On the Origin of Formamides in Diarylamine-Inhibited Autoxidations

&

The Development of Latent Radical Trapping Antioxidants for High-Temperature Applications

By
Matthew Dods

Master's thesis submitted to the Faculty of Science

In partial fulfillment of the M. Sc. of Chemistry

Supervisor Derek A. Pratt

Department of Chemistry & Biomolecular Sciences
University of Ottawa
Ottawa, Canada

Abstract

Autoxidation is a free radical chain reaction by which hydrocarbons undergo oxidative degradation. This process involves insertion of molecular oxygen into hydrocarbon-based materials such as oils, lubricants, polymers, etc. thereby altering their properties. Unlike living organisms, petroleum-derived products do not have inherent mechanisms to combat autoxidation. Therefore, they must be formulated with radical-trapping antioxidants (RTAs) which trap chain-propagating peroxyl radicals, terminating the radical chain. Although this technology has existed for decades, improvements are sought to keep up with ever more stringent environmental regulations, which requires internal combustion engines to operate at higher temperatures than previously, putting the lubricants under far greater oxidative stress. To improve RTAs, the process by which they are consumed and/or deactivated must be further understood.

Previous studies in our group revealed that *N*-formyl alkylated diphenylamines (ADPAs) are predominant products formed during ADPA-inhibited autoxidations of hydrocarbons at elevated temperatures. From previously known autoxidation products (acids, aldehydes, ketones, peracids, and alcohols), we hypothesized that *N*-formyl ADPAs arise from reactions of ADPAs with formate esters formed from Baeyer-Villiger oxidations of aldehydes. Herein we demonstrate that *N*-formyl ADPAs can be formed by this pathway. This was followed by a computational study to provide additional insight on the competition between formate ester and carboxylic acid formation, as the latter is almost exclusively observed in B-V oxidations of aldehydes. Surprisingly, the selectivity arising from these competing pathways has never been systematically evaluated as a function of temperature.

Additionally, to improve the stability – and therefore efficacy – of highly reactive diarylamine RTAs such as phenothiazine (PTZ) and phenoxazine (PNX), we have investigated the potential of *N*-acyl PTX and *N*-acyl PNZ derivatives as latent RTAs. Thus, we prepared various *N*-acyl derivatives that could serve as precursors to the reactive free amine by either intermolecular or intramolecular acyl substitution in situ. Additionally, we investigated the impact of para-substitution (relative to the amine) to investigate how electronics influence both the rate of release and the efficacy of the RTAs, which were determined in *n*-hexadecane autoxidations at 165 °C. Combining the performance metrics with kinetics of release will pave the way forward in RTA design.

Acknowledgements

To start, I would like to thank my supervisor Derek Pratt for taking a chance on me beginning as an undergraduate student 3 years ago. Over the last three and a bit years, I have learned an immense amount about both about science and life. Thank you for your mentorship and helping me be the best scientist I can be.

Secondly, I would like to thank my lab mates and other co-workers within the Department of Chemistry & Biomolecular Science that I have learned so much from over the years and for the fun times as well making it an enjoyable place to come to work every day. In particular I would like to thank Mel Mallais for being an amazing and supportive co-worker and friend. Thank you to Mike Donohoe not only for your help with all the computations and vast chemical knowledge but being an amazing friend and bringing the humour to the lab. I also want to thank Luke Farmer for his mentorship and conversation over the last three years, you've helped a lot. Lastly, I'd also like to thank Connor Bougonje, Mel Cyr, EJ Boisvert, Eda Kilic, Allison O'Rourke, Meredith Allen, and Zijun Wu for being amazing colleagues throughout my graduate studies.

I'd also like to thank my family (Mom, Dad and Zach), for being an amazing support network throughout my university career. You may not know what I'm talking about with my research but thank you for listening whenever I needed it.

Table of Contents

Table of Figures

Table of Schemes

Table of Tables

List of Abbreviations

ADPA	Alkylated diphenyl amine
APP	Anti periplanar
BDE	Bond dissociation energy
BHT	Butylated hydroxytoluene
BODIPY	Boron dipyrromethene
B-V	Baeyer-Villiger
EDG	Electron donating group
EWG	Electron withdrawing group
HAT	Hydrogen atom transfer
HPLC	High-pressure liquid chromatography
KIE	Kinetic isotope effect
m-CPBA	meta-chloroperoxybenzoic acid
NO_x	Nitrogen oxides
NMR	Nuclear magnetic resonance
PNX	Phenoxazine
PRA	Peroxyl radical addition
PTZ	Phenothiazine
RTA	Radical Trapping Antioxidant
TEMPO	(2,2,6,6-Tetramethylpiperidin-1-yl)oxyl
UPLC	Ultra performance liquid chromatography

Chapter 1: Background and Significance

1.1 – Autoxidation

Most things around us are made up of hydrocarbons – from petroleum-derived products (e.g. plastics and lubricants) to the lipids that make up cell membranes in living organisms.[1,2,3] Although it is necessary for life, molecular oxygen is simultaneously responsible for the destruction of all living and non-living organic structures, due to the oxidation of the hydrocarbons within them. The oxidation of lipids has been linked to cardiovascular disease and neurodegenerative diseases such as Parkinson's.[4] Likewise, oxidation of hydrocarbons/polymers via leads to the degradation of consumer and industrial products such as engine oil/lubricant and car tires. The mechanism by which this occurs is called autoxidation.

Autoxidation is a free radical chain reaction wherein molecular oxygen (O_2) is incorporated into a hydrocarbon. As typical in free radical chain reactions, the autoxidation mechanism is comprised of three different phases: initiation, propagation, and termination (**Scheme 1.1**). The rate of these steps can be influenced by a variety of factors such as substrate, temperature, potential initiators and the presence of inhibitors. These factors not only influence the rate of autoxidation itself but can also influence the distribution of products

formed – initially mostly peroxides but eventually acids, peracids, aldehydes, ketones and various alcohols, amongst others.[5]

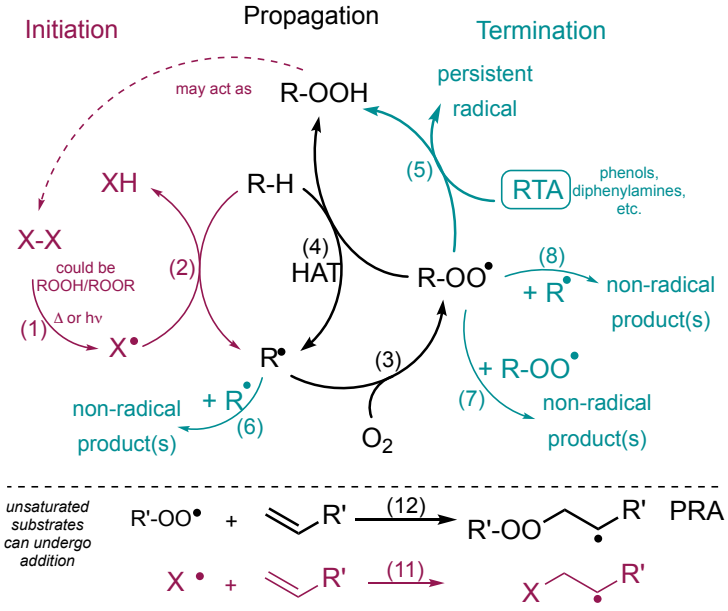

Scheme 1.1 – General autoxidation mechanism.

1.1.1. – Initiation

Radical chain reactions are typically initiated by light or heat (**Scheme 1.1-1 and 1.2**), which leads to the homolysis of a weak bond to form radicals. An example, and arguably the most important in the context of autoxidation, is the homolysis of O-O bonds in peroxides. Under physiological conditions however, homolysis due to light or heat is not generally responsible, but instead the cleavage of an O-O bond due to electron transfer from metal ions (i.e. Fe^{2+}).[3] The initiator-derived radical then abstracts a hydrogen atom from the hydrocarbon (a hydrogen atom transfer, HAT) which creates a carbon-centred radical (**Scheme 1.1-2**). Initiation can also occur via addition to an alkene (**Scheme 1.1-11**), which also leads to a carbon-centred radical. Autoxidations can be auto-initiated or self-initiated via the decomposition of product peroxides to initiating radicals. It has been proposed that at elevated

temperatures, even O_2 can act as an initiator, via the unlikely termolecular reaction with two equivalents of R-H as in **Scheme 1.3.**[6] Instead, it is more likely that trace hydroperoxides in the hydrocarbon serve as the initiator of otherwise uninitiated autoxidations. Regardless of the precise initiating species, due to the initiation step being highly endergonic, the rate of initiation (R_i) is significantly influenced by temperature.[1,3] The viscosity of the medium/substrate also plays a significant role, whereby the radical pair generated must escape the solvent cage to initiate the reaction.[1,3]

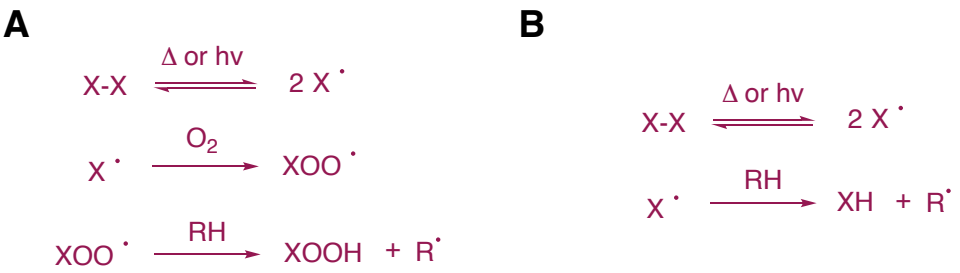

Scheme 1.2 – **(A)** Initiation of autoxidation where the initiator-derived radical reacts with molecular oxygen to give a peroxyl radical that starts the radical chain, e.g. X = AIBN or some other azo species. **(B)** Initiation where the initiator-derived radical directly reacts with the hydrocarbon to start the chain, e.g. X = hydroperoxide, alkyl peroxide.

Scheme 1.3 – Triplet oxygen acting as an initiator reacting with two equivalents of hydrocarbon generating two carbon centred radicals.

1.1.2 – Propagation

The carbon-centred radical generated in the initiation step combines with O_2 at near diffusion controlled rates ($k \approx 10^9$ M^{-1} s^{-1}) to create a peroxyl radical (**Scheme 1.1-3**).[1,3,7,8,9] The peroxyl radical can then abstract an H-atom from another substrate molecule to generate a hydroperoxide and another carbon-centred radical (**Scheme 1.1-4**). It can also add to a double bond via peroxyl radical addition (PRA) (**Scheme 1.1-12**) to form another carbon centred

radical.[3,7,10,11] HAT and PRA are the slower of the propagation steps which have rates highly dependent on the structure of the substrate where the propagation rate constant (k_p) $k_p \approx$ <1 to 100 M^{-1} s^{-1} for most hydrocarbons.[1] k_p is higher for substrates with weaker C-H bonds, such as those neighbouring aromatic ring, double bond or heteroatom (e.g. cumene, 1-hexadecene and THF, respectively).[12,13] This can be quantified from the rate of an initiated autoxidation, which obeys the following rate law, which can be derived under the assumption that the radical concentration remains constant ($R_i = R_t$, i.e. using the steady state approximation)[1,3]:

$$\frac{\mathrm{d[ROOH]}}{\mathrm{d}t} = -\frac{\mathrm{d[O_2]}}{\mathrm{d}t} = \frac{k_p[\mathrm{RH}]\sqrt{R_i}}{\sqrt{2k_t}} \quad \text{(I)}$$

1.1.3 - Termination

In competition with radical-molecule reactions which propagate the chain reaction, the radical species generated can combine in radical-radical reactions to create non-radical products. This includes the combination of two alkyl radicals, two peroxyl radicals, or an alkyl radical with a peroxyl radical (**Scheme 1.4-A**). Alkyl radical combination typically occurs quickly in isolation, however in the context of an autoxidation, the abundance of O_2 heavily favours the combination of the alkyl radical with O_2, therefore yielding a low concentration of alkyl radicals.[1,3,6] Thus, the combination of two peroxyl radicals is dominant, and yields a tetroxide intermediate which either homolyzes back to two peroxyl radicals or will form a ketone (or aldehyde), alcohol and O_2, in the so-called 'Russel Termination' process (**Scheme 1.4 – B**).[1,3,6,14]

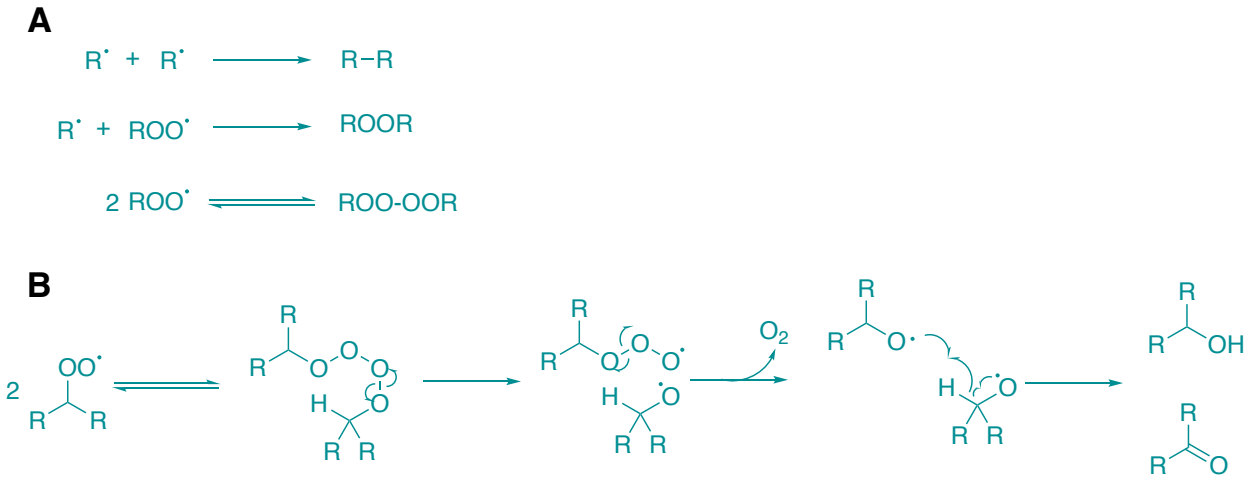

Scheme 1.4 – (A) Various modes of radical-radical termination which can, in principle, occur in an autoxidation. **(B)** The mechanism of peroxyl radical-mediated termination.

1.1.4 – Additional Products of High-Temperature Hydrocarbon Autoxidation

In addition to the primary hydroperoxides formed via HAT, peroxides formed via PRA and alcohols/ketones formed via termination reactions, several other products arise in the autoxidation of even simple aliphatic hydrocarbons. For example, intramolecular HAT in a

propagating peroxyl radical leads to the formation of carboxylic acids and methyl ketones via γ-hydroperoxyketones (**Scheme 1.5**).[3,15,16]

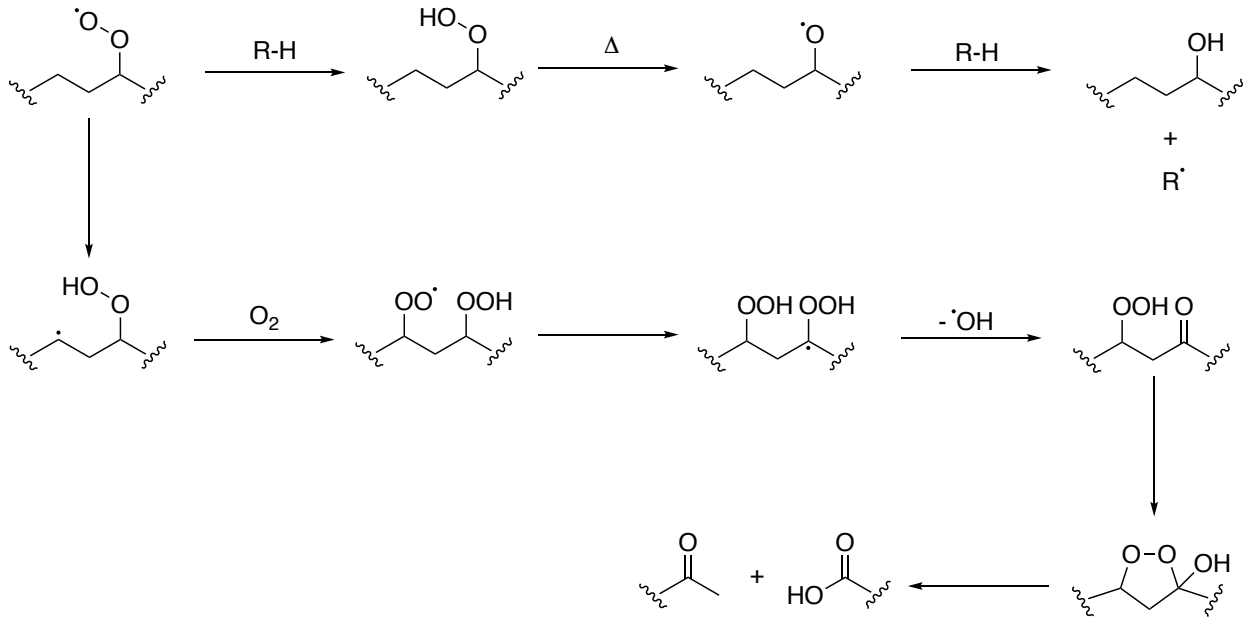

Scheme 1.5 – Generation of alcohols, ketones and acids from competing intermolecular and intramolecular HAT.

Aldehydes arise from β-scission of alkoxyl radicals formed via thermolysis (or photolysis, when appropriate) of hydroperoxides or peroxides (**Scheme 1.6**). Aldehydes themselves can be readily autoxidized (k_p ranging from 1-12 x 10^3 M^{-1} s^{-1}) yielding initially a peracid species that can then oxidize aldehydes and ketones to form acids and esters via Baeyer-Villiger (B-V) chemistry (**Scheme 1.7**).[6,17,18] In the context of high-temperature autoxidations, acid products are especially prominent due to the harsh environment of the system and significant accumulation can be observed.[5,15,19]

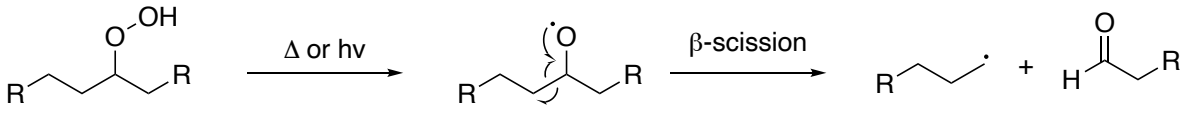

Scheme 1.6 – Aldehyde formation from hydroperoxides (heat or light initiated).

Peracid Formation

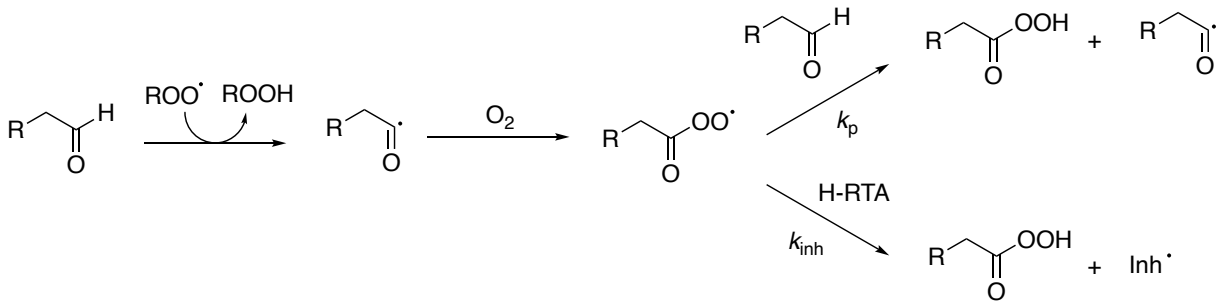

Acid/Ester Formation

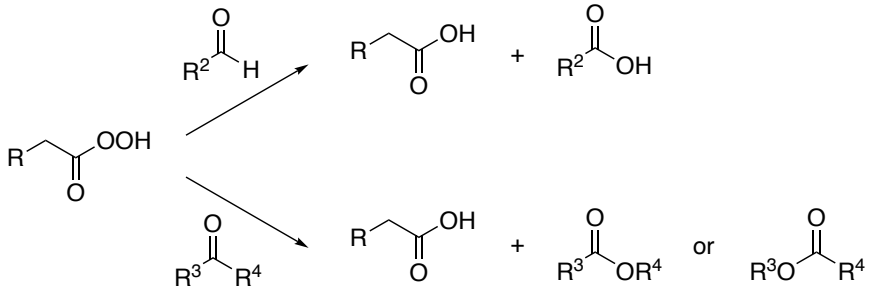

Scheme 1.7 – Formation of peracids, acids and esters from aldehydes in high-temperature autoxidations.

1.2.1 – Antioxidants

Inhibition of autoxidation by the intervention of hydrocarbon additives can be accomplished in several ways. Radical-trapping antioxidants (RTAs) 'trap' peroxyl radicals most commonly by donating a hydrogen atom via HAT, which forms a hydroperoxide and a persistent RTA-derived radical (**Schemes 1.1-5**).[3,6,20,21] HAT to the peroxyl radical as opposed to the carbon-centered radical is most important simply due to the rate at which carbon-centred radicals react with O_2. Thus, RTAs must be able to perform HAT or react in another fashion with the peroxyl radical faster than a peroxyl radical can perform HAT (or PRA) with a hydrocarbon (where k_p ranges from 1 to 100 M^{-1} s^{-1}).[1] The other type of antioxidants are secondary (preventative) antioxidants which decompose peroxides and other initiating species, slowing down the overall autoxidation process. Some common secondary antioxidants are organosulphur and organophosphorus compounds such as polysulphides and phosphines. In industry, secondary antioxidants are used in tandem with RTAs to slow the depletion of the stock of RTAs by retarding the rate of initiation.[3]

1.2.2 – Radical-Trapping or Chain-Breaking Antioxidants

The efficacy of RTAs is determined by how fast they undergo reactions with peroxyl radicals and the persistence of the radical formed as a result. The latter is especially key as the RTA is not acting as an antioxidant if the RTA-derived radical can propagate the chain. The rate constant characteristic of the reaction of the RTA with a peroxyl radical is called the inhibition rate constant (k_{inh}), which can be derived from the initial rate of an inhibited autoxidation:

$$\frac{\mathrm{d[ROOH]}}{\mathrm{d}t} = -\frac{\mathrm{d[O_2]}}{\mathrm{d}t} = \frac{k_p[\mathrm{RH}]R_i}{nk_{inh}[\mathrm{RTA}]} \quad \text{(II)}$$

Where:

$$n = \frac{t_{inh} R_i}{[\mathrm{RTA}]} \qquad \text{(III)}$$

Some common RTAs and their corresponding values of k_{inh} are included in **Figure 1.1**.[22,23] Importantly, even the least reactive of these representative compounds (BHT) still has a k_{inh} which is significantly greater than the k_p of most hydrocarbons (which are generally <100 M^{-1} s^{-1}). In an ideal world the 'perfect' RTA would possess a diffusion-limited k_{inh}. If an RTA could react this quickly, it would essentially trap peroxyl radicals as quickly as they form. For RTAs that react by HAT, k_{inh} is inversely correlated to the BDE of the bond to the hydrogen that is transferred.

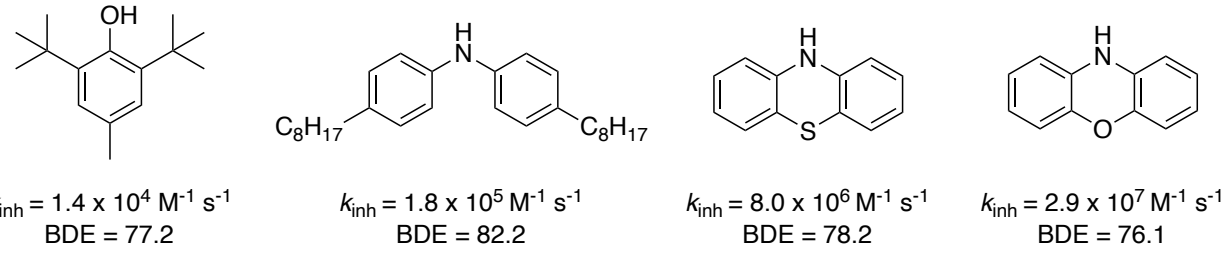

k_{inh} = 1.4 x 10^4 M^{-1} s^{-1} BDE = 77.2

k_{inh} = 1.8 x 10^5 M^{-1} s^{-1} BDE = 82.2

k_{inh} = 8.0 x 10^6 M^{-1} s^{-1} BDE = 78.2

k_{inh} = 2.9 x 10^7 M^{-1} s^{-1} BDE = 76.1

Figure 1.1 – Common radical trapping antioxidants with their associated k_{inh} and O-H or N-H BDE values (in kcal/mol).

The radical-trapping stoichiometry is key to antioxidant activity. Although the initial reaction of the RTA with the peroxyl radical dictates k_{inh} (and hence the initial rate of the inhibited autoxidation), the duration of the inhibited period depends on the number of radicals trapped per molecule of RTA. At ambient temperatures, RTAs generally trap 2 radicals – the first by HAT to a chain-propagating radical and the second by combination with another chain-propagating radical, as exemplified below for BHT. Importantly, the radical-trapping stoichiometry of BHT is eroded at elevated temperatures to n ~ 1 due to the reversibility of the second step (**Scheme 1.8**).[24]

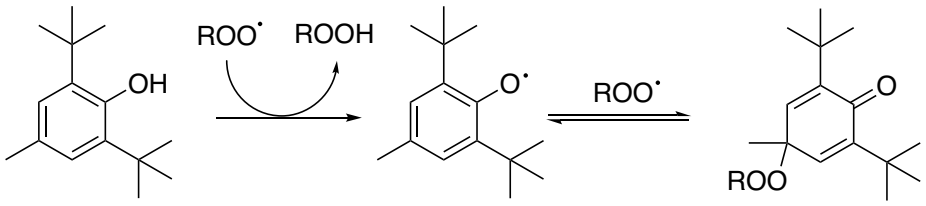

Scheme 1.8 – Trapping of two peroxyl radicals by BHT, the first via HAT and the second via radical combination.

An additional quality desirable for RTAs is their stability towards O_2 and/or peroxidic products of autoxidation, as this can deplete the RTA and possibly lead to chain-initiating radicals.[1,3] For example, phenoxazine is a very effective RTA at ambient temperatures, but at elevated temperatures (ie. 165 °C), its superb reactivity is curtailed somewhat due to reactions with molecular oxygen (**Scheme 1.11**).[25]

1.2.3 – Diarylamine RTAs

Alkylated-DPAs are some of the most widely used RTAs to protect hydrocarbon-based products (in particular, engine lubricants) at elevated temperatures. At ambient to moderate temperatures, aminic RTAs perform similarly to phenols like BHT (stoichiometries of n = 2).[26,27,28] However, at the elevated temperatures where BHT's stoichiometry decreases, ADPAs have been shown to possess very large stoichiometries. The origin of this 'catalytic' RTA activity at elevated temperatures is mainly due to conversion of ADPAs to their corresponding nitroxides, which enable them to participate in either the Korcek cycle (**Scheme 1.9-A**) or the peroxyl radical cross-dismutation cycle (**Scheme 1.9-B**), enabling one molecule of ADPA to trap two propagating radicals through each pass through either cycle.[3,5,15,16,25,29,30,31]

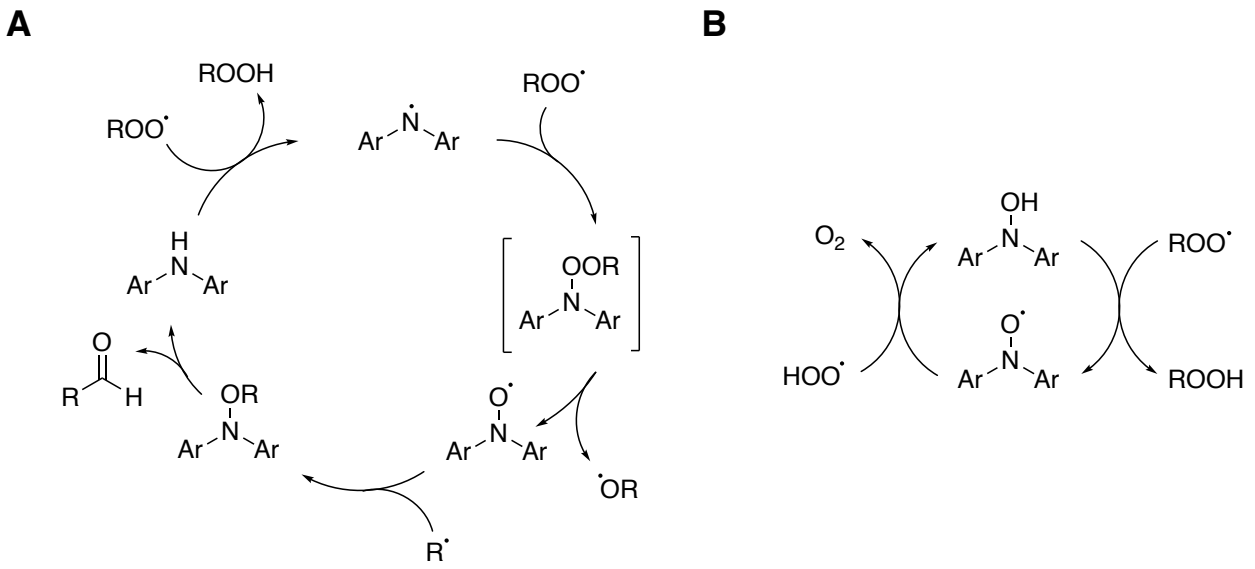

Scheme 1.9 – (A) Regeneration of diarylamines via the Korcek cycle. **(B)** Regeneration of diarylamines via the cross-dismutation pathway.

Given the unique reactivity offered by ADPAs, there has been much interest in structure-reactivity relationships in order to identify and/or design even more efficient high-temperature RTAs. Adding primary or secondary alkyl groups *para* to the amine can increase the stoichiometry (**Scheme 1.10**) of a diarylamine by trapping additional radicals, but the electrophilic reaction intermediates can also promote oligomer formation which can precipitate out of solution - a serious issue for engine lubricants.[29] Tertiary alkyl can be added in the *para*-position as well, which minimize oligomer formation, but also have reduced radical-trapping stoichiometry. Alkyl groups are slightly electron-donating and can therefore weaken the N-H, thus promoting HAT to occur faster with peroxyl radicals. Alkylation also increases the persistence of the eventual nitroxide species formed, which enables more efficient progress through the Korcek and cross-dismutation cycles.

Other electron donating groups (EDG) in the *para* and/or *ortho* positions will also weaken the N-H bond, leading to faster reactions with peroxyl radicals. This is demonstrated in

heteroatom-bridged diarylamines such as PTZ and PNX, where the heteroatom contributes towards a weakened N-H bond leading to increased activity, making them some of the most reactive scaffolds known at ambient temperature.[2]

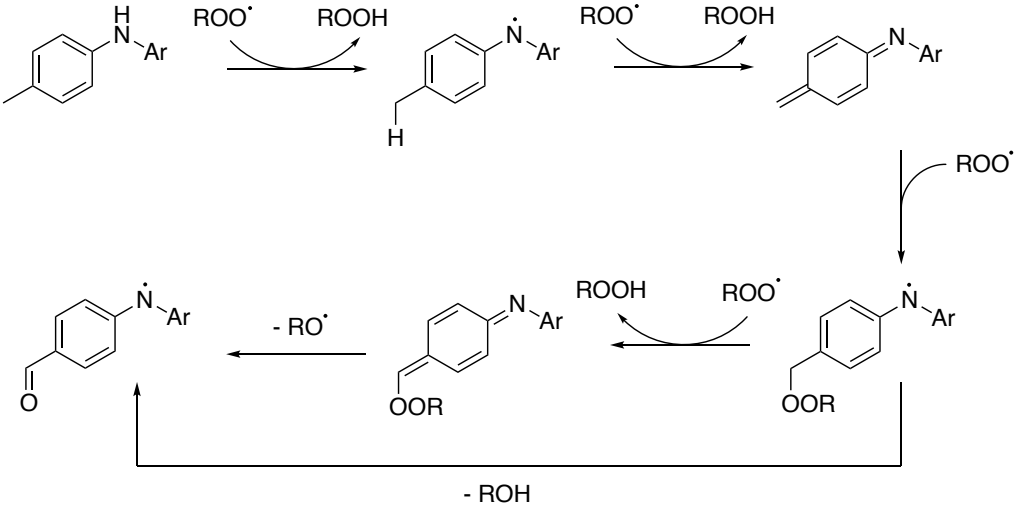

Scheme 1.10 – Increased RTA ability of diarylamines with alkyl groups para to the amine which contain accessible allylic hydrogens to increase stoichiometry.

1.2.4 – Challenges with Employing PTZ and PNX in High-Temperature Autoxidations

Despite having greatly superior k_{inh}s and lower N-H BDEs which contribute to longer inhibited periods than many diarylamines, phenoxazines and phenothiazines are not commonly used in as industrial antioxidants. Phenoxazines can react directly with O_2 at elevated temperatures, which leads to the formation of PNX-nitroxide, which has little RTA activity in saturated hydrocarbons (**Scheme 1.11**). Phenothiazine was extensively studied in the 1950's, 60's and 70's to inhibit oxidation in polyethylene oils and turbo-jet lubricants.[32] In the 1950's, Murphy and co-workers found phenothiazine to be a good inhibitor at ~163 °C when used at low concentrations (0.47 wt%), while in the 1960's, Strange and co-workers found that 1 and 0.6 wt% PTZ and PTZ-derived RTAs were only practical to ~150 °C.[32-33] At elevated temperatures and/or concentrations of PTZ, there are visible deposits of PTZ-derived products and increased

viscosity.[32,33] This is obviously undesirable for applications such as engine lubricants, since precipitates can clog filter screens or lubricants lines. Oligomerization presumably occurs due to off-cycle reactions of PTZ-derived radicals, which accumulate at increased concentrations of PTZ (**Scheme 1.12-A)**. In addition to the oligomers formed, PTZ can also form N-N dimers, *ortho* and/or *para* C-N dimers, phenothiazone, PTZ-sulfoxide and PTZ-sulfone (**Schemes 1.13**). Therefore, PTZ has not been investigated thoroughly since 1970's due to the detrimental structure-property relationships outweighing their potent inherent RTA activity.

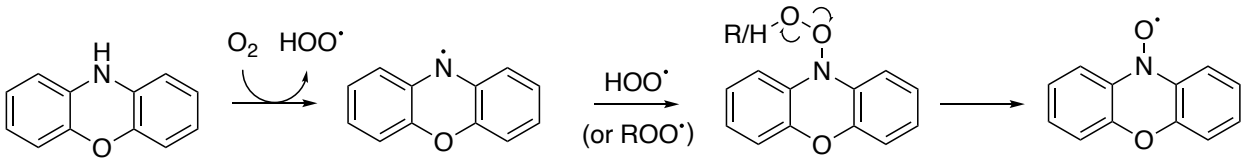

Scheme 1.11 – Autoxidation of PNX to its nitroxide.

A

B

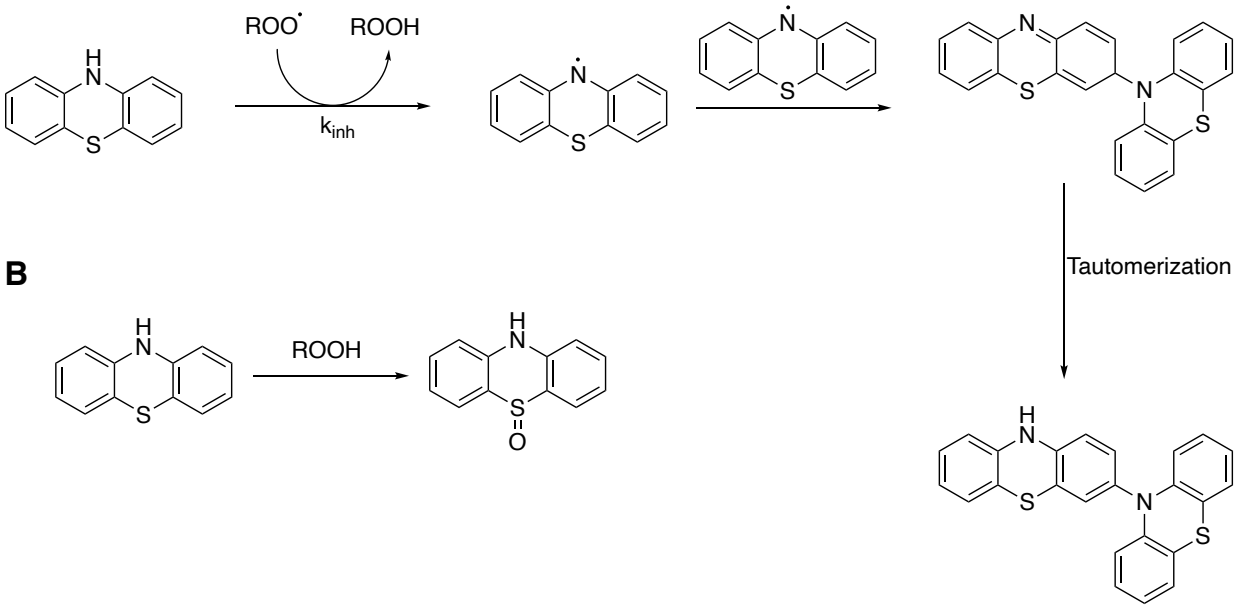

Scheme 1.12 – (A) The oligomerization of PTZ and **(B)** the direct oxidation of PTZ's sulfur atom during autoxidation. Both are undesired by-products which may cause precipitation at elevated concentrations of PTZ.

A

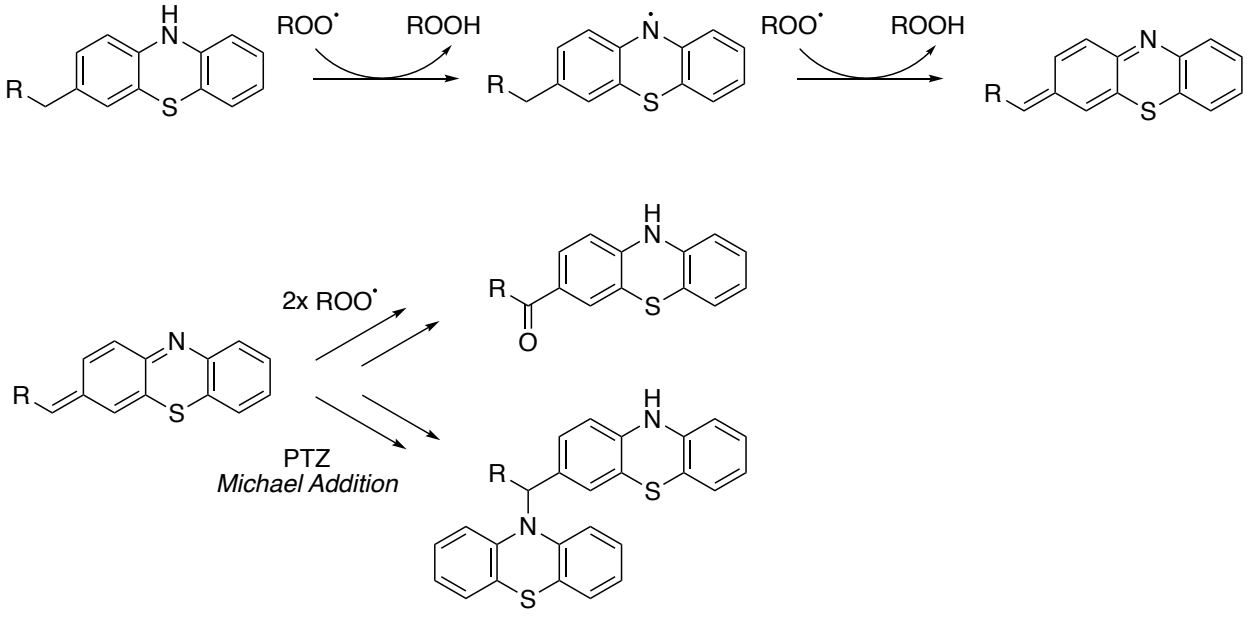

B

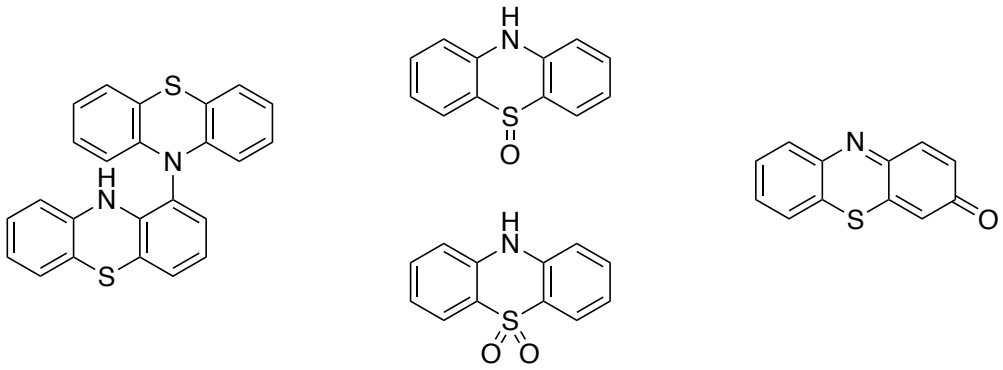

Scheme 1.13 – (A) Formation of PTZ-dimers or trapping of additional peroxyl radicals due to para-alkyl substituents. **(B)** Various off-cycle PTZ-based products which form during PTZ-inhibited autoxidations.

1.3.1 – Quantitative Measurement of Autoxidation Reaction Progress

Since mass transfer of O_2 can be rate-limiting in hydrocarbon autoxidation at elevated temperatures, experiments have been performed using stirred-flow reactors which were built of two flasks – a larger, outer flask containing the substrate and smaller inner flask which was perforated to deliver O_2.[5] In our group, we developed a more high-throughput and cost-effective method for carrying out multiple autoxidations simultaneously. We utilize test tubes of substrate which are heated in a circular 16-position aluminum block under a constant flow of O_2 supplied by Teflon tubing distributed to each test tube via an acrylic manifold (**Figure 1.2**). Aliquots are taken at various time points throughout the autoxidation and are analyzed for their hydroperoxide content.

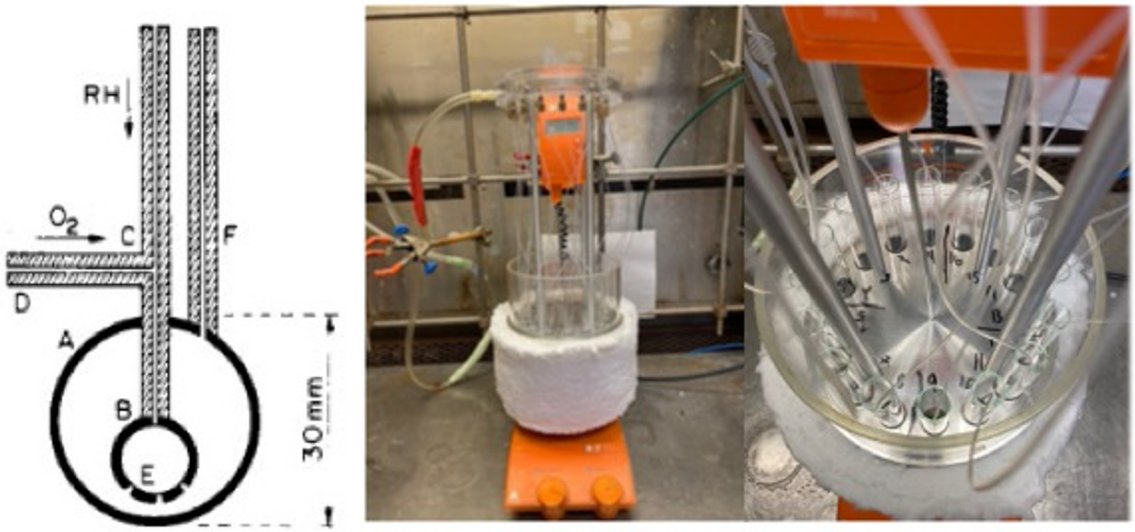

Figure 1.2 – (Left) A diagram of a stir-flowed reactor, such as that used by Korcek in seminal studies of high-temperature autoxidations. **(Centre, Right)** The stirred-flow autoxidation apparatus used in this work (front and top views).

The determination of [ROOH] is samples taken from autoxidations carried out at high temperatures can be time consuming, as it generally involves an iodometric titration or LC or GC analysis following reduction of the hydroperoxides to their corresponding alcohols.[5,19,34] In

2012, we reported a more high throughput approach utilizing a fluorogenic coumarin-conjugated phosphine (**Scheme 1.14**),[34] and in 2016, we reported a BODIPY-conjugated amine to measure acid formation (**Scheme 1.15**).[15] These probes can be used in tandem to simultaneously measure hydroperoxide and acid formation over the course of an autoxidation. In this method, aliquots are loaded into the wells of a 96-well microplate, acid probe and phosphine probe are then diluted in acetonitrile and dispensed by automated reagent dispensers into the microplate wells directly prior to the fluorescence measurement. The phosphine is oxidized by hydroperoxides which enhances the fluorescence of the probe as in **Scheme 1.14**. The concentration of hydroperoxide in each aliquot can be determined from the pseudo-first order rate of fluorescence increase.[15,34] The BODIPY-amine is protonated by acids generated during autoxidations (i.e. carboxylic acids) causing the BODIPY probe to undergo a fluorescence enhancement which is proportional to the acid concentration.[15] Using these methods, it is much more efficient to perform assays and learn about RTA structure-reactivity relationships.

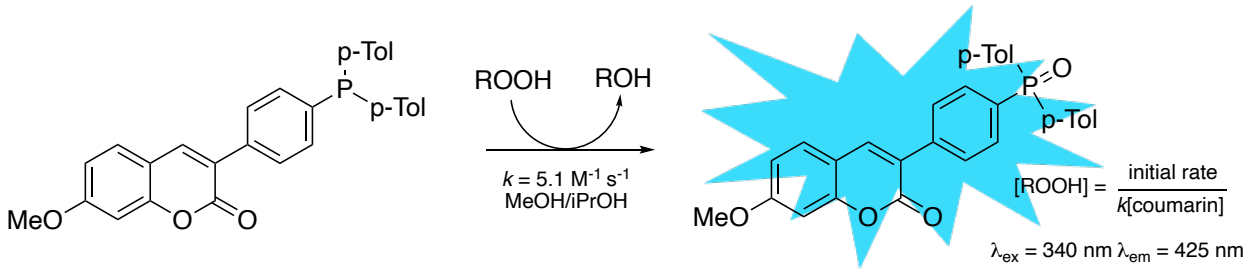

Scheme 1.14 – Oxidation of the phosphine-coumarin conjugate by hydroperoxides formed during autoxidations leads to a fluorescence enhancement, whose rate is proportional to the hydroperoxide concentration.

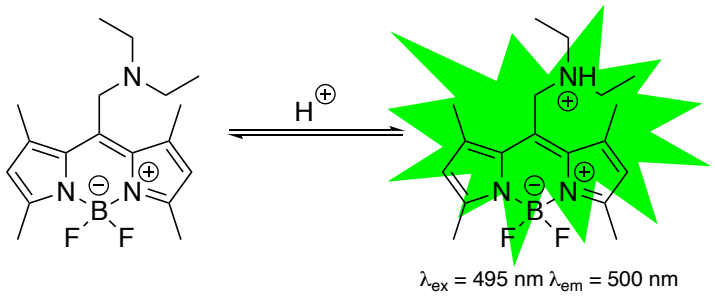

Scheme 1.15 – Protonation of the amino-BODIPY probe by acids formed during autoxidations leads to a fluorescence enhancement proportional to the amount of acid formed.

1.4 Research Objectives

1.4.1 – On the Origin of Formamides in Diarylamine-Inhibited Autoxidations

Our group recently determined that the most prominent ADPA-derived product in autoxidations inhibited by ADPAs at elevated temperatures are N-formyl ADPAs (**Scheme 1.16**). The mechanism by which this species forms is unclear, however, presumably this requires the generation of a formylating agent in situ. Unfortunately, to date none have been reported. We hypothesize that two products which are known to be formed in situ, aldehydes and peracids, react with each other to generate a formate ester via B-V oxidation. The formate ester in turn reacts with ADPA to generate N-formyl ADPA. Formate esters are not typically produced in B-V oxidations aside from a handful of cases, but this chemistry is not performed at the elevated temperatures at which saturated hydrocarbons undergo autoxidation.

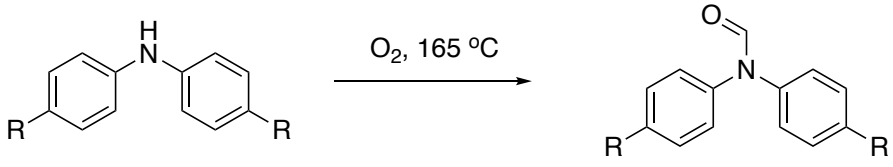

Scheme 1.16 – Formation of N-formyl-ADPA from ADPA under autoxidation conditions.

Therefore, we aim to investigate:

- Product distributions arising in Baeyer-Villiger oxidations with a model saturated aldehyde (1-hexadecanal) as a function of temperature.
- Corresponding oxidation of 1-d_1-hexadecanal to determine the kinetic isotope effect (KIE) on carboxylic acid formation.
- Computations of the competing migration of H (to form the typical carboxylic acid product) and the alkyl group (to form the formate ester), to corroborate our observations and understand the basis for the general preference for H-migration.

This will not only shed light onto the mechanism that leads to formation of formylated DPAs, but may lead to new applications for B-V oxidation chemistry.

1.4.2 – The Development of Latent Radical Trapping Antioxidants for High-Temperature Applications

Improved RTAs can increase the efficiency and longevity of fossil fuel-based products, therefore consuming less product and decreasing the carbon footprint of them. Despite their unprecedented potency, PTZ and PNX have significant drawbacks that must be addressed for possible commercial applications – specifically, these involve competing non-RTA reactions of PTZ (oligomerization) and PNX (direct reaction with O_2).

Therefore, we aim to investigate:

- Whether acyl groups can be used to protect PTZ and PNX from these deleterious reactions, and whether the small amounts of PTZ and PNX can be gradually released under autoxidative conditions by reactions with nucleophilic autoxidation products.

- The influence of both electron-donating and electron-withdrawing groups on both the release rates of PTZ and PNX under the autoxidative conditions and their overall performance as inhibitors of hydrocarbon autoxidation at elevated temperatures.
- An intramolecular approach for PTZ and PNX release, where an alcohol nucleophile is tethered to the acyl group; where release rate may be controlled by the tether length and therefore ring size of the eventual lactone product formed.

These preliminary studies will potentially unlock the untapped potential of PTZ and/or PNX as high temperature RTAs.

Chapter 2: On the Origin of Formamides in Diarylamine-Inhibited Autoxidations

2.1 – Introduction

Recent work in the group (Neill Penner, M.Sc. 2021) revealed that one of the most prominent antioxidant-derived products formed in high-temperature autoxidations inhibited by ADPAs are N-formylated derivatives. The origin of these products is unknown. While carbonyl containing compounds (aldehydes, ketones, acids, peracids) are known to accumulate in hydrocarbon autoxidations, they are not formylating agents. Carboxylic acid formation is attributed to both the Korcek fragmentation of γ-ketohydroperoxides and the Baeyer-Villiger (hereafter B-V) oxidation which take place in situ during the autoxidation of aldehydes to form these acids. B-V oxidations of aldehydes can theoretically produce formate esters if the alkyl group migrates in lieu of the proton. If the formate ester forms it could, in principle, formylate the diarylamine. This outcome, especially under acidic conditions which develop over the course of the autoxidation, gives reason for us to investigate this possibility.

2.1.1 – A Brief Review of the Baeyer-Villiger Reaction

The B-V reaction was discovered by Baeyer and Villiger over 100 years ago while studying the oxidative cleavage of cyclic ketones.[35–37] In general, it uses a peracid to transform ketones into esters and cyclic ketones into lactones. The mechanism originally proposed by Baeyer and Villiger (**Scheme 2.1**) involved a dioxirane intermediate, but this was proven to be incorrect by Criegee in the 1950's.[38] Using ^{18}O labeled benzophenone as a substrate, the experiment unambiguously excluded the symmetric intermediate, which would be expected to

yield a 50/50 distribution of ^{18}O labelled products.[39-40] To account for the observation that only the carbonyl oxygen was ^{18}O labelled in the products,

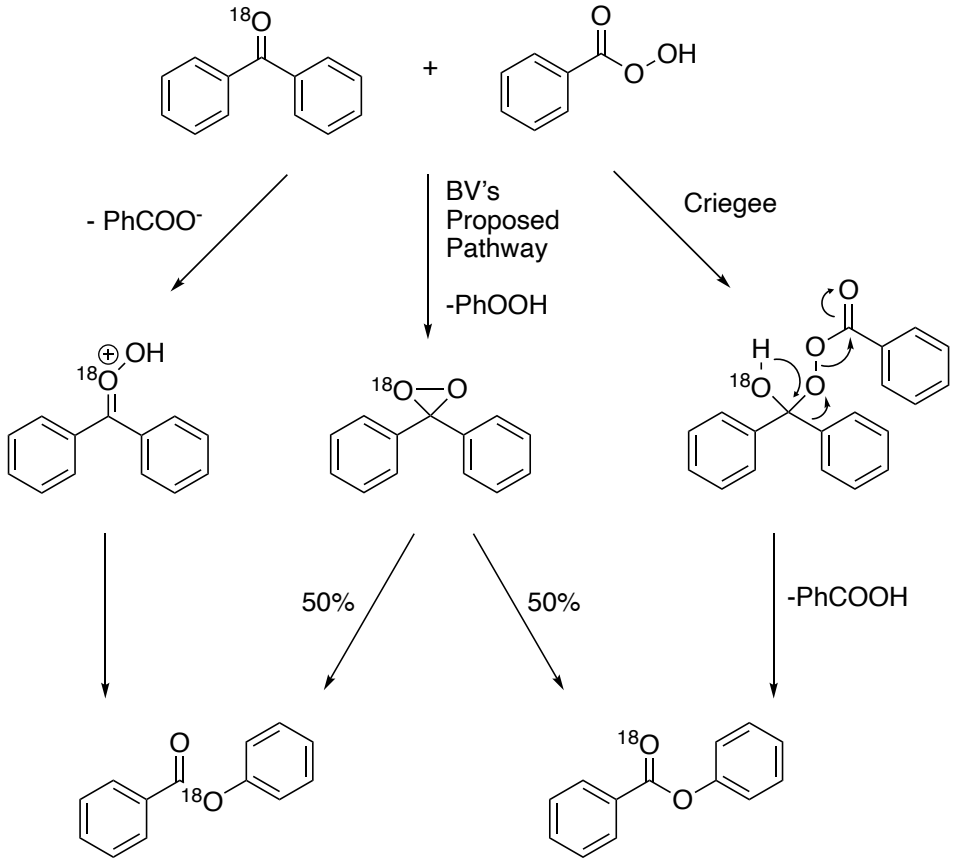

Scheme 2.1 – The original three proposed mechanisms of the Baeyer-Villiger reaction, where the Criegee intermediate/mechanism was determined via ^{18}O labelling.

Criegee proposed a tetrahedral intermediate where one of the aryl groups migrates to the proximal peroxidic oxygen atom to form an ester as the carbonyl is restored.[36,37] When the groups bound to the initial carbonyl are different, there are two possible products available depending on which group migrates. In general, the group which best stabilizes a positive charge migrates (i.e. t-Bu > s-Bu > Ar > ethyl > methyl, etc). When aryl groups are involved, EDG's/EWG's in the para-position can influence migratory aptitude, where EDG's boost migratory aptitude and EWG's hinder it. Ortho substituents make most ketones inert to B-V oxidations, presumably by slowing peroxyketal formation. In Doering and Speers' study of B-V

oxidations of camphor (**Scheme 2.2**) (also known as the 'Camphor Mystery' in many reviews), they discovered that changing the peracid or the pH can have a significant effect on product ratios, where either the bridgehead or methylene carbons migrate.[39] Under mildly acidic conditions, more methylene migration was observed, while under strongly acidic conditions, only 30% methylene migration product was observed.[36,37] In this scenario, the ketone can be attacked by the peracid in an endo or exo fashion (**Scheme 2.3**).The group that migrates is the group which gives the more energetically favourable chair structure as the final product. Therefore, if the peracid attacks the ketone in an endo fashion, migration of the methylene is preferred as it yields the product in a chair-like structure, whereas migration of the quaternary carbon would yield a boat-like structure. If the peracid attacks in an exo fashion, quaternary carbon migration is then preferred, as it would give the chair-like structure (**Scheme 2.3**).

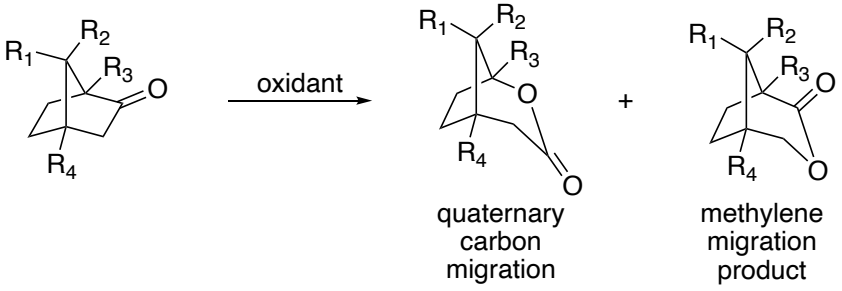

Scheme 2.2 – The 'Camphor Mystery' where under mildly acidic condition more methylene migration was observed, while under strongly acidic conditions only 30% of the methylene product is observed.

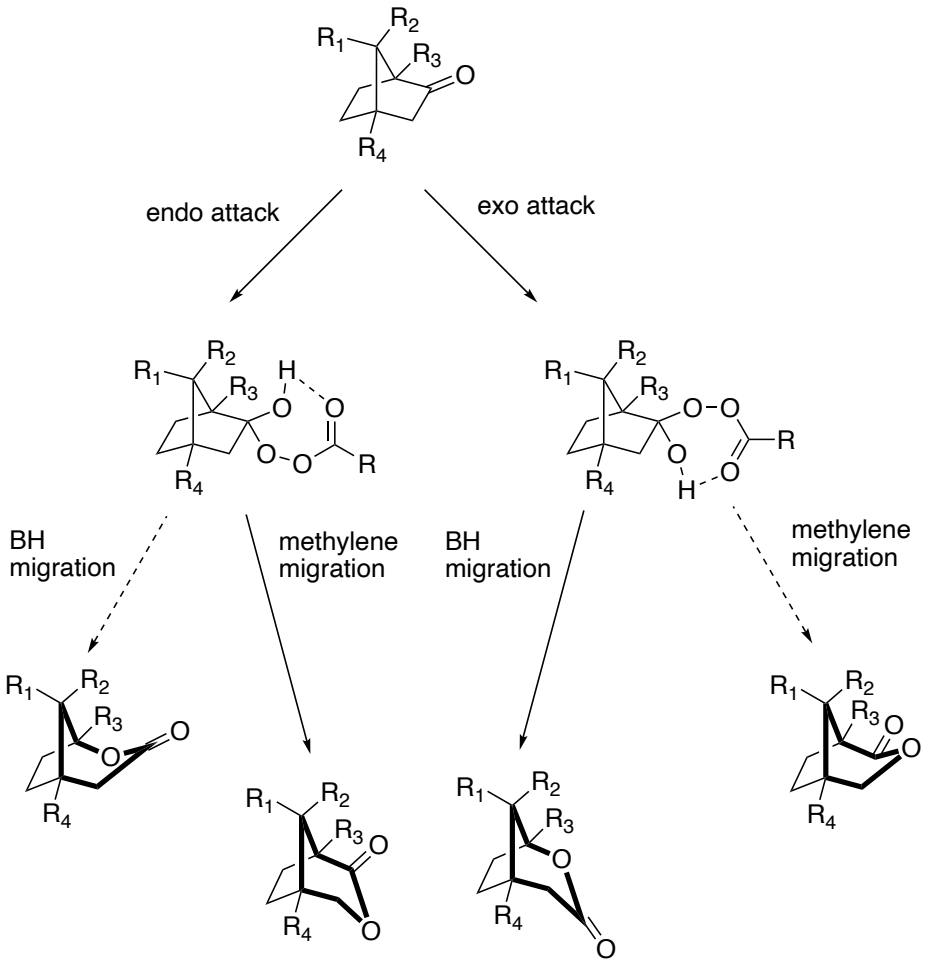

Scheme 2.3 – Product distribution of endo vs exo attack by the peracid on the bicyclic ketone from the Camphor mystery, where the preferred product adopts a chair-like structure and the non-preferred product adopts a boat-like structure.

In the context of acyclic ketones, the conformation adopted by the intermediate due to sterics and electronics effects plays a key role in the selectivity of the reaction. Two chair-like conformations are possible, with the peracid in an equatorial or axial position. H-bonding is more important in non-polar solvents as the intermediate will H-bond with itself to form a 7-membered chair conformation, while in H-bond accepting solvents, H-bonds with the solvent preclude conversion between chair structures allowing the H-migration to dominate. In **Scheme 2.4** there are two options for which group migrates based on which chair conformation is

adopted by the tetrahedral intermediate. Depending on the conformation, either group A or B will be anti-periplanar to the peracid and the group that is anti-periplanar will migrate to the oxygen (see **Figure 2.19** for orbital alignments).[41]

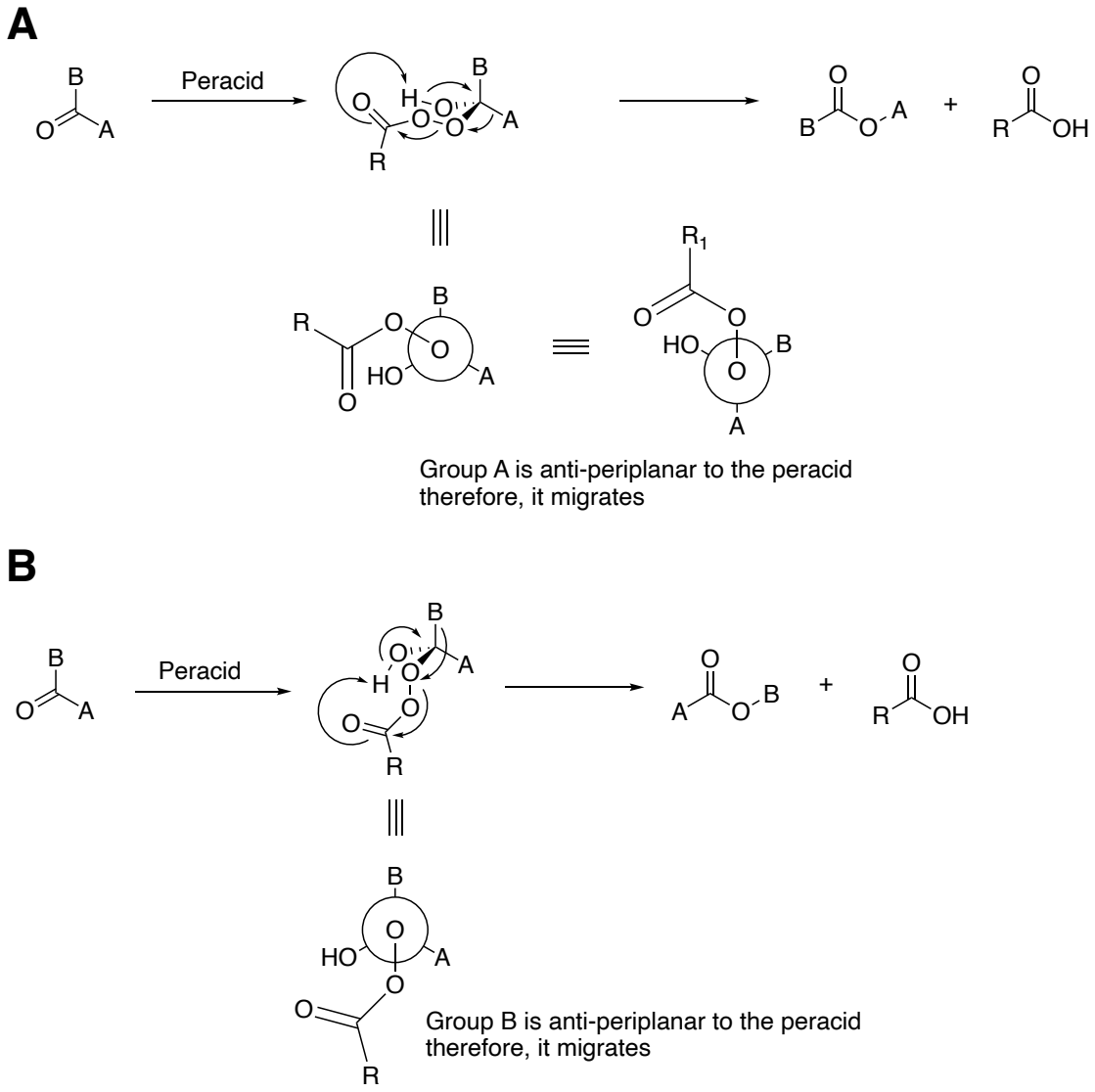

Scheme 2.4 – Chair conformations of Criegee intermediates where the group anti-periplanar to the nucleophilic peracid oxygen migrates.

Our knowledge about selectivity in B-V oxidations so far leans heavily on reactions of ketones – presumably since performing a B-V oxidation on an aldehyde in most cases yields carboxylic acids and there are many alternative approaches to oxidize an aldehyde to an acid. In 2010, Nakanishi et al. demonstrated that alkyl groups can migrate preferentially over an H-atom to form a B-V-like intermediate that yields a formate ester as opposed to an acid.[42] In fact, this was not a B-V reaction as no peracid was employed. Instead a hydrated *n*-aldehyde (or even a ketone) undergoes ligand exchange with a hypervalent aryl-λ^3-bromane(III), creating an activated Criegee-like intermediate, which undergoes reductive elimination to yield an ester (**Scheme 2.5**).[42] Formation of terminal esters from aldehydes was heavily favoured when employing this hypervalent bromane strategy, while reacting the aldehydes under classical B-V conditions formed acids exclusively. For example, butanal oxidation under the hypervalent bromane conditions forms a ratio of ester:acid of 4:1, while under classical conditions no formate ester is observed. An even better example is in the oxidation of *n*-heptanal, where under bromane conditions the ratio is 95:5, while classical conditions again yields no formate ester.[42]

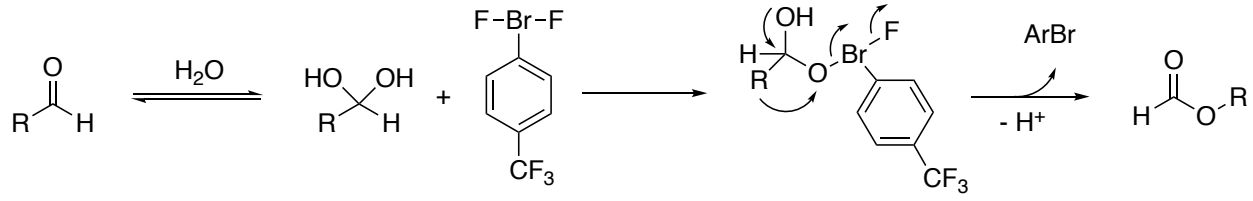

Scheme 2.5 – Formate esters synthesized from aldehyde and hypervalent bromanes via a Criegee-like intermediate.

Regarding aldehydes and B-V oxidations, transforming aldehydes to terminal esters via hypervalent bromane was the sole method until 2018. Inspired by Knochel's works, which

described the transformation of α-quaternary aldehydes to tertiary alcohols via B-V oxidation followed by reacting with KOH and MeOH (**Scheme 2.6**),[43] Kazmaier and co-workers employed this chemistry to in the stereoselective synthesis of β-hydroxyamino acids.[37] Their investigation eventually moved towards the preparation of formates from secondary aldehydes and tertiary aldehydes (**Scheme 2.8**) as these 'branched' aldehydes are closely related to the β-hydroxyamino acids (**Scheme 2.7**). Linear aldehydes were deemed "irrelevant" to the project and were therefore not investigated.[37]

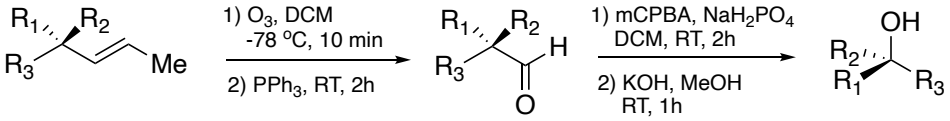

Scheme 2.6 – Proposed synthetic pathway from Kazmaier and coworkers to synthesize formate esters using classical B-V conditions.

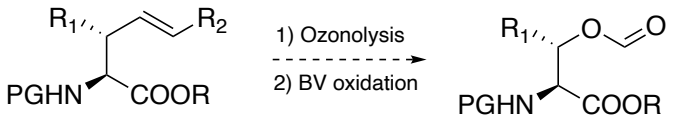

Scheme 2.8 – Proposed pathway from Kazmaier and coworkers to synthesize β-hydroxyamino acids.

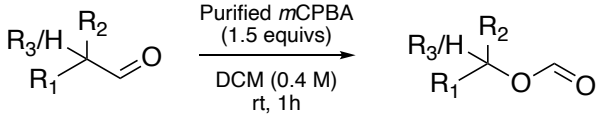

Scheme 2.7 – Synthesis of proprionaldehyde-based formate ester via classical B-V conditions.

After an investigation into various conditions that may favour formate formation, the ideal conditions used purified *m*-CPBA in DCM at room temperature, which typically resulted in complete conversion of the aldehyde within an hour.[37] Unpurified *m*-CPBA when used in an identical procedure leads to almost exclusively acid product, likely due to H-bonding with the water in commercial *m*-CPBA. Kazmaier's protocol is not only limited to secondary and tertiary

aldehydes, but can be used with more complex structures like steroidal structures, cinnamaldehydes and terpenoids such as myrtenal.[37]

2.1.2 – Formation of N-formyl Diarylamines

In his 2021 thesis, Penner proposed that *N*-formyl-4,4'-di-*tert*-butyldiphenylamine (*N*-formyl tBu_2DPA) is formed via reaction of 4,4'-di-*tert*-butyldiphenylamine (tBu_2DPA) with a formate ester (**Scheme 2.9-A**). Since aldehydes are common autoxidation products, and themselves undergo autoxidation to afford peracids, it is possible that the two react via B-V oxidation to form formate esters as shown in **Scheme 2.9-B**. While carboxylic acids are the typical reaction products (*vide supra*), at the elevated temperatures of the *n*-hexadecane autoxidation (165 °C), migration of the alkyl group and formation of the formate ester may be competitive. To investigate the *N*-formyl diarylamine formation, we synthesized the intermediates to determine if a preparative reaction under these conditions would be successful. We also investigated the dependence of the formate:acid product ratio on temperature and whether we could observe a kinetic isotope effect (KIE) on H-migration – first by performing B-V reactions of hexadecanal and hexadecanal-*d* with *m*-CPBA in DCE at varying temperatures – then also using computations of a model aldehyde (pentanal) and a model peracid (pervaleric acid). We sought to determine the difference in energy barrier for migration

of the alkyl group versus H and the corresponding formation of formate ester and acid respectively.

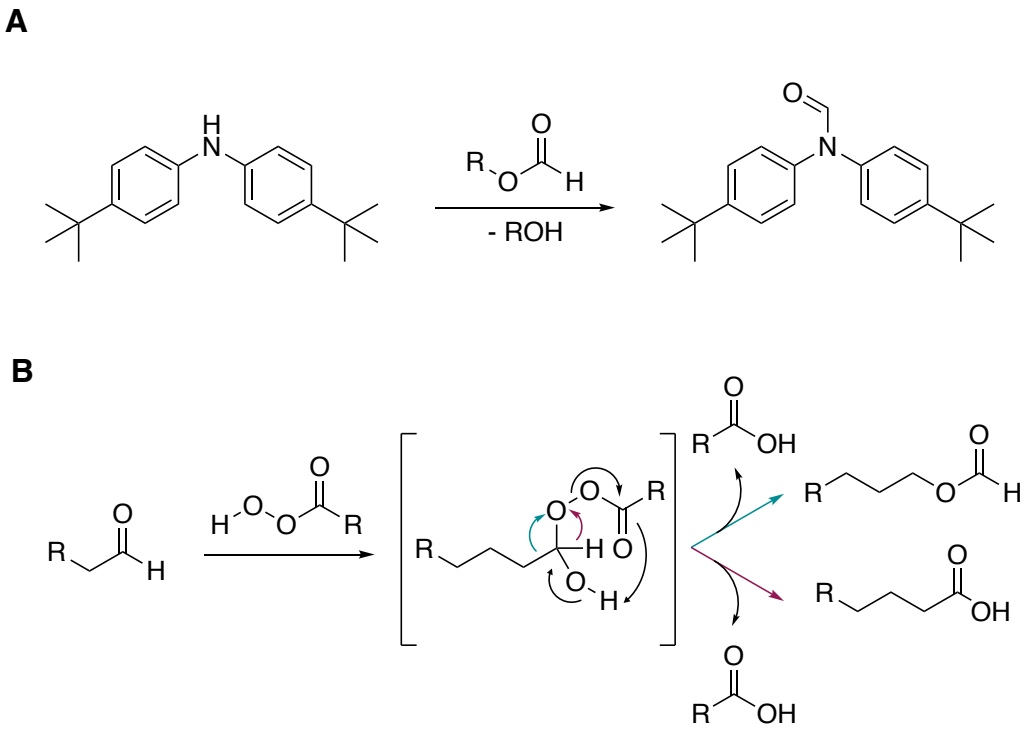

Scheme 2.9 – (A) Formation of *N*-formyl-di-t-butyl-DPA from reaction of di-t-butyl-DPA with a formate ester. **(B)** Competing formation of formate ester and acid derivatives from a B-V oxidation of an aldehyde.

2.2 – Results

2.2.1 – Formylation of tBu_2-DPA with n-Hexadecyl Formate

To confirm that a formate ester could serve as the source of a formyl group to produce the *N*-formyl ADPAs observed in ADPA-inhibited autoxidations, *n*-hexadecyl formate (**1**) was prepared as in **Scheme 2.10-1** and incubated with one equivalent of tBu_2DPA under N_2 in decane at 165 °C to simulate a high-temperature autoxidation.[3,25,29,44] To our initial dismay, no reaction occurred. However, when the reaction was carried out in the presence of palmitic acid

(5 mM), one of the acids that is known to be formed during the *n*-hexadecane autoxidation, the reaction was successful, yielding 58% of the *N*-formylated tBu_2DPA (**2**) (**Scheme 2.10-2**).

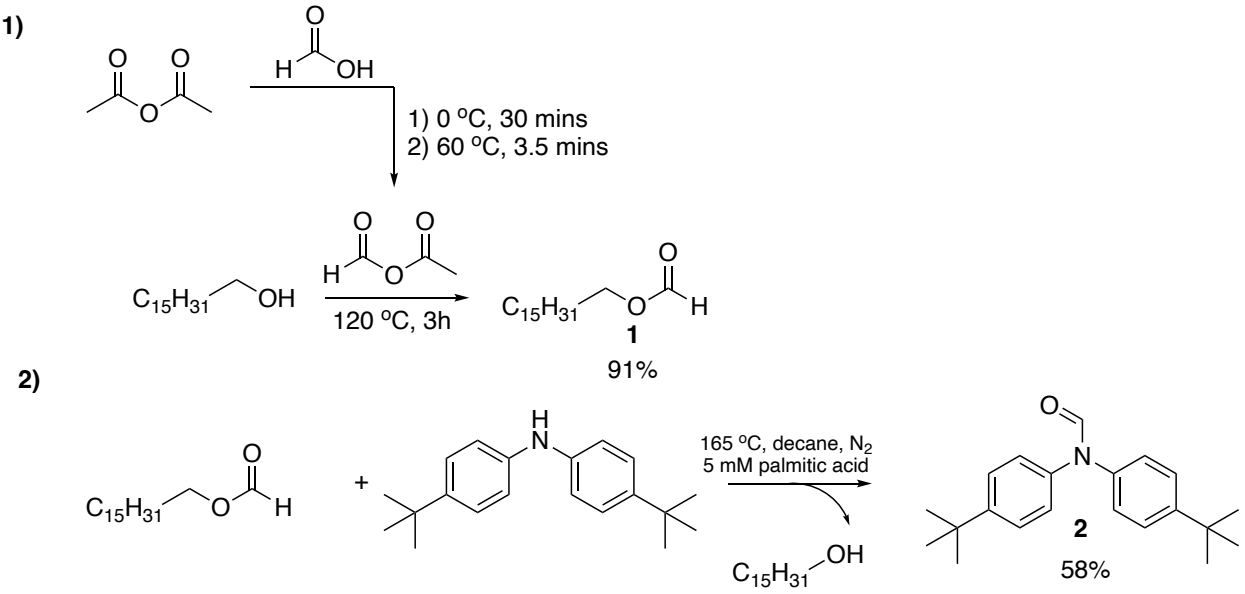

Scheme 2.10 – (1) The synthesis of *n*-hexadecyl formate (**1**) from dodecanol and a mixed anhydride. **(2)** The subsequent preparative reaction of hexadecyl formate with 4,4'-di-*tert*-butyldiphenylamine to form *N*-formyl-4,4'-di-*tert*-butyldiphenylamine (**2**).

2.2.2 – Phenyl-Propionaldehyde to Phenyl-Propionformate Ester Under B-V Conditions

To confirm that we could form formate esters from aldehydes and *m*-CPBA analogous to Kazmaier et al.'s results[37], we purified *m*-CPBA as stated in the paper, washing 30 g of *m*-CPBA (dissolved in 200 mL of diethyl ether) thrice with 150 mL of pH 7.5 $NaOH/KH_2PO_4$ buffer solution. The purified *m*-CPBA was then reacted with phenyl-propionaldehyde (**Scheme 2.13**). Using Kazmaier's optimized conditions we were able to reproduce their results, observing exclusive formation of the formate ester (**Figure 2.5**). If acid were formed, we would expect to see a quadruplet at δ 3.76, which is not present. However, the quadruplet at δ 6.00 ppm

(methine), doublet at 1.59 ppm (methyl) and singlet at 8.08 ppm (aldehyde) are all present and correspond to the formate product as reported by Kazmaier et al.[37]

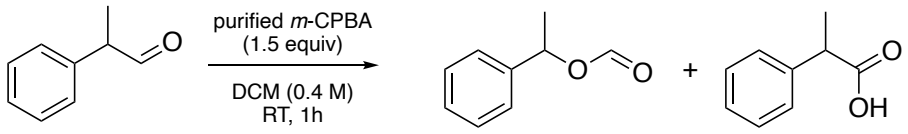

Scheme 2.11 – Formation of proprionformate from proprionaldehyde under B-V conditions.

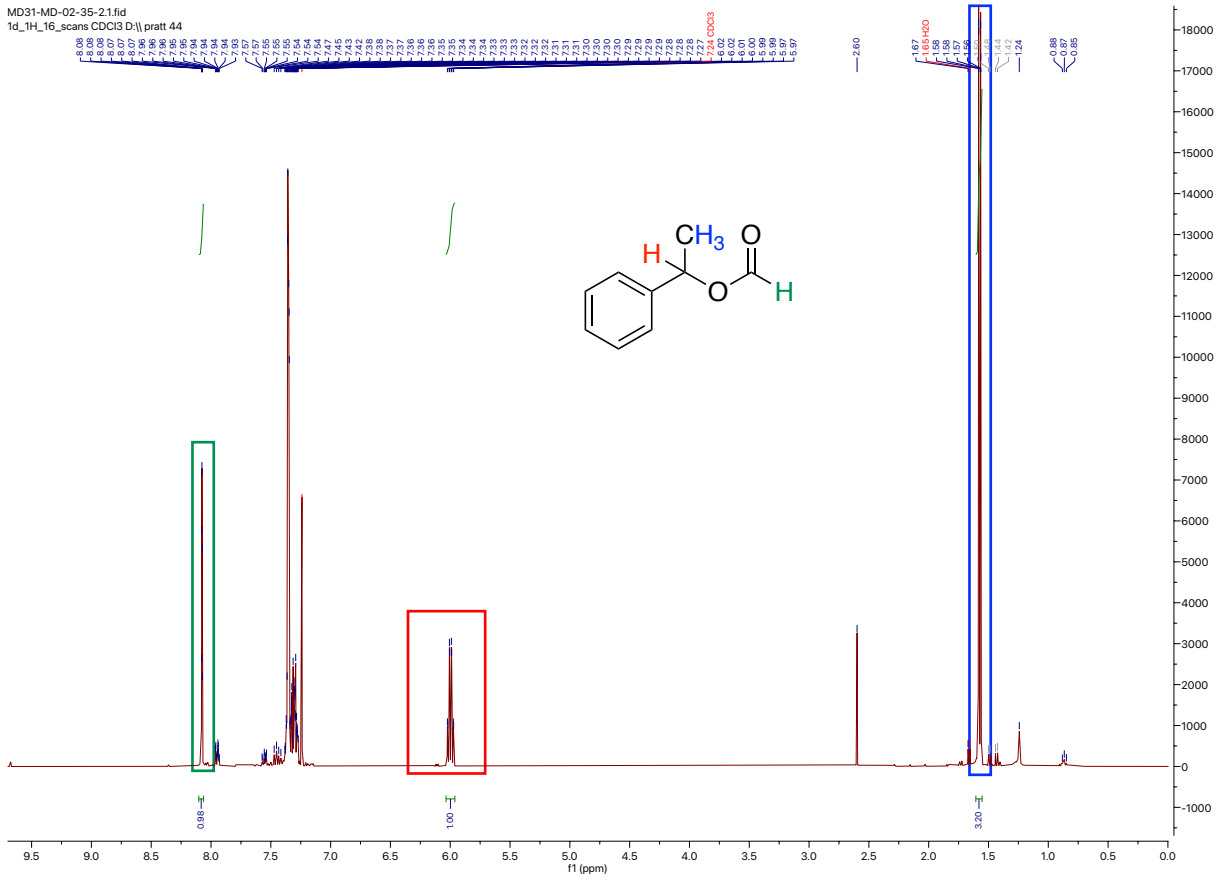

Figure 2.1 – ^{1}H NMR spectrum of proprionformate generated from proprionaldehyde under classical B-V conditions. With the aldehyde proton, sec-proton, and methyl protons highlighted.

2.2.3 – B-V Oxidation of Hexadecanal at Various Temperatures

Products arising from the reaction of *n*-hexadecanal with m-CPBA were investigated next. Thus, *n*-hexadecanal, prepared by oxidation of 1-hexadecanol with oxalyl chloride (**Scheme 2.11**), was reacted with purified *m*-CPBA in dichloroethane at each of room temperature, 40 °C, 60 °C and 80 °C. Dichloroethane was chosen as it is similar to Kazmaier's

conditions using DCM, except it can be used at temperatures greater than 39 °C. The 80 °C maximum was chosen as the limit in these experiments for safety reasons as using peracids at elevated temperatures can be hazardous. Each reaction was performed in the same manner, with 1 mmol of *n*-hexadecanal in DCE (0.4 M) and purified *m*-CPBA (1.5 equiv) in a round bottom flask (reaction scheme in **Scheme 2.12**) placed behind a blast shield for safety when ≥ 40 °C. Interestingly, both formate ester and carboxylic acid were observed under all experimental conditions.

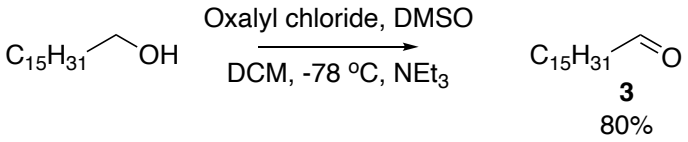

Scheme 2.12 – Synthesis of hexadecanal (**3**) from hexadecanol via Swern oxidation.

Product ratios were determined by integrating a peak unique to each product in a crude NMR spectrum so that no material was lost upon workup. For the formate ester, the triplet corresponding to the methylene adjacent to the oxygen atom (δ ~4.14 ppm) was selected, while for the carboxylic acid, the methylene next to the carbonyl (δ ~2.36 ppm) was used. Since they correspond to the same number of hydrogens, the integrations can be used directly to determine the product ratios. The product ratios determined in this way were [formate]:[acid] = 1:20.3, 1:11.1, 1:9.3 and 1:10.0 at 20, 40, 60 and 80 °C, respectively (**Figures 2.1-2.4**).

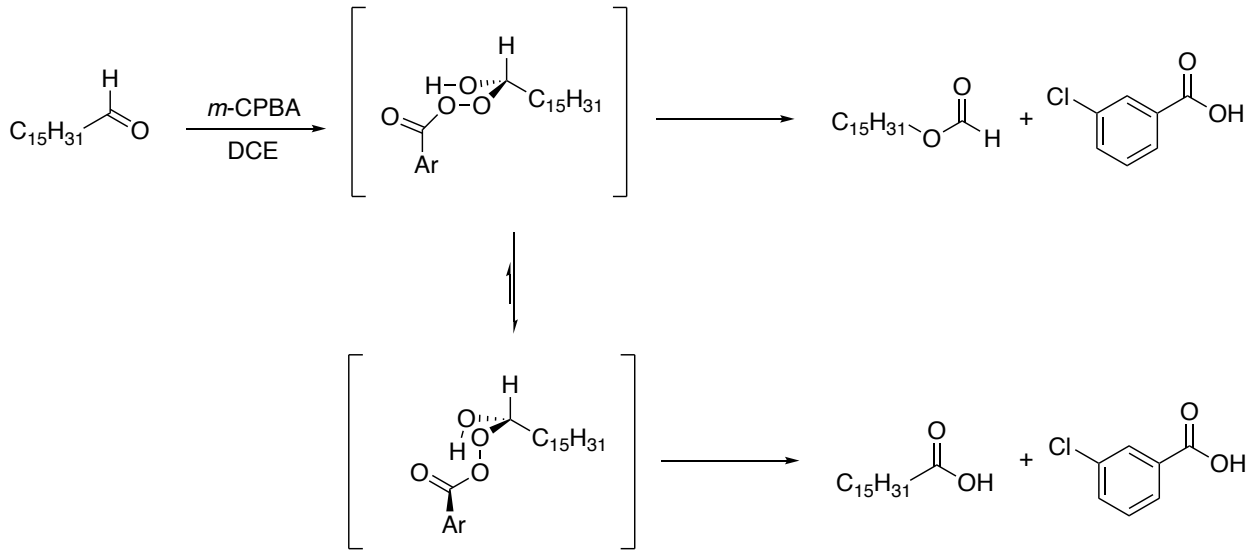

Scheme 2.13 – Criegee intermediates where the group antiperiplanar to the peroxide bond migrates which is dependent on conformation of the 7-memebered chair-like intermediate.

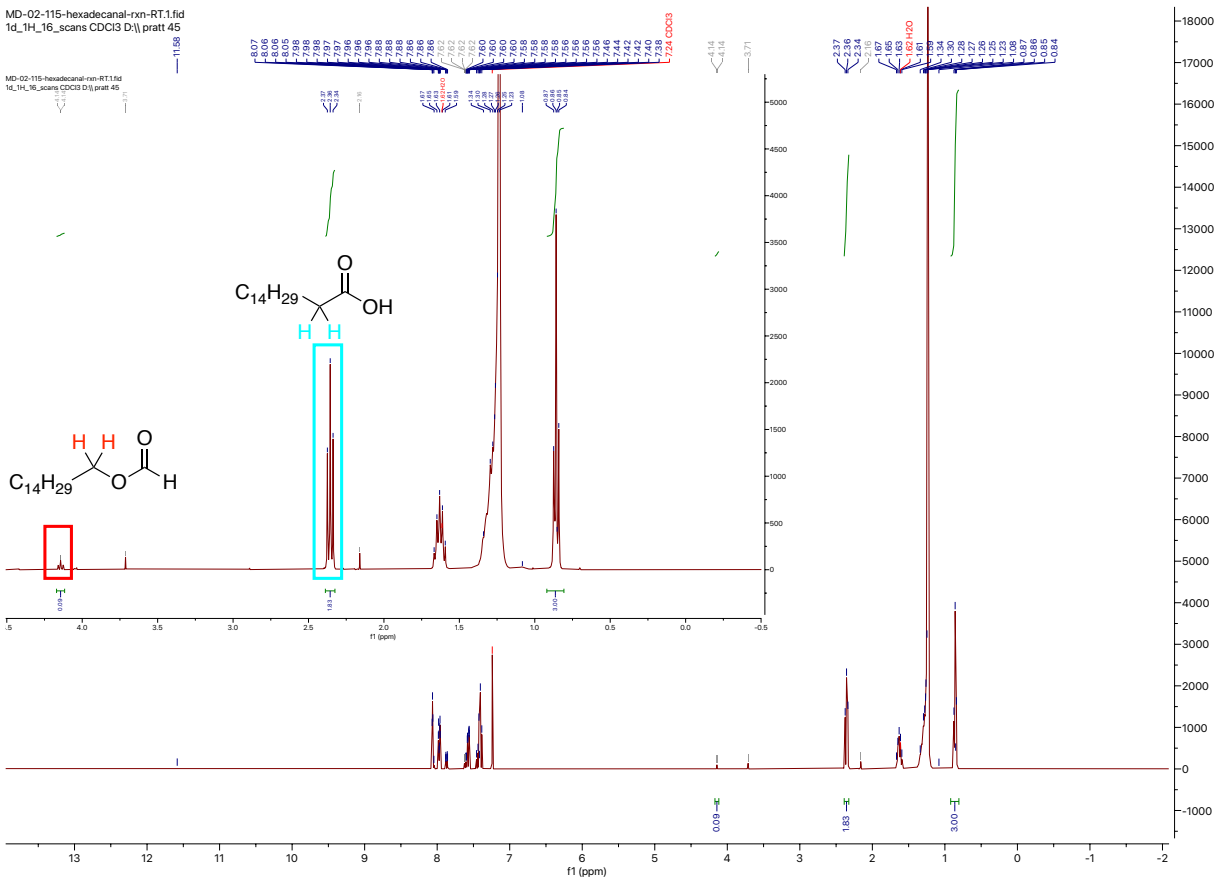

Figure 2.2 – ^{1}H NMR spectrum of the product mixture arising from the oxidation of *n*-hexadecanal with purified *m*-CPBA in CH_2Cl_2 at 20°C. Inset: Expansion of the region of interest, highlighting the distinct methylene peaks of the formate (δ ~ 4.14) and acid (δ ~ 2.36) products and the corresponding peak integrals for determination of the product ratios and mass balance.

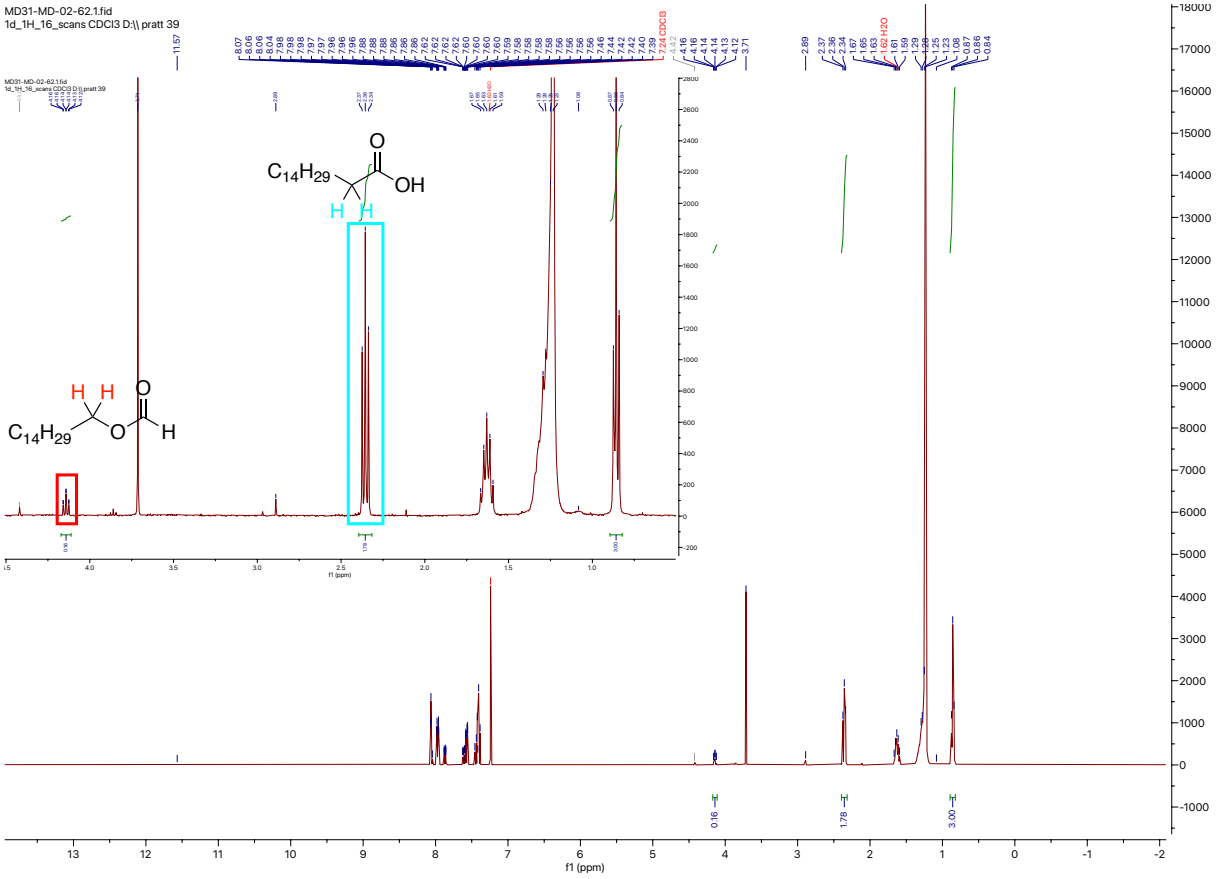

Figure 2.3 – ^{1}H NMR spectrum of the product mixture arising from the oxidation of n-hexadecanal with purified m-CPBA in CH_2Cl_2 at 40°C. Inset: Expansion of the region of interest, highlighting the distinct methylene peaks of the formate (δ ~ 4.14) and acid (δ ~ 2.36) products and the corresponding peak integrals for determination of the product ratios and mass balance.

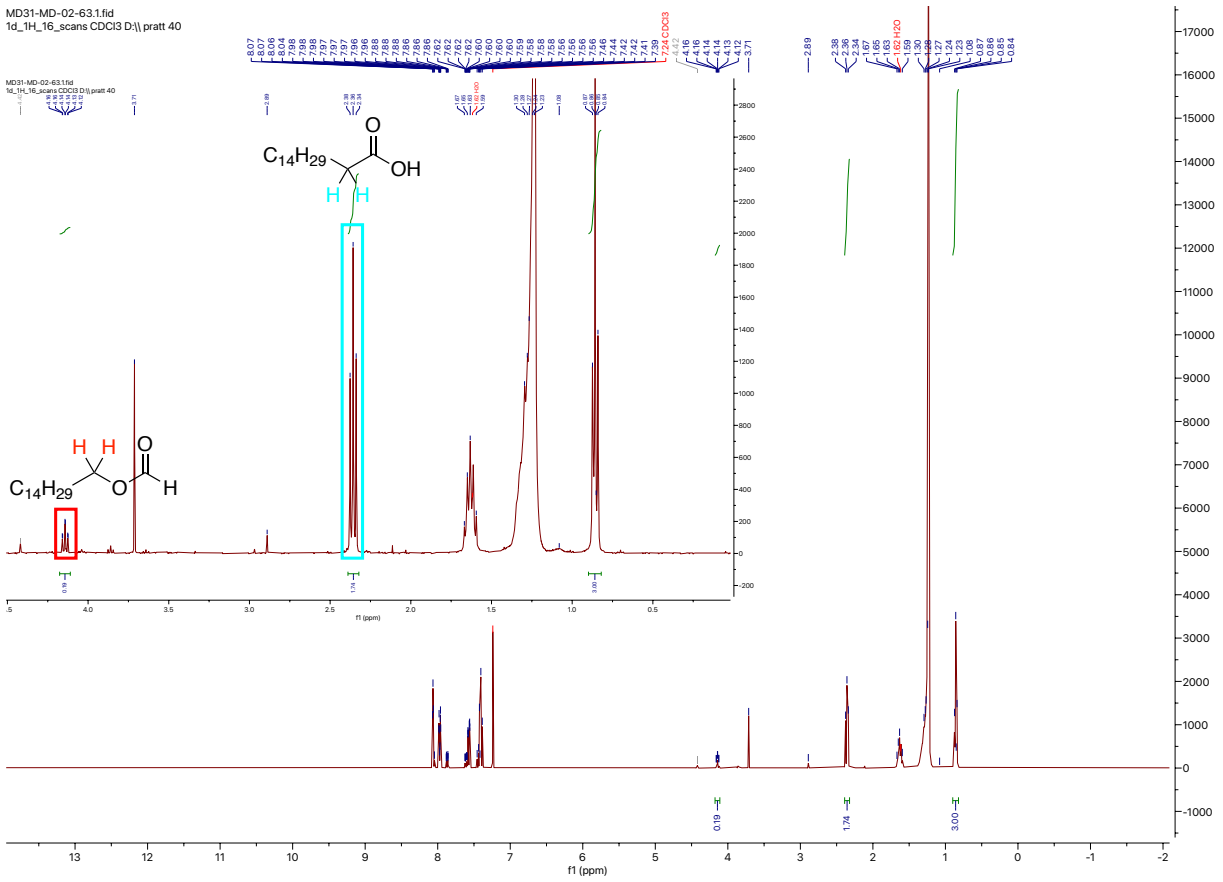

Figure 2.4 – ^{1}H NMR spectrum of the product mixture arising from the oxidation of *n*-hexadecanal with purified *m*-CPBA in CH_2Cl_2 at 60°C. Inset: Expansion of the region of interest, highlighting the distinct methylene peaks of the formate (δ ~ 4.14) and acid (δ ~ 2.36) products and the corresponding peak integrals for determination of the product ratios and mass balance.

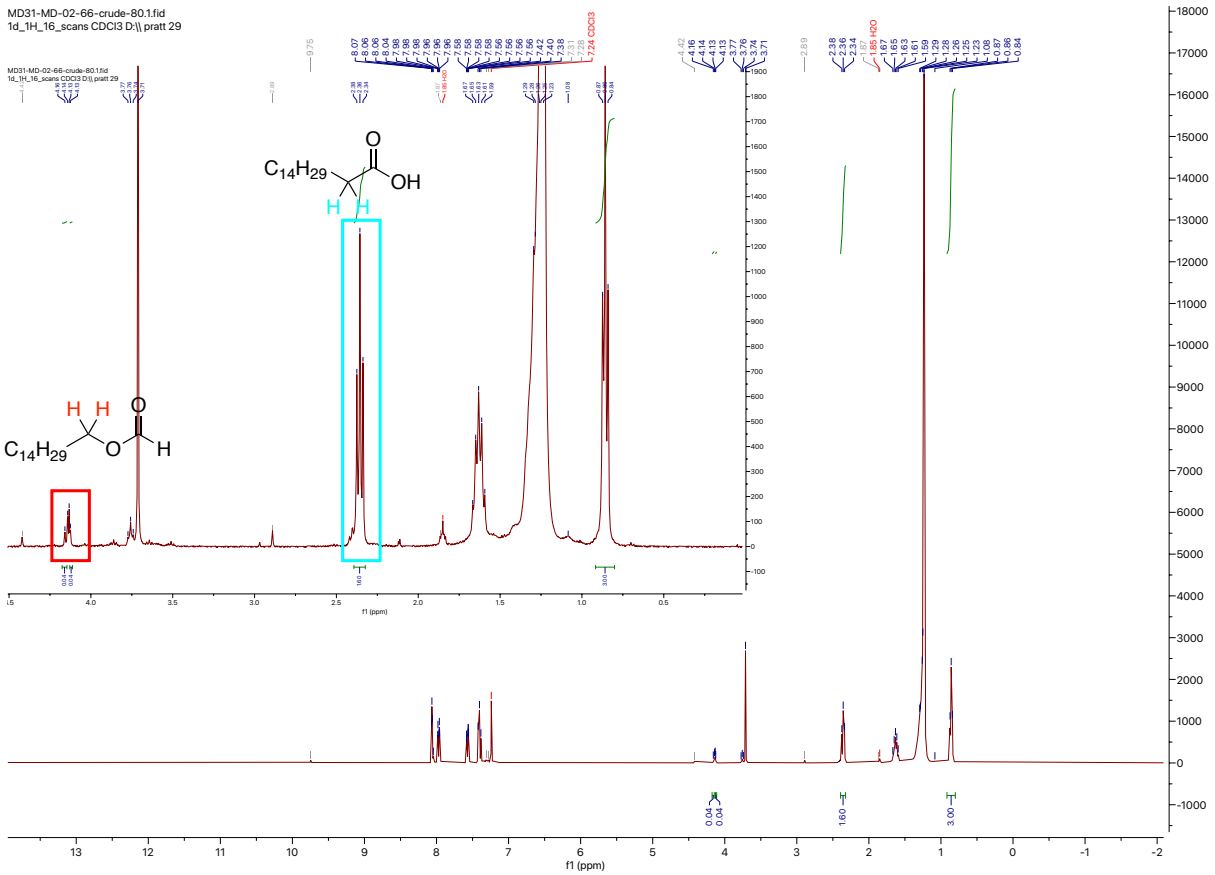

Figure 2.5 – ^{1}H NMR spectrum of the product mixture arising from the oxidation of n-hexadecanal with purified m-CPBA in CH_2Cl_2 at 80°C. Inset: Expansion of the region of interest, highlighting the distinct methylene peaks of the formate (δ ~ 4.14) and acid (δ ~ 2.36) products and the corresponding peak integrals for determination of the product ratios and mass balance.

2.2.4 – B-V Oxidations of Hexadecanal-*d* at Various Temperatures

To probe for a role for tunneling in the apparent universal preference for H migration in the B-V oxidation of aldehydes, hexadecanal-*d* (**5**) was prepared from commercial methyl palmitate using DIBAL-D (**Scheme 2.14**). Compound **5** was then subjected to the same B-V oxidation conditions as *n*-hexadecanal above yielding [formate]:[acid] product ratios of 1:15.1, 1:5.0, 1:4.4 and 1:2.3, affording KIEs of 1.34, 2.22, 2.11 and 4.35 at 20, 40, 60 and 80 °C, respectively (**Figures 2.6-2.9**). These data and the corresponding mass balances in the reactions are collected in **Table 2.1.**

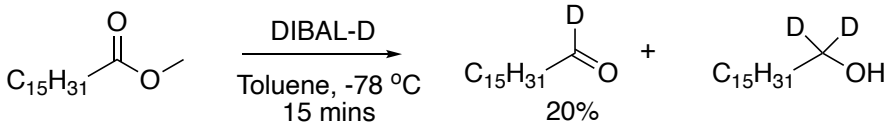

4 **5**

Scheme 2.14 – Synthesis of hexadecanal-*d* from methyl palmitate and hexadecanol-(CD_2).

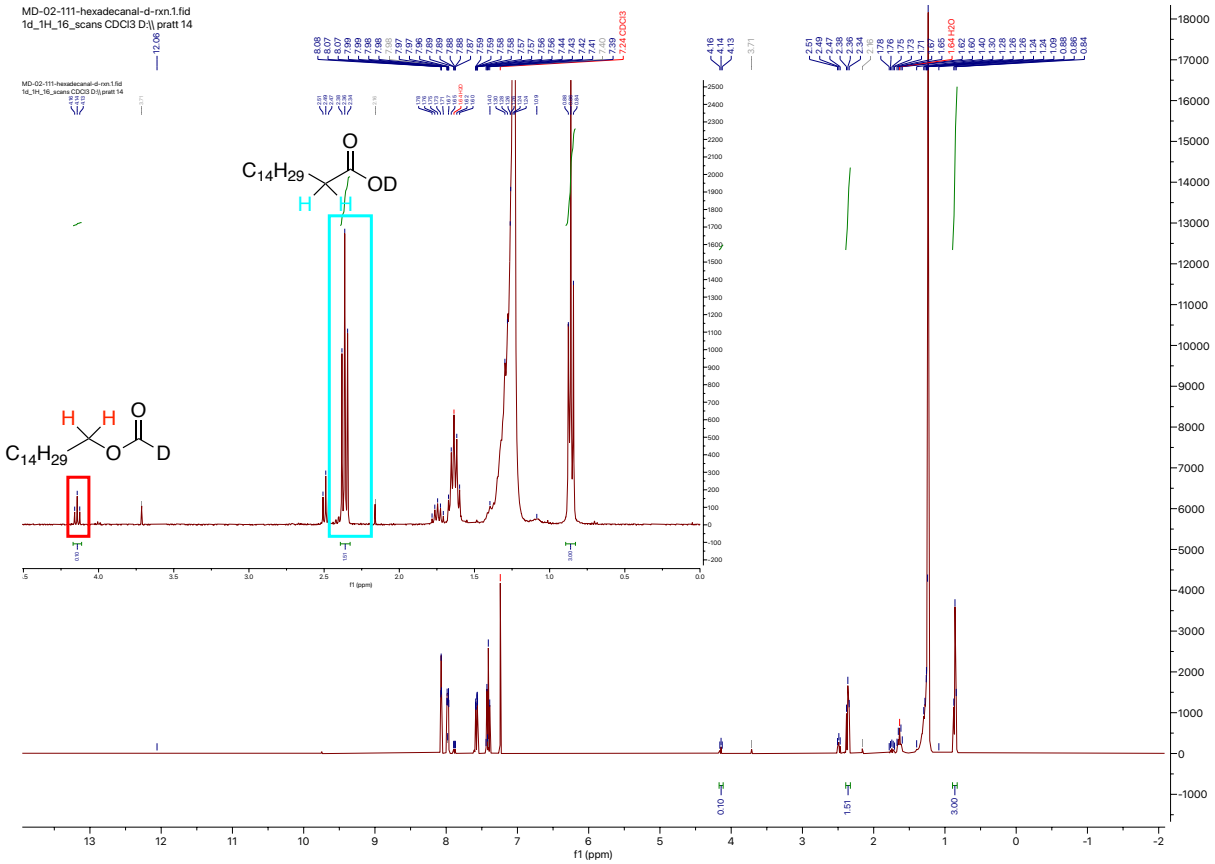

Figure 2.6 – ^{1}H NMR spectrum of the product mixture arising from the oxidation of n-hexadecanal-d with purified *m*-CPBA in CH_2Cl_2 at 20°C. Inset: Expansion of the region of interest, highlighting the distinct methylene peaks of the formate (δ ~ 4.14) and acid (δ ~ 2.36) products and the corresponding peak integrals for determination of the product ratios and mass balance.

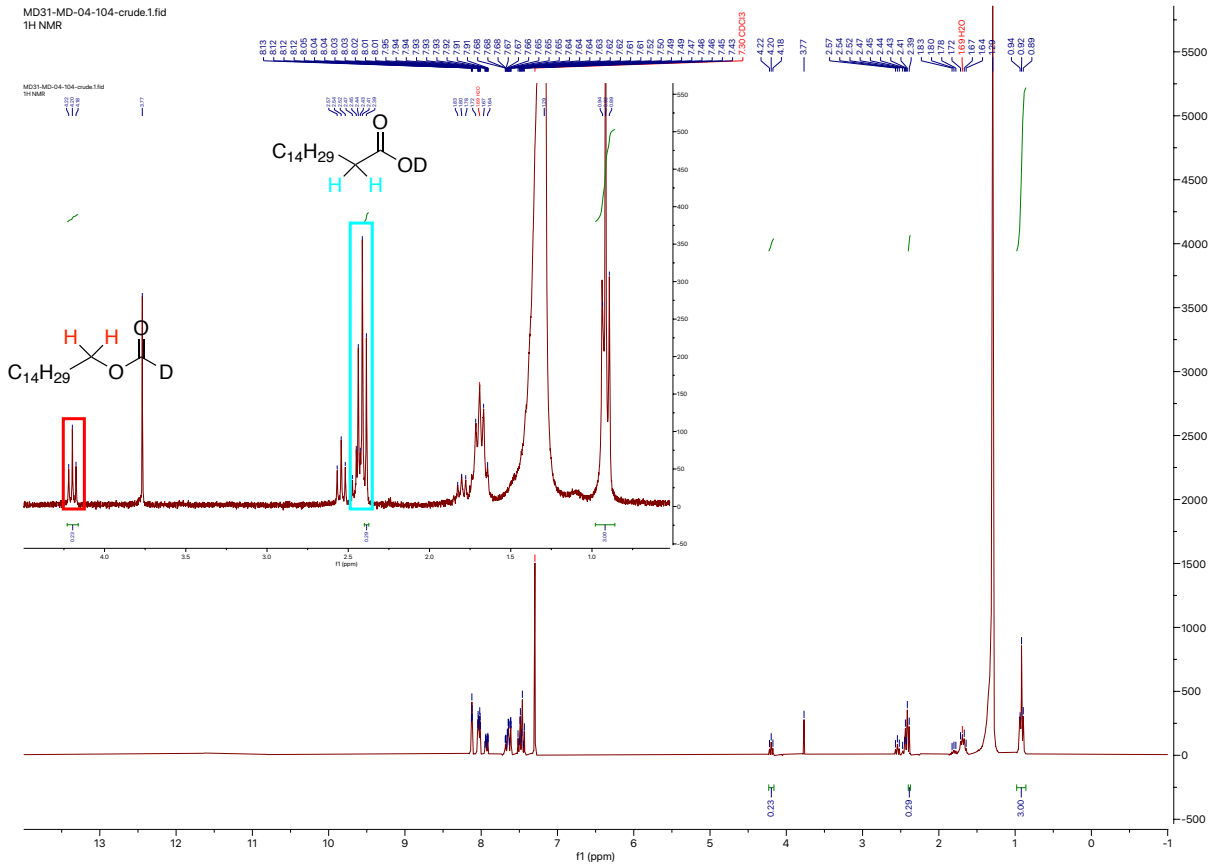

Figure 2.7 – ^{1}H NMR spectrum of the product mixture arising from the oxidation of n-hexadecanal-d with purified *m*-CPBA in CH_2Cl_2 at 40°C. Inset: Expansion of the region of interest, highlighting the distinct methylene peaks of the formate (δ ~ 4.14) and acid (δ ~ 2.36) products and the corresponding peak integrals for determination of the product ratios and mass balance.

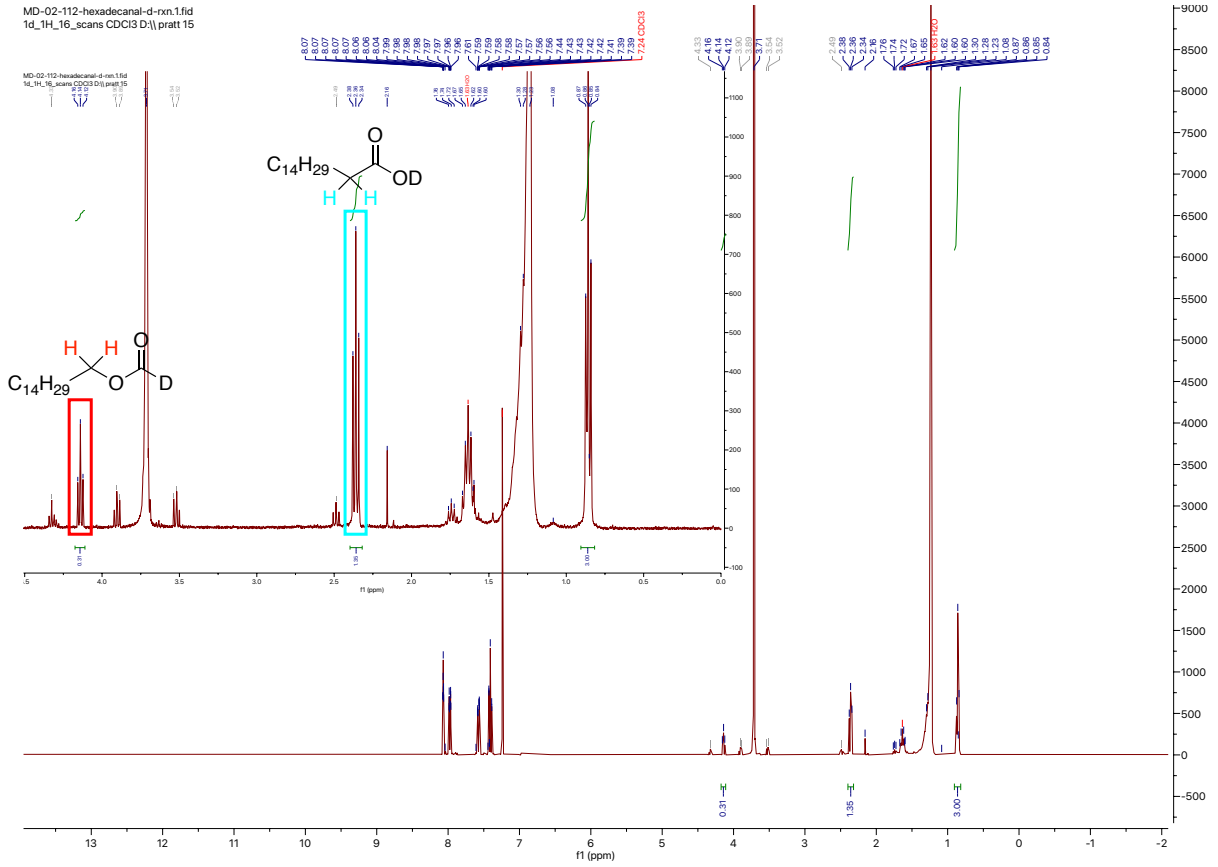

Figure 2.8 – ^{1}H NMR spectrum of the product mixture arising from the oxidation of n-hexadecanal-d with purified *m*-CPBA in CH_2Cl_2 at 60°C. Inset: Expansion of the region of interest, highlighting the distinct methylene peaks of the formate (δ ~ 4.14) and acid (δ ~ 2.36) products and the corresponding peak integrals for determination of the product ratios and mass balance.

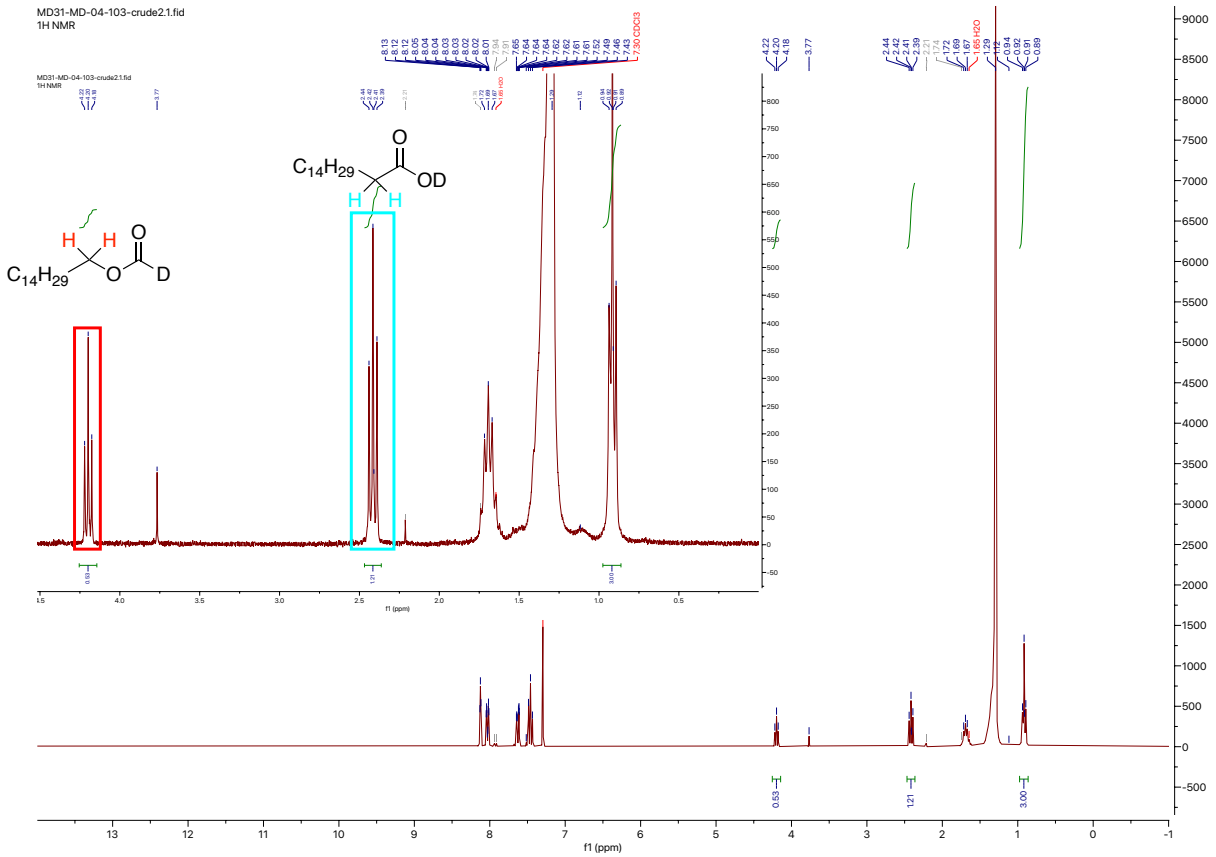

Figure 2.9 – ^{1}H NMR spectrum of the product mixture arising from the oxidation of n-hexadecanal-d with purified *m*-CPBA in CH_2Cl_2 at 40°C. Inset: Expansion of the region of interest, highlighting the distinct methylene peaks of the formate (δ ~ 4.14) and acid (δ ~ 2.36) products and the corresponding peak integrals for determination of the product ratios and mass balance.

Table 2.1 – Summary of ratios of formate ester to carboxylic acid products obtained from the oxidation of hexadecanal and hexadecanal-*d* with *m*-CPBA in CH_2Cl_2, associated mass balances and calculated kinetic isotope effects as a function of temperature.

Temperature (°C)	[Formate]: [Acid] (hexadecanal)	[Formate]: [Acid] (hexadecanal-*d*)	KIE for hexadecanal oxidation	Mass Balance (hexadecanal)	Mass Balance (hexadecanal-*d*)
20 °C	1:20.3	1:15.1	1.34	96%	80.5%
40 °C	1:11.1	1:5.0	2.22	97%	69.5%
60 °C	1:9.3	1:4.4	2.11	97.5%	83%
80 °C	1:10.0	1:2.3	4.35	82%	87%

2.2.5 – Computational Study of a Model B-V Oxidation

To aid in rationalizing our experimental observations, computations were carried out to investigate the fates of the two competing pathways of the peroxyacetal intermediate derived from a model aliphatic peracid (pervaleric acid) and a model aliphatic aldehyde (pentanal).

All geometry optimizations of reactants, products, and transitions states were carried out using the MN15 density functional along with the CBSB7+ basis set and the D3 version of Grimme's dispersion corrections with the Gaussian 16 suite of programs.[45–48] Convergence criteria were defined with Opt = Tight and solvent effects on stationary points were estimated for both *n*-hexadecane and DCE using the CPCM approach.[49] Computed structures of the chair-like intermediates and transition states for both pathways are shown in **Figures 2.10** & **2.11**.

At 25 °C, the difference in the computed TS free energies leading to the formate and acid products were −3.19, −2.29 and −1.42 kcal/mol in the gas phase, hexadecane and DCE, respectively (**Figures 2.12, 2.14 and 2.16**, respectively). The latter is in remarkably good agreement with the $\Delta\Delta G^{\ddagger}$ estimated based upon the product ratio observed in our experiments (−1.7 kcal/mol). We also computed the energy surface at 80 °C, and found marginally smaller differences in the computed TS free energies leading to the formate and acid products of −3.14, −2.23 and −1.35 kcal/mol in the gas phase, hexadecane and DCE, respectively (**Figures 2.13, 2.15 and 2.17**, respectively) – again consistent with the marginal increase in formate product

formed relative to acid in our experiments at this temperature, which corresponds to $\Delta\Delta G^{\ddagger}$ = -1.54 kcal/mol. These results are summarized in **Table 2.2**.

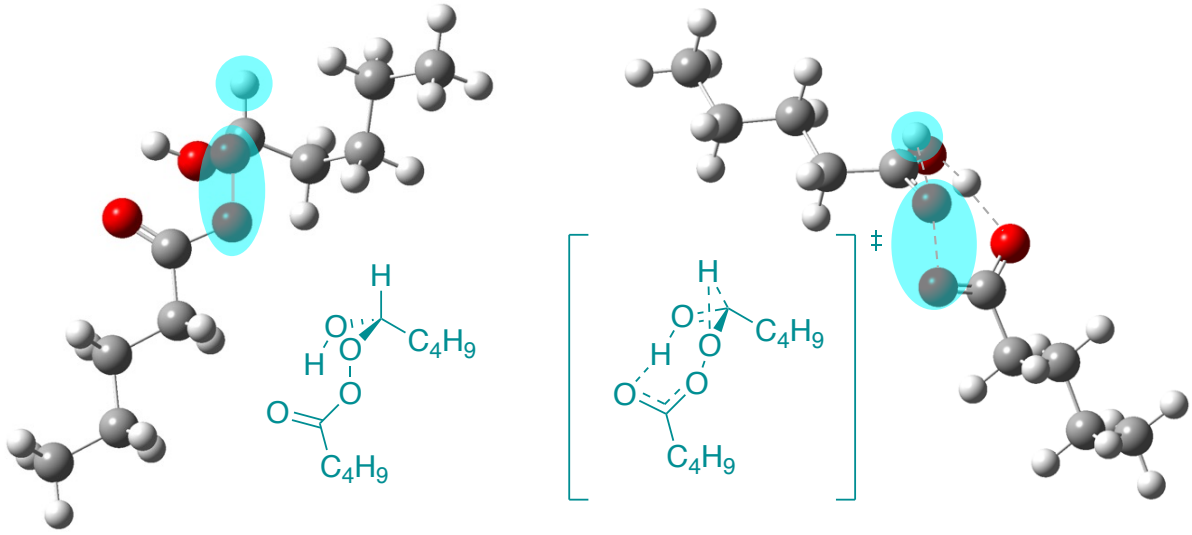

Figure 2.11 – Computed structures of the peroxyacetal conformer wherein the H and peroxide moiety are anti-periplanar and corresponding transition state for H-atom migration and formation of the carboxylic acid product.

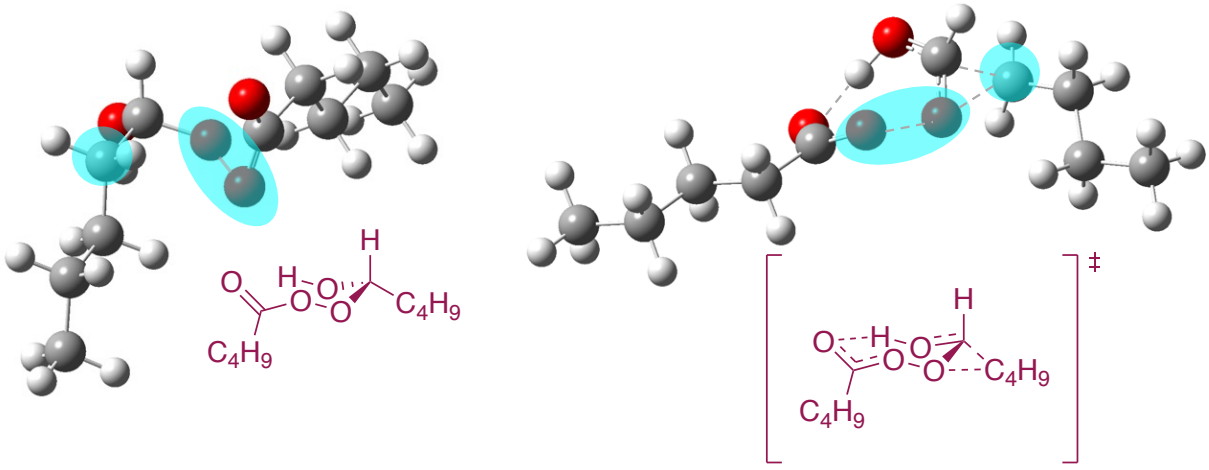

Figure 2.10 – Computed structures of the peroxyacetal conformer wherein the alkyl group and peroxide moiety are anti-periplanar and corresponding transition state for alkyl group migration and formation of the formate ester product.

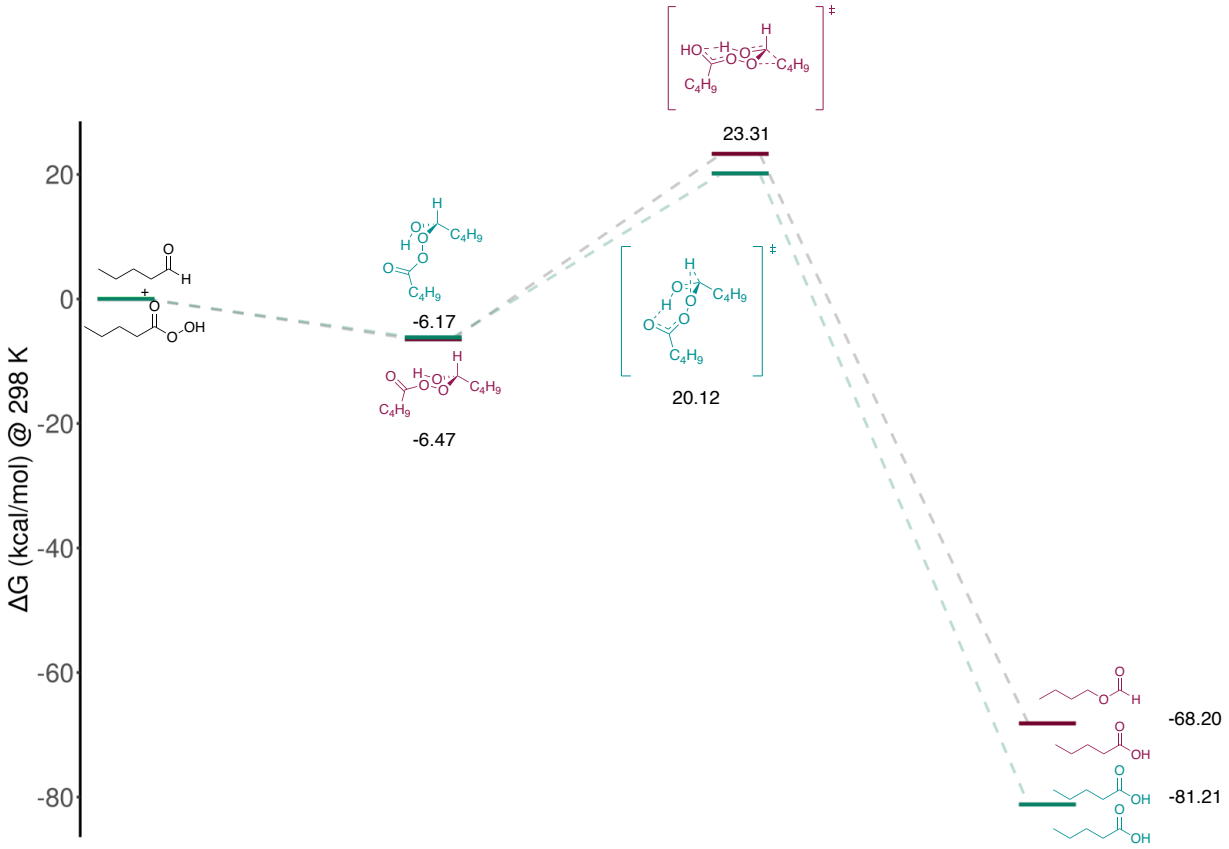

Figure 2.12 – Reaction coordinate diagram computed by MN15(D3)/CBSB7+ for the reaction of pentanal with pervaleric acid in the gas phase at 25 °C. The pathway leading to formate formation is in maroon, while the pathway leading to two acid products is in teal.

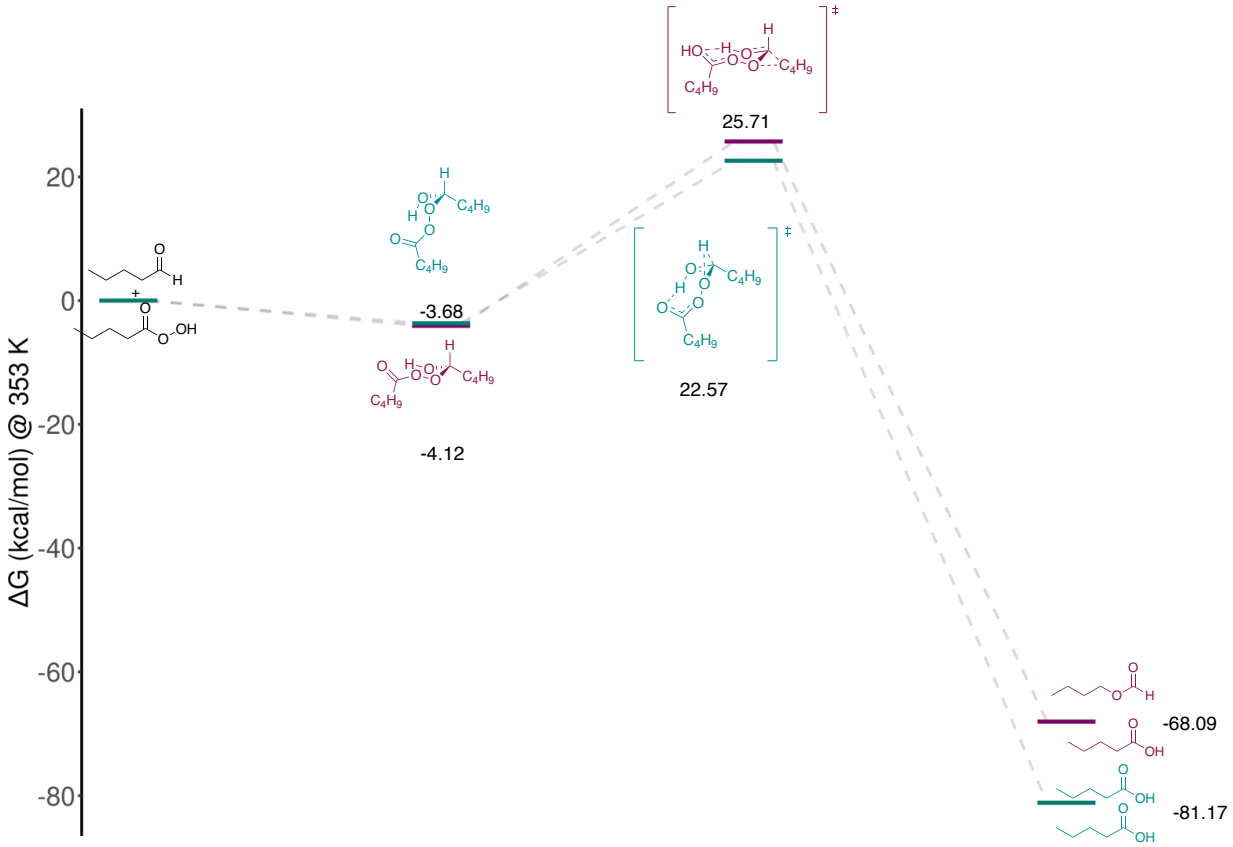

Figure 2.13 – Reaction coordinate diagram computed by MN15(D3)/CBSB7+ for the reaction of pentanal with pervaleric acid in the gas-phase at 80 °C. The pathway leading to formate formation is in maroon, while the pathway leading to two acid products is in teal.

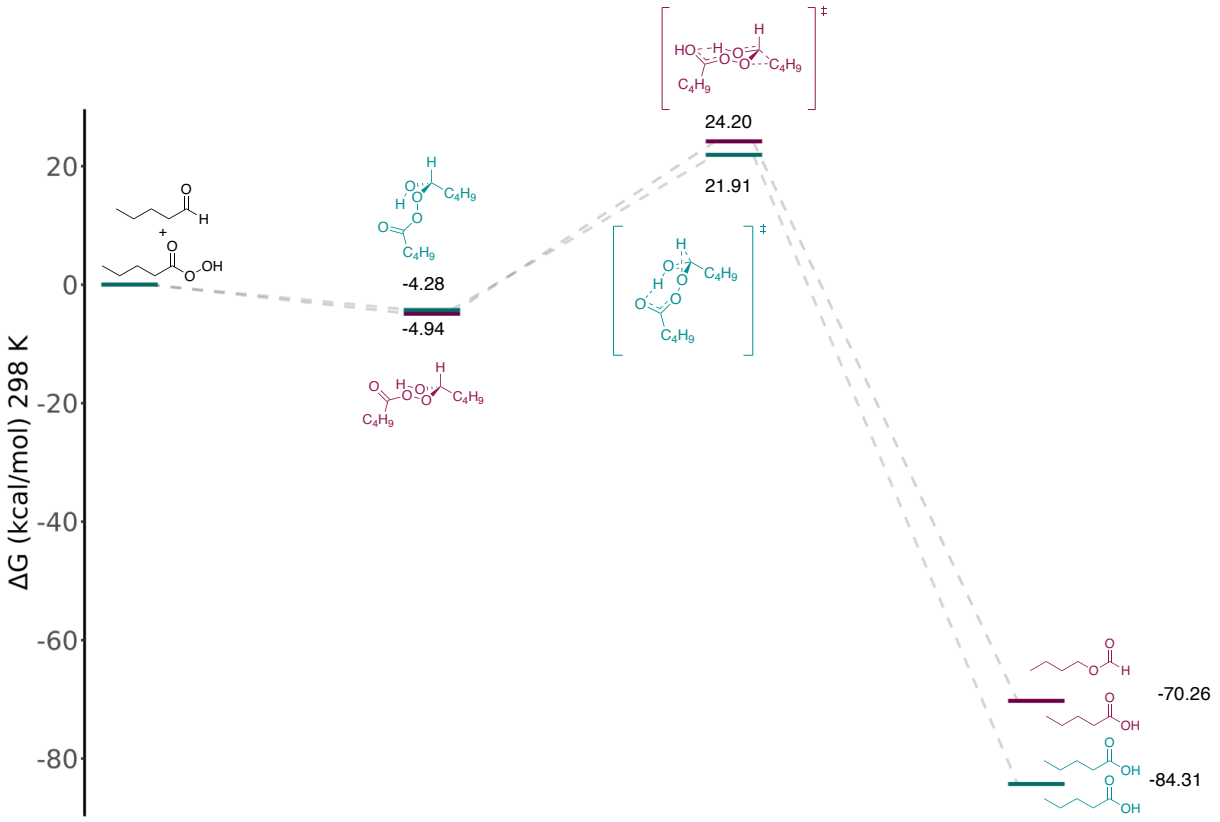

Figure 2.14 – Reaction coordinate diagram computed by MN15(D3)/CBSB7+ for the reaction of pentanal with pervaleric acid in n-hexadecane at 25 °C. The pathway leading to formate formation is in maroon, while the pathway leading to two acid products is in teal.

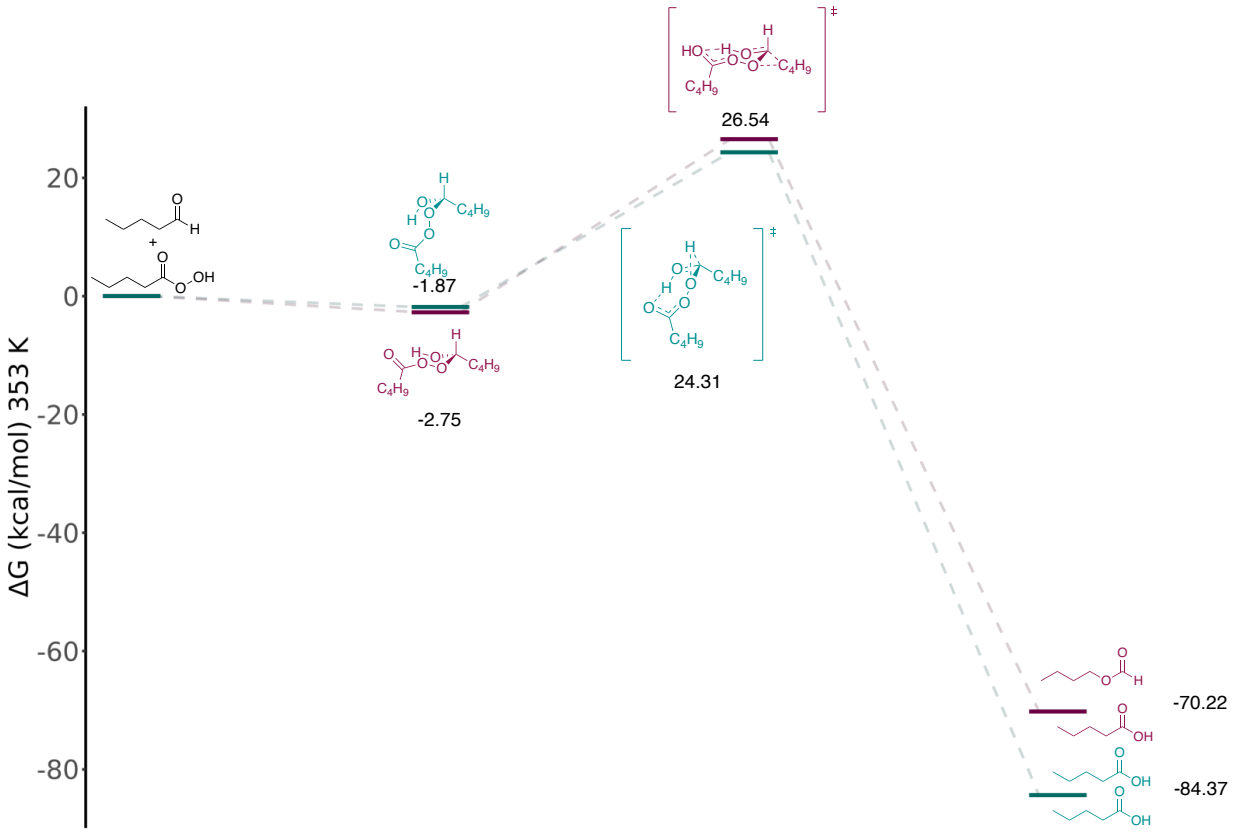

Figure 2.15 – Reaction coordinate diagram computed by MN15(D3)/CBSB7+ for the reaction of pentanal with pervaleric acid in n-hexadecane at 80 °C. The pathway leading to formate formation is in maroon, while the pathway leading to two acid products is in teal.

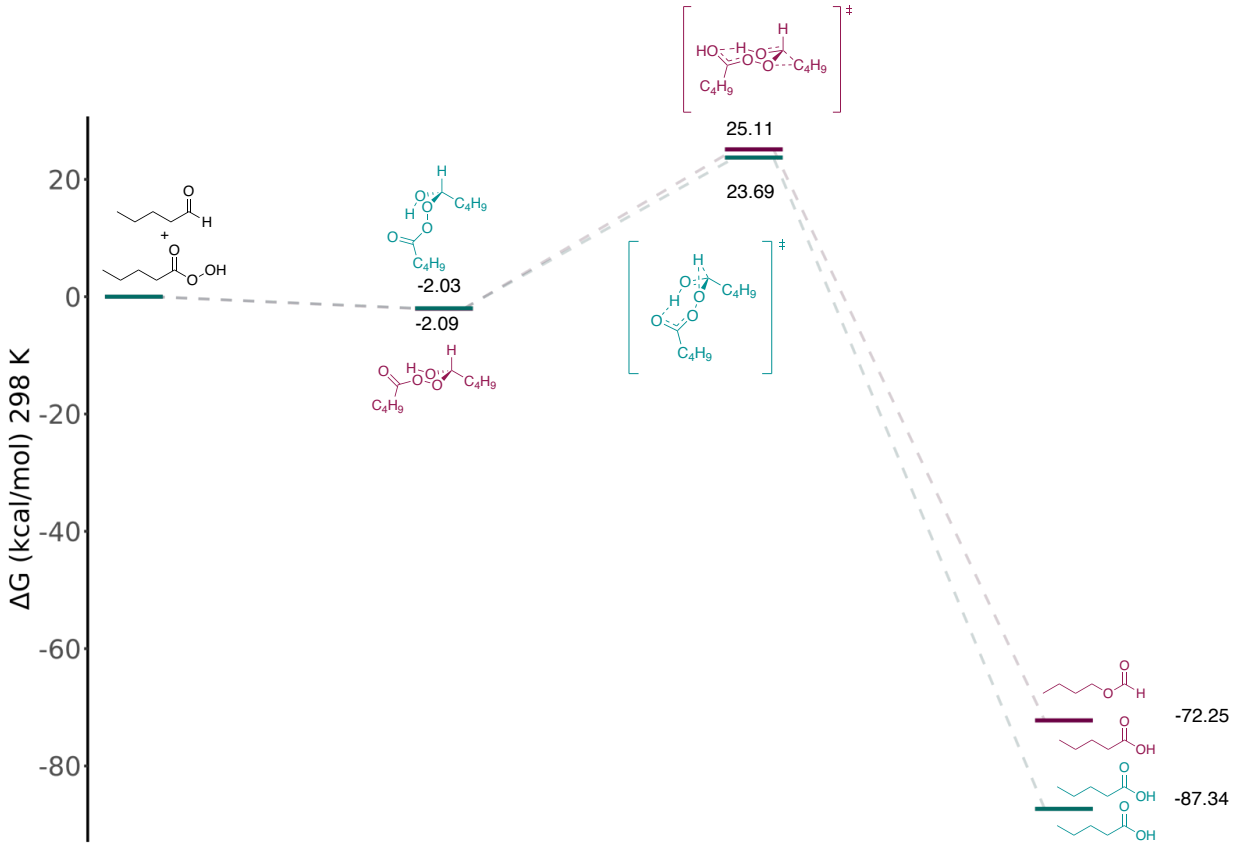

Figure 2.16 – Reaction coordinate diagram computed by MN15(D3)/CBSB7+ for the reaction of pentanal with pervaleric acid in DCE at 25 °C. The pathway leading to formate formation is in maroon, while the pathway leading to two acid products is in teal.

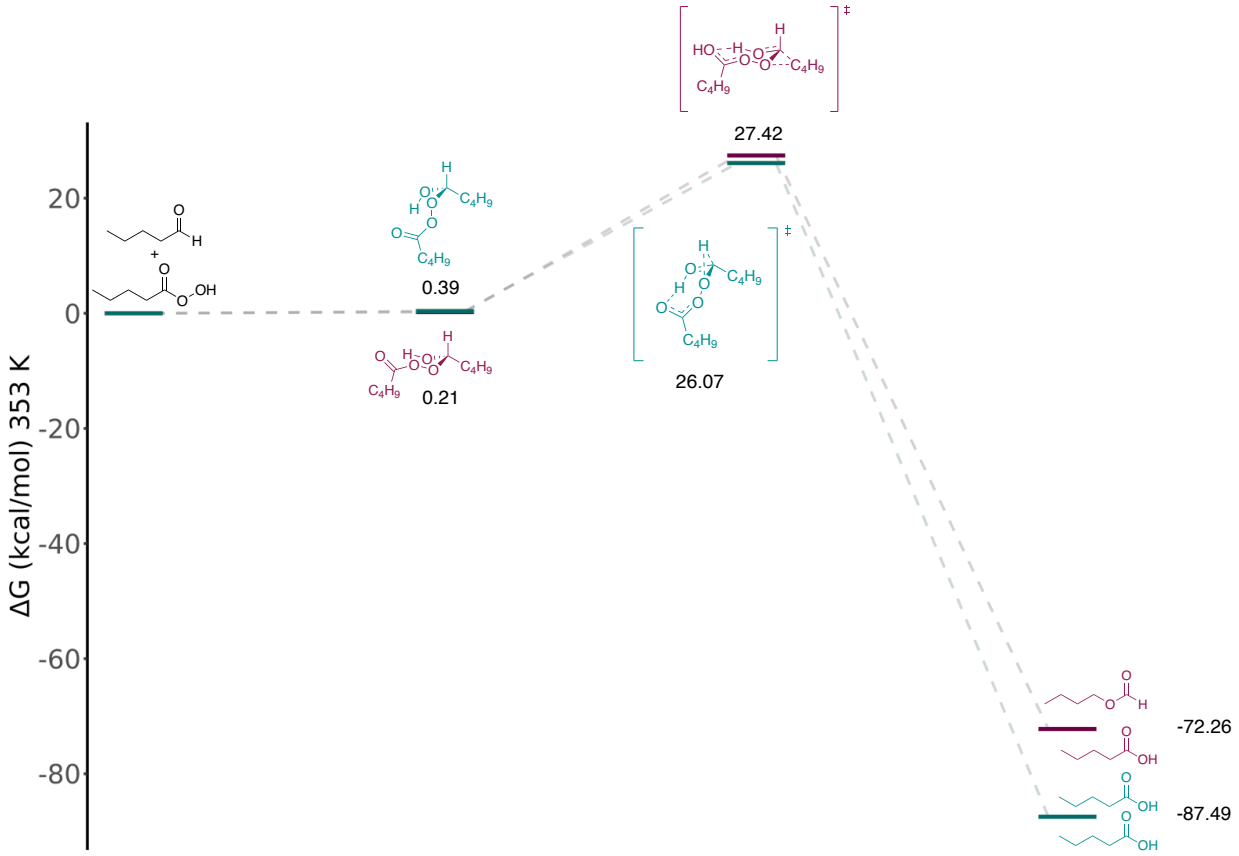

Figure 2.17 – Reaction coordinate diagram computed by MN15(D3)/CBSB7+ for the reaction of pentanal with pervaleric acid in DCE at 80 °C. The pathway leading to formate formation is in maroon, while the pathway leading to two acid products is in teal.

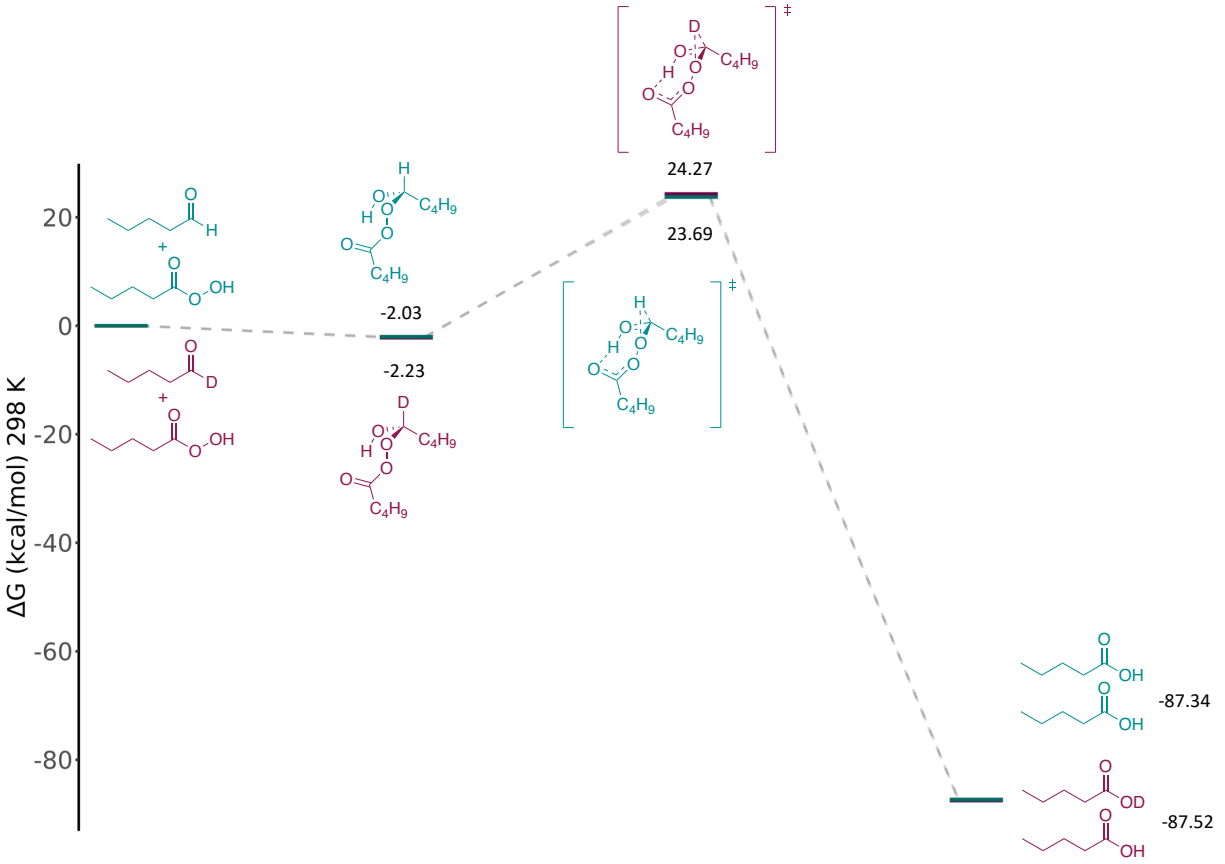

Figure 2.18 – Reaction coordinate diagram computed by MN15(D3)/CBSB7+ for the reaction of pentanal-d with pervaleric acid in DCE at 25 °C. The pathway leading to formate formation is in maroon, while the pathway leading to two acid products is in teal.

Table 2.2 – Summary of the $\Delta\Delta G^{\ddagger}$ leading to the formate and ester products of B-V oxidation of indicated aldehydes using indicated peracids.

Conditions	Solvent	Temperature (°C)	Exp or Comp	$\Delta\Delta G^{\ddagger}$ (kcal/mol)
Hexadecanal with *m*-CPBA	DCE	20	Exp	-1.70
Hexadecanal with *m*-CPBA	DCE	40	Exp	-1.43
Hexadecanal with *m*-CPBA	DCE	60	Exp	-1.41
Hexadecanal with *m*-CPBA	DCE	80	Exp	-1.54
Pentanal with pervaleric acid	DCE	25	Comp	-1.42

Pentanal with pervaleric acid	DCE	80	Comp	-1.35
Pentanal with pervaleric acid	Hexadecane	25	Comp	-2.29
Pentanal with pervaleric acid	Hexadecane	80	Comp	-2.23
Pentanal with pervaleric acid	Gas Phase	25	Comp	-3.19
Pentanal with pervaleric acid	Gas Phase	80	Comp	-3.14

2.3 – Discussion

Based on previous evidence that *N*-formyl ADPAs are one of the major products formed in ADPA inhibited autoxidations, we hypothesized that peracids and aldehydes which are formed in an autoxidation can react to form a formate ester which can formylate the diarylamine. Indeed, treating tBu_2DPA with a formate ester in the presence of a carboxylic acid (as a catalyst), yields the corresponding *N*-formyl tBu_2DPA. However, given the lack of precedent for the formation of formate esters from *n*-alkanals in B-V oxidations, we sought to determine the extent to which, if any, formate esters form. When *n*-hexadecanal was treated with *m*-CPBA in DCE at 20°C, formate ester forms in less than a 5:95 ratio with the acid derivative. However, as the temperature was increased to 80 °C, the product ratio more than doubled to 11:89. Extrapolating this trend to 165 °C as in our model experiments, the formate ester is likely to comprise an even larger fraction of the products. Looking at the reaction from the classical lens of migratory aptitudes, 1° alkyl chains are the least likely to migrate in a B-V oxidation compared to its 2° and 3° alkyl and aryl counterparts. Due to the poor migratory aptitude of the linear alkyl chains, the formate product is unlikely to form in higher quantities than the acids generated. What is likely to occur is the product ratios to become much closer,

potentially moving towards a 1:1 ratio as temperature is the difference in barrier heights is minimized. Although the mechanism by which these products form has been extensively studied, trends in the migratory aptitudes remain unclear – for example, the preference for H migration over alkyl migration. Given that tunneling may contribute to this preference, and seeking to maximize the formation of formate product (which arises due to the preference for alkyl migration over H migration in our reactions) we synthesized hexadecanal-d to see if a substantial KIE was observed.

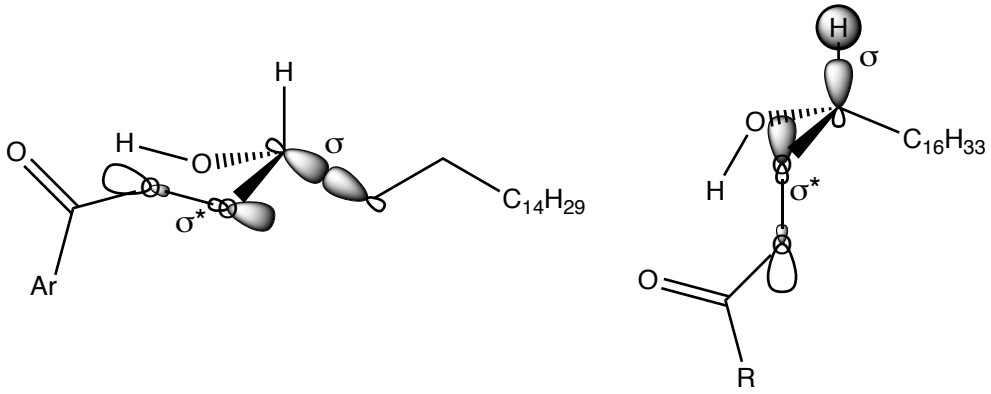

Figure 2.19 – Chair conformations of the two intermediates required for the respective alkyl and H-atom migrations. Shown are the sigma-orbitals of the migratory groups and of the peroxy-chair highlighting the alignment of each required for the respective migrations to occur. The left chair conformation demonstrates the alignment required for alkyl migration, while the right chair is the conformation required for H-atom migration.

The magnitude of the KIE derived from these experiments are consistent with a classical primary KIE and imply no significant contribution of quantum mechanical tunneling. Interestingly, the KIE was found to increase with an increase in temperature (KIE = 1.34 at 20 °C, 2.22 at 40 °C, 2.11 at 60 °C and 4.35 at 80 °C). Intuitively, KIE should decrease with temperature. Although, it must be acknowledged that these experiments were performed only once due to the small amount of deuterated material which was synthesized. Our computations

predict a KIE of 1.99 at 25 °C in DCE, consistent with the majority of the experimental observations.

In our experimental study, we demonstrated that using *m*-CPBA in a non-protic solvent, it is possible to shift the product ratio towards formate ester formation by increasing the temperature of the system, with a product ratio approaching parity at 80 °C. In a practical context, the formation of a formate ester in situ now means the formation of a good electrophile. In the more 'sterile' scenario of *n*-hexadecane and ADPA being the only other components of the system, ADPA is the sole reactant, (forming *N*-formyl ADPA), however, industrial formulations contain many components such as overbased detergents, viscosity modifiers, and anti-wear agents such as molybdenum dithiocarbamates (MDTCs) and zinc dialkyldithiophosphates (ZDDPs). How formate esters interact with these additional additives, or if formate esters even form in the presence of these additives has yet to be explored. However, due to their structures and mechanisms, some hypotheses can be made. Overbased detergents such as phenates, sulfonates and salicylates, simply participate in acid/base chemistry and are poor nucleophiles.[50] Potentially their role of reducing the amount of acid in the system may retard the formation of formate esters and/or the formylation of the ADPA, which we found to be acid-catalyzed, however this is yet to be explored. Although MDTCs and ZDDPs contain sulphur, neither are particularly nucleophilic, and are believed to oxidize to presumably even less nucleophilic species. Based on the lack of nucleophilic species in formulations, it is still likely that formate esters will react with ADPAs, forming their *N*-formylated derivatives. Since this abrogates their activity as an RTA, the addition of a sacrificial

nucleophile may serve to liberate the free RTA, extending the lifetime of ADPAs. This will be explored in the next chapter.

2.4 – Conclusion

By independently demonstrating the feasibility of two reactions that could occur to yield the *N*-formyl-diarylamines formed in situ in high temperature hydrocarbon autoxidations, we have provided support for our proposed mechanism and provide insight into some unexplored chemistry which may occur during lubricant autoxidation. In our study we demonstrated that in non-protic solvents you can not only form formate product at room temperature, but that formate formation increases with temperature (1:21 to 1:8) when increasing from RT to 80 °C. This ratio can be further minimized by switching the aldehyde hydrogen to a deuterium due to a kinetic isotope effect on the H migration that is key to the formation of the acid product. Computations of the competing reaction pathways provided good quantitative agreement with the experiments – in terms of each of the product ratios, the temperature dependence and the magnitude of the kinetic isotope effect. To further build on this work, conducting a systematic study with other solvents, aldehydes and oxidants could be beneficial to afford a better understanding of selectivity in high-temperature B-V oxidations and more detailed analyses of the electronics of the transition states structures could lead to a better understanding of the selectivity of B-V oxidations, in general.

2.5 – Experimental

2.5.1 – Synthesis of hexadecyl formate (1)

Formic acid (8.7 mL, 230 mmol) and acetic anhydride (21.2 mL, 224 mmol) were stirred at 0 °C for 30 minutes and then at 60 °C for 3.5 hours. After this time, hexadecanol (1.7 g, 7.0 mmol) of as added and the reaction heated to reflux for 3h. The reaction was then left to cool, EtOAc was added and washed thrice with sodium bicarbonate and then brine. The organic phase was then dried using $MgSO_4$, filtered and the solvent evaporated in vacuo. The crude mixture was run through a silica plug with 9:1 hexanes:EtOAc, which afforded 1.7 g (6.4 mmol) of a white solid in 91% yield. ^{1}H NMR (400 MHz, $CDCl_3$): δ 8.04 (1H, s), 4.12-4.15 (2H, t), 1.60-1.67 (2H, m), 1.23-1.135 (12H, m), 0.84-0.87 (3H, t). The spectroscopic characterization was consistent with that reported in the literature [51]

2.5.2 – Synthesis of N-formyl t_2Butyl-DPA from hexadecyl formate (2)

Under an inert atmosphere, hexadecyl formate (271 mg, 1 mmol) and di-*t*-butyl-DPA (281 mg, 1 mmol) were heated to 168 °C with 5 mM of palmitic acid (64.1 mg) in decane (50 mL) and left to stir overnight. The reaction was then left to cool, EtOAc was added and washed thrice with sodium bicarbonate and once with brine. The organic phase was then dried using $MgSO_4$, filtered and the solvent evaporated in vacuo. The residue was then purified via column chromatography on silica gel using 9:1 hexanes:EtOAc, which afforded 179.5 mg (0.58 mmol) of white needles in 58% yield. ^{1}H NMR (300 MHz, C_6D_6): δ 8.52 (1H, s), 7.29-7.33 (2H, dt, J= 8.7, 6.5, 2.0), 7.13-7.17 (2, dt, J= 8.7, 6.5, 2.0), 6.99-7.03 (2H, dt, J= 8.7, 6.5, 2.0), 6.69-6.74 (2H, dt,

J= 8.7, 6.5, 2.0), 1.09-1.11 (18H, d). The spectroscopic characterization was consistent with that reported in the literature.[52]

2.5.3 – Synthesis of hexadecanal (3)

To a flame-dried Schlenk flask, evacuated and back-filled with N_2, 15 mL of dry DCM was added and cooled to -78 °C in an acetone/dry ice bath. Oxalyl chloride (0.61 mL, 7.08 mmol) was added via syringe, followed by 1 mL of DMSO in 15 mL of DCM also dropwise via syringe and the mixture was allowed to stir for 15 minutes. 1-Hexadecanol (1.7 g, 7.0 mmol) was dissolved in a minimum of DCM and added dropwise. After 15 minutes of stirring, 4.7 mL of triethylamine (in 10 mL of DCM) was added dropwise. The reaction was then left to stir for 1h. Once deemed complete by TLC (disappearance of hexadecanol), the reaction mixture was mixed carefully with saturated sodium bicarbonate in a properly sized beaker and left to stir until bubbling subsided. This mixture was extracted thrice with DCM, dried with $MgSO_4$ and solvent evaporated in vacuo. The crude product was then purified with a silica plug using 95:5 hexanes:EtOAc which afforded 1.3 g (5.6 mmol) of a white solid in 80% yield. ^{1}H NMR (400 MHz, $CDCl_3$): δ 9.74-9.75 (1H, t), 2.38-2.42 (2H, td), 1.54-1.64 (2H, m), 1.23-1.31 (26H, m), 0.84-0.87 (3H, t). The spectroscopic characterization was consistent with that reported in the literature.[53]

2.5.4 – Synthesis of methyl hexadecanoate (4)

Palmitic acid (18.9 g, 74 mmol) was dissolved in 100 mL of a 1M solution of HCl in MeOH to which 3 drops of H_2SO_4 were added and the reaction heated to reflux overnight. Once cooled the reaction mixture was poured on saturated sodium bicarbonate solution and extracted thrice with EtOAc. The organic layer was dried with $MgSO_4$, filtered and the solvent evaporated

in vacuo. The crude product was run through a silica plug using 95:5 hexanes:EtOAc to afford 6.4 g (23.7 mmol) of a white solid in 32% yield. ^{1}H NMR (400 MHz, $CDCl_3$): δ 3.64 (3H, s), 2.26-2.30 (2H, t), 1.57-1.63 (2H, m), 1.23-1.27 (26H, m), 0.84-0.87 (3H, t). The spectroscopic characterization was consistent with that reported in the literature.[54]

2.5.5 – Synthesis of hexadecanal-*d* (5)

Methyl hexadecanoate (1.9 g, 7 mmol) was dissolved in 10 mL of dry DCM under an inert atmosphere and the mixture cooled to -78 °C using an acetone/dry ice bath. DIBAL-*d* (12.5 mL of a 0.7 M solution in toluene, 8.75 mmol) was added dropwise. After 15 minutes 2N HCl was added to quench the DIBAL-*d* so the aldehyde was not over reduced. The mixture was extracted with DCM, dried with $MgSO_4$ and the solvent evaporated in vacuo. The crude product was purified using column chromatography, with a reverse gradient of 95:5 to 99:1 hexanes:EtOAc affording 340 mg (1.4 mmol) of an off-white solid in 20% yield. ^{1}H NMR (400 MHz, $CDCl_3$): δ 2.37-2.41 (2H, t), 1.57-1.64 (2H, t), 1.23-1.32 (24H, m), 0.84-0.87 (3H, t). The spectroscopic characterization was consistent with that reported in the literature.[55]

2.6 – Appendix

^{1}H-NMR ($CDCl_3$, 400 MHz)

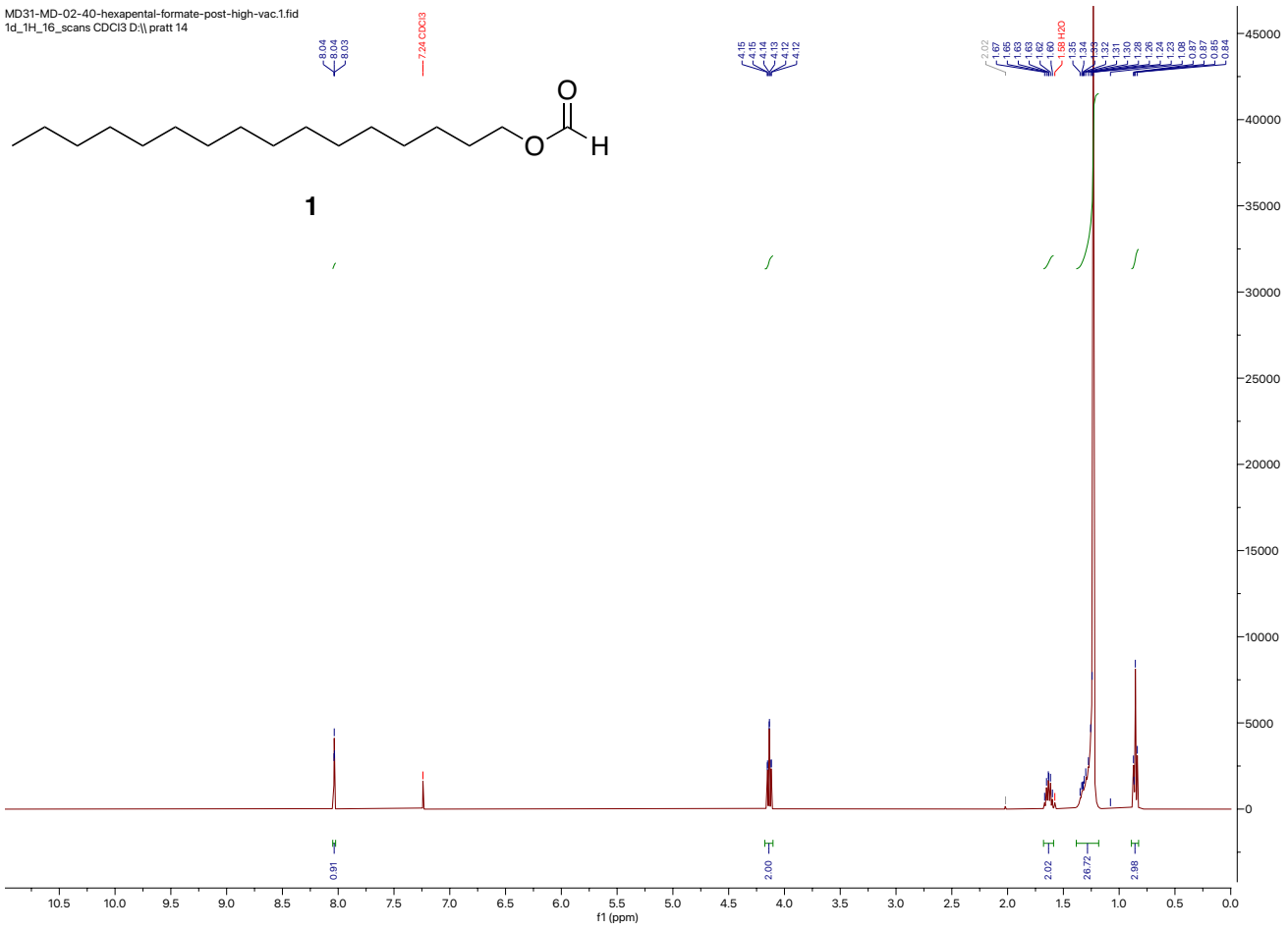

^{1}H-NMR (C_6D_6, 400 MHz)

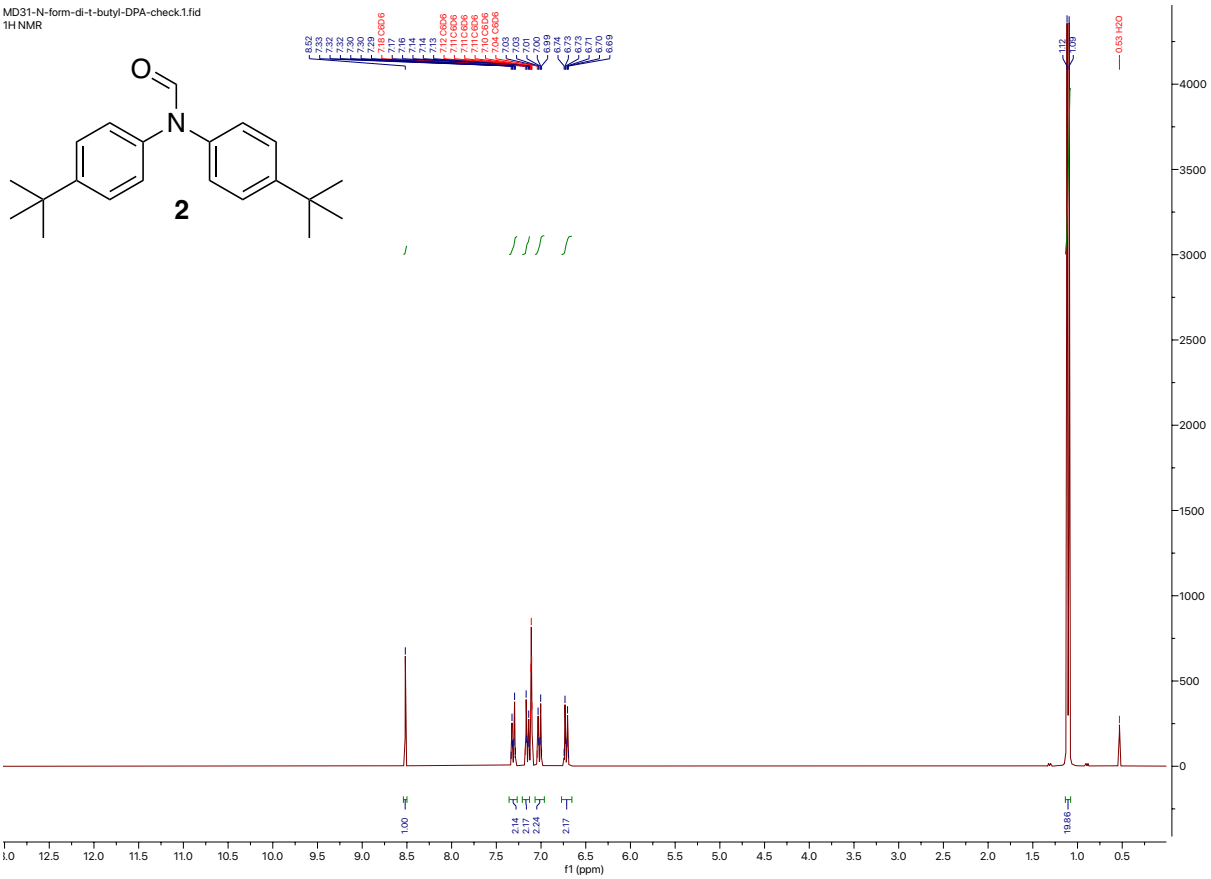

^{1}H-NMR ($CDCl_3$, 400 MHz)

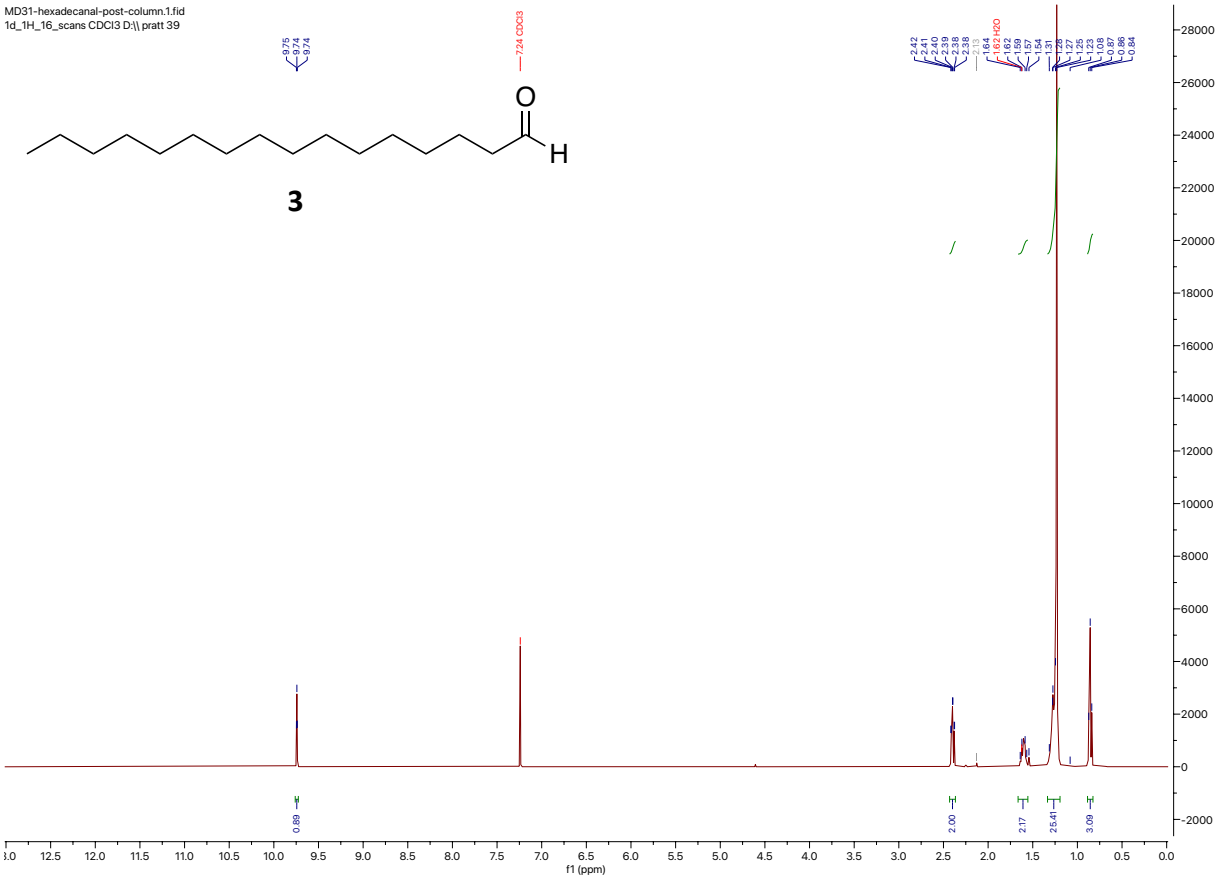

^{1}H-NMR ($CDCl_3$, 400 MHz)

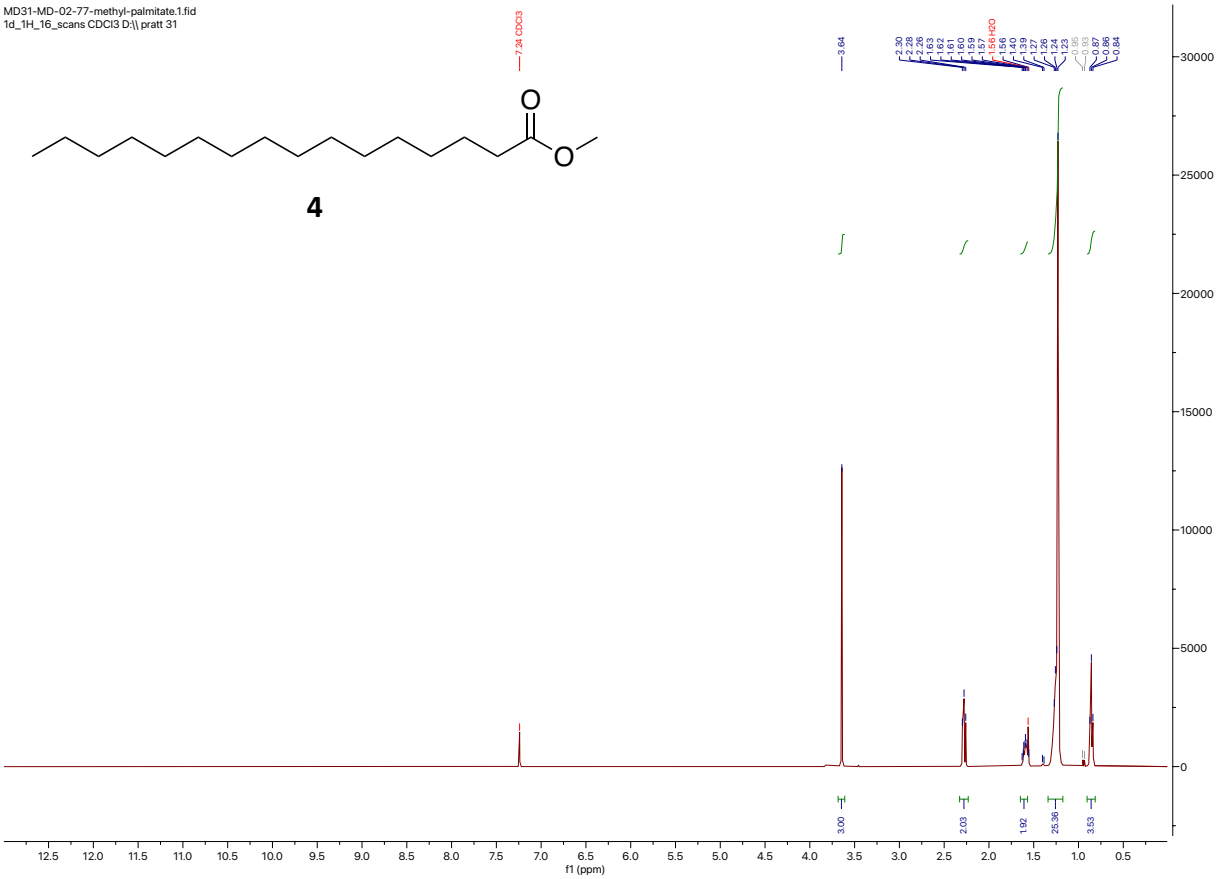

4

^{1}H-NMR ($CDCl_3$, 400 MHz)

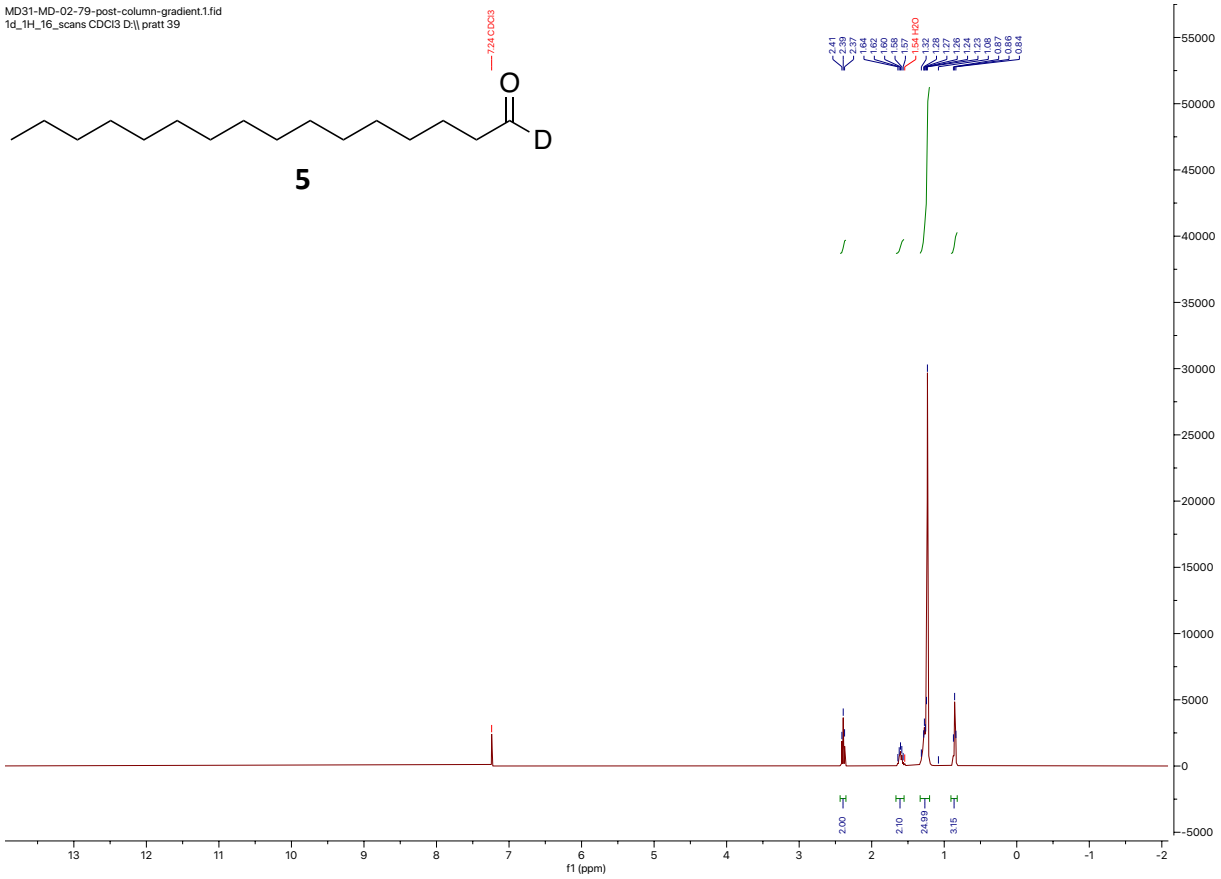

Cartesian Coordinates and Energies of Optimized Structures

Pentanal

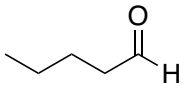

Gas Phase RT:
MN15/CBSB7+ Enthalpy = -170276.6881 kcal/mol
MN15/CBSB7+ Free Energy = -170302.0207 kcal/mol

Gas Phase 80 °C:
MN15/CBSB7+ Enthalpy = -170275.0566 kcal/mol
MN15/CBSB7+ Free Energy = -170306.8148 kcal/mol

Hexadecane RT:
MN15/CBSB7+ Enthalpy = -170278.6083 kcal/mol
MN15/CBSB7+ Free Energy = -170303.9346 kcal/mol

Hexadecane 80 °C:
MN15/CBSB7+ Enthalpy = -170276.9768 kcal/mol
MN15/CBSB7+ Free Energy = -170308.7287 kcal/mol

DCE RT:
MN15/CBSB7+ Enthalpy = -170280.403 kcal/mol
MN15/CBSB7+ Free Energy = -170305.7167 kcal/mol

DCE 80 °C:
MN15/CBSB7+ Enthalpy = -170278.7715 kcal/mol
MN15/CBSB7+ Free Energy = -170310.5171 kcal/mol

Pervaleric Acid

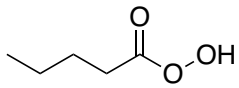

Gas Phase RT:
MN15/CBSB7+ Enthalpy = -264572.7166 kcal/mol
MN15/CBSB7+ Free Energy = -264601.8769 kcal/mol

Gas Phase 80 °C:
MN15/CBSB7+ Enthalpy = -264570.627 kcal/mol
MN15/CBSB7+ Free Energy = -264607.4178 kcal/mol

Hexadecane RT:
MN15/CBSB7+ Enthalpy = -264570.627 kcal/mol

MN15/CBSB7+ Free Energy = -264575.9482 kcal/mol

Hexadecane 80 °C:
MN15/CBSB7+ Enthalpy = -264573.8649 kcal/mol
MN15/CBSB7+ Free Energy = -264610.4048 kcal/mol

DCE RT:
MN15/CBSB7+ Enthalpy = -264578.9666 kcal/mol
MN15/CBSB7+ Free Energy = -264607.8194 kcal/mol

DCE 80 °C:
MN15/CBSB7+ Enthalpy = -264576.8832 kcal/mol
MN15/CBSB7+ Free Energy = -264613.3038 kcal/mol

Alkyl Group Antiperiplanar Chair Intermediate:

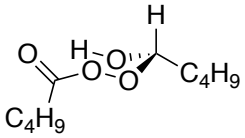

Gas Phase RT:
MN15/CBSB7+ Enthalpy = -434868.7006 kcal/mol
MN15/CBSB7+ Free Energy = -434910.3659 kcal/mol

Gas Phase 80 °C:
MN15/CBSB7+ Enthalpy = -434864.9669 kcal/mol
MN15/CBSB7+ Free Energy = -434918.3491 kcal/mol

Hexadecane RT:
MN15/CBSB7+ Enthalpy = -434871.5244 kcal/mol
MN15/CBSB7+ Free Energy = -434921.882 kcal/mol

Hexadecane 80 °C:
MN15/CBSB7+ Enthalpy = -434867.7844 kcal/mol
MN15/CBSB7+ Free Energy = -434921.882 kcal/mol

DCE RT:
MN15/CBSB7+ Enthalpy = -434873.9528 kcal/mol
MN15/CBSB7+ Free Energy = -434915.6257 kcal/mol

DCE 80 °C:
MN15/CBSB7+ Enthalpy = -434870.2066 kcal/mol
MN15/CBSB7+ Free Energy = -434923.6139 kcal/mol

H-Atom Antiperiplanar Chair Intermediate:

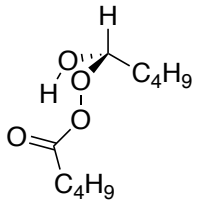

Gas Phase RT:
MN15/CBSB7+ Enthalpy = -434869.1336 kcal/mol
MN15/CBSB7+ Free Energy = -434910.066 kcal/mol

Gas Phase 80 °C:
MN15/CBSB7+ Enthalpy = -434865.4124 kcal/mol
MN15/CBSB7+ Free Energy = -434917.9099 kcal/mol

Hexadecane RT:
MN15/CBSB7+ Enthalpy = -434871.9825 kcal/mol
MN15/CBSB7+ Free Energy = -434913.1157 kcal/mol

Hexadecane 80 °C:
MN15/CBSB7+ Enthalpy = -434868.2551 kcal/mol
MN15/CBSB7+ Free Energy = -434921.0035 kcal/mol

DCE RT:
MN15/CBSB7+ Enthalpy = -434874.4988 kcal/mol
MN15/CBSB7+ Free Energy = -434915.563 kcal/mol

DCE 80 °C:
MN15/CBSB7+ Enthalpy = -434870.7588 kcal/mol
MN15/CBSB7+ Free Energy = -434923.4319 kcal/mol

Alkyl Migration Transition State:

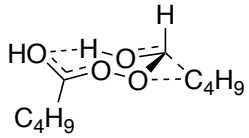

Gas Phase RT:
MN15/CBSB7+ Enthalpy = -434839.1449 kcal/mol
MN15/CBSB7+ Free Energy = -434880.5875 kcal/mol
Imaginary frequency: 1 cm^{-1}

Gas Phase 80 °C:
MN15/CBSB7+ Enthalpy = -434835.4426 kcal/mol
MN15/CBSB7+ Free Energy = -434888.5236 kcal/mol
Imaginary frequency: 1 cm^{-1}

Hexadecane RT:
MN15/CBSB7+ Enthalpy = -434843.0982 kcal/mol
MN15/CBSB7+ Free Energy = -434884.6393 kcal/mol
Imaginary frequency: 1 cm^{-1}

Hexadecane 80 °C:
MN15/CBSB7+ Enthalpy = -434839.3834 kcal/mol
MN15/CBSB7+ Free Energy = -434892.5899 kcal/mol
Imaginary frequency: 1 cm^{-1}

DCE RT:
MN15/CBSB7+ Enthalpy = -434846.788 kcal/mol
MN15/CBSB7+ Free Energy = -434896.3988 kcal/mol
Imaginary frequency: 1 cm^{-1}

DCE 80 °C:
MN15/CBSB7+ Enthalpy = -434843.0543 kcal/mol
MN15/CBSB7+ Free Energy = -434896.3988 kcal/mol
Imaginary frequency: 1 cm^{-1}

H-Atom Migration Transition State

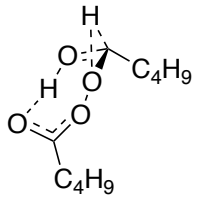

Gas Phase RT:
MN15/CBSB7+ Enthalpy = -434842.5962 kcal/mol
MN15/CBSB7+ Free Energy = -434883.774 kcal/mol
Imaginary frequency: 1 cm^{-1}

Gas Phase 80 °C:
MN15/CBSB7+ Enthalpy = -434838.9127 kcal/mol
MN15/CBSB7+ Free Energy = -434891.6612 kcal/mol
Imaginary frequency: 1 cm^{-1}

Hexadecane RT:
MN15/CBSB7+ Enthalpy = -434845.7338 kcal/mol
MN15/CBSB7+ Free Energy = -434886.9297 kcal/mol
Imaginary frequency: 1 cm^{-1}

Hexadecane 80 °C:

MN15/CBSB7+ Enthalpy = -434842.0377 kcal/mol
MN15/CBSB7+ Free Energy = -434894.8238 kcal/mol
Imaginary frequency: 1 cm^{-1}

DCE RT:
MN15/CBSB7+ Enthalpy = -434848.5889 kcal/mol
MN15/CBSB7+ Free Energy = -434889.8476 kcal/mol
Imaginary frequency: 1 cm^{-1}

DCE 80 °C:
MN15/CBSB7+ Enthalpy = -434844.8804 kcal/mol
MN15/CBSB7+ Free Energy = -434897.748 kcal/mol
Imaginary frequency: 1 cm^{-1}

Formate Ester Product

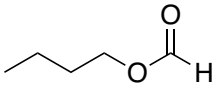

Gas Phase RT:
MN15/CBSB7+ Enthalpy = -217452.7959 kcal/mol
MN15/CBSB7+ Free Energy = -217485.3511 kcal/mol

Gas Phase 80 °C:
MN15/CBSB7+ Enthalpy = -217451.0138 kcal/mol
MN15/CBSB7+ Free Energy = -217490.4276 kcal/mol

Hexadecane RT:
MN15/CBSB7+ Enthalpy = -217455.7766 kcal/mol
MN15/CBSB7+ Free Energy = -217482.5273 kcal/mol

Hexadecane 80 °C:
MN15/CBSB7+ Enthalpy = -217453.9945 kcal/mol
MN15/CBSB7+ Free Energy = -217487.6038 kcal/mol

DCE RT:
MN15/CBSB7+ Enthalpy = -217458.5941 kcal/mol
MN15/CBSB7+ Free Energy = -217485.3511 kcal/mol

DCE 80 °C:
MN15/CBSB7+ Enthalpy = -217456.8057 kcal/mol
MN15/CBSB7+ Free Energy = -217490.4276 kcal/mol

Acid Product

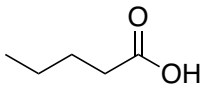

Gas Phase RT:
MN15/CBSB7+ Enthalpy = -217465.3587 kcal/mol
MN15/CBSB7+ Free Energy = -217492.5549 kcal/mol

Gas Phase 80 °C:
MN15/CBSB7+ Enthalpy = -217463.5138 kcal/mol
MN15/CBSB7+ Free Energy = -217497.7005 kcal/mol

Hexadecane RT:
MN15/CBSB7+ Enthalpy = -217469.2618 kcal/mol
MN15/CBSB7+ Free Energy = -217496.571 kcal/mol

Hexadecane 80 °C:
MN15/CBSB7+ Enthalpy = -217467.4169 kcal/mol
MN15/CBSB7+ Free Energy = -217501.7542 kcal/mol

DCE RT:
MN15/CBSB7+ Enthalpy = -217472.9013 kcal/mol
MN15/CBSB7+ Free Energy = -217500.4364 kcal/mol

DCE 80 °C:
MN15/CBSB7+ Enthalpy = -217471.0564 kcal/mol
MN15/CBSB7+ Free Energy = -217505.6573 kcal/mol

Pentanal-d

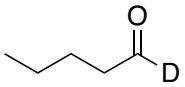

DCE RT:
MN15/CBSB7+ Enthalpy = -170282.2792 kcal/mol
MN15/CBSB7+ Free Energy = -170307.7749

Alkyl Group Antiperiplanar Chair Intermediate (deuterated)

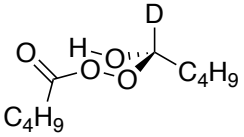

DCE RT:
MN15/CBSB7+ Enthalpy = -434876.1429 kcal/mol
MN15/CBSB7+ Free Energy = -434917.9161 kcal/mol

H-Atom Antiperiplanar Chair Intermediate (deuterated)

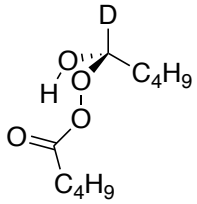

DCE RT:
MN15/CBSB7+ Enthalpy = -434876.6637 kcal/mol
MN15/CBSB7+ Free Energy = -434917.8283 kcal/mol

Formate Ester Product Transition State (deuterated)

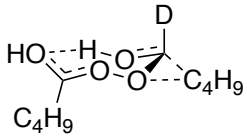

DCE RT:
MN15/CBSB7+ Enthalpy = -434848.8588 kcal/mol
MN15/CBSB7+ Free Energy = -434890.6132 kcal/mol
Imaginary Frequency: 1 cm^{-1}

Acid Products Transition State (deuterated)

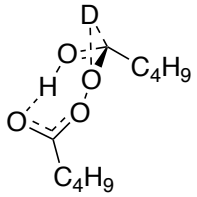

DCE RT:
MN15/CBSB7+ Enthalpy = -434849.9318 kcal/mol
MN15/CBSB7+ Free Energy = -434891.3286 kcal/mol
Imaginary Frequency: 1 cm^{-1}

Formate Ester Product (deuterated)

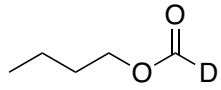

DCE RT:
MN15/CBSB7+ Enthalpy = -217460.5394 kcal/mol
MN15/CBSB7+ Free Energy = -217487.4658 kcal/mol

Acid Product (deuterated)

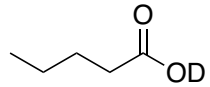

DCE RT:
MN15/CBSB7+ Enthalpy = -217474.9282 kcal/mol

MN15/CBSB7+ Free Energy = -217500.4364 kcal/mol

Chapter 3: The Development of Latent Radical Trapping Antioxidants for High-Temperature Applications

3.1 – Introduction

As humanity moves away from the use of the combustion engines, one might believe there is no need to invest in new RTAs to improve the properties of the lubricant that are key to their operation. However, this transition will take time, particularly in the developing world – and the electrification of heavy machinery, ships and transport trucks is a far greater challenge than that of passenger vehicles. The continued environmental impact can, in part, be mitigated by continued improvements in combustion engine technology and lubricant performance and longevity.

As part of our group's efforts to develop new RTA technology, we found that substitution of highly potent *N*-heterocyclic diarylamines, [29,56] PTZs or PNXs with methyl groups or other 1° and/or 2° alkyl groups could dramatically extend the inhibited period observed in high-temperature (>160 °C) autoxidations of *n*-hexadecane as shown in **Scheme 1.10.**[29] Based on some product analyses, we surmised that after the initial HAT reaction, another equivalent of peroxyl radical can abstract a hydrogen atom from a 1° and/or 2° alkyl group (BDE ~62.9 kcal/mol) to form a *p*-iminoquinone methide. The *p*-iminoquinone methide can then undergo PRA with yet another equivalent of peroxyl radical eventually forming a ketone and/or aldehyde depending on the alkyl group.[29]

However, when increasing the loading of these RTAs to the levels that would be required to protect a lubricant or consumer product over the typical lifetime of the product (generally at least 1 wt%), many insoluble by-products are formed, as shown for the PTZ-based RTAs in **Figure 3.2**. Given evidence for the formation of oligomeric species in MS analyses, we presumed that it was due to Michael addition of unreacted RTAs to the iminoquinone methide intermediates. Consistent with this hypothesis, the addition of a sacrificial nucleophile such as dodecanol or another lipophilic alcohol was able to reduce precipitation (**Figure 3.2**).

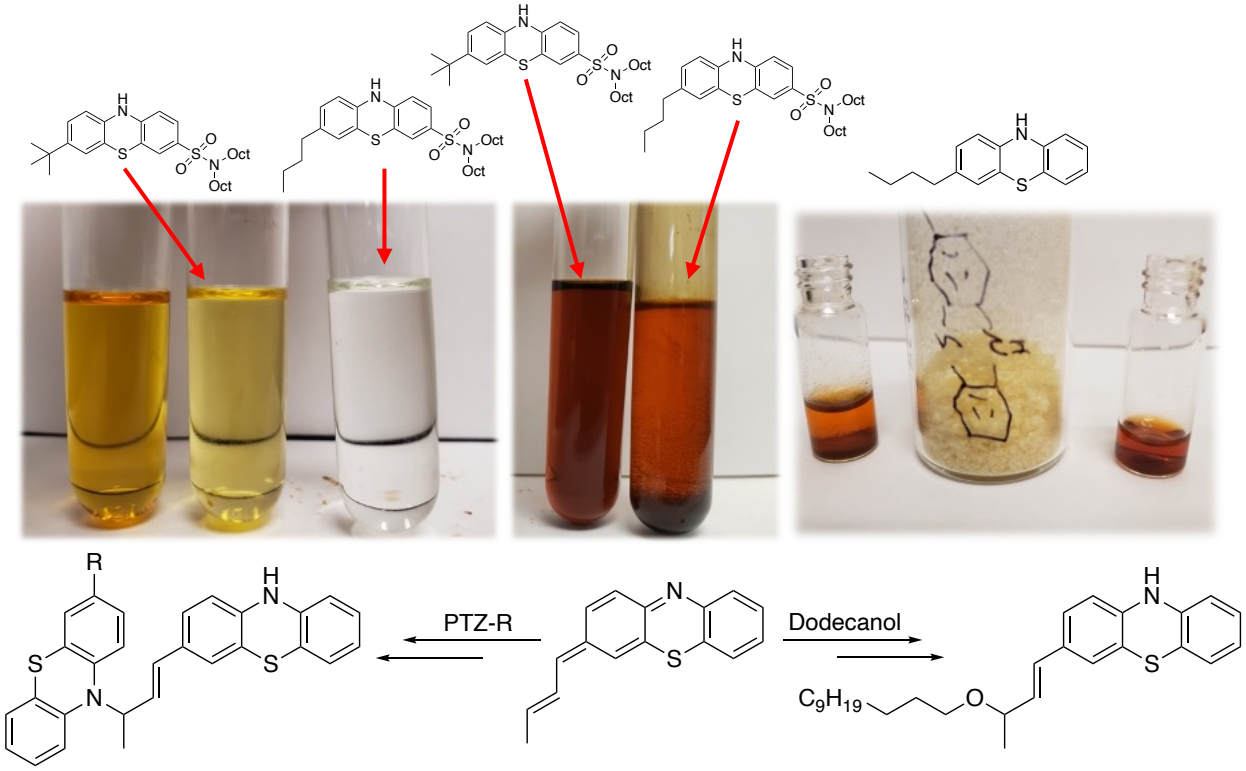

Figure 3.1 – (Top Left) Appearance of samples from *n*-hexadecane autoxidations at at 165 °C after 5h where the left tube is uninhibited, the middle tube contains 150 μM 3-$SO_2N(Oct)_2$7-t-butyl-PTZ and the tube on the right 150 μM 3-$SO_2N(Oct)_2$-7-n-butyl-PTZ. **(Top middle)** Appearance of samples from *n*-hexadecane autoxidations at 165 °C inhibited by 10 mM of 3-$SO_2N(Oct)_2$-7-t-butyl-7-sulfonamide-PTZ (left tube) and 10 mM of 3-$SO_2N(Oct)_2$-7-n-butyl-7-sulfonamide-PTZ (right tube. **(Top right)** Appearance of samples from *n*-hexadecane autoxidations at 165 °C inhibited by 1 mM 3-*n*-butyl-PTZ, the left vial contains no added dodecanol, while the right vial has added dodecanol. **(Bottom)** Michael-acceptor has two options: oligomerize with PTZ or dodecanol is used as a sacrificial nucleophile to eliminate precipitation.

3.1.2 – Design and Performance of 3-$SO_2N(Oct)_2$-7-R-PTZs

At first, we considered that in lieu of adding dodecanol to the autoxidations containing alkyl-PTZs, perhaps incorporation of a very lipophilic group would improve the solubility of any oligomeric species that may form. For ease of synthesis and what could be obtained as inexpensive precursors, it was decided that the alkyl group would be at the 7-position and a di-octyl-sulfonamide at the 3-position (both *para* to the amine). To compare to the previous mono-alkylated PTZs studied by the group, the series of compounds in **Figure 3.2** were synthesized to combine the increased lipophilicity with the various alkyl substituents which increase radical-trapping stoichiometry, and therefore the duration of the inhibited period.

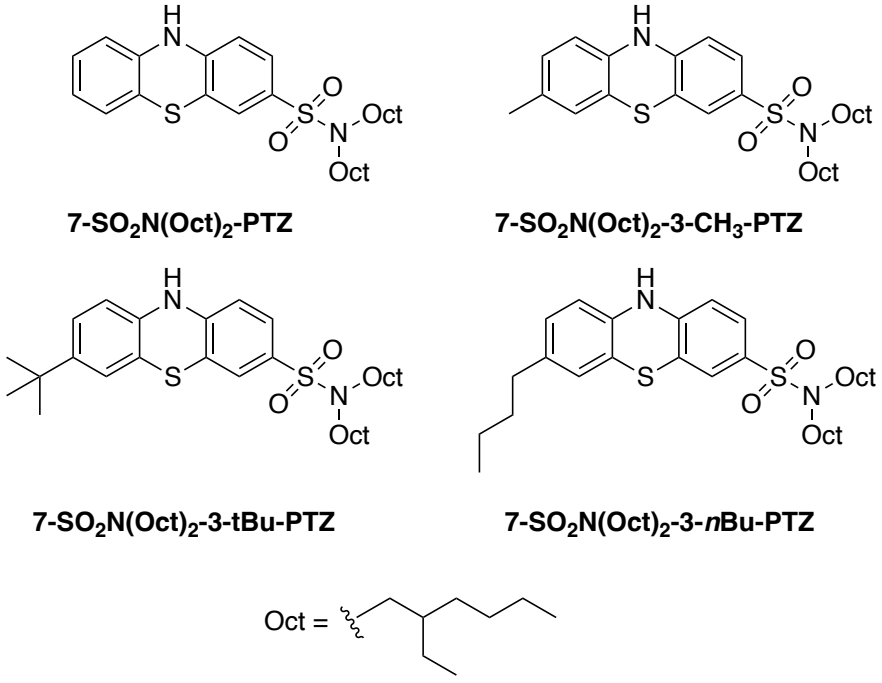

Figure 3.2 – Previous 3-$SO_2N(Oct)_2$-7-alkyl-PTZ RTAs synthesized by the Pratt Group where it was expected that primary alkyl groups would increase the stoichiometry while the lipophilic octyl chains would hopefully limit precipitation by increasing the solubility of by-products.

Inhibited autoxidations of *n*-hexadecane carried out at 165 °C revealed that, consistent with our previous results with the non-sulfonylated analogs, the PTZs which contained a 1° or 2° alkyl group in the *para* position relative to the reactive amine have increased stoichiometry, as demonstrated by their longer inhibited periods (where t_{inh} trend as *t*-Bu < H < CH_3 < *n*-Bu) (**Figure 3.3**).

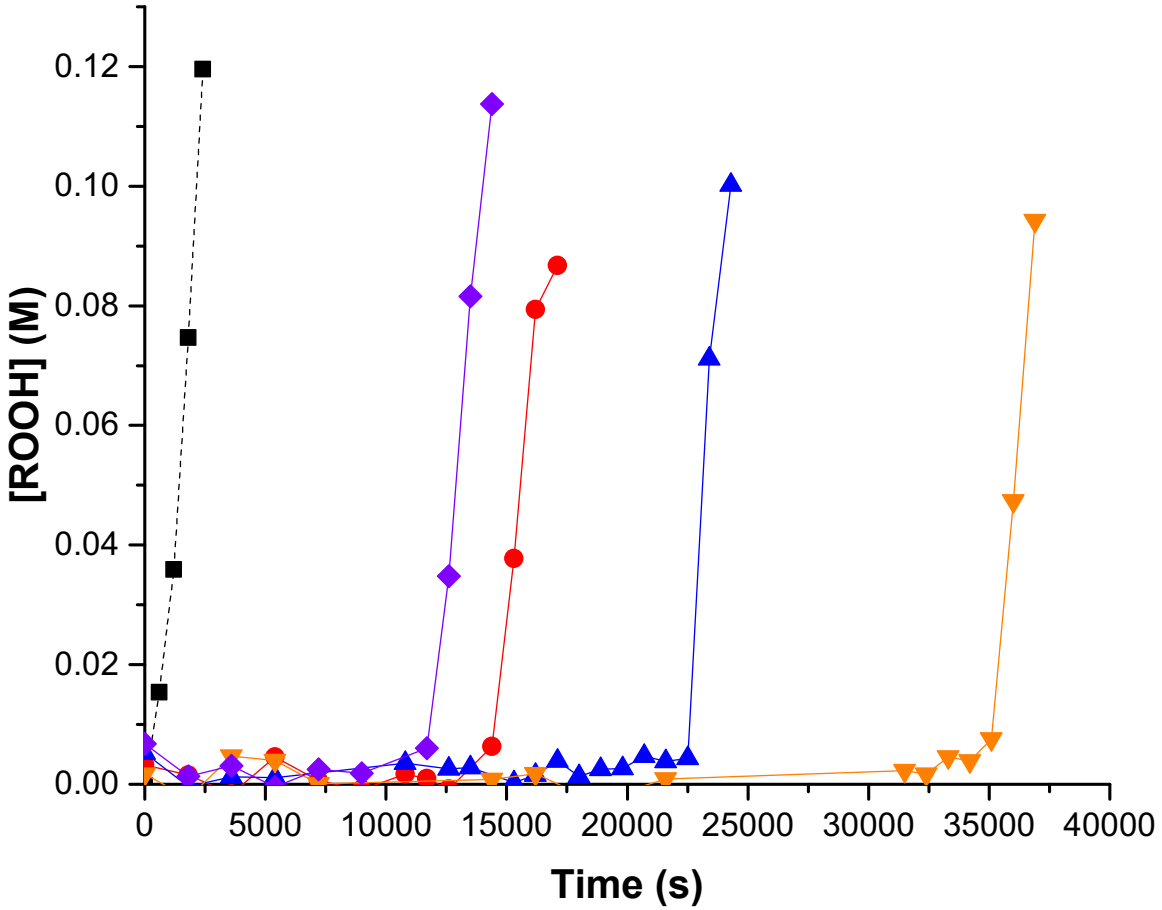

Figure 3.3 – Hydroperoxide formation from autoxidations of *n*-hexadecane at 165 °C in the presence of 3-$SO_2N(Oct)_2$-7-alkyl-PTZ at concentrations of 150 μM respectively. Where alkyl = t-Bu, H, CH_3 and n-Bu.

The observation of t_{inh} ~ 10 h for the *n*-butylated compound was rather remarkable. For context, the industry standards BHT and tBu_2DPA have t_{inh} ~1 h 45 and ~0.5 h, respectively, at the same concentration (150 μM) under these experimental conditions.[57] The two most

effective sulfonamide-PTZs are the *n*-butyl and *iso*-propyl derivatives. Indeed, these are the two most potent high-temperature RTAs synthesized yet by the group, and to our knowledge, the most potent reported to date. It is important to note that the unprecedented potency is not due to an increase in inherent reactivity of the aminic site since, at 37 °C in PhCl, the compounds all have similar reactivity to peroxyl radicals (**Table 3.1**). Although the k_{inh} values determined under these conditions are slightly larger with alkyl groups at the 3-position as opposed to without, this cannot account for the differences since the *t*-Bu-substituted compound has an even shorter inhibited period than the unsubstituted compound at elevated temperatures. Instead, it is clear that the additional reducing equivalents provided by the alkyl sidechain contribute to the greater radical-trapping stoichiometry, especially at elevated temperatures where peroxyl radical addition to the aryl ring is reversible, demonstrated in **Scheme 1.10**.

Table 3.1 - Inhibited periods and inhibition rate constants of 3-$SO_2N(Oct)_2$-7-R-PTZs at 37 °C determined from PBD-BODIPY/dioxane co-autoxidations (inhibitor concentration of 4 μM) and at 165 °C determined from *n*-hexadecane autoxidations (inhibitor concentration of 150 μM).

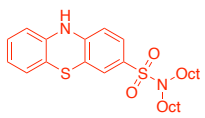
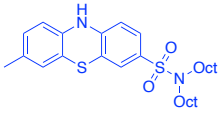
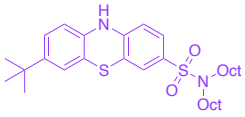
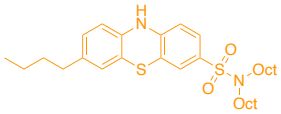

$t_{inh}^{37°C}$:	56 min	52 min	52 min	56 min
$k_{inh}^{37°C}$:	2.7 x 10^5 M^{-1} s^{-1}	4.8 x 10^5 M^{-1} s^{-1}	5.1 x 10^5 M^{-1} s^{-1}	5.3 x 10^5 M^{-1} s^{-1}
$t_{inh}^{168°C}$:	225 min	360 min	195 min	585 min

In order to determine if inclusion of the *N,N*-dioctylsulfonamide groups on the PTZ core help reduce precipitation of the RTA-derived oxidation products over the course of an

autoxidation, we also ran autoxidations at 10 mM RTA in *n*-hexadecane at 165 °C and visually inspected the solutions (**Figure 3.4**). At 10 mM the sulfonamide-PTZs all suppressed autoxidation completely and likely would have done so beyond the 5 hours of the experiment. However, similarly to the previous PTZ-based RTAs studied in the group, significant formation of precipitates did unfortunately occur.

Figure 3.4 – Appearance of *n*-hexadecane autoxidations samples in the presence of 10 mM 3-$SO_2N(Oct)_2$-7-R-PTZs at 0 h, 3 h and 5 h. Precipitation is extremely prominent in tubes dosed with alkyl groups which contain benzylic hydrogens, due to the formation of Michael-acceptors and subsequent oligomerization.

3.1.3 – Design of Latent RTAs

Given our expectation that dimerization/oligomerization of the RTA at high concentrations is driven by the reactivity of the aminic site of the RTA as both a H-atom donor and nucleophile, we considered whether installation of a protecting group that would be slowly cleaved at a well-defined (or tunable) rate in situ could minimize these deleterious reactions. This would allow for a low basal concentration to inhibit autoxidation while the reserve RTA remains inactive. This would protect the PTZ-based compounds from oligomerizing and could protect the PNX-based compounds from rapid autoxidation at elevated temperatures which erodes its otherwise best-in-class RTA activity.[2,25]

As mentioned in Chapter 2, Neill Penner's work in the Pratt group revealed the prominent formation of *N*-formyl tBu_2DPA in HMBC NMR analyses (among other methods) of samples taken during high temperature autoxidations of *n*-hexadecane inhibited by t-Bu_2DPA. Although *N*-formyl tBu_2DPA showed no RTA activity by itself, autoxidations carried out in its presence surprisingly showed the same 'fingerprint' of products by HMBC analyses as observed in autoxidations inhibited by tBu_2DPA – suggesting that the formyl group was eventually cleaved in situ. As such, we wondered if a formyl group or other acyl group, could serve as a protecting group for aminic RTAs (**Scheme 3.1**). While Penner's observation that *N*-formyl tBu_2DPA had no RTA activity suggests that perhaps cleavage of *N*-formyl-DPA is too slow under the reaction conditions to inhibit autoxidation, it was expected that the significantly higher

intrinsic reactivity of PTZ or PNX would require less RTA to be released to efficiently inhibit autoxidation.

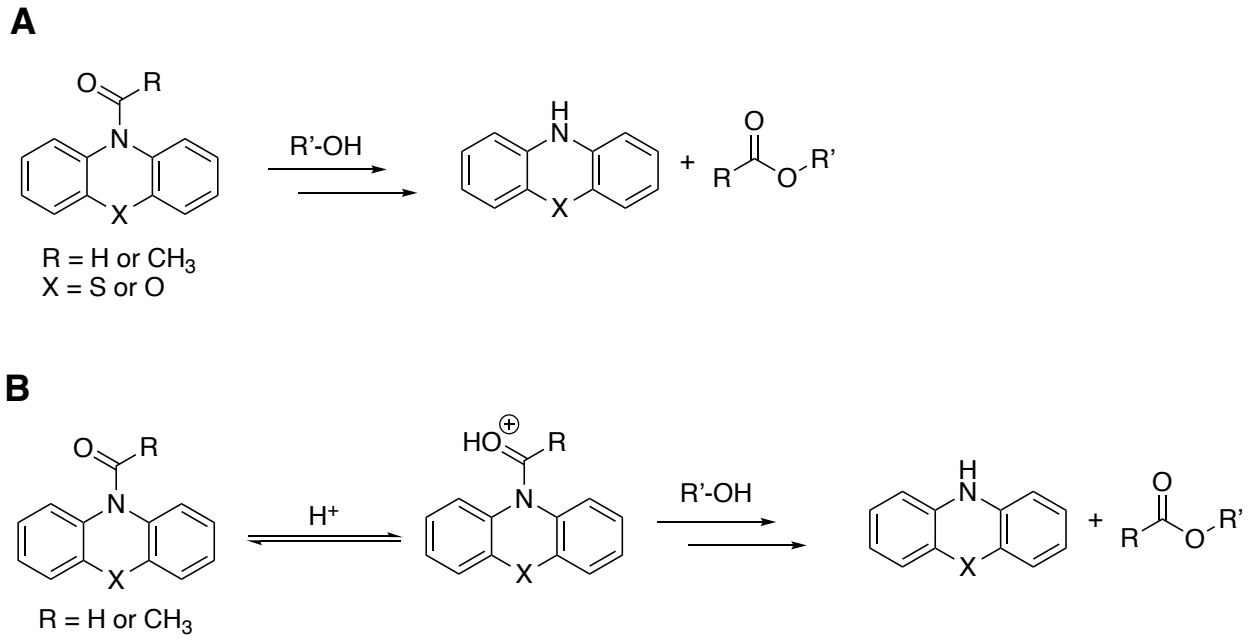

Scheme 3.1 – The cleavage of formyl/acetyl protecting groups on heteroatom bridged diarylamines using a long-chain alcohol nucleophile in both an uncatalyzed fashion (**A**) and acid-catalyzed fashion (**B**).

3.2 – Results

For proof-of-principle experiments we prepared *N*-formyl-PTZ and *N*-acetyl-PTZ by heating PTZ with formic acid to reflux and mixing PTZ with acetyl chloride at room temperature, respectively. The compounds were then heated to reflux in ethylene glycol (5 mL) (at 198 °C) in sealed tubes in the presence or absence of sulfuric acid (0.5 mL) to determine if the amides could be cleaved in the presence of a nucleophile and whether this required an acid catalyst. TLC analysis (**Figure 3.5**) revealed that although the acetyl group was not cleaved in the absence of acid under these conditions, the formyl group was steadily cleaved. Moreover, the addition of sulfuric acid expectedly accelerated the rate of reaction, such that the formamide was

essentially quantitatively cleaved by ~8 h. Addition of acid also lead to cleavage of a significant amount of acetamide by this point.

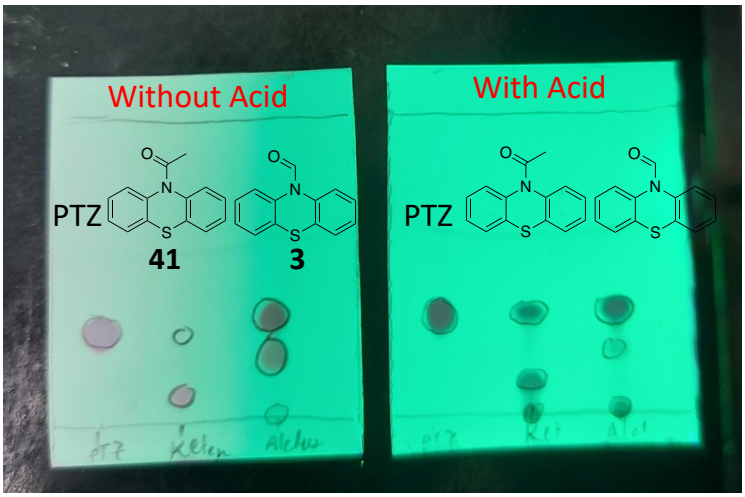

Figure 3.5 – Representative TLC analyses of *N*-formyl PTZ (**3**) and *N*-acetyl PTZ (**41**) in neat ethylene glycol at reflux in the absence and presence of sulfuric acid.

3.2.1 – *N*-Formyl-PTZ and *N*-Formyl-PNX as Latent Inhibitors of n-Hexadecane Autoxidation

Given that PTZ could be liberated from *N*-formyl-PTZ (**3**) without the addition of acid, we sought to investigate whether **3** and the corresponding *N*-formyl-PNX (**4**) (prepared in an analogous manner to **3**) could inhibit *n*-hexadecane autoxidation. We carried out these autoxidations in the parallel stirred-flow reactor introduced in **Section 1.3.1**. Test tubes were loaded with 10 mL of purified *n*-hexadecane and heated to 165 °C (under N_2). Once at temperature, 0.1 mmol of either *N*-formyl-PTZ or *N*-formyl-PNX (dissolved in a minimum of benzene) was added to the tubes via Pasteur pipette. Once the latent RTAs were loaded, the gas flow was switched from N_2 to O_2 to commence the experiment. Aliquots were taken via Pasteur pipette at various time points and total hydroperoxide concentration was determined using the phosphine-coumarin conjugate as introduced in **Section 1.3.1**. The results are shown in **Figure 3.6**, where *N*-formyl-PNX showed very little activity (inhibiting for less than an hour)

and *N*-formyl-PTZ had a modest, but well-defined, inhibited period (~1 h). Interestingly, it appeared to 'switch on' once [ROOH] accumulated, leading to eventual suppression in [ROOH] formation. Since *n*-hexadecane autoxidation will provide a nucleophile for transformylation (ROOH or ROH derived from ROOH) as well as some acid to catalyze it, this profile seems reasonable. It is noteworthy that the *n*-hexadecane was very viscous at the end of the experiment, implying that although *N*-formyl-PTZ could be activated to supress autoxidation, it may have been 'too little, too late'. Viscous *n*-hexadecane or other hydrocarbon substrate is characteristic of the destruction of the substrate in both uninhibited and inhibited autoxidations.

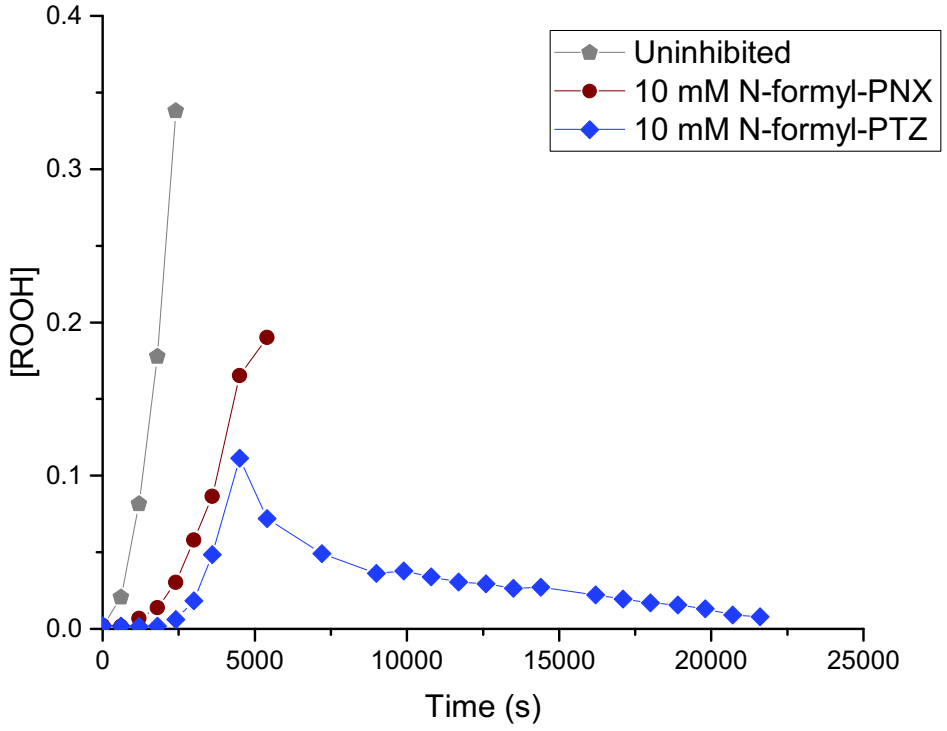

Figure 3.6 – Hydroperoxide formation from the autoxidation of *n*-hexadecane at 165 °C in the presence of 10 mM *N*-formyl-PNX and *N*-formyl-PTZ, respectively.

Given this result, we added a lipophilic alcohol (1-dodecanol) and/or acid (palmitic acid) along with the latent RTA to establish whether this could accelerate removal of the formyl group. We also varied the amount of latent RTA (2, 5 and 10 mM) to provide some insight on the dose-response relationship under these conditions. The results are shown in **Figure 3.7**. While the additives themselves did not have a significant impact on the rate of the uninhibited autoxidation, their presence lead to the complete suppression of the autoxidation by both *N*-formyl-PTZ and *N*-formyl-PNX when present at 10 mM. Reducing the concentrations of the latent RTAs to 5 mM and 2 mM had no impact on complete suppression by *N*-formyl-PNX, but a concentration dependence emerged for *N*-formyl-PTZ, with inhibited periods of ~2 h and ~4h 45 at 2 mM and 5 mM, respectively, while 10 mM inhibited for >6.5 h.

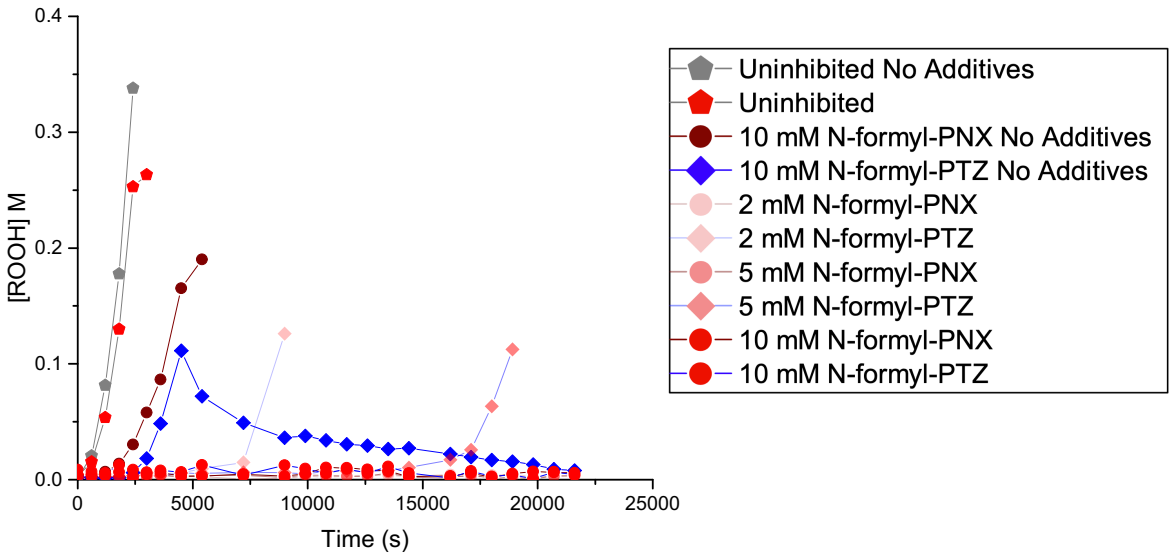

Figure 3.7 – Hydroperoxide formation from the autoxidation of *n*-hexadecane at 165 °C in the presence of *N*-formyl-PTZ and *N*-formyl-PNX with added nucleophile (5% dodecanol) and acid (5 mM palmitic acid) at various concentrations of inhibitor. Red symbols indicate the presence of 5% dodecanol and 5 mM of palmitic acid.

Given the complete suppression of autoxidation by *N*-formyl-PNX trough the 2-10 mM concentration range, we decreased the test concentration to 150 μM, 300 μM and 1 mM to look for a concentration dependence. We were additionally encouraged by the possibility of direct comparison to an equivalent amount of 'free' PNX. In the presence of additives, even 150 μM of N-formyl-PNX was effective, with an inhibited period of ~1 h, which increased to ~1.5 h at 300 μM and was >12 h at 1 mM, as shown in **Figures 3.8 and 3.9**. Remarkably, *N*-formyl-PNX was a more effective inhibitor than free PNX at 1 mM (**Figure 3.9**)!

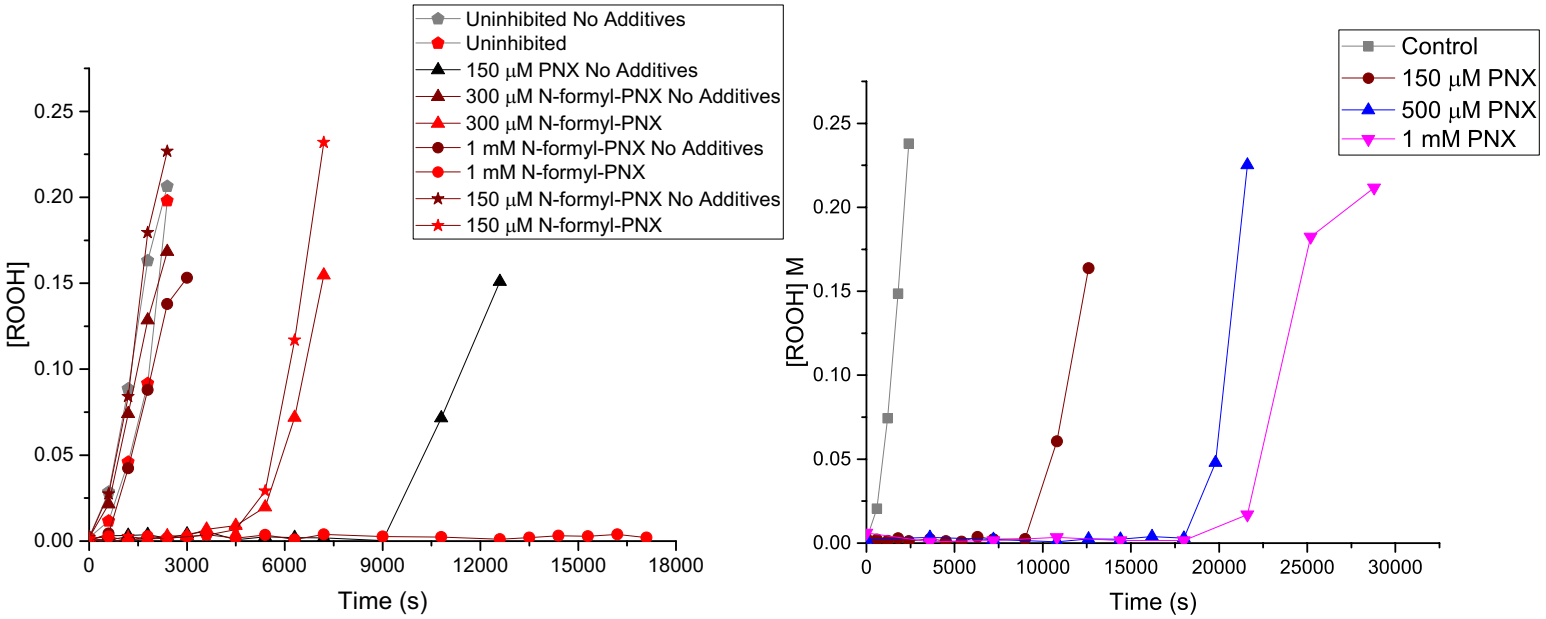

Figure 3.8 – (Left) Hydroperoxide formation from the autoxidation of *n*-hexadecane at 165 °C in the presence of *N*-formyl-PNX and PNX with and without added nucleophile (5% dodecanol) and acid (5 mM palmitic acid) at 150 μM, 300 μM or 10 mM of inhibitor. Red symbols indicating the presence of dodecanol and palmitic acid. **(Right)** Hydroperoxide formation from the autoxidation of *n*-hexadecane at 165 °C in the presence of 150 μM, 500 μM and 1 mM of PNX at 165 °C, demonstrating the lack of return on investment when increasing the concentration of PNX.

The superior antioxidant activity of *N*-formyl-PNX compared to PNX at 1 mM validates the latent RTA approach (**Figure 3.9**). Importantly, increasing the amount of PNX does not lead to a corresponding increase in inhibited period. For example, 150 μM of PNX has a t_{inh} of 2.5h,

and when the [PNX] is increased to 1 mM (~7 fold), the inhibited period is increased only by ~50% to ~5-5.5 h (**Figure 3.9**). This is consistent with our previous results that showed that PNX is depleted rapidly by direct reaction with O_2 (as in **Scheme 1.10 (B)**) to form the comparatively ineffective PNX-derived nitroxide and/or loss via other deleterious pathways.

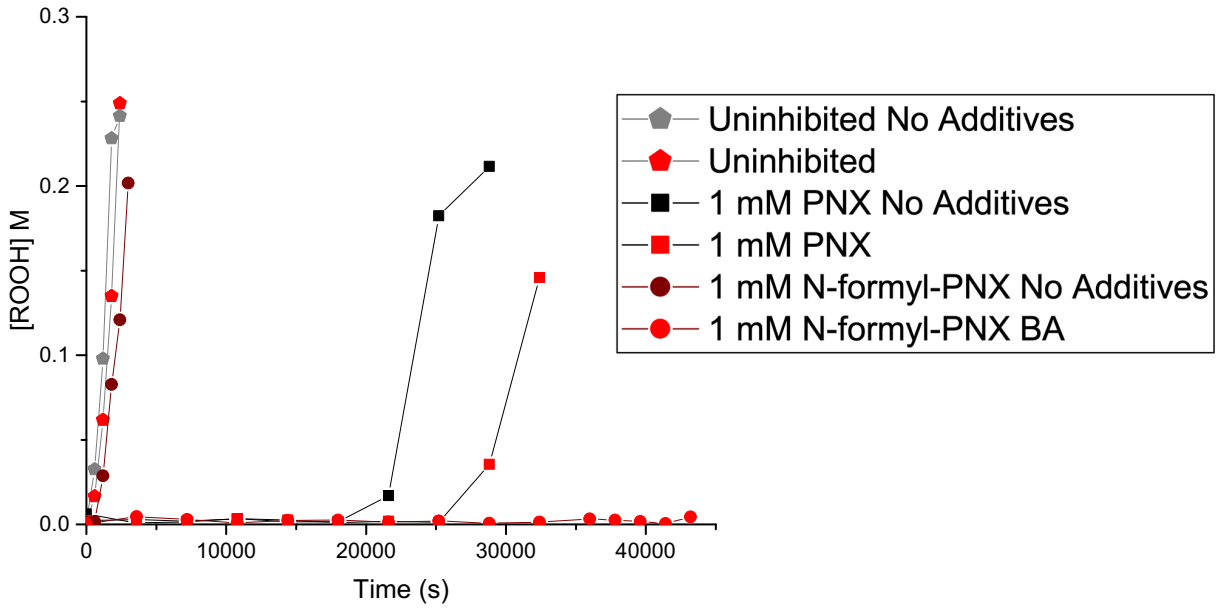

Figure 3.9 – Hydroperoxide formation from the autoxidation of n-hexadecane at 165 °C in the presence of N-formyl-PNX and PNX with and without added nucleophile (5% dodecanol) and acid (5 mM palmitic acid) at 1 mM of inhibitor respectively. Red symbols indicating the presence of 5% dodecanol and 5 mM palmitic acid.

N-formyl PTZ, however, performs worse than its PNX counterpart at 1 mM. There is still significant inhibition at 1 mM but speaking in terms of t_{inh} only, it does not outperform free-PTZ head-to-head at 1 mM, as its t_{inh} is ~3.5 h and free PTZ has a t_{inh} > 7.5 h (**Figure 3.10**). However, there may still be an advantage with respect to minimizing oligomerization and precipitate formation (*vide infra*).

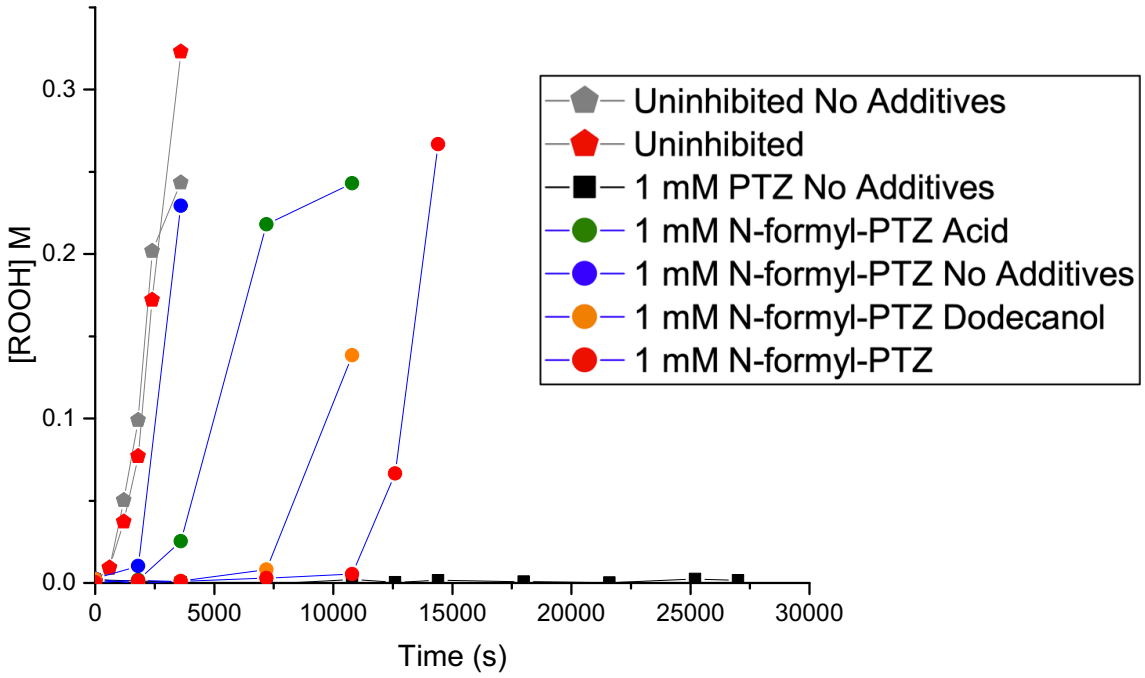

Figure 3.10 – Hydroperoxide formation from the autoxidation of *n*-hexadecane at 165 °C in the presence of 1 mM of PTZ of *N*-formyl-PTZ with various combinations of dodecanol (5%) and palmitic acid (5 mM). Red symbols indicating the presence of 5% dodecanol and 5 mM palmitic acid, green symbols indicating the presence of just 5 mM palmitic acid and organge symbols indicating just the presence of 5% dodecanol.

To evaluate whether this strategy may be used more broadly to improve the activity of other aminic RTAs, we added acyl groups to the amines shown in **Figure 3.11**. Therefore, *N*-formyl- and *N*-acetyl-di-aza-DPA (**7** & **8**), *N*-formyl-naphthalene-DPA (**6**) and *N*-formyl tBu_2DPA (**9**) were synthesized. Unfortunately, **7** and **8** showed little to no inhibition (<1 h) at a concentration of 10 mM (**Figure 3.12**). The aza-derivatives likely suffered poor performance due to protonation of their basic nitrogen atoms in the presence of added acid, which renders them

unreactive.[56] At 10 mM, *N*-formyl tBu_2DPA (**9**) showed some activity, but did not fully supress autoxidation as did *N*-formyl-PNX and -PTZ, presumably since it is significantly less reactive.

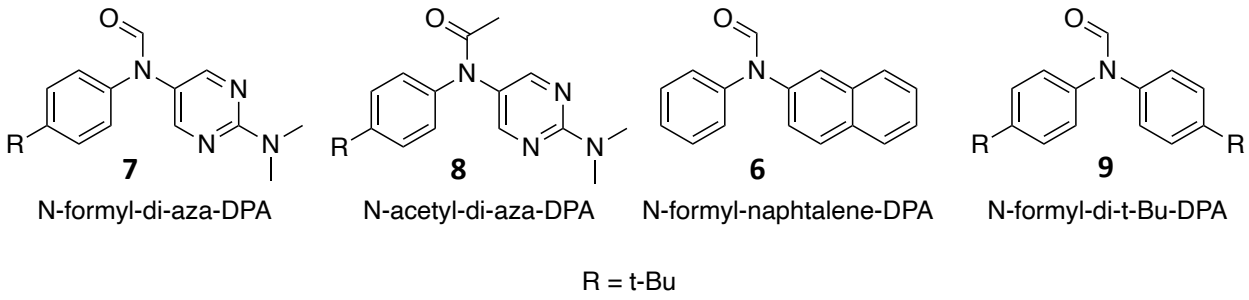

Figure 3.11 – Scope of other protected aminic RTAs tested at 10 mM in *n*-hexadecane high-temperature autoxidations.

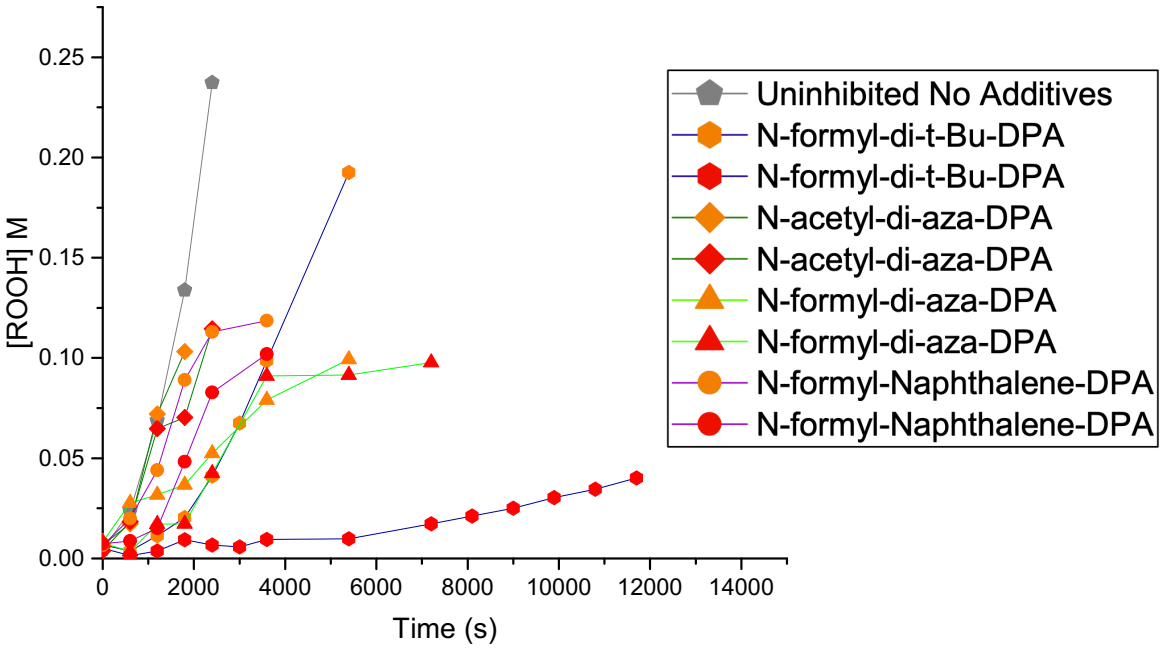

Figure 3.12 – Hydroperoxide formation from the autoxidation of n-hexadecane at 165 °C in the presence of *N*-formyl-tBu_2-DPA (10 mM with 5% doecanol and 5% dodecanol and 5 mM palmitic acid respectively), *N*-acetyl-di-aza-DPA (10 mM with 5% doecanol and 5% dodecanol and 5 mM palmitic acid respectively), *N*-formyl-di-aza-DPA (10 mM with 5% doecanol and 5% dodecanol and 5 mM palmitic acid respectively) and *N*-formyl-Naphthelene-DPA (10 mM with 5% doecanol and 5% dodecanol and 5 mM palmitic acid respectively). Dod = dodecanol, BA = both additives. Red symbols indicate the presence of 5% doecanol and 5 mM palmitic acid and orange symbols indicate the presence of just 5% dodecanol.

3.2.2 – Electronic Effects and Their Influence on Release of Protected RTAs

The observation that *N*-formyl-PNX is deformylated faster than *N*-formyl-PTZ, and that performance of *N*-formyl-PNX relative to PNX is very different from *N*-formyl-PTZ relative to PTZ suggests that the electronic differences can have a significant impact on latent RTA activity. Thus, we sought to investigate how systematic changes in the electronics of the PNX and PTZ rings impact the activity of the *N*-formylated derivatives. We synthesized PNX and PTZ derivatives with either a methoxy substituent as an electron-donating group (EDG) or a trifluoromethyl substituent as an electron-withdrawing group (EWG) at the 3-position (*para* to the amine) to enable assessment of electronic effects unimpacted by steric effects.

The substituted *N*-formyl-PNX derivatives were prepared as shown in **Scheme 3.2**. In general, a phenol undergoes an S_NAr reaction with a nitro-aryl derivative where the EDG or EWG is *para* to the nitro group with the halogen *ortho* to the nitro group. The nitro group is then reduced to an amine on the diarylether intermediate, where the crude product is then

formylated using formic acid. The formylated intermediate is then subjected to CuI-catalyzed Ullmann-type C-N cross-coupling conditions to afford the desired products.

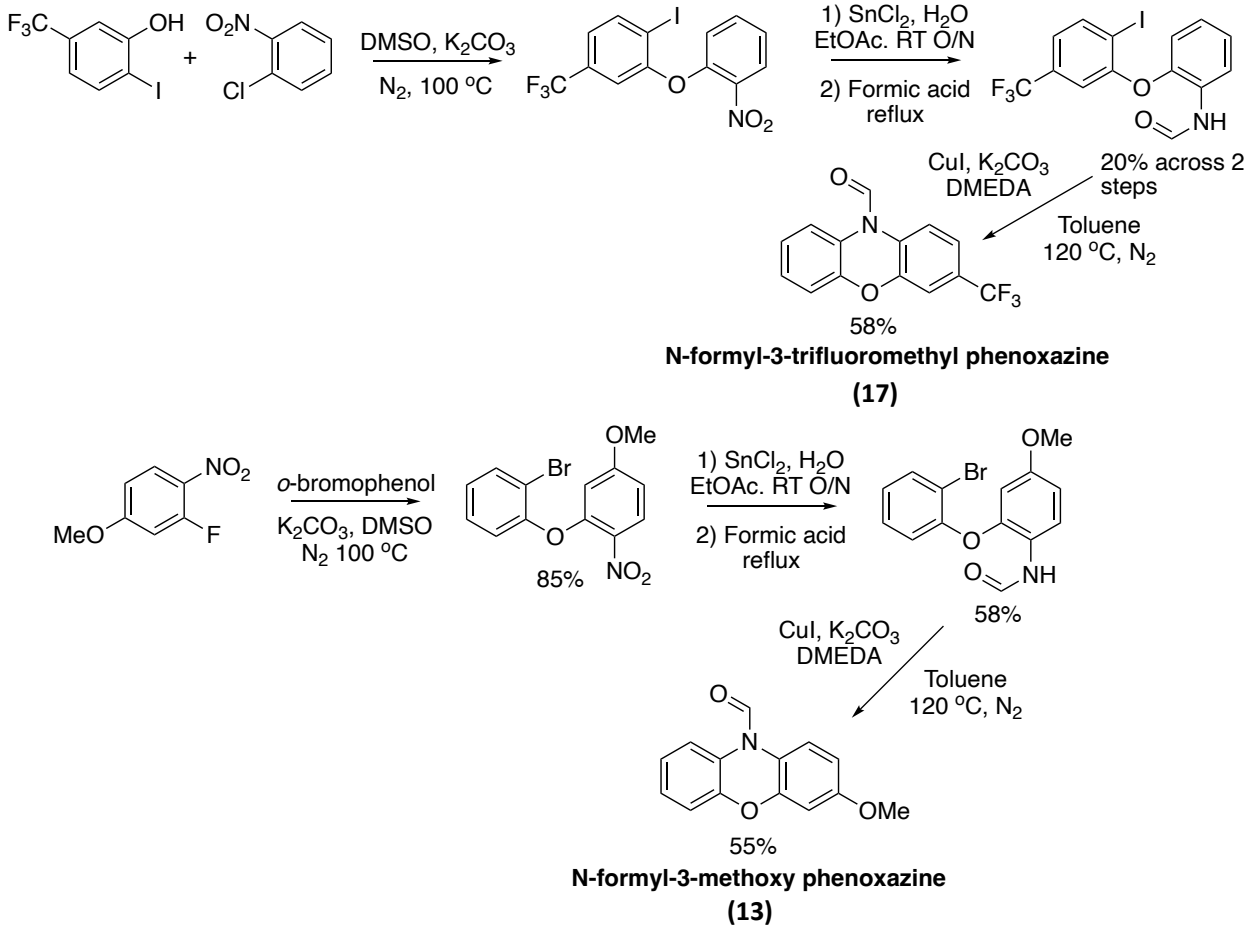

Scheme 3.2 – Synthetic approaches to *N*-formyl-3-CF_3-PNX and *N*-formyl-3-OCH_3-PNX.

With these derivatives in hand, and to better understand how cleavage rates contribute to efficacy in inhibited autoxidations, we quantified PNX formation under the *n*-hexadecane autoxidation conditions (with additives) under N_2. The data, which was determined by HPLC/UV analysis of samples withdrawn periodically from reaction mixtures are presented in **Figure 3.13.** They reveal the expected trends in that the methoxy substituent slows deformylation while the trifluoromethyl substituent accelerates it – consistent with their impact on the electrophilicity of the formyl group. However, importantly, the difference is relatively modest – as the half-lives

of the unsubstituted-, methoxy- and trifluoromethyl-N-formyl-PNX's are 11 h, 26 h and 4.5 h, respectively.

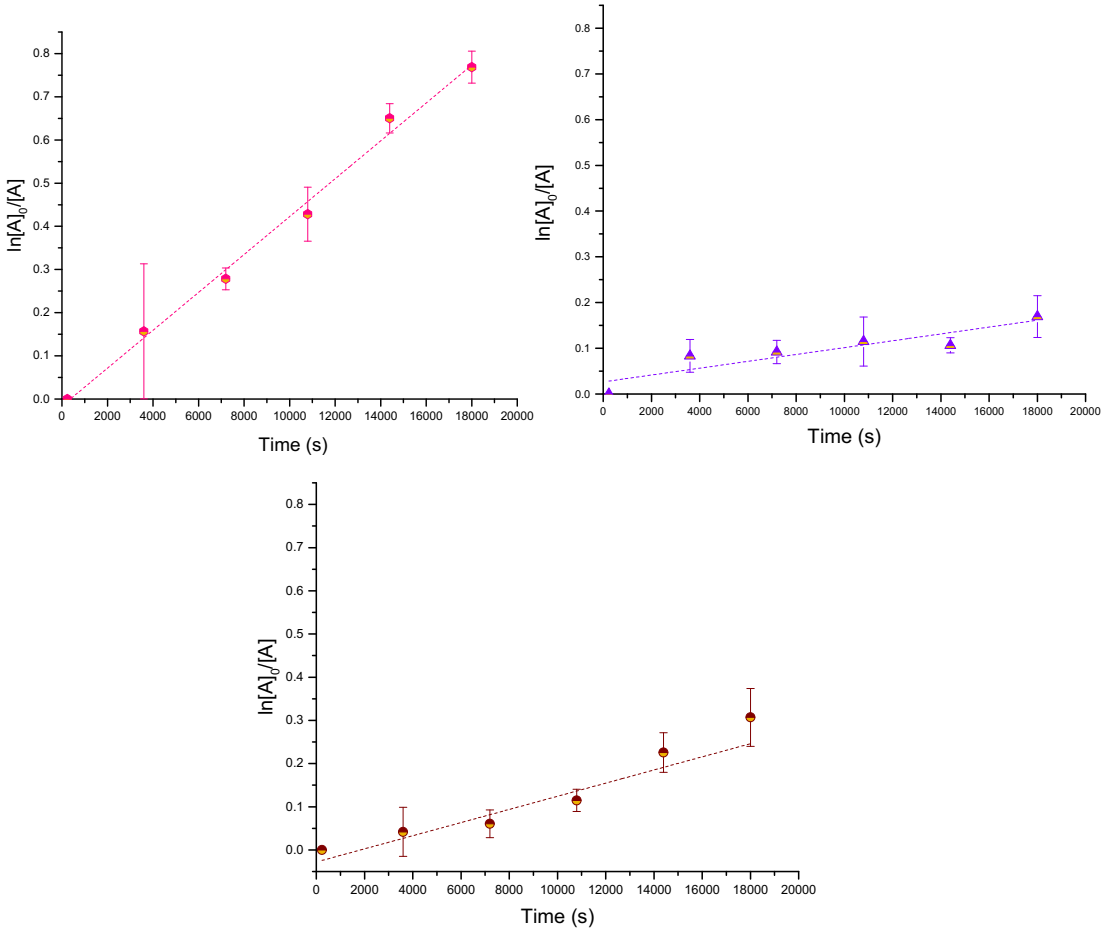

Figure 3.13 – (Top Left) Formation of CF_3-PNX from 500 μM 3-CF_3-*N*-formyl-PNX (**17**) in *n*-hexadecane containing 5% dodecanol and 5 mM palmitic acid at 165 °C under N_2. **(Top right)** Formation of 3-OMe-PNX from 500 μM 3-OMe-*N*-formyl-PNX (**13**) in *n*-hexadecane containing 5% dodecanol and 5 mM palmitic acid at 165 °C under N_2. **(Bottom)** Formation of PNX from 500 μM *N*-formyl-PNX in *n*-hexadecane containing 5% dodecanol and 5 mM palmitic acid at 165 °C under N_2. Average of measurements made in duplicate shown.

In inhibited autoxidations (**Figure 3.14**), **17** afforded an inhibited period of ~5 h 45, while adding 5 mM of palmitic acid to the system reduced the inhibited period to ~4 h 45. Despite having shorter inhibited periods than **13** and **4** (with additives), **17** does have the ability to release without the addition of acid, requiring only dodecanol. The slowest to release of the

set is **13** ($t_{1/2}$ = 26 h), and like **4** ($t_{1/2}$ = 11 h), it shows little to no efficacy without the addition of both palmitic acid and dodecanol to the system. However, despite releasing the slowest, its t_{inh} is > 5.5 h, fully supressing autoxidation for the duration of the experiment. This is somewhat remarkable because one may have anticipated that the release rate is key to keep up with the autoxidation. However, cleavage seems to be fast enough to be effective and additionally the methoxy group is able to weaken the N-H bond by donating electron density, making the liberated compound more reactive towards HAT. Unsubstituted *N*-formyl-PNX also supressed autoxidation fully for the duration of the experiment when both palmitic acid and dodecanol

were added. A summary of inhibited periods and half-lives of the *N*-formyl protected PNXs are given in **Table 3.2**

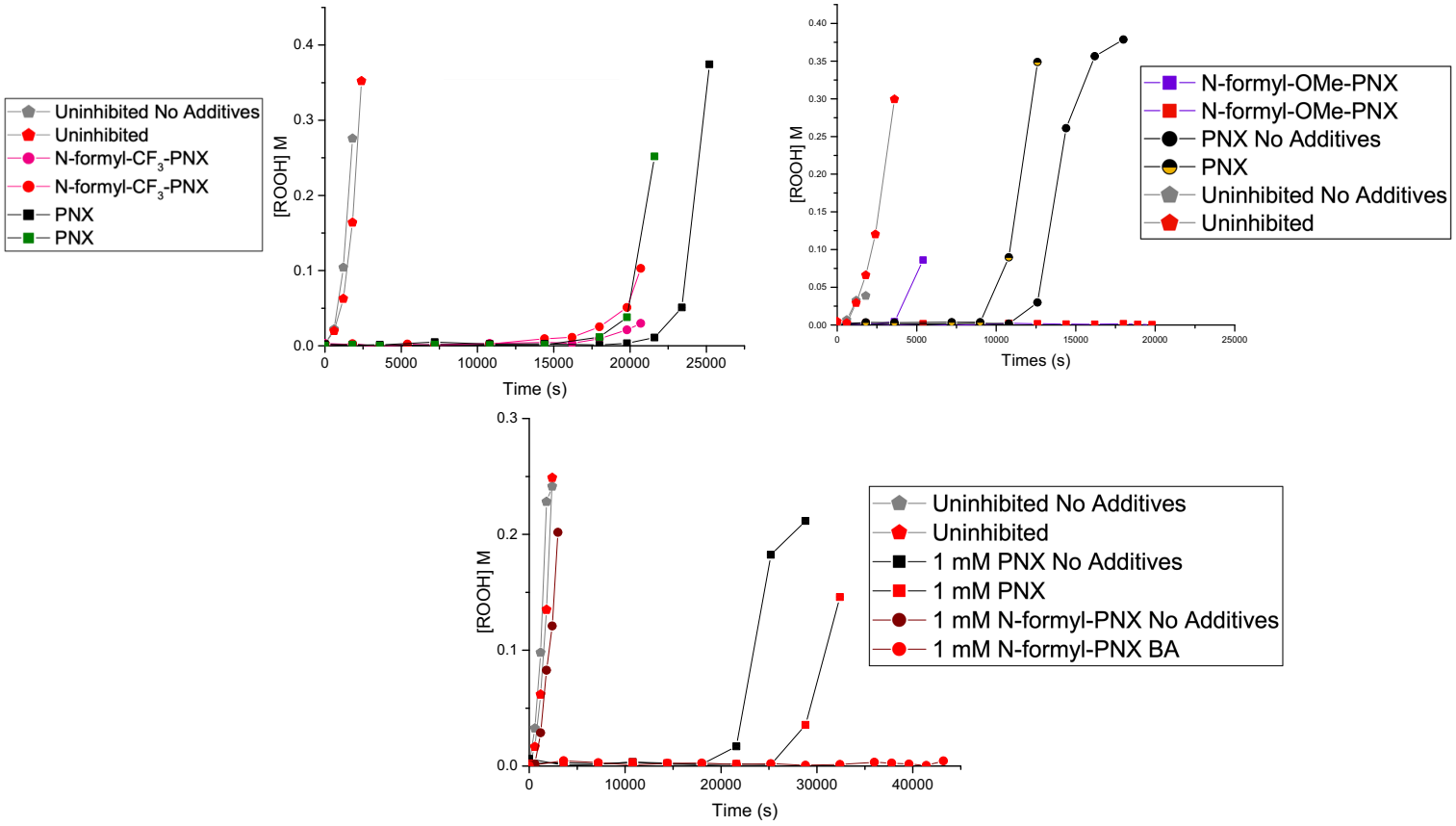

Figure 3.14 – Hydroperoxide formation in an *n*-hexadecane autoxidation in the presence of 1 mM of *N*-formyl-3-CF_3-PNX (top left), *N*-formyl-PNX (top right), *N*-formyl-3-OMe-PNX (bottom) (with dodecanol and with both additives) at 165 °C. (Dod = just dodecanol, BA = both dodecanol and acid). Red Symbols Indicating the presence of 5% dodecanol and 5 mM palmitic acid and green symbols indicating the presence of 5 mM palmitic acid.

Visual inspection of the autoxidations provides additional insight into the advantages of the latent RTAs. PNX-inhibited autoxidations become purple immediately upon switching the gas flow from N_2 to O_2 due to the formation of the PNX-nitroxide, while *N*-formyl-PNX-inhibited autoxidations do not show this colour immediately. At about 10 minutes there is a faint colour which intensifies ever so slightly at 60 minutes (**Figure 3.15**), but it is nowhere near the intensity of the purple colour for the tubes which contain free PNX. In the autoxidations inhibited by **13** at 1 mM, after >5.5 h of inihbition time, there is only a mild development of purple colour (**Figure 3.16**). This is unique for autoxidations inhibited by PNX, as even at concentrations in the μM range, the purple colour arising from nitroxide formation is still very prominent.

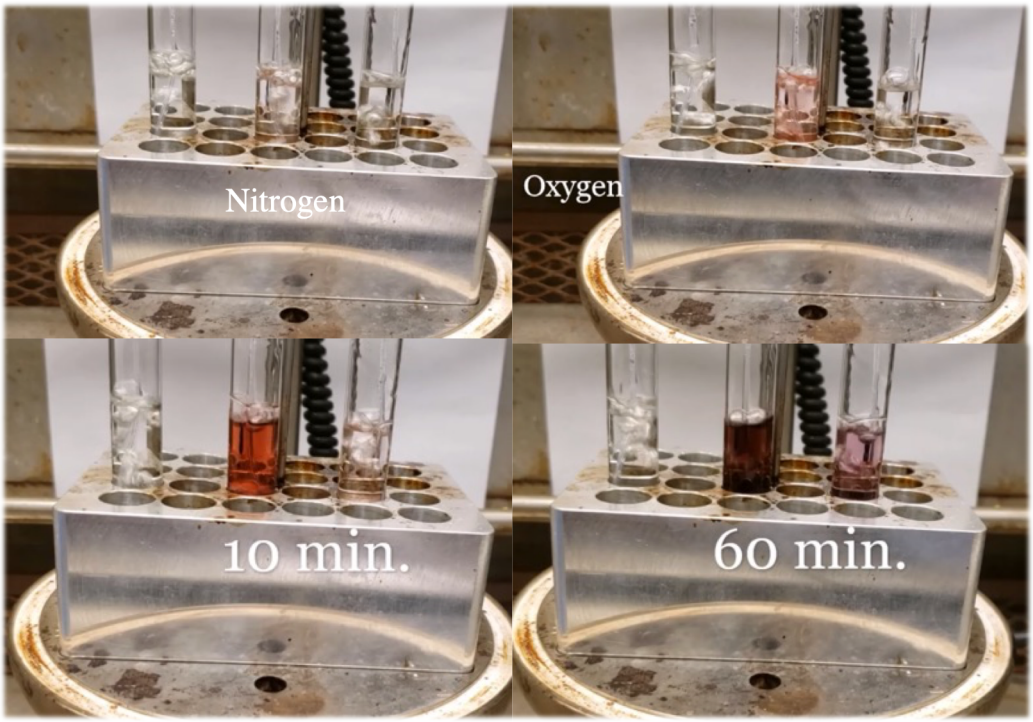

Figure 3.15 – Appearance of *n*-hexadecane autoxidation samples in the presence of no inhibitor (left tube), 1 mM PNX (middle tube) and 1 mM of N-formyl-PNX (right tube). The purple colour is characteristic of PNX-nitroxide. Thus, the protecting group limits the amount of free PNX, therefore the oil has less purple colour.

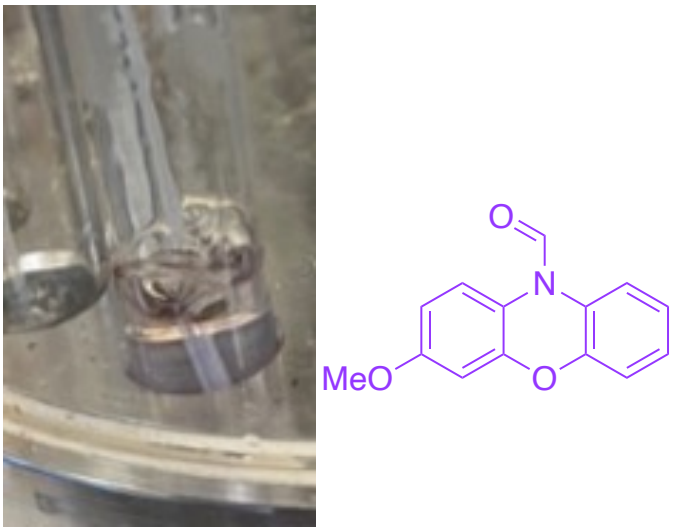

Figure 3.16 – Appearance of *n*-hexadecane autoxidation samples inhibited by 1 mM of **13**, at ~5.5 h.

We next carried out analogous structure-reactivity studies on the *N*-formyl-PTZ derivatives. Again, 3-OMe and 3-CF_3 were chosen as the substituents, and the compounds were synthesised as shown in **Scheme 3.3**.

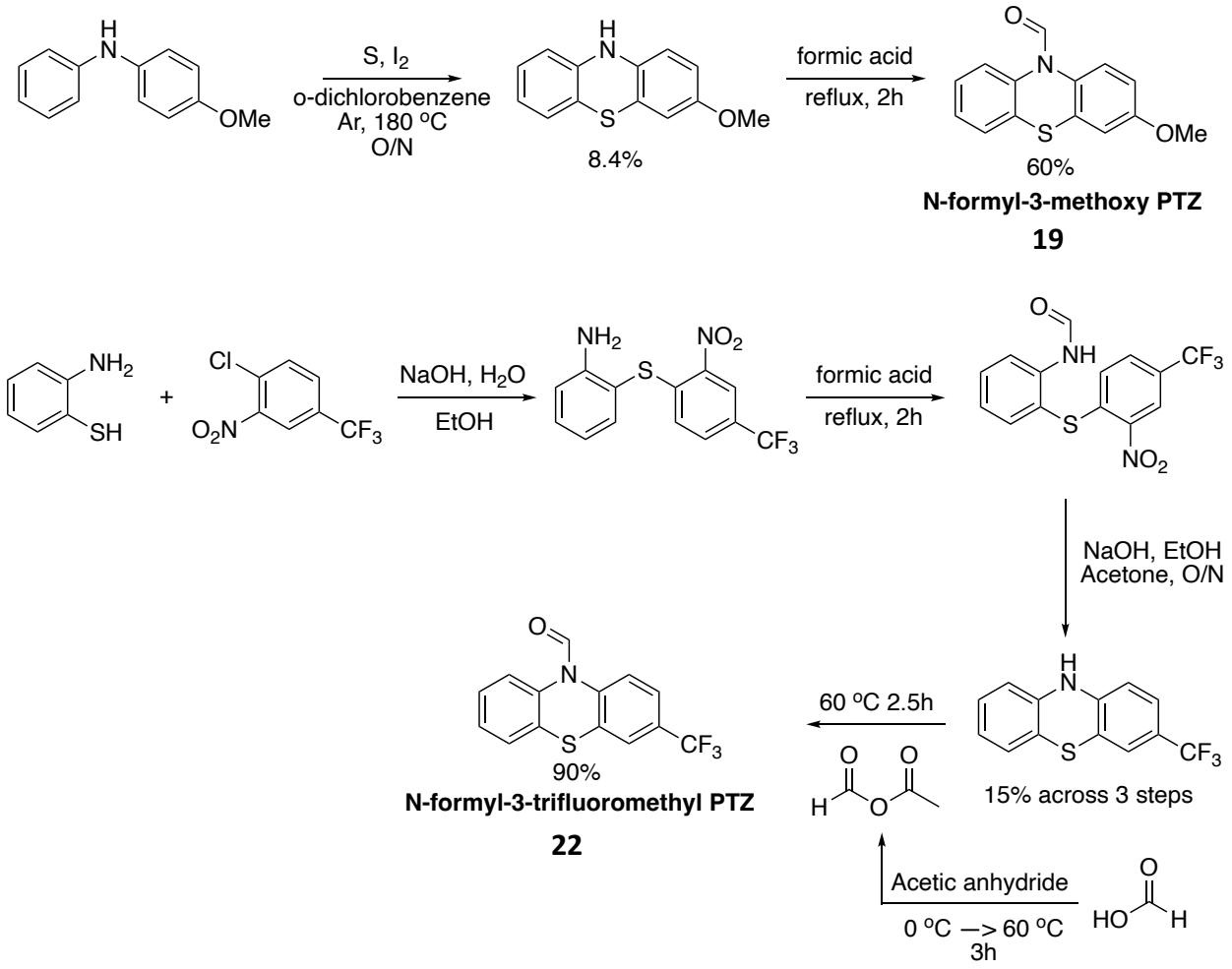

Scheme 3.3 – Synthetic approaches to **19** and **22.**

Similarly to the PNX derivatives, trifluoromethylated **22** ($t_{1/2}$ = 55 h with just dodecanol and $t_{1/2}$ = 36 h with both additives) was the fastest releasing of the *N*-formyl PTZs. Unlike the *N*-formyl-PNXs, this would appear to be most desirable as PTZ is less reactive towards oxygen and the *N*-formyl-PTZ derivatives transformylate more slowly compared to the *N*-formyl-PNXs, i.e. the fastest cleaving *N*-formyl-PTZ has a half-life that is 7 h longer than the slowest *N*-formyl-

PNX, thus there is less free PTZ at the same concentrations. The inhibited period observed in the presence of **19** was ~2 h ($t_{1/2}$ = 49 h), which is 90 minutes less than that observed for **3** (a t_{inh} of ~3.5 h) (**Figures 3.17** and **3.19**). The longest inhibiting *N*-formyl-PTZ was **22**, which inhibited for 4 h with just dodecnaol and 5.5 h with acid and dodecanol (**Figure 3.18**).

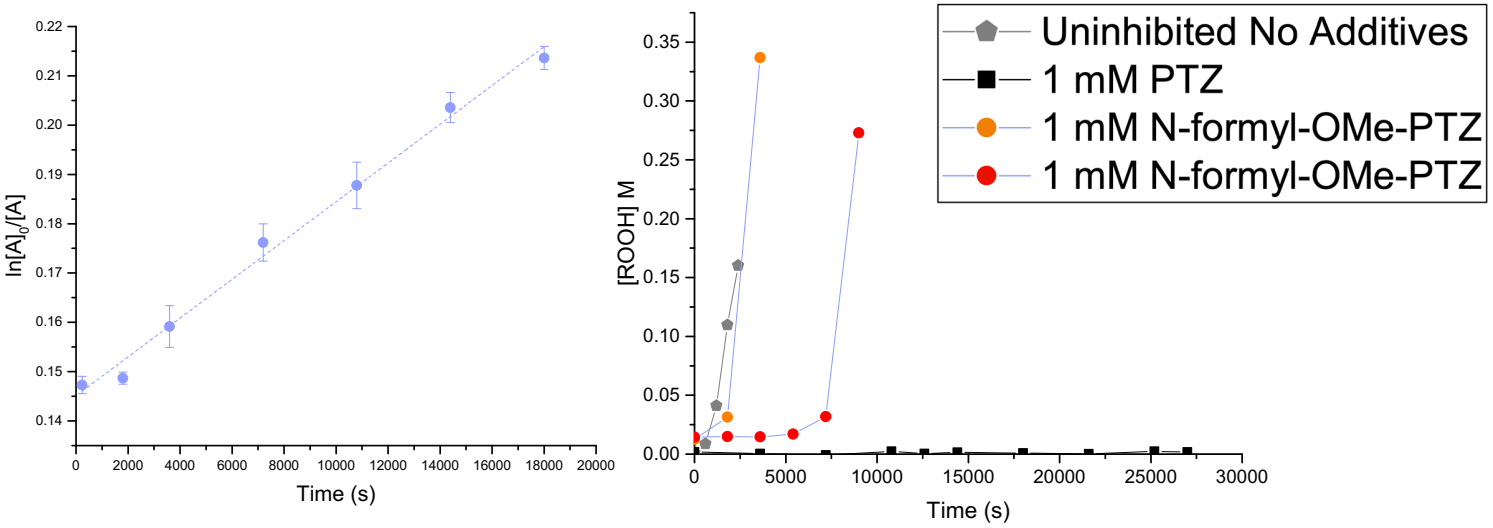

Figure 3.17 – (Left) Formation of OMe-PTZ from 500 μM **19** in *n*-hexadecane containing 5% dodecanol and 5 mM palmitic acid at 165 °C under N_2 (average of measurements made in triplicate shown). **(Right)** Hydroperoxide formation in a representative *n*-hexadecane autoxidation in the presence of 1 mM of **19** and either dodecanol or dodecanol and palmitic acid at 165 °C. Red symbols indicating the presence of 5% dodecanol and 5 mM palmitic acid and orange symbols indicating the presence of 5% dodecanol.

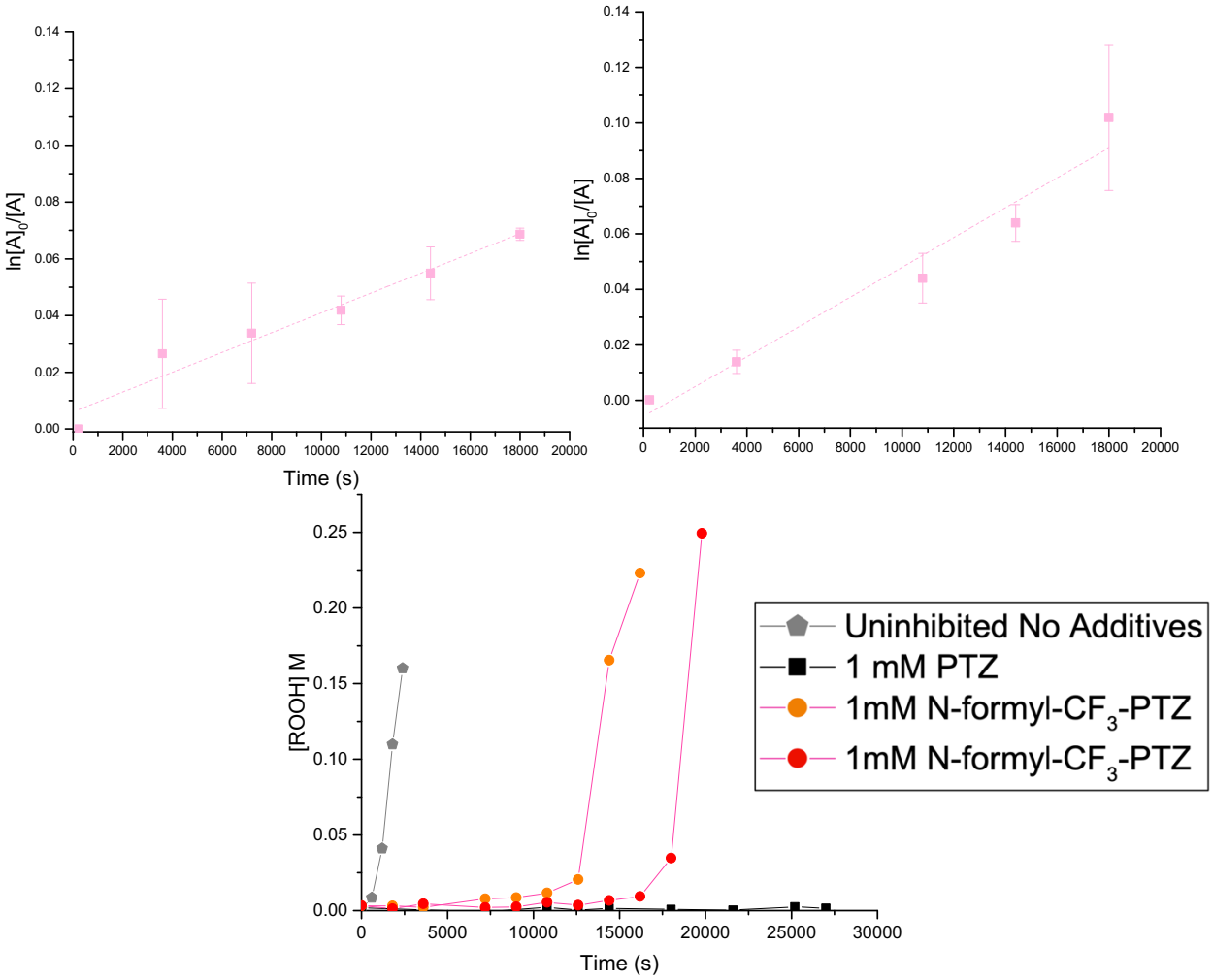

Figure 3.18 – Formation of CF_3-PTZ from 500 μM **22** in in *n*-hexadecane at 165 °C under N_2 in the presence of either 5% dodecanol **(Top Left)** or 5% dodecanol and 5 mM palmitic acid **(Top Right)** (average of measurements made in triplicate shown). **(Bottom)** Hydroperoxide formation in a representative *n*-hexadecane autoxidation in the presence of 1 mM of **22** and either dodecanol or dodecanol and palmitic acid at 165 °C. Red symbols indicating the presence of 5% dodecanol and 5 mM of palmitic acid and orange symbols indicating the presence 5% dodecanol.

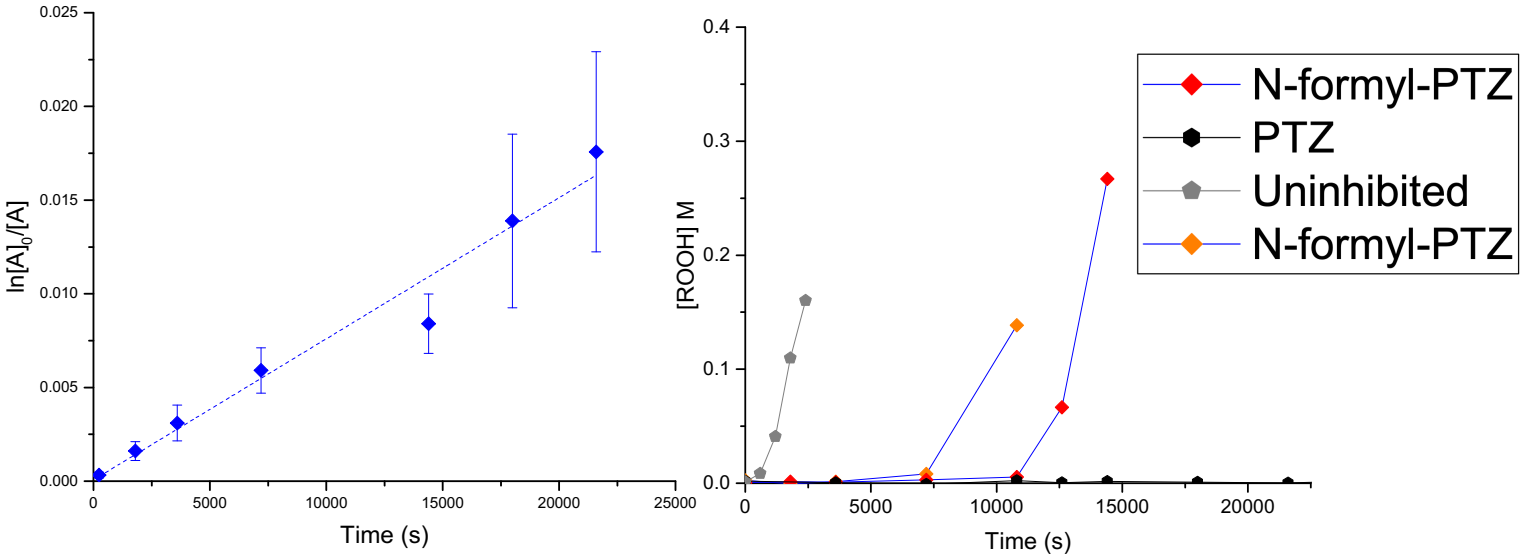

Figure 3.19 – (Left) Formation of PTZ from 500 μM **3** in *n*-hexadecane containing 5% dodecanol and 5 mM palmitic acid at 165 °C under N_2 (average of measurements made in duplicate shown). (**Right**) Hydroperoxide formation in a representative *n*-hexadecane autoxidation in the presence of 1 mM of **3** and either dodecanol or dodecanol and palmitic acid at 165 °C. Red symbols indicating the presence of 5% dodecanol and 5 mM of palmitic acid and orange symbols indicating the presence 5% dodecanol.

Table 3.2 – Summary of inhibited periods, pseudo-first order rate constants for deformylation and corresponding half-lives for the *N*-formyl-protected PNXs and PTZs.

Compound	t_{inh} (dodecanol) 1 mM	t_{inh} (dodecanol & acid) 1 mM	k_{obs} (dodecanol) s^{-1} 500 μM	k_{obs} (dodecanol & acid) s^{-1} 500 μM	$t_{1/2}$ (no acid)	$t_{1/2}$ (with acid)
N-formyl-PNX	< 1 h	> 7 h	Too slow	1.7×10^{-5}	---	11 h
N-formyl-OMe-PNX	< 1 h	> 7 h	Too slow	7.5×10^{-6}	---	26 h
N-formyl-CF_3-PNX	5.5 h	5.5 h	Too slow	4.3×10^{-5}	---	4.5 h
N-formyl-PTZ	2 h	3.5 h	Too slow	7.5×10^{-7}	---	255 h
N-formyl-OMe-PTZ	< 10 min	2 h	Too slow	3.9×10^{-6}	---	49 h
N-formyl-CF_3-PTZ	4 h	5.5 h	3.49×10^{-6}	5.4×10^{-6}	55 h	36 h
N-formyl-3-sulfonamide-7-methyl-PTZ	4 h	6 h	---	---	---	---

3.2.3 – Acylated PNXs and PTZs with Pendant Nucleophiles as RTAs

In order to subvert the requirement for an added nucleophile to liberate the RTA from its acylated precursor, we envisioned that a nucleophile could be tethered to the *N*-acyl group where activation would now be an intramolecular process (**Scheme 3.4**). Although the *N*-acetylated PNX and PTZ derivatives were initially found to be deacylated very slowly (**Figure 3.5**), we hypothesized that the intramolecular cleavage could make up the difference due to the lower entropic barrier.

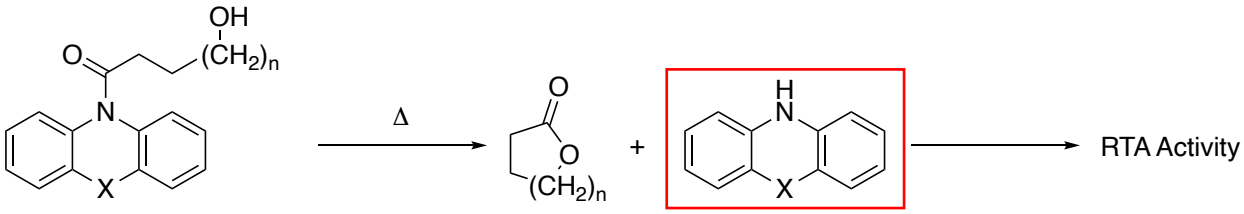

Scheme 3.4 – Proposed cleavage of acyl protecting groups on PTZ/PNX using a pendant nucleophile, generating free RTA and a lactone.

To evaluate the entropic effects on the cleavage of acylated-PTZ and acylated-PNX, we set out to prepare the series of compounds shown in **Figure 3.20**, which feature varying chain lengths of the tethered nucleophiles and are expected to release RTA along with the formation of γ-butyrolactone (from the 5R-compounds), δ-valerolactone (from the 6R-compounds) and ε-caprolactone (from the 7R-compounds). The various lactones are expected to be innocuous, simply remaining in solution as their boiling points are 204 °C, 230 °C and 241 °C respectively.

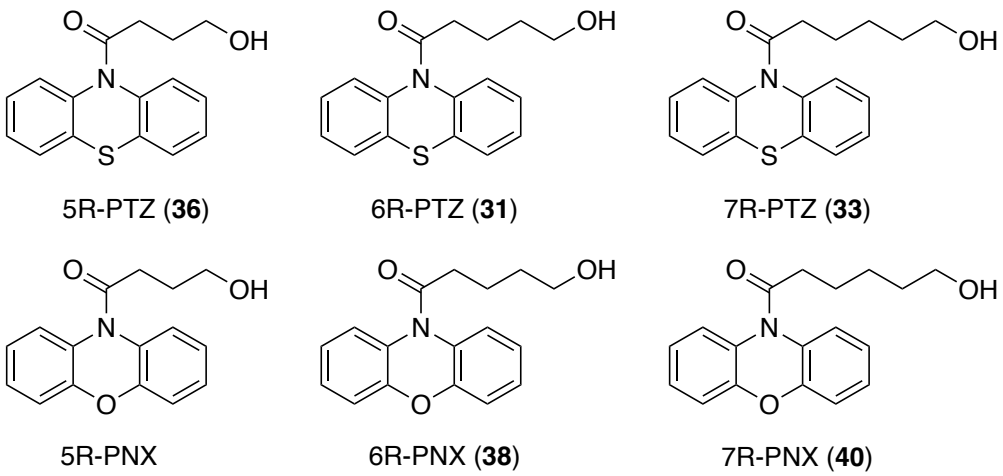

Figure 3.20 – Acylated PTZs and PNXs with pendant nucleophiles.

To synthesize the acylating agents with pendant nucleophiles, a procedure from Heathcock et al's 1992 paper was followed to synthesize the 'tethers' of varying lengths. Beginning from the desired diol each step was carried forward with the crude product (as per the procedure) eventually forming a tether with an acid chloride on one side (where the RTA can be attached) and a benzyloxy protecting group on the other side (to mask the nucleophile during synthesis).[58] Thus, the 5R-derivatives were synthesized from benzyloxy-butanoic acid, while the synthesis of the 6R and 7R-derivatives began from the appropriate diols (**Schemes 3.5 & 3.6**). The PNX-based pendant nucleophile derivatives had a slightly different synthetic route

when reacting PNX with the acyl chloride as, using DMAP was less effective than deprotonating the amine with n-BuLi, then adding the acyl chloride.

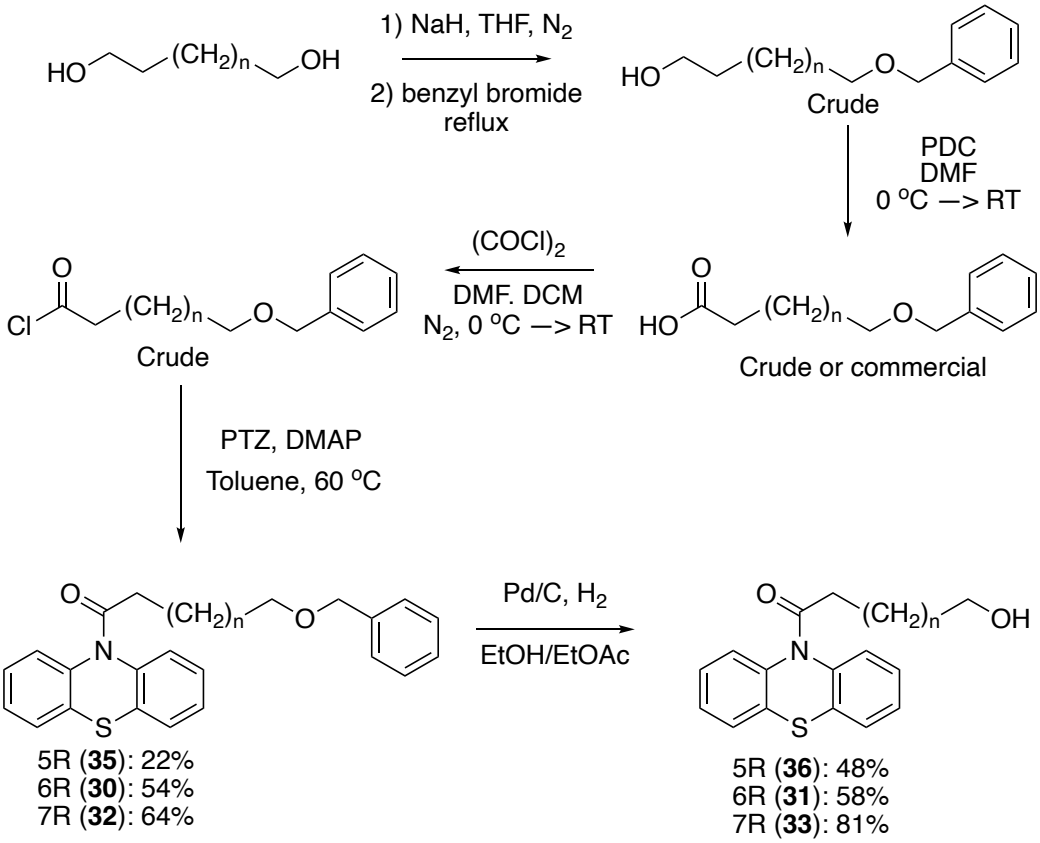

Scheme 3.5 – Synthetic approaches to 5R-PTZ, 6R-PTZ and 7R-PTZ.

Synthesizing the 5R-PNX derivative was unfortunately not attainable due to its reactivity, even with the benzyloxy protecting group. To confirm that the acyl chloride was made, we successfully synthesized it using oxalyl chloride or thionyl chloride and reacted each with MeOH to form the ester and isolated for an NMR. We hypothesize that the benzyloxy protecting group is too reactive itself and therefore attacks the carbonyl to yield PNX, benzyl alcohol or benzyl chloride (visible via NMR) with no trace of the starting material. One last synthetic route was attempted where PNX was reacted with methyl 4-chloro-oxo-butyrate to

yield an *N*-acyl-PNX with a pendant ester that could be reduced**.** The ester was then hydrolyzed to the acid using LiOH. However, upon treatment with borane-THF, only PNX was isolated, suggesting that cyclization occurs directly upon reduction to the alcohol.

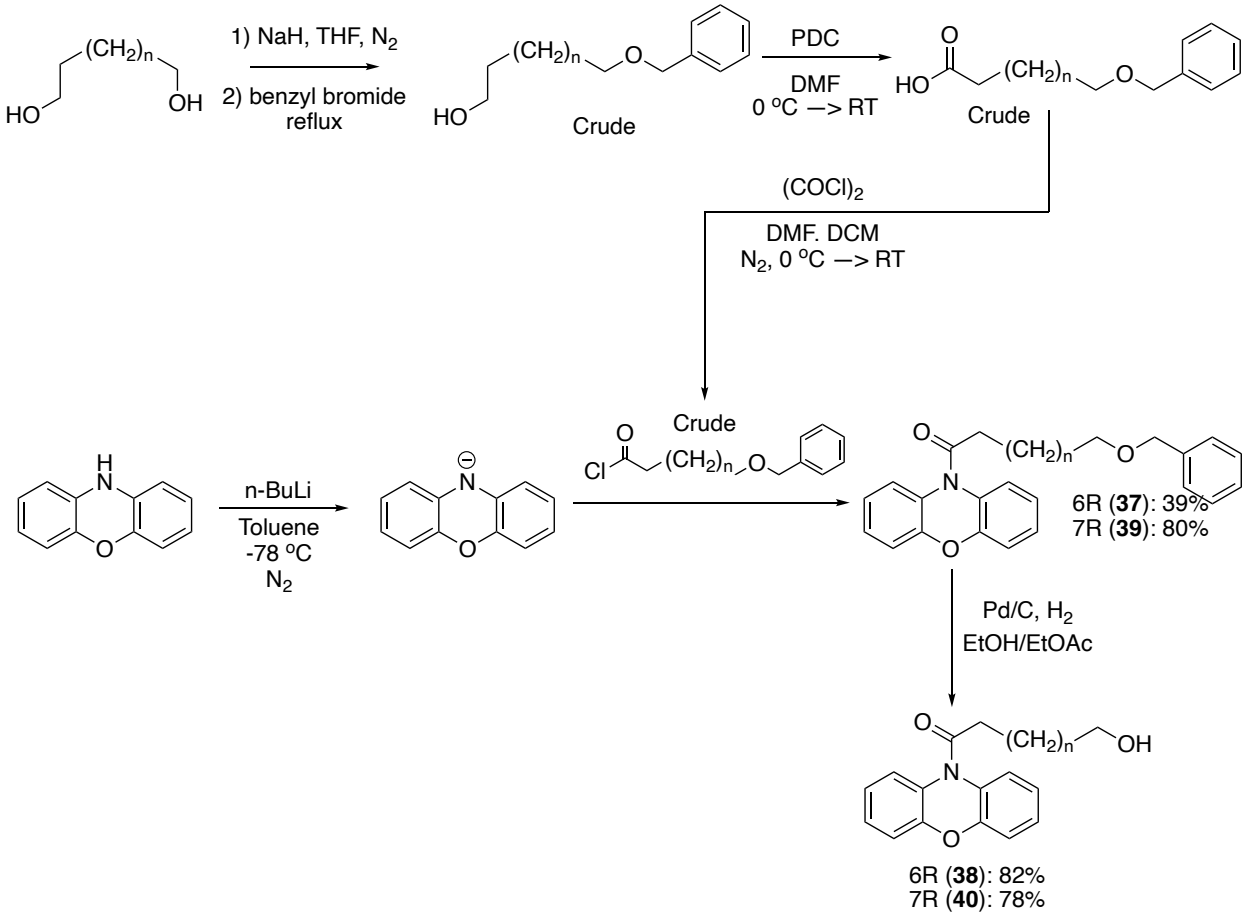

Scheme 3.6 – Synthetic approaches to **38** and **40**.

3.2.4 – Performance of Acyl-RTAs With Pendant Nucleophiles

The acyl-RTAs with pendant nucleophiles showed very promising activity, being competitive with the parent amines, or even outperforming them. Compound **40** showed modest efficacy without added acid (t_{inh} ~1 h) (**Figure 3.21 - Bottom**); which doubled in the presence of palmitic acid (~2 h). Compound **38** fared much better than **40** such that without acid, it inhibited for ~3 h, and with acid it even outcompeted free PNX by suppressing

autoxidation for >4.5 h. When attempting to determine half-lives of the acylated derivatives, the only two scenarios where kinetic data could be obtained were for **40** (with acid) which had a $t_{1/2}$ = 96 h and **38** (without acid) which had a $t_{1/2}$ = 53 h. Both **40** (without acid) and **38** (with acid) were deacylated too slowly and too quickly, respectively, to obtain reliable data. *N*-acetyl-PNX (**42**) inhibited for 20-30 minutes with and without acid (with dodecanol), and was used in these assays as a control for comparing intramolecular and intermolecular acyl group cleavage.

The acyl-PTZs with pendant nucleophiles also showed promising activity. Similarly to the acylated-PNXs, **41** and **33** showed only modest, if any, RTA activity – inhibiting for less than 1 h with and without added acid. However, **31** and **36** showed excellent potency with and without acid, suppressing autoxidation longer than their PNX counterparts (**Figure 3.22**). 6R-PTZ inhibited autoxidation for ~7 h – even in the absence of palmitic acid – which is 4 h longer than **38** without acid and 2.5 h longer than **38** with acid. This is likely due to too much PNX being released, rather than not enough PNX being released. Compounds **31** (with acid) and **36** (both

with and without acid) have inhibited periods >7.5 h (the duration of the experiment), as does free PTZ at 1mM.

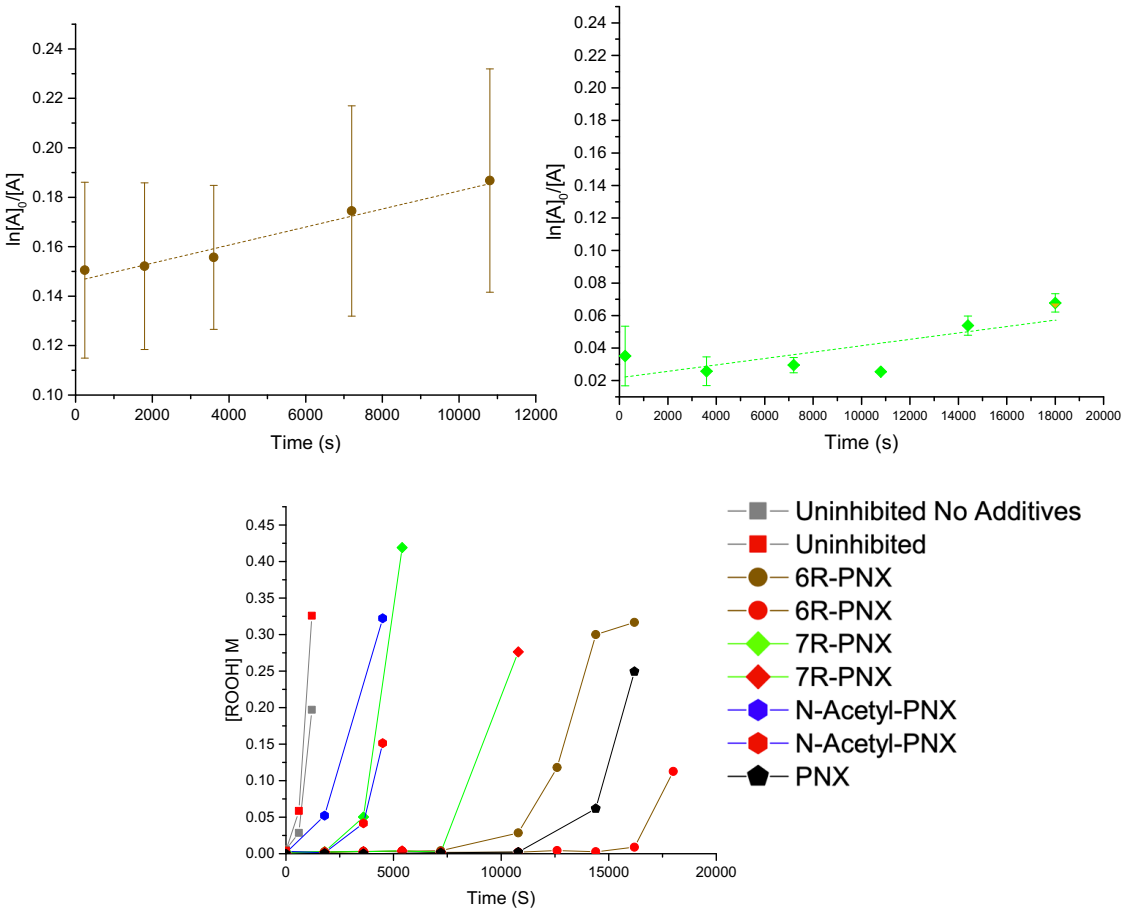

Figure 3.21 – (**Top Left**) Formation of PNX from 500 μM of **38** in *n*-hexadecane at 165 °C under N_2 (**Top Right**) Formation of PNX from 500 μM of **40** in *n*-hexadecane containing 5 mM palmitic acid at 165 °C under N_2 (**Bottom**) Hydroperoxide formation from the autoxidation of *n*-hexadecane at 165 °C in the presence of **38** (1 mM, with and without 5 mM of palmitic acid), **40** (1 mM, with and without 5 mM of palmitic acid) and **42** with dodecanol (5%) (1 mM, with and without 5 mM of palmitic acid). Red symbols indicating the presence of 5 mM palmitic acid.

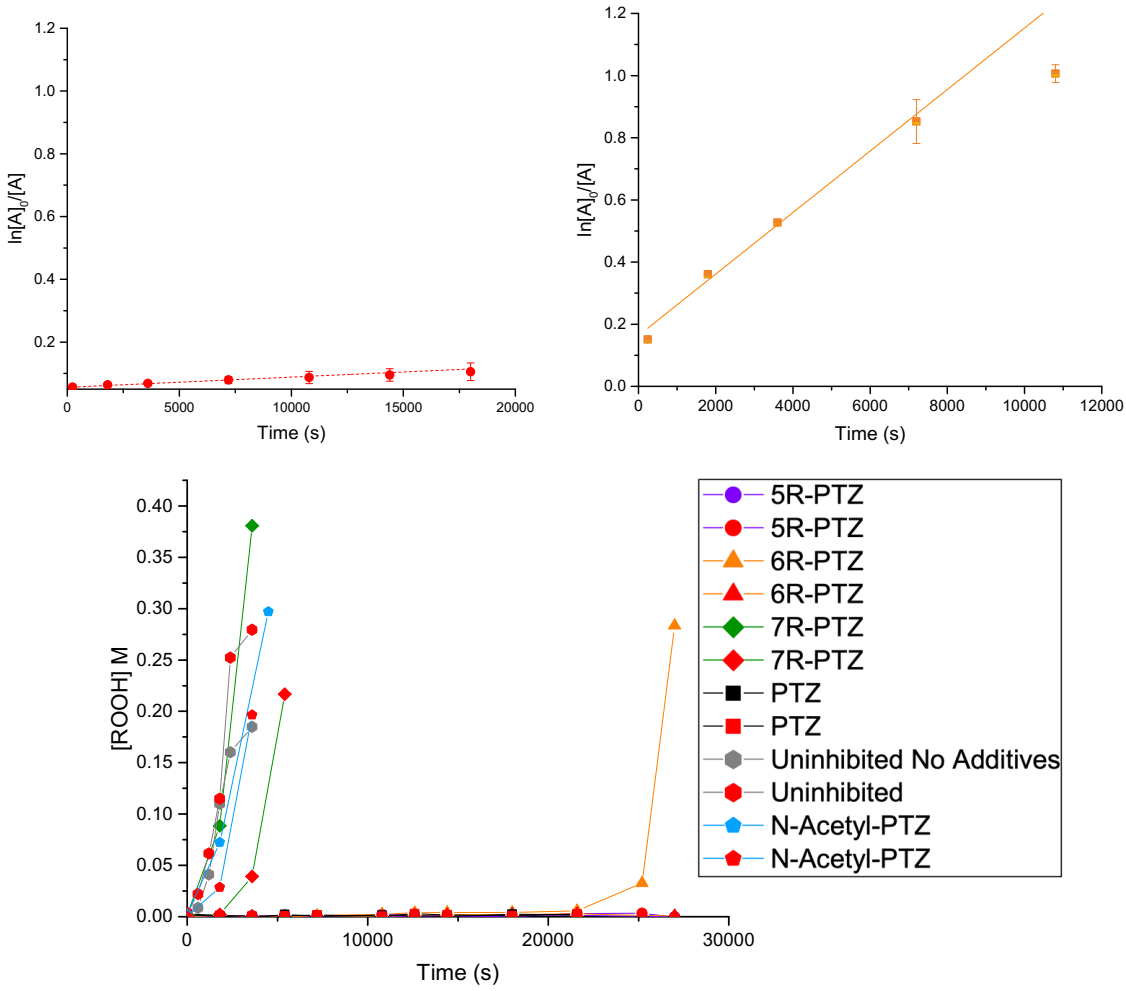

Figure 3.22 – (**Top Left**) Formation of PTZ from 500 μM of **36** in *n*-hexadecane at 165 °C under N_2. (**Top Right**) Formation of PTZ from 500 μM of **33** in *n*-hexadecane containing 5 mM palmitic acid at 165 °C under N_2. (**Bottom**) Hydroperoxide formation from the autoxidation of *n*-hexadecane at 165 °C in the presence of 5R-PTZ (1 mM, with and without 5 mM of palmitic acid), **31** (1 mM, with and without 5 mM of palmitic acid), **33** (1 mM, with and without 5 mM of palmitic acid) and **41** with dodecanol (5%) (1 mM, with and without 5 mM of palmitic acid). Red symbols indicating the presence of 5 mM palmitic acid.

Commpound **36** underwent deacylation in the absence of acid with $t_{1/2}$ = 59 h (very similar to **38**, no acid) (**Figure 3.23**). In contrast, **31** had $t_{1/2}$ = 2 h in the presence of acid. Representative chromatograms of samples taken from these experiments are shown in **Figures 3.23-3.26** and a summary of inhibited periods and deacylation half-lives is given in **Table 3.3**.

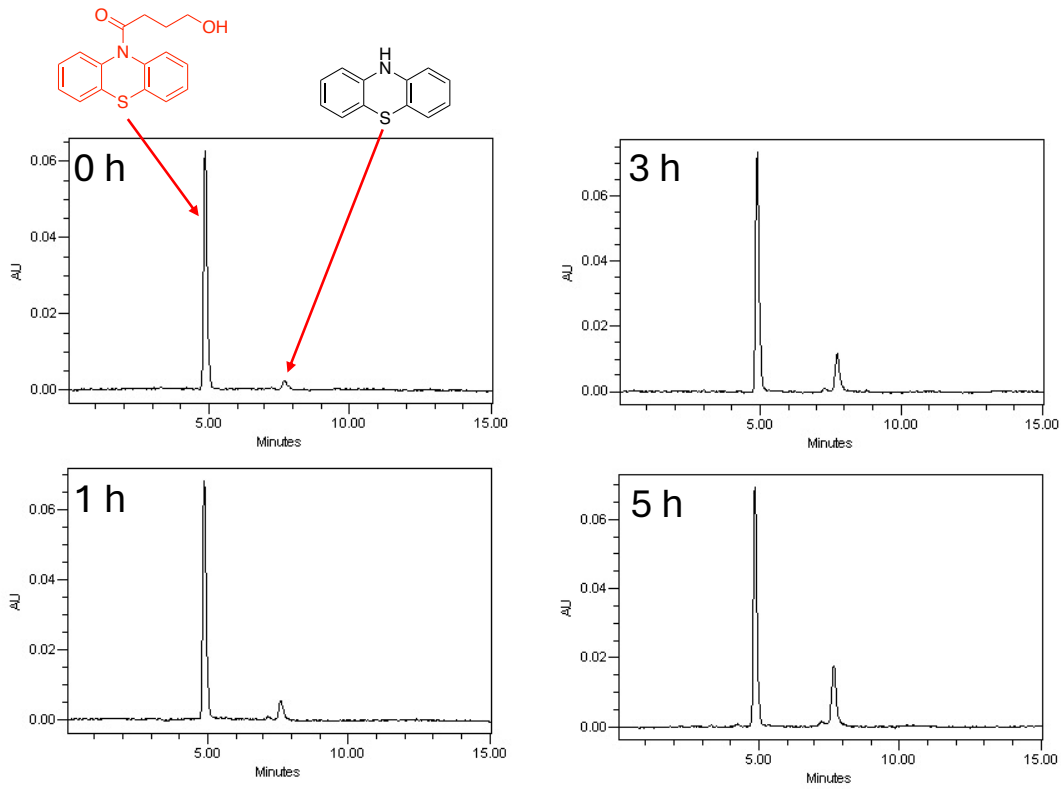

Figure 3.23 – UPLC chromatogram (with detection at 252.5 nm) of the formation of PTZ from 500 μM of 5R-PTZ in *n*-hexadecane at 165 °C in the absence of palmitic acid under N_2 at 0 h, 1 h, 3 h and 5 h.

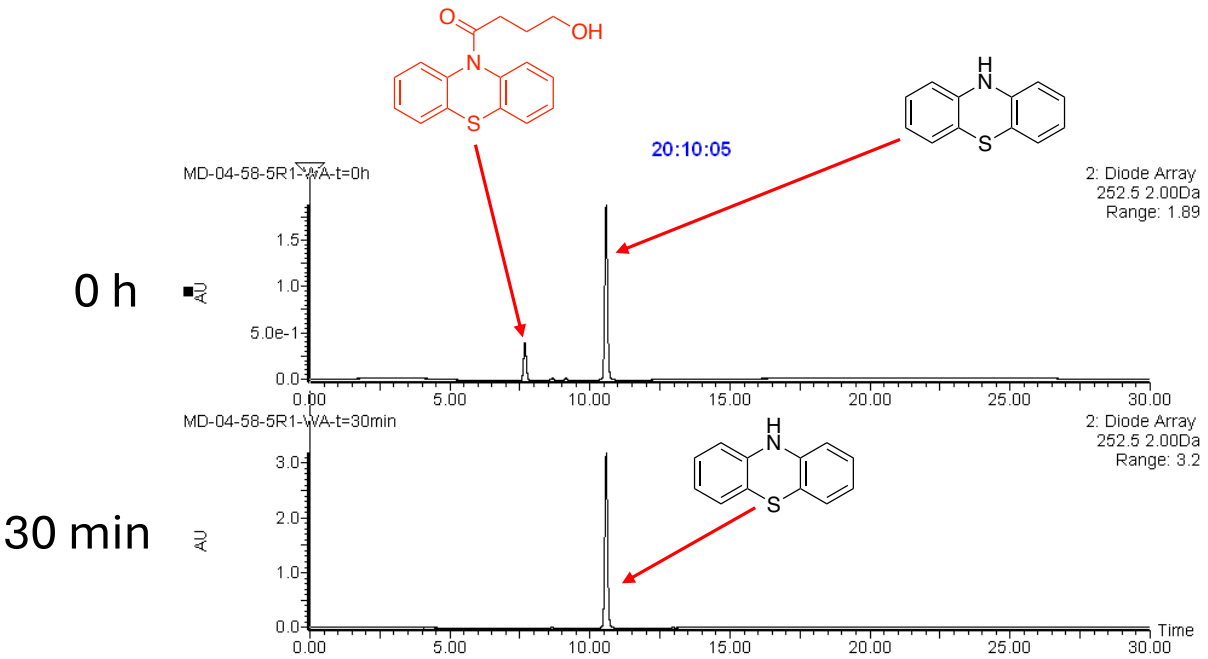

Figure 3.25 – UPLC chromatograms (with detection at 252.5 nm) of the formation of PTZ from 500 μM of 5R-PTZ in *n*-hexadecane at 165 °C with 5 mM of palmitic acid under N_2 at 0 h, and 30 minutes.

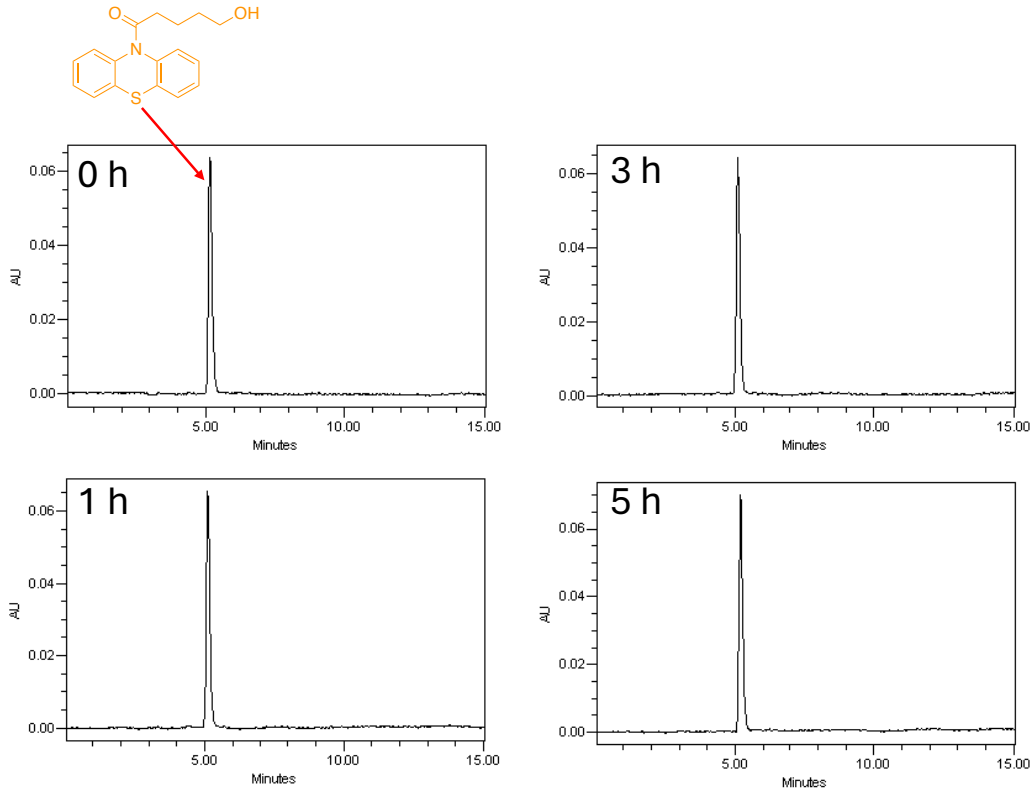

Figure 3.24 –UPLC chromatogram (with detection at 252.5 nm) of the lack of formation of PTZ from 500 μM of 6R-PTZ in *n*-hexadecane at 165 °C with the absence of palmitic acid under N_2 at 0 h, 1 h, 3 h and 5 h.

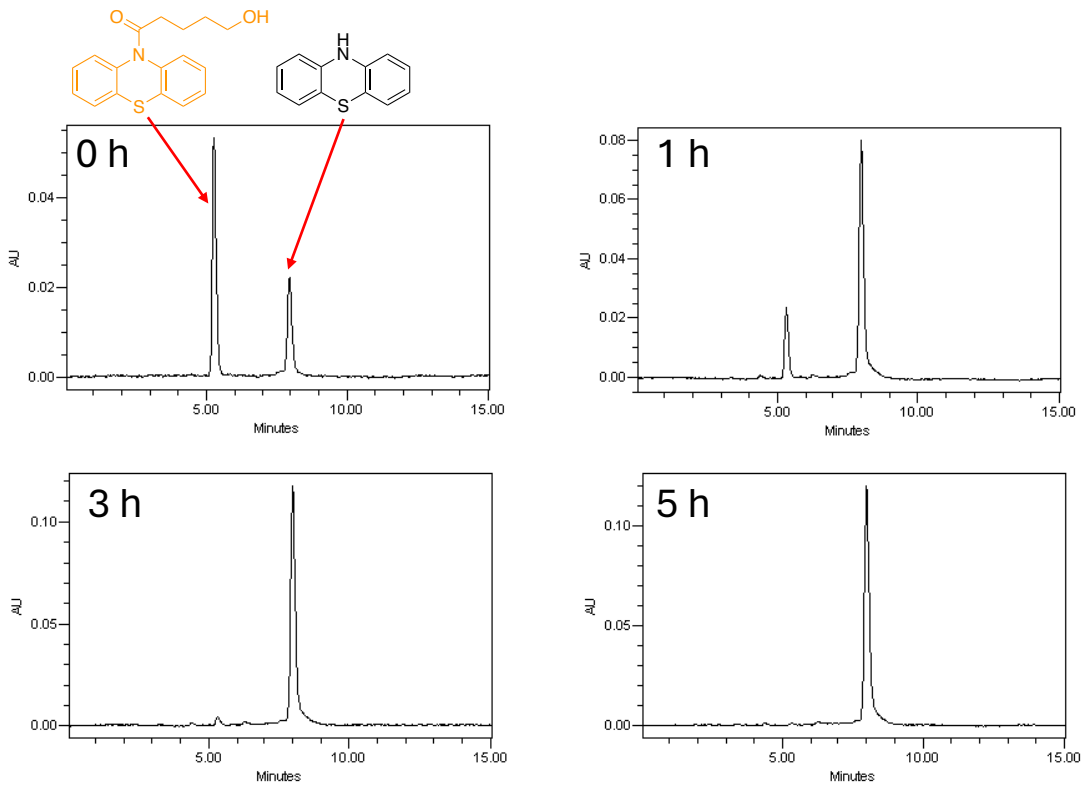

Figure 3.26 – UPLC chromatograms (with detection at 252.5 nm) of the formation of PTZ from 500 µM of 6R-PTZ in *n*-hexadecane at 165 °C with 5 mM of palmitic acid under N_2 at 0 h, 1 h, 3 h and 5 h.

Given the encouraging results with the *N*-acyl-PTZs with pendant nucleophiles, autoxidations inhibited with these compounds at a lower concentration (150 μM) were performed to enable better comparison to free PTZ (**Figure 3.27**). In the absence of acid, **36** inhibited for 4 h, while with acid t_{inh} = 4.5 h (equivalent to free PTZ with acid). The equivalent inhibited periods suggest that deacylation is complete within the initial minutes of the experiment, consistent with the rapid release of **36** in the presence of acid. The shorter inhibited period of **36** in the absence of acid is consistent with this being a little slower. Compound **31** (with acid) also inhibited for 4.5 h (also due to its rapid diacylation – $t_{1/2}$ = 2 h), while without acid protecting group cleavage was too slow to inhibit autoxidation. In the presence and absence of acid **33** did not show any significant inhibition of autoxidation at 150 μM.

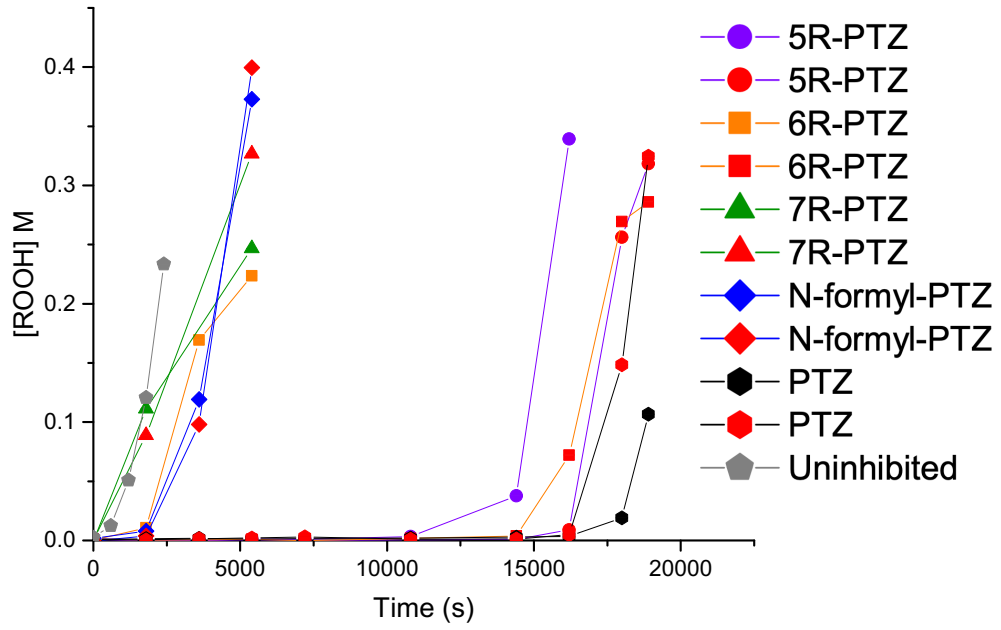

Figure 3.27 – Hydroperoxide formation from the autoxidation of *n*-hexadecane at 165 °C in the presence of 5R-PTZ (150 μM, with and without 5 mM of palmitic acid), 6R-PTZ (150 μM, with and without 5 mM of palmitic acid), and 7R-PTZ (150 μM, with and without 5 mM of palmitic acid).

Table 3.3 – Summary of inhibited periods and rate constants and associated half-lives of diacylation of *N*-acylated PNXs and PTZs with pendant nucleophiles.

Structure	t_{inh} (1 mM) No Acid	t_{inh} (1 mM) w/ 5mM palmitic acid	k_{obs} no acid s^{-1}	k_{obs} (5 mM palmitic acid) s^{-1}	$t_{1/2}$ (no acid)	$t_{1/2}$ (with acid)
5R-PTZ	> 7.5 h	> 7.5 h	3.26×10^{-6}	Too fast	59 h	---
6R-PTZ	7 h	> 7.5 h	Too slow	9.9×10^{-5}	---	2 h
7R-PTZ	< 10 min	1 h	Too slow	Too slow	---	---
N-Acetyl-PTZ	< 10 min	< 10 min	---	---	---	---
6R-PNX	3.5 h	4.5 h	3.65×10^{-6}	Too fast	53 h	---
7R-PNX	1 h	2 h	Too slow	1.96×10^{-6}	---	98 h
N-Acetyl-PNX	< 10 min	< 20 min	---	---	---	---

3.2.5 – Expanding Studies to Industrially Relevant Conditions

Despite the formylated PTZs not being able to outcompete the free PTZ derivatives at 1 mM, we proceeded to synthesize a *N*-formyl derivative of 3-$SO_2N(Oct)_2$-7-methyl PTZ to see if there was a qualitative impact, by reducing or eliminating by-products that precipitate out of the *n*-hexadecane. Recall that while 3-$SO_2N(Oct)_2$-7-methyl PTZ was a highly efficacious inhibitor with a t_{inh} of ~6 h 15 when at a concentration of 150 μM in an *n*-hexadecane, it also had the most precipitation visually when used at 10 mM in an *n*-hexadecane autoxidation (**Figure 3.4**). Therefore, we conducted a high-temperature autoxidation where 1 mM of the *N*-formylated 3-$SO_2N(Oct)_2$-7-methyl PTZ (**23**), 1 mM 3-$SO_2N(Oct)_2$-7-methyl PTZ (**2**) and one tube of each compound at a concentration of 10 mM. Compound **23**, at a concentration of 1 mM, inhibited for ~5 h, where it did not outperform **2**, which inhibted for the duration of the

experiment (**Figure 3.28**). The high concentrations of each compound (10 mM) suppressed the autoxidation for the duration of the experiment (> 6 h).

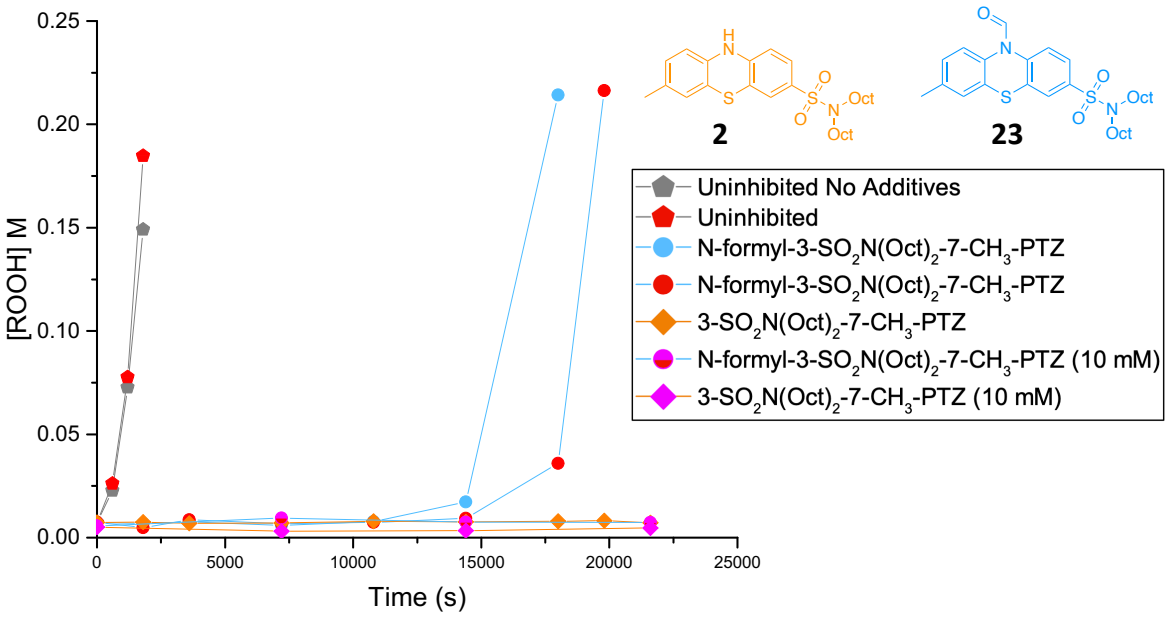

Figure 3.28 – Hydroperoxide formation from the autoxidation of *n*-hexadecane at 165 °C inhibited by *N*-formyl 3-$SO_2N(Oct)_2$-7-CH_3-PTZ and 3-$SO_2N(Oct)_2$-7-CH_3-PTZ at 1 mM and 10 mM with and without dodecanol (5%) and 5 mM of palmitic acid. Red symbols indicating. The presence of 5% doecanol and 5 mM palmitic acid.

Impressively, despite not inhibiting the autoxidation for longer (at least at lower concentrations), the addition of a protecting group very clearly prevents precipitation during the autoxidation (**Figures 3.29 & 3.30**). At the elevated concentration, although both the free amine and the *N*-formylated counterpart suppress autoxidation for the duration of the experiment, there is a stark contrast in the appearance of the *n*-hexadecane. At 30 minutes, the hexadecane containing the unprotected compound is very dark in colour and somewhat opaque, consistent with the formation of oxidized oligomers and/or other precipitates while the translucent red-brown colour of the autoxidation containing the *N*-formyl-PTZ is characteristic of oxidized PTZ (sulfone, PTZ-S-oxide, PTZ-S-dioxide, etc). This red colour is, to our

knowledge, not detrimental because it is still observable at lower concentrations (ie. 150 μM) over the course of a PTZ-inhibited autoxidation and does not contribute precipitates nor change the viscosity of the substrate significantly. Remarkably, even after the *n*-hexadecane cooled down to room temperature, nothing precipitated out of the sample which contained **23**.

Previously, other alkyl-sulfonamide-PTZs which seemed ‘cleaner’ at elevated concentrations (such as the *t*-butylated derivative), still contained precipitates once the *n*-hexadecane cooled.

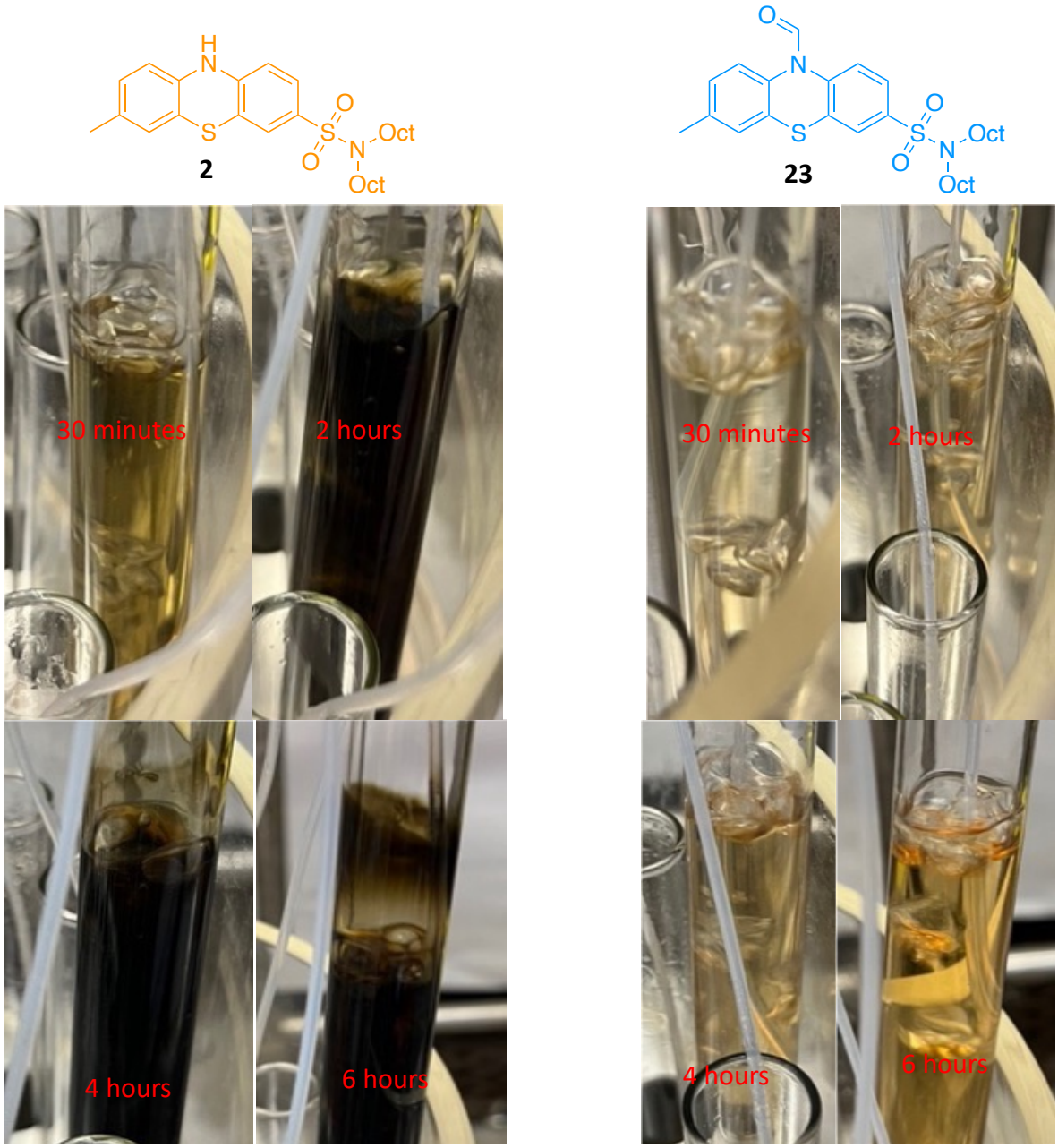

Figure 3.29 – Appearance of samples from *n*-hexadecane autoxidations inhibited by 10 mM of **2** and **23** at 165 °C at 30 min, 2 h, 4 h and 6 h respectively.

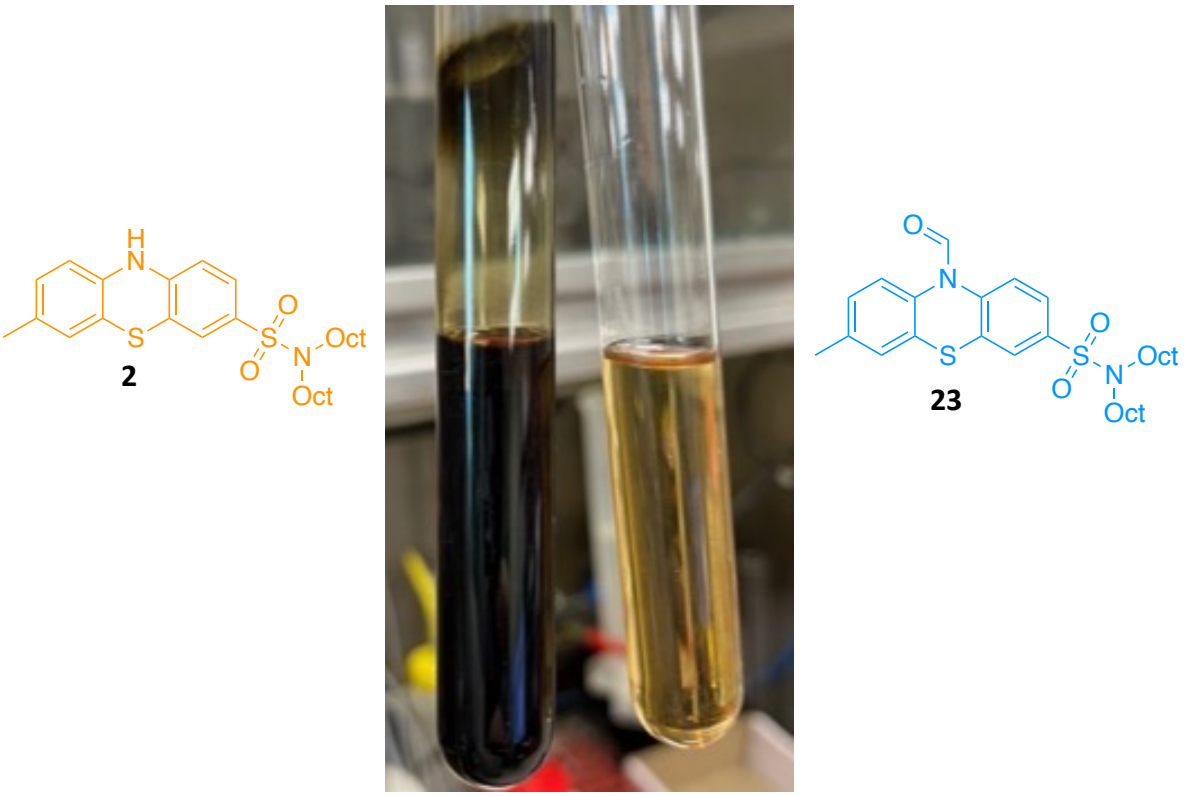

Figure 3.30 – Appearance of samples from *n*-hexadecane autoxidations inhibited by 10 mM of **2** and **23** once cooled (~14 h after the conclusion of the experiment).

Moving further toward translation of our findings to a real-world application, we evaluated the performance of **4** in a model lubricant formulation provided by our industry collaborators. Two formulations were investigated: one which contained 1 wt% of the industry standard ADPA, and another formulated without this RTA such that the *N*-formyl-PNX could be added in its place. Otherwise, the lubricant compositions are as follows**:** polyisobutylsuccinimidepolyalkylamine (< 10 wt%), calcium sulphonate overbased detergent (< 5 wt%), zinc dialkyldithiophosphate (< 2 wt%), polydimethylsiloxane (< 0.01 wt%), viscosity modifier (< 10 wt%), and group III base oil. In order for the autoxidations to be carried out over

a convenient time period, the lubricant formulations were diluted with base oil for our autoxidations to such an extent where the starting RTA concentration was roughly 250 μM.

Gratifyingly, the formulation containing **4** performed far better than that containing the industrial ADPA for the duration of the experiment, suppressing autoxidation for over 4.5 h (**Figure 3.31**). Previous studies in our lab have shown that PNX itself does not fare well under these conditions due to its rapid oxidation, suggesting that the protecting group approach is worthy of further development. The added nucleophile (dodecanol) is still apparently needed in the formulation to release PNX (at least at the early stages where little oxidation has taken place to provide nucleophiles in situ), however, it is quite interesting that added acid is no longer needed. This may arise since the formulations contain various bases, which may provide base catalysis for transformylation in lieu of the acid catalysis employed in our model experiments. The base catalysis was unexpected, as we previously found that primary hindered amines did not facilitate release – although this was not thoroughly investigated.

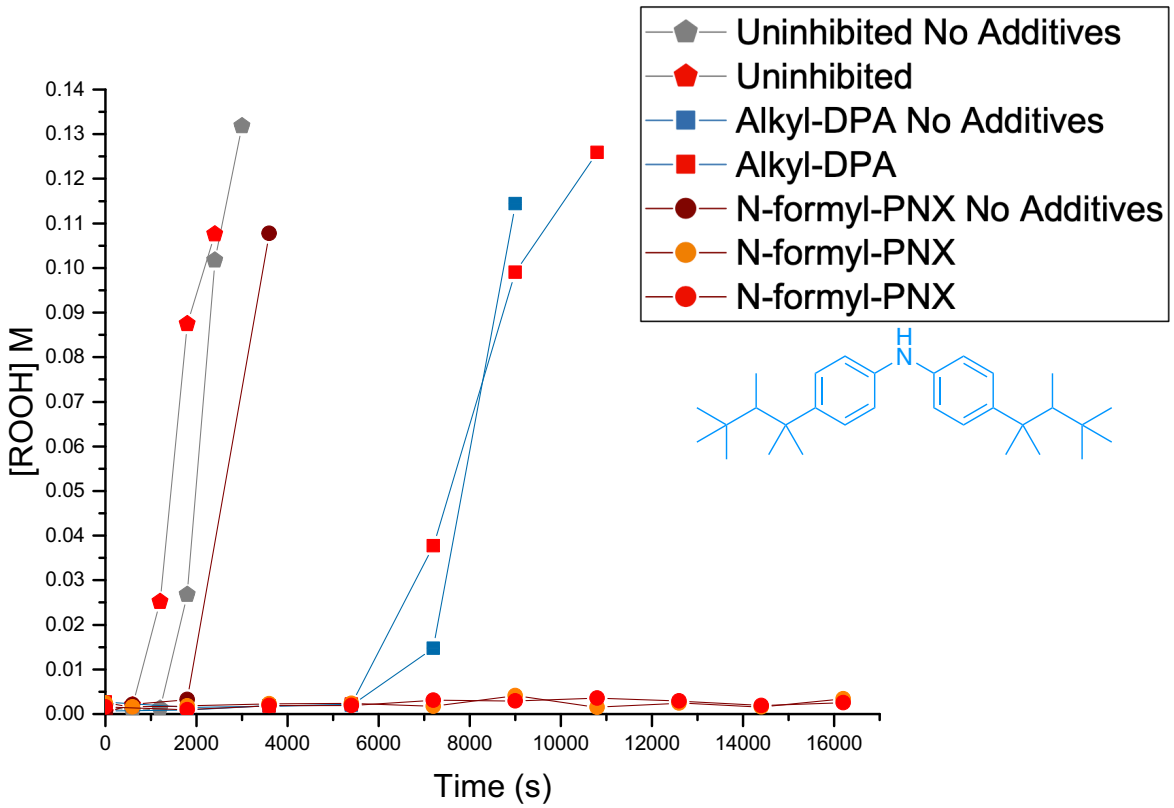

Figure 3.31 – Hydroperoxide formation in an autoxidation at 165 °C of Infineum's base oil blends in the presence of 250 μM **4** with/without dodecanol (5%) and with/without 5 mM palmitic acid or 250 μM of di-alkylated-DPA. Red symbols indicate the presence of 5% dodecanol and 5 mM of palmitic acid and orange symbols indicate the presence of 5% doecanol.

3.3 – Discussion

With the need for improved RTAs for oils, lubricants, and other hydrocarbon-based products due to environmental regulations associated with both emissions and wildlife reproductive toxicity concerns, alternatives to the gold-standard ADPAs are being sought. Heteroatom-bridged diarylamines previously explored such as PTZ and PNX have greater intrinsic reactivity, but issues associated with precipitates and oxidative stability, which have been known since the 1960's/70's, have precluded their development. Previous work in our group demonstrated that aza-analogs of ADPAs and incorporation of non-tertiary alkyl groups could substantially increase radical-trapping stoichiometry, leading to compounds of unprecedented potency. Some of these structures are shown in **Figure 3.32**. In *n*-hexadecane autoxidations at 160 °C, aza-DPA derivatives *p*-Me-2 and neopent-2 afforded inhibited periods of ~9.5 h and ~7 h, respectively. These results cannot be directly compared with those obtained with the current compounds, as they were obtained with 300 μM of RTA, the *n*-hexadecane contained 2 mM of primene, and the autoxidations were carried out at 160 °C. The standard conditions of the autoxidations above were 150 μM RTA at 165 °C. The primene was included in the autoxidations inhibited by the aza-DPA analogues to prevent protonation of the heterocycles, which deactivates the diarylamine to HAT. Even though lubricants are formulated with overbased detergents, they are used to neutralize acid build-up over the course of the

autoxidation, not necessarily to control the pH of the environment. Therefore, over time a potentially mildly acidic environment will render the aza-analogues useless.

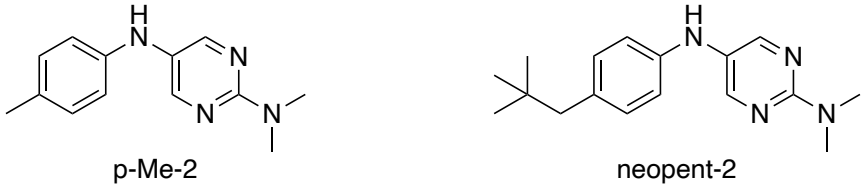

Figure 3.32 – Alkyl-di-aza-DPAs previously synthesized and tested by the Pratt group which were the most potent RTAs (under basic conditions) until the 3-alkyl-PTZ were synthesized.

Replacement of the *t*-Bu group with a methyl or neo-pentyl group in these di-aza analogues has since been shown to translate to the PTZ and PNX scaffolds, too. Introducing these types of substituents increases the inhibited period of PTZ from 5 h at 150 μM to over 9h in the cases of 3-sulfonamide-7-*n*-butyl-PTZ and 3-sulfonamide-7-*i*-propyl-PTZ. A methyl group at the 3-position also increases the inhibited period of autoxidation by almost 2 additional hours. Despite these significant improvements, and the addition of the lipophilic di-octyl-sulfonamide substituent at the 3-position, issues of PTZ oligomerization and precipitates are accentuated, especially in the case of the methyl derivative (**Scheme 1.13**). To minimize formation of these products, we have explored the use of acyl protecting groups which would cleave gradually over time to minimize deleterious reactions of 'free' RTA by maintaining a low basal concentration.

Adding acyl protecting groups to the PTZ and PNX derivatives has proved a viable strategy for protecting the active RTA from deleterious chemistry. Using substituents of differing electronics, such as methoxy (EDG) and trifluoromethyl or sulfonamides (EWG), we can modulate the reactivity of the *N*-acyl functionality. *N*-formyl-PNXs are cleaved about an

order of magnitude more rapidly than their *N*-formyl PTZ counterparts under our experimental conditions. In terms of inhibited periods, at 1 mM, the poorest performing *N*-formyl PNX is **17** (t_{inh} = 5.5 h), but it is as efficacious as the most efficacious *N*-formyl PTZ, which is also a CF_3-derivative (**22**) (t_{inh} = 5.5 h). However, despite the equivalent inhibited periods, their half-lives differ – 4.5 h for the former and 36 h for the latter. This suggests that the two compounds stop inhibiting the autoxidation for different reasons: *N*-formyl-CF_3-PNX because it is being cleaved to its free compound too quickly and is subsequently being depleted by reactions with O_2 and *N*-formyl-CF_3-PTZ because it is not being cleaved fast enough to keep up. The fastest releasing compound that inhibits the autoxidation for the duration of the experiment is **4** ($t_{1/2}$ = 11 h), suggesting that to be an effective *N*-formylated RTA *under our test conditions*, the half-life of cleavage of the formyl group must fall between 11 h-26 h. The upper limit of this half-life 'window' is the half-life of *N*-formyl OMe-PNX which also supressed autoxidation for the duration of the experiment at 1 mM.

Excellent activity was also observed when using *N*-acyl RTAs which contain a pendant nucleophile. Despite *N*-acyl protecting group cleavage still being slower for the PTZ derivatives compared to the PNX derivatives, the PTZ-derivatives outperformed their PNX counterparts *under our test conditions*. Compound **36** was the best performing and inhibited for the duration of the experiment (>7.5 h) both without and with 5 mM of palmitic acid. However, consideration of the half-lives for *N*-acyl cleavage unveils why it is so successful in both sets of conditions. In the presence of acid, as the chromatograms in **Figure 3.24** show, the PTZ is fully released within minutes of the experiment commencing, such that it is no different than PTZ itself. As such, this will offer no advantage at elevated concentrations where formation of

oligomers and/or precipitates would still occur. Compound **31** also performed well at 1 mM under the experimental conditions, inhibiting for 7 h in the absence of acid, and >7.5 h in the presence of acid, but it didn't release at all in the absence of acid when under N_2, suggesting that acid generated in the autoxidation is sufficient to enable the deprotection. Still, it would seem that the rapid release of **31** in the presence of acid ($t_{1/2}$ ~ 2 h) will be detrimental at elevated concentrations. Although **38** showed some efficacy at 1 mM in both the presence and absence of palmitic acid, it likely undergoes deacylation too quickly since it is similarly potent to PNX at 1 mM. In the absence of acid, its half-life is 53 h – however, due to the acid generated in situ, this half-life is likely much faster in an autoxidation under O_2 whereby it falls outside of the 11-26 h window where these latent RTAs seem to be effective at concentrations of 1 mM.

Based on the foregoing, it is clear that the effectiveness of the acylated RTAs will be highly concentration dependent, whereby at industrially relevant concentrations, slower releasing compounds should be used. This is likely to make some of the *N*-formyl and 7R compounds which were less efficacious at 1 mM practical at elevated concentrations. Also looking through an 'industrial lens' the acyl-protected RTAs do not have to be the most potent of those synthesized, they only have to be more potent than the compounds currently available, while not leading to deleterious precipitates. The next phase of this work should combine the knowledge of how electronic and entropic effects influence the cleavage of these protecting groups with various alkyl substituents which can boost their radical-trapping stoichiometry. Increased stoichiometries could potentially allow for even slower compounds to be used in inhibiting autoxidations.

Latent RTAs can also potentially improve diarylamines activity in autoxidations containing NO_x, since free amines (and phenols) are known to react directly with NO_x as in **Scheme 3.7**. This was demonstrated by Penner in 2021, where the inhibited period in the presence of di-tBuDPA was reduced from ~9 h to ~1 h 45 with 10 mM of RTA switching from pure oxygen to 765 ppm NO_2.

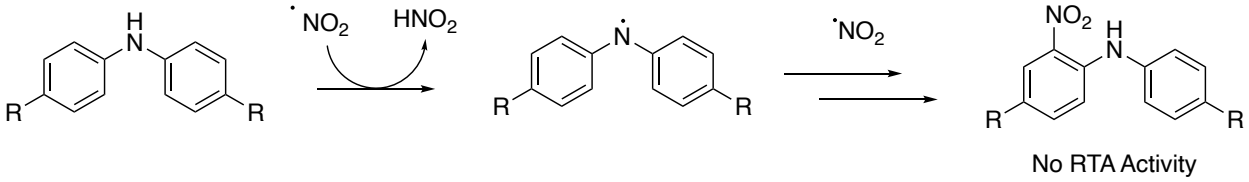

Scheme 3.7 – The direct reaction of NO_x with DPAs, which neutralizes their RTA activity.

3.4 – Conclusions

Protecting heteroatom-bridged diarylamines with acyl protecting groups which are slowly displaced by both intermolecular and intramolecular nucleophiles has proved a viable strategy for inhibiting high temperature hydrocarbon autoxidation. These protecting groups not only improve the efficacy of PTZ and PNX-based RTAs, but they also mitigate, if not eliminate, free PTZ and free PNX from forming oligomers which precipitate out of *n*-hexadecane/oil or reacting directly with oxygen, respectively. Substitution of a methoxy group (EDG), trifluoromethyl or sulfonamide (EWGs) at the 3- or 7-positions (*para* to the amine) and varying the chain length of protecting groups with pendant nucleophiles can enhance or slow the release of PTZ and PNX-based RTAs to tailor the rate of release of the free RTA. Tailoring the rate of release specific to the RTA will keep a low basal concentration of active RTA that can fully inhibit hydrocarbon autoxidation without by-product formation or deactivation of the RTA. The minimization of off-cycle reactions will maximize RTA regeneration via the Korcek and cross-dismutation cycles believed to operate in saturated and unsaturated hydrocarbons,

respectively. This study allows for the combination of our knowledge of improving stoichiometry/efficacy using alkyl substituents as well as using protecting groups to improve the structure-property relationships which has hindered the deployment of many diarylamine RTAs for commercial applications. By combining these improvements, RTAs with unprecedented potency may be developed to extend the lifetime of oils, lubricants, and other hydrocarbon-based products. This will lead to less oil and other petroleum derived products that need to be manufactured, thus reducing emissions, and reducing our carbon footprints.

3.5 – References

(1) Ingold, K. U.; Pratt, D. A. Advances in Radical-Trapping Antioxidant Chemistry in the 21st Century: A Kinetics and Mechanisms Perspective. *Chem. Rev.* **2014**, *114* (18), 9022–9046. https://doi.org/10.1021/cr500226n.

(2) Farmer, L. A.; Haidasz, E. A.; Griesser, M.; Pratt, D. A. Phenoxazine: A Privileged Scaffold for Radical-Trapping Antioxidants. *J. Org. Chem.* **2017**, *82* (19), 10523–10536. https://doi.org/10.1021/acs.joc.7b02025.

(3) Helberg, J.; Pratt, D. A. Autoxidation *vs.* Antioxidants – the Fight for Forever. *Chem. Soc. Rev.* **2021**, *50* (13), 7343–7358. https://doi.org/10.1039/D1CS00265A.

(4) Valko, M.; Leibfritz, D.; Moncol, J.; Cronin, M. T. D.; Mazur, M.; Telser, J. Free Radicals and Antioxidants in Normal Physiological Functions and Human Disease. *Int. J. Biochem. Cell Biol.* **2007**, *39* (1), 44–84. https://doi.org/10.1016/j.biocel.2006.07.001.

(5) Jensen, R. K.; Korcek, S.; Mahoney, L. R.; Zinbo, M. Liquid-Phase Autoxidation of Organic Compounds at Elevated Temperatures. 1. The Stirred Flow Reactor Technique and Analysis of Primary Products from n-Hexadecane Autoxidation at 120-180.Degree.C. *J. Am. Chem. Soc.* **1979**, *101* (25), 7574–7584. https://doi.org/10.1021/ja00519a018.

(6) Ingold, K. U. Inhibition of the Autoxidation of Organic Substances in the Liquid Phase. *Chem. Rev.* **1961**, *61* (6), 563–589. https://doi.org/10.1021/cr60214a002.

(7) Howard, J. A.; Ingold, K. U. Absolute Rate Constants for Hydrocarbon Autoxidation. VI. Alkyl Aromatic and Olefinic Hydrocarbons. *Can. J. Chem.* **1967**, *45* (8), 793–802. https://doi.org/10.1139/v67-132.

(8) Maillard, B.; Ingold, K. U.; Scaiano, J. C. Rate Constants for the Reactions of Free Radicals with Oxygen in Solution. *J. Am. Chem. Soc.* **1983**, *105* (15), 5095–5099. https://doi.org/10.1021/ja00353a039.

(9) Von Sonntag, C.; Schuchmann, H. The Elucidation of Peroxyl Radical Reactions in Aqueous Solution with the Help of Radiation-Chemical Methods. *Angew. Chem. Int. Ed. Engl.* **1991**, *30* (10), 1229–1253. https://doi.org/10.1002/anie.199112291.

(10) Bolland, J. L. Kinetics of Olefin Oxidation. *Q. Rev. Chem. Soc.* **1949**, *3* (1), 1. https://doi.org/10.1039/qr9490300001.

(11) Do, Q.; Lee, D. D.; Dinh, A. N.; Seguin, R. P.; Zhang, R.; Xu, L. Development and Application of a Peroxyl Radical Clock Approach for Measuring Both Hydrogen-Atom Transfer and Peroxyl Radical Addition Rate Constants. *J. Org. Chem.* **2021**, *86* (1), 153–168. https://doi.org/10.1021/acs.joc.0c01920.

(12) Luo, Y.-R. *Handbook of Bond Dissociation Energies in Organic Compounds*, 0 ed.; CRC Press, 2002. https://doi.org/10.1201/9781420039863.

(13) *Encyclopedia of Radicals in Chemistry, Biology, and Materials*; Chatgilialoglu, C., Studer, A., Eds.; John Wiley & Sons: Chichester, West Sussex ; Hoboken, N.J, 2012.

(14) Lee, R.; Gryn'ova, G.; Ingold, K. U.; Coote, M. L. Why Are Sec-Alkylperoxyl Bimolecular Self-Reactions Orders of Magnitude Faster than the Analogous Reactions of Tert-Alkylperoxyls? The Unanticipated Role of CH Hydrogen Bond Donation. *Phys. Chem. Chem. Phys.* **2016**, *18* (34), 23673–23679. https://doi.org/10.1039/C6CP04670C.

(15) Shah, R.; Pratt, D. A. Determination of Key Hydrocarbon Autoxidation Products by Fluorescence. *J. Org. Chem.* **2016**, *81* (15), 6649–6656. https://doi.org/10.1021/acs.joc.6b01032.

(16) Jalan, A.; Alecu, I. M.; Meana-Pañeda, R.; Aguilera-Iparraguirre, J.; Yang, K. R.; Merchant, S. S.; Truhlar, D. G.; Green, W. H. New Pathways for Formation of Acids and Carbonyl Products in Low-Temperature Oxidation: The Korcek Decomposition of γ-Ketohydroperoxides. *J. Am. Chem. Soc.* **2013**, *135* (30), 11100–11114. https://doi.org/10.1021/ja4034439.
(17) Zaikov, G. E.; Howard, J. A.; Ingold, K. U. Absolute Rate Constants for Hydrocarbon Autoxidation. XIII. Aldehydes: Photo-Oxidation, Co-Oxidation, and Inhibition. *Can. J. Chem.* **1969**, *47* (16), 3017–3029. https://doi.org/10.1139/v69-500.
(18) Bäckström, H. L. J. THE CHAIN-REACTION THEORY OF NEGATIVE CATALYSIS [1]. *J. Am. Chem. Soc.* **1927**, *49* (6), 1460–1472. https://doi.org/10.1021/ja01405a011.
(19) Jensen, R. K.; Korcek, S.; Zinbo, M.; Johnson, M. D. Initiation in Hydrocarbon Autoxidation at Elevated Temperatures. *Int. J. Chem. Kinet.* **1990**, *22* (10), 1095–1107. https://doi.org/10.1002/kin.550221008.
(20) Howard, J. A.; Ingold, K. U. THE INHIBITED AUTOXIDATION OF STYRENE: PART I.THE DEUTERIUM ISOTOPE EFFECT FOR INHIBITION BY 2,6-DI- *Tert* -BUTYL-4-METHYLPHENOL. *Can. J. Chem.* **1962**, *40* (9), 1851–1864. https://doi.org/10.1139/v62-281.
(21) Lucarini, M.; Pedulli, G. F. Free Radical Intermediates in the Inhibition of the Autoxidation Reaction. *Chem. Soc. Rev.* **2010**, *39* (6), 2106. https://doi.org/10.1039/b901838g.
(22) Lucarini, M.; Pedrielli, P.; Pedulli, G. F.; Valgimigli, L.; Gigmes, D.; Tordo, P. Bond Dissociation Energies of the N−H Bond and Rate Constants for the Reaction with Alkyl, Alkoxyl, and Peroxyl Radicals of Phenothiazines and Related Compounds. *J. Am. Chem. Soc.* **1999**, *121* (49), 11546–11553. https://doi.org/10.1021/ja992904u.
(23) Franchi, P.; Lucarini, M.; Pedrielli, P.; Pedulli, G. F. Nitroxide Radicals as Hydrogen Bonding Acceptors. An Infrared and EPR Study. *Chemphyschem Eur. J. Chem. Phys. Phys. Chem.* **2002**, *3* (9), 789–793. https://doi.org/10.1002/1439-7641(20020916)3:9<789::AID-CPHC789>3.0.CO;2-Z.
(24) Valgimigli, L.; Amorati, R.; Fumo, M. G.; DiLabio, G. A.; Pedulli, G. F.; Ingold, K. U.; Pratt, D. A. The Unusual Reaction of Semiquinone Radicals with Molecular Oxygen. *J. Org. Chem.* **2008**, *73* (5), 1830–1841. https://doi.org/10.1021/jo7024543.
(25) Poon, J.-F.; Farmer, L. A.; Haidasz, E. A.; Pratt, D. A. Temperature-Dependence of Radical-Trapping Activity of Phenoxazine, Phenothiazine and Their Aza-Analogues Clarifies the Way Forward for New Antioxidant Design. *Chem. Sci.* **2021**, *12* (33), 11065–11079. https://doi.org/10.1039/D1SC02976B.
(26) Brownlie, I. T.; Ingold, K. U. The Inhibited Autoxidation of Styrene. Part VI. The Relative Efficiencies and the Kinetics for Inhibition by *N* -Aryl Anilines and *N* -Alkyl Anilines. *Can. J. Chem.* **1967**, *45* (20), 2419–2425. https://doi.org/10.1139/v67-390.
(27) Beckwith, A. L. J.; Bowry, V. W.; Ingold, K. U. Kinetics of Nitroxide Radical Trapping. 1. Solvent Effects. *J. Am. Chem. Soc.* **1992**, *114* (13), 4983–4992. https://doi.org/10.1021/ja00039a005.
(28) Thomas, J. R.; Tolman, C. A. **Oxidation Inhibition by Diphenylamine**. *J. Am. Chem. Soc.* **1962**, *84* (15), 2930–2935. https://doi.org/10.1021/ja00874a017.
(29) Shah, R.; Poon, J.-F.; Haidasz, E. A.; Pratt, D. A. Temperature-Dependent Effects of Alkyl Substitution on Diarylamine Antioxidant Reactivity. *J. Org. Chem.* **2021**, *86* (9), 6538–6550. https://doi.org/10.1021/acs.joc.1c00365.

(30) Baschieri, A.; Valgimigli, L.; Gabbanini, S.; DiLabio, G. A.; Romero-Montalvo, E.; Amorati, R. Extremely Fast Hydrogen Atom Transfer between Nitroxides and HOO · Radicals and Implication for Catalytic Coantioxidant Systems. *J. Am. Chem. Soc.* **2018**, *140* (32), 10354–10362. https://doi.org/10.1021/jacs.8b06336.
(31) Jensen, R. K.; Korcek, S.; Zinbo, M.; Gerlock, J. L. Regeneration of Amine in Catalytic Inhibition of Oxidation. *J. Org. Chem.* **1995**, *60* (17), 5396–5400. https://doi.org/10.1021/jo00122a014.
(32) Murphy, C. M.; Ravner, H.; Smith, N. L. Mode of Action of Phenothiazine-Type Antioxidants. *Ind. Eng. Chem.* **1950**, *42* (12), 2479–2489. https://doi.org/10.1021/ie50492a027.
(33) Strange, H. O.; McGrath, J. J.; Pellegrini, J. P. Improved Phenothiazine Antioxidants for Synthetic Lubricants. *IEC Prod. Res. Dev.* **1967**, *6* (1), 33–35. https://doi.org/10.1021/i360021a005.
(34) Hanthorn, J. J.; Haidasz, E.; Gebhardt, P.; Pratt, D. A. A Versatile Fluorescence Approach to Kinetic Studies of Hydrocarbon Autoxidations and Their Inhibition by Radical-Trapping Antioxidants. *Chem. Commun.* **2012**, *48* (81), 10141. https://doi.org/10.1039/c2cc35214a.
(35) Baeyer, A.; Villiger, V. Einwirkung Des Caro'schen Reagens Auf Ketone. *Berichte Dtsch. Chem. Ges.* **1899**, *32* (3), 3625–3633. https://doi.org/10.1002/cber.189903203151.
(36) Renz, M.; Meunier, B. 100 Years of Baeyer-Villiger Oxidations. *Eruopean J. Org. Chem.* **1998**, *1999* (4), 737–958.
(37) Horn, A.; Kazmaier, U. Purified mCPBA, a Useful Reagent for the Oxidation of Aldehydes. *Eur. J. Org. Chem.* **2018**, *2018* (20–21), 2531–2536. https://doi.org/10.1002/ejoc.201701645.
(38) Criegee, R. Die Umlagerung Der Dekalin-peroxydester Als Folge von Kationischem Sauerstoff. *Justus Liebigs Ann. Chem.* **1948**, *560* (1), 127–135. https://doi.org/10.1002/jlac.19485600106.
(39) Doering, W. V. E.; Speers, L. The Peracetic Acid Cleavage of Unsymmetrical Ketones [1]. *J. Am. Chem. Soc.* **1950**, *72* (12), 5515–5518. https://doi.org/10.1021/ja01168a041.
(40) Doering, W. V. E.; Dorfman, E. Mechanism of the Peracid Ketone—Ester Conversion. Analysis of Organic Compounds for Oxygen-18 [1]. *J. Am. Chem. Soc.* **1953**, *75* (22), 5595–5598. https://doi.org/10.1021/ja01118a035.
(41) Snowden, M.; Bermudez, A.; Kelly, D. R.; Radkiewicz-Poutsma, J. L. The Preference for Anti over Gauche Migration in the Baeyer−Villiger Reaction. *J. Org. Chem.* **2004**, *69* (21), 7148–7156. https://doi.org/10.1021/jo0491307.
(42) Ochiai, M.; Yoshimura, A.; Miyamoto, K.; Hayashi, S.; Nakanishi, W. Hypervalent λ [3] -Bromane Strategy for Baeyer−Villiger Oxidation: Selective Transformation of Primary Aliphatic and Aromatic Aldehydes to Formates, Which Is Missing in the Classical Baeyer−Villiger Oxidation. *J. Am. Chem. Soc.* **2010**, *132* (27), 9236–9239. https://doi.org/10.1021/ja104330g.
(43) Leuser, H.; Perrone, S.; Liron, F.; Kneisel, F. F.; Knochel, P. Highly Enantioselective Preparation of Tertiary Alcohols and Amines by Copper-Mediated Diastereoselective Allylic SN2′ Substitutions. *Angew. Chem. Int. Ed.* **2005**, *44* (29), 4627–4631. https://doi.org/10.1002/anie.200500672.

(44) Harrison, K. A.; Haidasz, E. A.; Griesser, M.; Pratt, D. A. Inhibition of Hydrocarbon Autoxidation by Nitroxide-Catalyzed Cross-Dismutation of Hydroperoxyl and Alkylperoxyl Radicals. *Chem. Sci.* **2018**, *9* (28), 6068–6079. https://doi.org/10.1039/C8SC01575A.
(45) Frisch, M. J.; Trucks, G.; Schlegel, H. B.; Scuseria, G. E.; Robb, M. A.; Farkas, O.; Foresman, J. B.; Fox, D. J. Gaussian 16, Rev. A.03, 2016.
(46) Zhao, Y.; Truhlar, D. G. The M06 Suite of Density Functionals for Main Group Thermochemistry, Thermochemical Kinetics, Noncovalent Interactions, Excited States, and Transition Elements: Two New Functionals and Systematic Testing of Four M06-Class Functionals and 12 Other Functionals. *Theor. Chem. Acc.* **2008**, *120* (1–3), 215–241. https://doi.org/10.1007/s00214-007-0310-x.
(47) Montgomery, J. A.; Frisch, M. J.; Ochterski, J. W.; Petersson, G. A. A Complete Basis Set Model Chemistry. VI. Use of Density Functional Geometries and Frequencies. *J. Chem. Phys.* **1999**, *110* (6), 2822–2827. https://doi.org/10.1063/1.477924.
(48) Grimme, S.; Antony, J.; Ehrlich, S.; Krieg, H. A Consistent and Accurate *Ab Initio* Parametrization of Density Functional Dispersion Correction (DFT-D) for the 94 Elements H-Pu. *J. Chem. Phys.* **2010**, *132* (15), 154104. https://doi.org/10.1063/1.3382344.
(49) Barone, V.; Cossi, M. Quantum Calculation of Molecular Energies and Energy Gradients in Solution by a Conductor Solvent Model. *J. Phys. Chem. A* **1998**, *102* (11), 1995–2001. https://doi.org/10.1021/jp9716997.
(50) O'Connor, S. P.; Crawford, J.; Cane, C. Overbased Lubricant Detergents – a Comparative Study. *Lubr. Sci.* **1994**, *6* (4), 297–325. https://doi.org/10.1002/ls.3010060402.
(51) King, J. F.; Loosmore, S. M.; Aslam, M.; Lock, J. D.; McGarrity, M. J. Betylates. 3. Preparative Nucleophilic Substitution by Way of [2]-, [3]-, and [4]Betylates. Stoichiometric Phase Transfer and Substrate-Reagent Ion-Pair (SRIP) Reactions of Betylates. *J. Am. Chem. Soc.* **1982**, *104* (25), 7108–7122. https://doi.org/10.1021/ja00389a038.
(52) Penner, N. Insights on the Fates of Diarylamine Radical-Trapping Antioxidants During Inhibited Autoxidations Using Isotopically-Enriched Compounds, 2020.
(53) Mudugamuwa, C. J.; Xie, Y.; Zhang, K.; Nicholls, T. P.; Chalker, J. M.; Jia, Z. Nitroxide Radical Surfactants Enable Electrocatalytic Oxidation of Fatty Alcohols in Water. *Green Chem.* **2023**, *25* (8), 3086–3094. https://doi.org/10.1039/D3GC00785E.
(54) Tung, N. H.; Uto, T.; Sakamoto, A.; Hayashida, Y.; Hidaka, Y.; Morinaga, O.; Lhieochaiphant, S.; Shoyama, Y. Antiproliferative and Apoptotic Effects of Compounds from the Flower of Mammea Siamensis (Miq.) T. Anders. on Human Cancer Cell Lines. *Bioorg. Med. Chem. Lett.* **2013**, *23* (1), 158–162. https://doi.org/10.1016/j.bmcl.2012.10.127.
(55) Taguchi, H.; Paal, B.; Armarego, W. L. F. Glyceryl-Ether Monooxygenase [EC 1.14.16.5]. Part 9. Stereospecificity of the Oxygenase Reaction. *J. Chem. Soc. Perkin 1* **1997**, No. 3, 303–308. https://doi.org/10.1039/a603533g.
(56) Shah, R.; Haidasz, E. A.; Valgimigli, L.; Pratt, D. A. Unprecedented Inhibition of Hydrocarbon Autoxidation by Diarylamine Radical-Trapping Antioxidants. *J. Am. Chem. Soc.* **2015**, *137* (7), 2440–2443. https://doi.org/10.1021/ja5124144.
(57) Farmer, L. A.; Pratt, D. A. Non-Tertiary Alkyl Substituents Enhance High-Temperature Radical Trapping by Phenothiazine and Phenoxazine Antioxidants. *Submitted* **2024**.
(58) Heathcock, C. H.; Stafford, J. A. Daphniphyllum Alkaloids. 13. Asymmetric Total Synthesis of (-)-Secodaphniphylline. *J. Org. Chem.* **1992**, *57* (9), 2566–2574. https://doi.org/10.1021/jo00035a010.

(59) Vishwakarma, L. C.; Martin, A. R. Tetracyclic Phenothiazines. VI. Attempted Pummerer Cyclization of 10-(2-Keto-3-methylsulfinylpropyl)Phenothiazine. *J. Heterocycl. Chem.* **1982**, *19* (1), 103–105. https://doi.org/10.1002/jhet.5570190118.
(60) Brewster, K.; Chittenden, R. A.; Harrison, J. M.; Inch, T. D.; Brown, C. Oxidation of Some Dibenz[b,f][1,4]Oxazepines by Peracetic Acid. *J. Chem. Soc. Perkin 1* **1976**, No. 12, 1291. https://doi.org/10.1039/p19760001291.
(61) Vantourout, J. C.; Law, R. P.; Isidro-Llobet, A.; Atkinson, S. J.; Watson, A. J. B. Chan–Evans–Lam Amination of Boronic Acid Pinacol (BPin) Esters: Overcoming the Aryl Amine Problem. *J. Org. Chem.* **2016**, *81* (9), 3942–3950. https://doi.org/10.1021/acs.joc.6b00466.
(62) Schönewerk, J.; Hartmann, H. On the Formation and ^{1}H NMR-Spectroscopic Characterization of N,N-Diaryl-Substituted Formamide Chlorides. *Z. Für Naturforschung B* **2012**, *67* (4), 277–284. https://doi.org/10.1515/znb-2012-0401.
(63) Tietze, L. F.; Eichhorst, C.; Hungerland, T.; Steinert, M. A Fast Way to Fluorescence: A Fourfold Domino Reaction to Condensed Polycyclic Compounds. *Chem. – Eur. J.* **2014**, *20* (39), 12553–12558. https://doi.org/10.1002/chem.201402961.
(64) Cui, M.; Sung, H. H. Y.; Williams, I. D.; Jia, G. Alkyne Metathesis with d ^{2} Re(V) Alkylidyne Complexes Supported by Phosphino-Phenolates: Ligand Effect on Catalytic Activity and Applications in Ring-Closing Alkyne Metathesis. *J. Am. Chem. Soc.* **2022**, *144* (14), 6349–6360. https://doi.org/10.1021/jacs.2c00368.
(65) Chen, M.; Lee, Y.; Huang, Z.; Chen, D.; Chou, P. Tuning Electron-Withdrawing Strength on Phenothiazine Derivatives: Achieving 100 % Photoluminescence Quantum Yield by NO_2 Substitution. *Chem. – Eur. J.* **2020**, *26* (31), 7124–7130. https://doi.org/10.1002/chem.202000754.
(66) Yale, H. L.; Sowinski, F.; Bernstein, J. 10-(3-Dimethylaminopropyl)-2-(Trifluoromethyl)-Phenothiazine Hydrochloride (VESPRIN ^{1}) and Related Compounds. I. *J. Am. Chem. Soc.* **1957**, *79* (16), 4375–4379. https://doi.org/10.1021/ja01573a037.
(67) Matralis, A. N.; Kourounakis, A. P. Design of Novel Potent Antihyperlipidemic Agents with Antioxidant/Anti-Inflammatory Properties: Exploiting Phenothiazine's Strong Antioxidant Activity. *J. Med. Chem.* **2014**, *57* (6), 2568–2581. https://doi.org/10.1021/jm401842e.
(68) Farmer, L. A.; Wu, Z.; Poon, J.-F.; Zilka, O.; Lorenz, S. M.; Huehn, S.; Proneth, B.; Conrad, M.; Pratt, D. A. Intrinsic and Extrinsic Limitations to the Design and Optimization of Inhibitors of Lipid Peroxidation and Associated Cell Death. *J. Am. Chem. Soc.* **2022**, *144* (32), 14706–14721. https://doi.org/10.1021/jacs.2c05252.

3.6 – Experimental

3.6.1 – Synthesis of 3,4-Difluoro-1-(SO_2N-Oct_2) (1)

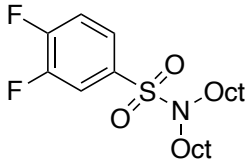

Di-(2-ethylhexyl)amine (7.24 g, 30 mmol) and triethylamine (6.07 g, 60.0 mmol) were added to 150 mL of dichloromethane and cooled to 0 °C. A solution of of 3,4-difluorobenzenesulfonyl-chloride (6.38 g, 30 mmol) in 40 mL of DCM was added dropwise. The mixture was allowed to come to room temperature and stirred overnight. After the addition of H_2O, the crude product was extracted with DCM, and the organic phase dried with $MgSO_4$. Purification via column chromatography (SiO_2 / DCM:EtOAc = 95:5) afforded 27.7 mmol (11.6 g) of the product as a colourless oil in 92% yield. ^{1}H NMR (400 MHz, $CDCl_3$): δ 7.63-7.58 (1H, m, J_{ortho} = 7.68 Hz, J_{para} = 1.2), 7.57-7.53 (1H, dm), 7.31-7.25 (1H, d), 3-2.8 (4H, m), 1.56-1.53 (2H, t), 1.40-1.13 (16H, m), 0.88-0.80 (12H, m). ^{13}C NMR (100 MHz, $CDCl_3$) δ 154.3, 154.1, 151.7, 151.4, 149.00, 148.86, 136.8, 136.7, 124.5, 124.4, 124.4, 118.1, 117.9, 117.4-117.2, 53.4, 37.8, 30.6, 28.9, 23.8, 23.2, 14.2, 10.7. HRMS (EI, magnetic sector) calcd for $C_{22}H_{33}F_2NO_4S$: 445.2098, found: 445.2083.

3.6.2 – General Synthesis of 3-$SO_2N(Oct)_2$-7-R-Phenothiazines via Smiles Rearrangement

Under an inert atmosphere, 35 mL of DMF was added to a Schlenk flask. To the flask was added 3,4-diflouro-1-(SO_2N-Oct_2) (sulfonamide) (3.1 g, 7 mmol), an equivalent of the desired aminothiophenol and K_2CO_3 (2.4 g, 17.5 mmol). The mixture was left to stir at 130°C for 1 h. The

flask was then removed from the oil bath and left to cool to room temperature. NaH (279.9 mg of a 60% suspension in mineral oil, 7.0 mmol) was then added portion-wise and the mixture was stirred overnight. The mixture was then extracted with ethyl acetate, and the organic phase dried with $MgSO_4$ and solvent evaporated in vacuo. The crude mixture was purified via column chromatography (SiO_2 / hexanes:EtOAc 9:1)

3-$SO_2N(Oct)_2$-7-methyl-phenothiazine (2)

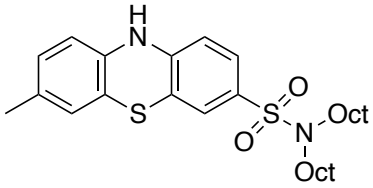

Isolated 530 mg (0.98 mmol) of a grey-red solid in 14% yield. ^{1}H NMR (400 MHz, DMSO-d6): δ 8.98 (1H, s), 7.30-7.28 (1H, dd, J = 8.10, 1.67), 7.13 (1H, d, J = 2.11), 6.79-6.76 (1H, dd, J = 8.02, 1.18), 6.71-6.70 (1H, d, J = 1.30), 6.69-6.67 (1H, d, J = 8.45), 6.55-6.53 (1H, d, J = 8.04), 2.86 (4H, m), 2.09 (3H, s), 1.32-1.09 (17H, m), 0.82-0.74 (13H, m). ^{13}C NMR (100 MHz, DMSO) δ 145.9, 137.7, 132.0, 130.6, 130.6, 128.3, 127.3, 126.6, 124.8, 116.9, 115.4, 114.8, 113.7, 53.2, 40.12, 39.9, 39.7, 39.5, 39.3, 39.1, 38.9, 37.3, 29.8, 28.2, 28.1, 23.1, 22.5, 19.9, 13.9, 10.42, 10.39. HRMS (EI, magnetic sector) calcd for $C_{29}H_{40}N_2O_4S_2$: 516.2844, found: 516.2871

3.6.3 – Synthesis of *N*-formyl-phenothiazine (3)

PTZ (10.0 g, 50.0 mmol) and formic acid (150 mL) were heated to reflux overnight. The mixture was then left too cool, poured over ice, and filtered. The crude solid was recrystallized from ethanol, affording 1.2 g (5.4 mmol) of white fluffy needles in 54% yield. ^{1}H NMR (400 MHz, $CDCl_3$): δ 8.64 (1H, s), 7.71-7.73 (1H, dd, J=8.1, 1.3), 7.19-7.39 (7H, m). The spectroscopic characterization was consistent with that reported in the literature. [59]

3.6.4 – Synthesis of *N*-formyl-phenoxazine (4)

PNX (1.0 g, 5.5 mmol), 10 mL of formic acid and 2 mL of acetic anhydride were combined and heated to reflux together for 2h. The mixture was then poured onto ice, the solid was filtered and recrystallized from MeOH affording 530.0 mg (2.5 mmol) of a fluffy white solid, in 46% yield. ^{1}H NMR (400 MHz, $CDCl_3$): δ 8.67 (1H, s), 7.95 (1H, br s), 7.05-7.20 (7H, m). HRMS (EI, magnetic sector): calcd for $C_{13}H_9NO_2$: 211.0633, found: 211.0610. The spectroscopic characterization was consistent with that reported in the literature.[60]

3.6.5 – Synthesis of *N*-Phenyl-2-naphthylamine (5)

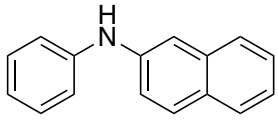

2-Naphthol (2.88 g, 20.0 mmol), aniline (5.59 g, 60 mmol) and *p*-toluenesulfonic acid (344 mg, 2 mmol) were added to a sealed tube purged with argon and heated to 120 °C for 48h. The crude mixture was then run through a silica column (hexanes:EtOAc 8:2) and recrystallized from EtOH affording 789 mg (3.6 mmol) of an off-white solid in a 18% yield**.** ^{1}H NMR (400 MHz, DMSO-d6): δ 8.39 (1H, s), 7.69-7.75 (2H, m), 7.63-7.65 (1H, dd, J = 8.2, 1.1), 7.43 (1H, d, J =2.2), 7.31-7.7.35 (1H, tt, J= 6.8, 2.7, 1.4), 7.15-7.28 (6H, m), 6.83-6.87 (1H, tt, J= 7.2, 2.3, 1.2). The spectroscopic characterization was consistent with that reported in the literature. [61]

3.6.6 – Synthesis of *N*-(2-naphthyl)-N-phenylformamide (6)

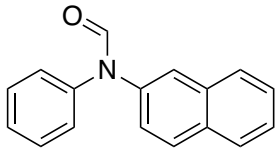

Formic acid (1.4 mL, 36.3 mmol) and acetic anhydride (3.3 mL, 35.2 mmol) was stirred at 0 °C for 30 minutes and then 60 °C for 3.5 h. N-Phenyl-2-naphthylamine (241 mg, 1.1 mmol) was then added and the mixture was heated to reflux for 2 hours. The reaction mixture was then stirred in saturated sodium bicarbonate and extracted 3 times with EtOAc. The organic layer was dried with $MgSO_4$, filtered and solvent evaporated in vacuo. The product was then purified via column chromatography on silica gel using hexanes:EtOAc 8:2 affording 230 mg (0.97 mmol) of the products as a white solid in 88% yield. ^{1}H NMR (400 MHz, DMSO-d6): δ 8.72-8.76 (1H, d), 7.79-7.95 (4H, m), 7.48-7.55 (2H, m), 7.39-7.44 (2H, m), 7.23-7.34 (2H, m). HRMS (EI, magnetic sector) calcd for $C_{17}H_{13}NO$: 247.0997, found: 247.0997. The spectroscopic characterization was consistent with that reported in the literature.[62]

3.6.7 – Synthesis of *N*-acetyl-(4-(tert-butyl)phenyl)-N,N-dimethylpyrimidine-2,5-diamine (7)

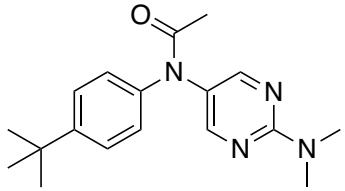

To a solution of N-(4-(tert-butyl)phenyl)-N,N-dimethylpyrimidine-2,5-diamine (811.1 mg, 3.0 mmol) in toluene (10 mL), acetyl chloride (243.3 mg, 3.1 mmol) was added dropwise and then the reaction was heated to 60 °C. NEt_3 (0.43 mL, 3.1 mmol) was then added and the mixture was left to stir for 1.5 h. The mixture was then poured into water and extracted with EtOAc

thrice. The organic layer was then washed with brine, dried with $MgSO_4$ and the solvent evaporated in vacuo. The residue was purified via column chromatography on silica gel (DCM:EtOAc 1:1) affording 690 mg (2.2 mmol) of the products as an off-white solid in 74% yield. ^{1}H NMR (400 MHz, $CDCl_3$): δ 8.22 (2H, s), 7.36 (2H. br s), 7.13-7.16 (2H, d), 3.15 (6H, s), 2.05 (3H, s), 1.28 (9H, s). ^{13}C NMR (100 MHz, $CDCl_3$) δ 170.9, 160.1, 156.9, 155.4, 151.2, 140.2, 127.5, 126.8, 126.1, 77.4, 77.3, 77.1, 76.7, 37.3, 34.6, 31.3, 23.3. HRMS (EI, magnetic sector) calcd for $C_{18}H_{24}N_4O$: 312.1950, found: 312.1972.

3.6.8 – Synthesis of *N*-formyl-(4-(tert-butyl)phenyl)-N,N-dimethylpyrimidine-2,5-diamine (8)

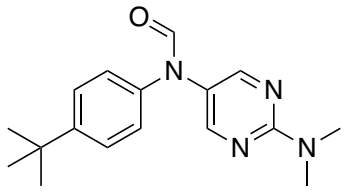

Formic acid (0.67 mL, 17.8 mmol) and acetic anhydride (1.63 mL, 17.3 mmol) were stirred at 0 °C for 30 minutes then 60 °C for 3.5 h. To the mixed anhydride, N-(4-(tert-butyl)phenyl)-N,N-dimethylpyrimidine-2,5-diamine (146 mg, 0.54 mmol) was added and the reaction heated to reflux for 3h. The mixture was then poured on saturated sodium bicarbonate and extracted thrice with EtOAc. The organic phase was washed with brine and dried with $MgSO_4$ and filtered. The solvent was evaporated in vacuo and purified via column chromatography on silica gel (DCM:EtOAc, 1:1) affording 106 mg (0.32 mmol) of the product as an off-white solid in 60% yield. ^{1}H NMR (400 MHz, $CDCl_3$): δ 8.40-8.62 (1H, d), 8.19-8.22 (2H, d), 7.35-7.40 (2H, t), 7.19-7.24 (1H, m), 7.06-7.08 (1H, m), 3.17-3.19 (6H, d), 1.28-1.30 (9H, d). ^{13}C NMR (100 MHz, $CDCl_3$) δ 162.0, 161.3, 160.5, 155.7, 155.4, 150.4, 149.7, 138.4, 137.0, 126.8, 126.2, 125.4, 124.4,

123.9, 123.7, 77.4, 77.2, 77.0, 76.7, 37.4, 37.4, 34.6, 34.6, 31.3. HRMS (EI, magnetic sector) calcd for $C_{18}H_{24}N_4O$: 298.1793, found: 298.1768.

3.6.9 – Synthesis of 4,4'-Di-tert-butyldiphenylamine (9)

N-formyl tBu_2-DPA used in this work was courtesy of Neill Penner and was synthesized as described in Shah *et al.*[29]

3.6.10 – Synthesis of 2-fluoro-4-methoxy-nitrobenzene (10)

2-Fluoro-4-hydroxy-nitrobenzene (2.37 g, 15 mmol) was dissolved in THF (6 mL) and stirred at 0 °C under a nitrogen atmosphere. To the solution, NaH (720 mg of a 60% suspension in mineral oil, 18 mmol) was added portion-wise. After the reaction warmed to room temperature methyl iodide (0.93 mL, 15 mmol) was added and the reaction was heated to reflux overnight. Once cooled, the reaction was quenched with 120 mL of water and extracted with 3x75 mL EtOAc. The organic phases were collected and dried with magnesium sulphate, filtered and the solvent evaporated in vacuo. The residue was purified via column chromatography on silica gel (hexanes:EtOAc, 4:1) to afford 770 mg (4.5 mmol) of the product as a white solid in 30% yield. ^{1}H NMR (400 MHz, $CDCl_3$): δ 8.05-8.10 (1H, tt, J= 1.2, 8.8), 6.70-6.76 (2H, m), 3.88 (3H, s). The spectroscopic characterization was consistent with that reported in the literature.[63]

3.6.11 – Synthesis of 2-(2-bromophenoxy)-4-methoxy-1-nitrobenzene (11)

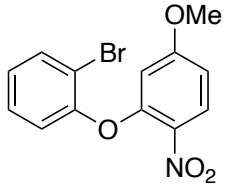

2-Fluoro-4-methoxy-nitrobenzene (684.5 mg, 4 mmol), ortho-bromophenol (709.3 mg, 4.1 mmol) and K_2CO_3 (2.3 g, 9.2 mmol) were combined in DMSO and stirred under a nitrogen

atmosphere at 100 °C overnight. Once cooled, the reaction mixture was poured into water and extracted 3 times with EtOAc. The organic phases were collected and dried with magnesium sulphate, filtered and the solvent evaporated in vacuo. The residue was purified by column chromatography on silica gel (hexanes:EtOAc, 85:15) to afford 1.1 g (3.4 mmol) of the product as a grey-red solid in 85% yield. ^{1}H NMR (400 MHz, $CDCl_3$): δ 8.09-8.11 (1H, d, J=9.2), 7.83-7.85 (1H, dd, J=7.9, 1.6), 7.28-7.33 (1H, td, J=15.6, 8.0, 1.6), 7.09-7.11 (1H, td, J=15.4, 7.9, 1.4), 7.00-7.03 (1H, dd, J=8.1, 1.5), 6.65-6.68 (1H, dd, J=9.2, 2.7), 6.26-6.27 (1H, d, J=2.7), 3.77 (3H, s). ^{13}C NMR (100 MHz, $CDCl_3$) δ 164.5, 152.6, 152.1, 134.2, 133.7, 129.0, 128.5, 126.4, 121.1, 115.1, 108.4, 104.7, 77.4, 77.0, 76.7, 56.0. HRMS (EI, magnetic sector) calcd for $C_{13}H_{10}BrNO_4$: 322.9793, found: 322.9765.

3.6.12 – Synthesis of 2-(2-bromophenoxy)-4-methoxy N-formyl-aniline (12)

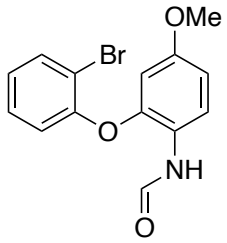

A mixture of 2-(2-bromophenoxy)-4-methoxy-1-nitrobenzene (972.4 mg, 3 mmol), anhydrous $SnCl_2$ (2.84 g, 15 mmol), 10 equivalents of water and a minimum of EtOAc to dissolve the mixture was stirred overnight. The mixture was poured slowly into saturated sodium bicarbonate solution and left to stir for 30 minutes. The mixture was then extracted 5 times with EtOAc, the organic phases were combined, dried with magnesium sulphate, filtered and the solvent evaporated in vacuo. The crude product was used in the subsequent step where it was dissolved in 10 mL of formic acid and heated to reflux overnight. The mixture was then

cooled, poured into saturated sodium bicarbonate, extracted thrice with EtOAc, dried with $MgSO_4$, filtered and the solvent evaporated in vacuo. The crude material was purified with a silica plug (hexanes:EtOAc, 4:1) affording 550 mg (1.71 mmol) of the product as a grey-off-white solid in 57% yield. ^{1}H NMR (400 MHz, DMSO-d6): δ 9.64 (1H, s), 8.17 (1H, d J= 1.8), 7.98-8.00 (1H, d, J= 9.1), 7.62-7.64 (1H, dd, J = 1.4, 7.9), 7.21-7.25 (1H, td, J = 1.4, 7.5), 7.06-7.12 (2H, m), 6.97-6.98 (1H, d, J = 2.9). ^{13}C NMR (150 MHz, $CDCl_3$) δ 161.6, 158.8, 157.5, 156.4, 136.9, 136.4, 133.4, 133.1, 132.9, 132.0, 128.3, 128.2, 127.9, 127.7, 127.2, 127.0, 123.4, 122.9, 122.4, 121.5, 121.4, 121.1, 120.3, 120.1, 117.3, 117.1, 77.3, 77.1, 76.9, 55.8, 55.7. HRMS (EI, magnetic sector) calcd for $C_{14}H_{12}BrNO_3$: 321.0000, found: 320.9986.

3.6.13 – Synthesis of *N*-formyl-3-methoxy-phenoxazine (13)

2-(2-Bromophenoxy)-4-methoxy *N*-formyl-aniline (250 mg, 0.78 mmol) was dissolved in 3.5 mL of toluene and stirred under a nitrogen atmosphere at room temperature. CuI (10 mg, 0.05 mmol), DMEDA (8.5 μL, 0.08 mmol) and K_2CO_3 (232.1 mg, 1.68 mmol) were then added and the mixture was stirred at 120 °C overnight. The reaction was then cooled, poured onto water and extracted thrice with EtOAc. The organic phases were collected and dried with magnesium sulphate, filtered and the solvent evaporated in vacuo. The residue was purified via column chromatography on silica gel (hexanes:EtOAc, 8:2) affording 102 mg (0.43 mmol) of the product as a white powder in 55% yield. ^{1}H NMR (400 MHz, $CDCl_3$): δ 8.62 (1H, s), 7.85-7.96 (1H, d, J = 7.6), 7.05-7.17 (4H, m), 6.63-6.65 (1H, d, J=9.5), 3.79 (3H, s). ^{13}C NMR (100 MHz, $CDCl_3$): δ 160.0, 158.5, 127.0, 124.3, 123.6, 123.2, 118.6, 118.0, 117.3, 109.6, 108.8, 103.2, 102.5, 77.4, 77.2, 77.0, 76.7, 55.7. HRMS (EI, magnetic sector) calcd for $C_{14}H_{11}NO_3$: 241.0738, found: 241.0759.

3.6.14 – Synthesis of 2-iodo-5-(trifluoromethyl)phenol (14)

To *m*-Trifluromethylphenol (2.4 mL, 20 mmol) dissolved in toluene (60 mL) and placed under a nitrogen atmosphere, NaH (1.2 g of a 60% suspension in mineral oil, 30 mmol) was added portion-wise and stirred for 5 minutes at room temperature after the last portion was added. Iodine (5.08 g, 20 mmol) was then added and the reaction was stirred for 16h. The reaction mixture was then poured onto water and extracted thrice with EtOAc. The organic extracts were combined, dried with $MgSO_4$, filtered and the solvent evaporated in vacuo. The crude mixture was purified by column chromatography on silica gel (hexanes:EtOAc 9:1) affording 3.8 g (13.2 mmol) of the product as beige needles in 66% yield. ^{1}H NMR (400 MHz, $CDCl_3$): δ 7.75-7.78 (1H, dd, J = 8.2, 0.9), 7.20-7.21 (1H, d, J = 1.8), 6.90-6.93 (1H, ddd, J = 8.2, 1.8, 0.9). 5.57 (1H, s). The spectroscopic characterization was consistent with that reported in the literature.[64]

3.6.15 – Synthesis of 1-Iodo-2-(2-nitrophenoxy)-4-(trifluoromethyl)benzene (15)

2-Iodo-5-trifluormethylphenol (1.53 g, 5.3 mmol), 2-nitrochlorobenzene (787.8 mg, 5 mmol) and K_2CO_3 (1.55 g, 11.2 mmol) were combined in DMSO (7.5 mL) and heated to 100 °C in a Schlenk tube under an inert atmosphere overnight. The next day the reaction mixture was cooled and run through a silica plug (hexanes:EtOAC, 9:1). The semi-purified product was used in the subsequent step. ^{1}H NMR (300 MHz, $CDCl_3$): δ 8.26-8.27 (1H, d, J = 2.3), 7.57-7.71 (2H, m), 7.38-7.44 (1H, tdd, J = 7.6, 1.6, 0.5), 7.16-7.24 (2H, m), 6.83-6.87 (1H, dd, J = 8.8, 0.5). The spectroscopic characterization was consistent with that reported in the literature.[2]

3.6.16 – Synthesis of 1-Iodo-2-(2-N-formylanilinephenoxy)-4-(trifluoromethyl)benzene (16)

The crude material from the previous step was combined with $SnCl_2$ (2.51 g, 13.2 mmol) and water (0.48 mL) in a minimum volume of ethyl acetate required to dissolve the mixture and left to stir at room temperature overnight. The mixture was then poured on saturated sodium bicarbonate and left to stir for 30-40 minutes. The mixture was then extracted thrice with EtOAc and concentrated in vacuo before being taken up in 10 mL of formic acid and heated to reflux until the starting amine was consumed (judged by TLC). The mixture was then stirred in saturated sodium bicarbonate solution and extracted thrice with ethyl acetate. The organic layer was then dried with $MgSO_4$, filtered and the solvent evaporated in vacuo. The product was recrystallized from hexanes affording 218.6 mg (0.53 mmol) of the product as a white fluffy solid in 20% yield over 3 steps. ^{1}H NMR (400 MHz, $CDCl_3$) 8.47-8.81 (2H, m), 7.99-8.01 (1H, d, J = 8.5), 7.66-7.73 (1H, br d), 7.03-7.38 (4H, m), 6.73-6.81 (1H, dd rotamers) ^{13}C NMR (150 MHz, $CDCl_3$) δ 161.3, 158.8, 158.8, 155.8, 155.7, 145.3, 144.4, 141.0, 140.9, 132.8, 132.6, 128.5, 128.2, 125.8, 125.3, 125.1, 124.8, 124.1, 122.5, 122.5, 122.3, 122.0, 118.5, 118.5, 117.0, 115.6, 115.5, 115.5, 115.5, 115.2, 93.0, 77.2, 77.0, 76.8. HRMS (EI, magnetic sector) calcd for $C_{14}H_9F_3INO_2$: 406.9630, found: 406.9644.

3.6.17 – Synthesis of *N*-formyl-3-triflruoromethyl-phenoxazine (17)

1-Iodo-2-(2-N-formylanilinephenoxy)-4-(trifluoromethyl)benzene (218.6 mg, 0.54 mmol) was dissolved in 3.5 mL of toluene and stirred under a nitrogen atmosphere at room temperature. CuI (10 mg, 0.05 mmol), DMEDA (8.5 μL, 0.08 mmol) and K_2CO_3 (232.1 mg, 1.68 mmol) were added and the mixture was stirred at 120 °C overnight. The reaction was then cooled, poured on water and extracted thrice with EtOAc. The organic phases were combined, dried with magnesium sulphate, filtered and the solvent removed in vacuo. The residue was purified by

column chromatography on silica gel (hexanes:EtOAc 8:2) to afford 87 mg (0.31 mmol) of the product as a fluffy white solid in 58% yield. ^{1}H NMR (600 MHz, $CDCl_3$): δ 8.64 (1H, s), 7.89-8.02 (1H, br d), 7.30-7.32 (1H, dd, J = 0.8, 5.6), 7.26 (1H, s), 7.16 (2H, br s), 7.07-7.10 (1H, td, J = 1.0, 5.5, 10.2), 7.02-7.04 (1H, d, J = 13.72) ^{13}C NMR (150 MHz, $CDCl_3$) δ 160.0, 127.6, 126.1, 124.8, 124.3, 123.5, 122.5, 121.3, 120.7, 118.0, 117.5, 114.7, 114.1, 105.3, 77.2, 77.0, 76.8, 29.7. HRMS (EI, magnetic sector) calcd for $C_{14}H_8F_3NO_2$: 279.0507, found: 279.0475.

3.6.18 – Synthesis of 3-methoxy-phenothiazine (18)

1,2-Dichlorobenzene (20 mL) and a stir bar was added to a sealed tube (with a Teflon cap) and purged with argon for 20 minutes. 3-Methoxydiphenylamine (1.99 g, 10 mmol), sulphur (641.4 mg, 20 mmol) and iodine (73.6 mg, 0.29 mmol) were then added and the tube sealed and heated to 180 °C overnight. The cooled reaction mixture was poured on water and extracted thrice with EtOAc. The organic phases were combined, dried with magnesium sulphate, filtered and concentrated in vacuo. The crude mixture was then run through silica plug to eliminate the dichlorobenzene and the product was recrystallized from hexanes and toluene affording 190 mg (0.84 mmol) of the product as a white solid in 8.4% yield. ^{1}H NMR (400 MHz, C_6D_6): δ 6.95-6.97 (1H, dd, J= 7.5, 1.5), 6.82-6.87 (1H, td, J= 9.2, 7.5, 1.3), 6.55-6.69 (2H, m), 6.54-6.57 (1H, dd, J= 8.5, 2.8), 6.05-6.07 (1H, dd, J= 8.0, 1.3), 5.95-5.97 (1H, d, J= 8.5), 4.98 (1H, bs), 3.25 (3H, s). The spectroscopic characterization was consistent with that reported in the literature.[65]

3.6.19 – Synthesis of *N*-formyl-3-methoxy-phenothiazine (19)

3-Methoxy-PTZ (100 mg, 0.44 mmol) was dissolved in 5 mL of formic acid and heated to reflux for 2 hours. The mixture was poured on ice, filtered, and the product recrystallized from hexanes to afford 67 mg (0.26 mmol) of the white solid in 60% yield. ^{1}H NMR (400 MHz, C_6D_6): δ

8.19-8.23 (1H, d, J= 13.1), 7.72-7.88 (1H, dd, J=12.1), 6.27-7.01 (6H, m), 3.07 (3H, s). ^{13}C NMR (150 $CDCl_3$) δ 206.9 (acetone), 161.1, 161.1, 158.5, 158.2, 137.7, 135.6, 132.4, 130.7, 130.4, 129.3, 128.0, 127.8, 127.7, 127.4, 127.1, 127.1, 126.9, 126.3, 125.6, 122.8, 121.9, 113.3, 112.9, 112.7, 112.3, 77.3, 77.1, 76.8, 55.8, 55.7, 30.9 (acetone). HRMS (EI, magnetic sector) calcd for $C_{14}H_8F_3NO_2$: 257.0510, found: 257.0512.

3.6.20 – Synthesis of *N*-formyl-[2-(2-nitro-5-trifluoromethyl-phenylsulfanyl)-anilide] (20)

2-Aminothiophenol (6.3 g, 50 mmol), 2-chloro-5-trifluormethyl-nitrobenzene (11.28 g, 50 mmol) and NaOH (2.0 g, 50 mmol, in 15 mL of water) were dissolved in 200 mL of ethanol and stirred for 2h at room temperature before being heated to reflux for 30 minutes. Once the mixture cooled, it was filtered and washed with water. The crude product was then dissolved in 130 mL of formic acid and heated to reflux overnight. Once cooled, the reaction was poured over ice and the product crystallized from ethanol used crude in the subsequent step per the literature procedure. ^{1}H NMR (400 MHz, C_6D_6): δ 9.77 (1H, br s), 8.48-8.56 (1H, t, J= 14.1), 8.35-8.38 (1H, dd, J= 8.4, 1.3), 8.14 (1H, d, J= 2.0), 7.89-7.92 (1H, dd, J= 8.6, 1.9), 7.69-7.71 (1H, dd, J= 8.6, 1.9), 7.59-7.63 (1H, td, J= 8.4, 1.6), 7.27-7.34 (1H, td, J= 7.7, 1.4), 6.78-6.80 (1H, d, J= 9.4). The spectroscopic characterization was consistent with that reported in the literature.[66]

3.6.21 – Synthesis of 3-trifluoromethyl-phenothiazine (21)

The crude N-formyl-[2-(2-nitro-5-trifluoromethyl-phenylsulfanyl)-anilide] was dissolved in 50 mL of acetone and stirred at room temperature. To the solution was added two portions of KOH (each containing 0.65 g, 11.6 mmol dissolved in 16.25 mL of ethanol). The mixture was then heated to reflux for 1h. The acetone and most of the ethanol was then evaporated in

vacuo and the crude mixture was poured on water and extracted thrice with EtOAc. The organic phases were combined, dried with magnesium sulphate, filtered and concentrated in vacuo. The crude mixture was then run through a silica plug (hexanes:EtOAc, 4:1) and then the product was recrystallized from ethanol to afford 1.2 g (4.53 mmol) of golden platelets in 14.2% yield. ^{1}H NMR (400 MHz, DMSO-d_6): δ 9.04 (1H, s), 7.29-7.32 (1H, dd, J= 8.4, 2.1), 7.23-7.24 (1H, d, J= 1.8), 7.00-7.04 (1H, td, J= 9.1, 7.5, 1.4), 6.92-6.94 (1H, dd, J= 7.6, 1.3), 6.78-6.82 (1H, td, J= 8.9, 7.7, 1.4), 6.75-6.77 (1H, d, J= 8.3), 6.68-6.70 (1H, dd, J = 7.9, 1.3). The spectroscopic characterization was consistent with that reported in the literature [66]

3.6.22 – Synthesis of *N*-formyl-3-trifluoromethyl-phenothiazine (22)

Formic acid (0.68 mL, 17.9 mmol) and acetic anhydride (1.75 mL, 18.5 mmol) were stirred at 0 °C for 30 minutes and then heated at 60 °C for 3h. To the mixed anhydride, 3-trifluoromethyl-phenothiazine (149.7 mg, 0.56 mmol) was added, and the mixture was heated to reflux for 2h. The mixture was allowed to cool and poured into saturated $NaHCO_3$ and stirred until the vigorous bubbling subsided. The solution was then extracted with ethyl acetate thrice. The organic phases were combined, dried with magnesium sulphate, filtered and the solvent evaporated in vacuo. The residue was purified by column chromatograph on silica gel using hexanes:EtOAc (8:2) to afford 148 mg (0.50 mmol) of a fluffy white solid in 90% yield. ^{1}H NMR (400 MHz, DMSO-d_6): δ 8.78 (1H, s), 7.96 (1H, s), 7.37-7.84 (6H, m). ^{13}C NMR (150 MHz, $CDCl_3$): δ 161.0, 160.6, 136.8, 130.8, 129.9, 128.3, 127.9, 127.6, 125.9, 125.7, 124.9, 124.6, 124.1, 121.9, 77.2, 77.0, 76.8, 30.9.^{19}F (400 MHz, DMSO-d_6): δ -60.9. HRMS (EI, magnetic sector) calcd for $C_{14}H_8F_3NOS$: 295.0278, found: 295.0293.

3.6.23 – Synthesis of *N*-formyl-3-$SO_2(Oct_2)$-7-methyl-phentothiazine (23)

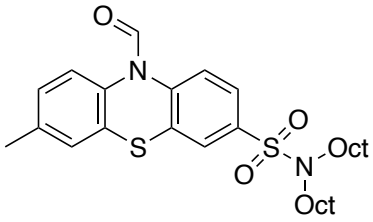

Formic acid (1.39 mL, 36.8 mmol) and acetic anhydride (3.59 mL, 37.95 mmol) were stirred at 0 °C for 30 minutes, then heated at 60 °C for 3h. To the mixed anhydride, 3-$SO_2(Oct_2)$-7-methyl-phenothiazine (624 mg, 1.15 mmol) was added, and the solution heated to reflux overnight. Once the reaction was cooled, it was poured into EtOAC and extracted with 1 M HCl. The extracts were monitored by TLC until no amine remained in the organic phase. The organic phases were combined, dried with magnesium sulphate, filtered and the solvent removed in vacuo to afford 0.4 g (0.7 mmol) of the product as a dark resin in 67% yield. ^{1}H NMR (400 MHz, $CDCl_3$): δ 8.63-8.64 (1H, d), 7.58-7.86 (3H, m), 7.09-7.34 (3H, m), 2.81-3.02 (4H, m), 2.33-2.35 (2H, d). ^{13}C NMR (100 MHz, $CDCl_3$) δ 207.1, 161.0, 138.9, 138.1, 138.0, 134.2, 131.1, 129.5, 129.1, 128.5, 128.4, 128.0, 126.9, 126.6, 126.6, 126.0, 125.9, 121.9, 121.7, 77.4, 77.2, 77.0, 53.9, 53.5, 38.1, 37.9, 32.1, 31.1, 30.6, 30.6, 29.8, 29.8, 29.5, 28.9, 28.9, 23.8, 23.8, 23.2, 22.8, 21.0, 14.3, 14.2, 14.2, 10.8, 10.7. HRMS (EI, magnetic sector) calcd for $C_{30}H_{44}N_2O_3S_2$: 544.2793, found: 544.2794.

3.6.24 – General Synthesis of 5-(benzyloxy)-1-pentanol (24) and 6-(benzyloxy)-1-hexanol (25)

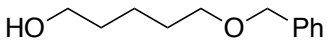

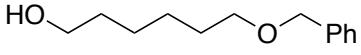

Diol (105 mmol) was dissolved in 150 mL of THF in a Schlenk flask under a nitrogen atmosphere. NaH (4.2 g of a 60% suspension in mineral oil, 105 mmol) was added portion-wise over 10-20 minutes with vigorous stirring. The mixture was then heated to reflux for 4.5h. Benzyl bromide (17.9 g, 105 mmol) was then added, and the mixture was kept at reflux for a further 22h. The reaction was then cooled, filtered and the solid NaBr was washed with THF. The filtrate was then concentrated in vacuo to a yellow oil. The yellow oil was taken up in ether and washed with water until no starting diol remained via TLC. The organic phase was then washed with brine, dried with magnesium sulphate, filtered and concentrated in vacuo. The product was used in the subsequent step without further purification as per the literature procedure.[58] **24:** ^{1}H NMR (400 MHz, $CDCl_3$): δ 7.24-7.35 (5H, m), 4.48 (2H, s), 3.59-3.62 (2H, t), 3.45-3.48 (2H, t), 1.61-1.67 (2H, m), 1.52-1.58 (2H, m), 1.39-1.47 (2H, m). **25:** ^{1}H NMR (300 MHz, $CDCl_3$): δ 7.24-7.38 (5H, m), 4.50 (2H, s), 3.72-3.79 (1H, t), 3.61-3.65 (1H, t), 3.45-3.50 (2H, m), 1.81-1.88 (1H, m), 1.53-1.66 (3H, m), 1.37-1.42 (3H, m), 0.84-0.89 (1H, t). The spectroscopic characterization were consistent with those reported in the literature [58]

3.6.25 – General Synthesis of 5-(benzyloxy)-pentanoic acid (26) and (6-benzyloxy)-hexanoic acid (27)

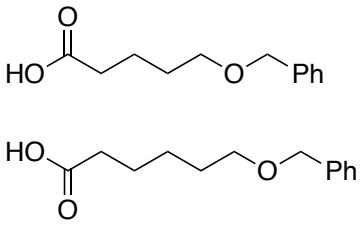

Each of the crude mono-benzylated diols (4 g) were dissolved in 15.8 mL of dry DMF and added dropwise to pyridinium dichromate (13.47 g, 35.8 mmol) in 32 mL of DMF at 0 °C and stirred for 2h. The reaction was then allowed to warm to room temperature and stirred for a further 9h.

The mixture was then poured into 250 mL of water and extracted thrice with diethyl ether. The organic extracts were combined, filtered through celite to remove any residual PDC and extracted with 5x20 mL of 0.5N NaOH solution. The combined aqueous extracts were washed with ether, the basic layer re-acidified with HCl to a pH of ~2-3 and then extracted three times with ether. The organic phases were combined, dried with magnesium sulphate, filtered and the solvent evaporated in vacuo. The crude product was used in the subsequent step without further purification per the literature procedure. **26:** ^{1}H NMR (400 MHz, $CDCl_3$): δ 7.24-7.35 (5H, m), 4.49 (2H, s), 3.46-3.49 (2H, t), 2.35-2.39 (2H, t), 1.62-1.77 (4H, m). **27:** ^{1}H NMR (300 MHz, $CDCl_3$): δ 11.34 (1H, br s), 7.25-7.38 (5H, m), 4.51 (2H, s), 3.46-3.51 (2H, t), 2.34 (2H, t), 1.60-1.72 (4H, m), 1.39-1.49 (2H, m). The spectroscopic characterization were consistent with those reported in the literature [58]

3.6.26 – Synthesis of 5-(benzyloxy)pentanoyl chloride (28) and 6-(benzyloxy)hexanoyl chloride (29)

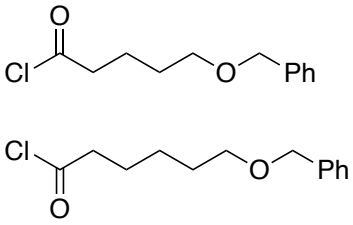

Each of the crude carboxylic acids (1 g) were dissolved in dry DCM (purged with argon) in a Schlenk flask. The solution was cooled to 0 °C in an ice bath and then oxalyl chloride (0.453 mL, 5.3 mmol) and 3 drops of DMF were added. The mixture was stirred for 30 minutes after which gas evolution subsided. The solvent was then evaporated in vacuo to give a yellow oil with some solid dispersed. The oil with solid was filtered through glass wool to give just the oil,

removing some solid that formed. The oil was reacted immediately in the subsequent without further purification.

3.6.27 – Synthesis of *N*-(5-benzyloxypentanoyl)phenothiazine (30)

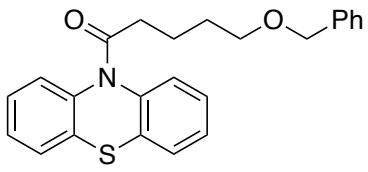

The crude acid chloride **28** (500 mg) and DMAP (50 mg, 0.41 mmol) were dissolved in dry toluene and stirred at room temperature for 5 minutes. PTZ (598 mg, 3 mmol) was then added and the reaction stirred for 2h. The mixture was then poured into water and extracted thrice with EtOAc and washed once with brine. The organic phases were combined, dried with magnesium sulphate, filtered and the solvent evaporated in vacuo. The residue was purified by column chromatography on silica gel (hexanes/EtOAc, 4:1) to afford 429 mg (1.1 mmol) of the product as an off-white solid in 54% yield. ^{1}H NMR (400 MHz, $CDCl_3$): δ 7.40-7.49 (4H, m), 7.18-7.33 (9H, m), 4.41 (2H, s), 3.38 (2H, t), 2.47 (2H, t), 1.66-1.73 (2H, m), 1.52-1.59 (2H, m). ^{13}C NMR (100 MHz, $CDCl_3$): δ 172.0, 138.9, 138.6, 133.3, 128.4, 128.0, 127.6, 127.5, 127.3, 127.0, 126.8, 77.4, 77.3, 77.1, 76.7, 72.8, 7.0, 34.0, 29.0, 22.2. HRMS (EI, magnetic sector) calcd for $C_{24}H_{23}NO_2S$: 389.1449, Found: 389.1455.

3.6.28 – Synthesis of *N*-(5-hydroxypentanoyl)phenothiazine (31)

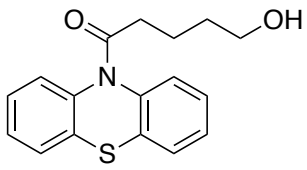

Compound **30** (400 mg, 1.03 mmol) was dissolved in 10 mL of 7:3 EtOH:EtOAc in a round bottom flask sealed with a rubber septum. The solution was sparged with an argon balloon for

20 minutes and then Pd/C (dry matrix) 30 wt% (120.0 mg) was added and the suspension sparged again for 5 minutes with an argon balloon. The solution was then sparged for 20 minutes with two balloons (double layered) of H_2 and was maintained under an atmosphere of H_2 while stirring overnight. The mixture was then filtered through celite and the filter cake was rinsed with DCM. The solvent was then evaporated in vacuo and the residue purified by column chromatography on silica gel (hexanes:EtOAc 7:3) to afford 178.3 mg (0.59 mmol) of the product as an off-white solid in 58% yield. ^{1}H NMR (400 MHz, DMSO-d6): δ 7.60-7.64 (2H, d, J= 10.7, 1.9), 7.55-7.558 (2H, ddd, J= 10.2, 2.1, 0.6), 7.38-7.43 (2H, td, J= 10.5, 2.1, 0.6), 7.28-7.34 (2H, td, J= 10.2, 1.9), 4.32 (1H, t), 3.26 (2H, q), 2.44 (2H, t), 1.43-1.53 (2H, m), 1.18-1.34 (2H, m). ^{13}C NMR (150 MHz, $CDCl_3$): δ 172.3, 138.8, 133.3, 128.1, 127.3, 127.0, 126.9, 77.3, 77.1, 76.8, 62.1, 33.8, 32.0, 21.1. HRMS (EI, magnetic sector) calcd for $C_{17}H_{17}NO_2S$: 299.0980, Found: 299.0917.

3.6.29 – Synthesis of *N*-(6-benzyloxyhexanoyl)phenothiazine (32)

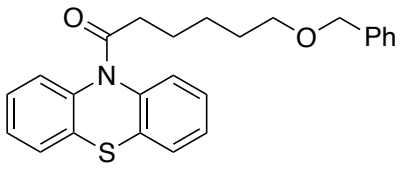

The crude acid chloride **29** (641 mg) and DMAP (64.1 mg, 0.52 mmool) were dissolved in dry toluene and stirred at room temperature for 5 minutes. PTZ (717.4 mg, 3.6 mmol) was then added and the reaction stirred for 2h. The mixture was then poured into water and extracted thrice with EtOAc and washed once with brine. The organic phases were combined, dried with magnesium sulphate, filtered and solvent evaporated in vacuo. The residue was purified by column chromatography on silica gel using hexanes and EtOAc 4:1 to afford 930 mg (2.30

mmol) of the product as an off-white/grey solid in 64% yield. ^{1}H NMR (400 MHz, $CDCl_3$): δ 7.47-7.49 (2H, d, J= 8.0), 7.41-7.43 (2H, dd, J= 7.7, 1.3), 7.18-7.34 (9H, m), 4.44 (2H, s), 3.38 (2H, t), 2.44 (2H, t), 1.48-1.64 (4H, m), 1.23-1.35 (2H, m).^{13}C NMR (100 MHz, $CDCl_3$): δ 172.2, 138.9, 138.6, 128.4, 128.0, 127.6, 127.5, 127.3, 127.0, 126.8, 72.9, 70.2, 34.2, 29.5, 25.7, 25.1. HRMS (EI, magnetic sector) calcd for $C_{25}H_{25}NO_2S$: 403.1606, found: 403.1578.

3.6.30 – Synthesis of *N*-(6-hydroxyhexanoyl)phenothiazine (33)

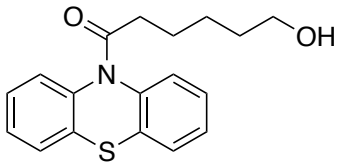

Compound **32** (698, 1.73 mmol) was dissolved in 11 mL of 7:3 EtOH:EtOAc in a round bottom sealed with a rubber septum. The solution was sparged with an argon balloon for 20 minutes and then 30 wt% Pd/C (209 mg, 0.2 mmol) was added and the suspension sparged again for 5 minutes with an argon balloon. The solution was then sparged for 20 minutes with two balloons (double layered) of H_2 and was then maintained under an atmosphere of H_2 while stirring overnight. The mixture was then filtered through celite (frit already wet with DCM) and the filter cake was rinsed with DCM. The solvent was then evaporated in vacuo and the residue purified by column chromatography on silica gel (hexanes:EtOAc 7:3) to afford 439 mg (1.4 mmol) of the product as a white powder in 81% yield. ^{1}H NMR (400 MHz, $CDCl_3$): δ 7.47-7.49 (2H, d, J 8.0 7.41-7.44 (2H, dd, J= 7.7, 1.5), 7.28-7.33 (2H, td, J= 9.3, 7.9, 1.5), 7.19-7.23 (2H, td, J= 8.9, 7.5, 1.3), 3.56 (2H, q), 2.46 (2H, t), 1.60 (2H, m), 1.46 (2H, m), 1.29 (3H, m). ^{13}C NMR (100 MHz, $CDCl_3$): δ 172.3, 139.0, 128.1, 127.5, 127.1, 127.0, 77.5, 77.4, 77.2, 76.8, 62.8, 34.3, 32.4, 31.1, 25.3, 25.0. HRMS (EI, magnetic sector) calcd for $C_{18}H_{19}NO_2S$: 313.1136, found: 313.1132.

3.6.31 – Synthesis of 4-(benzyloxy)butanoyl chloride (34)

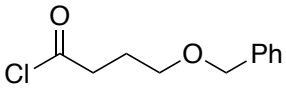

To a flame-dried flask, 4-(benzyloxy)butanoic acid (1.48 g, 7 mmol) was dissolved in 12.5 mL of dry benzene. Under nitrogen atmosphere, the solution was cooled to 0 °C, $SOCl_2$ (1.1 mL, 15.2 mmol) and 5 μL of DMF were added, and the solution allowed to warm to room temperature. After 3 h, the solvent was evaporated in vacuo and the crude acid chloride was used in the subsequent step.

3.6.32 – Synthesis of *N*-(4-benzyloxybutanoyl)phenothiazine (35)

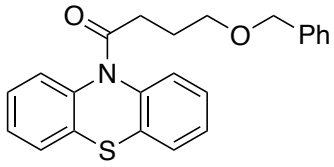

In a flame dried flask PTZ (1.69 g, 8.75 mmol) was dissolved in 12.5 mL of dry toluene. The solution was heated to 60 °C and then crude **34** was added dropwise and the reaction stirred for 4 h. Once cooled, the mixture was poured into water and extracted thrice with EtOAc. The organic phase was washed with brine, dried with $MgSO_4$ and filtered. The solvent was evaporated in vacuo and the residue purified by column chromatography on silica gel (hexanes:EtOAc 4:1) to afford 739 mg (1.9 mmol) of the product in 22.5% yield. ^{1}H NMR (400 MHz, $CDCl_3$): δ 7.48-7.50 (2H, d, J = 7.4), 7.40-7.43 (2H, dd, J = 1.5, 7.7), 7.18-7.32 (9H, m), 4.42 (2H, s), 3.44-3.47 (2H, t), 2.56-2.59 (2H, t), 1.89-1.96 (2H, m). ^{13}C NMR (100 MHz, $CDCl_3$): δ 171.9, 138.9, 138.5, 133.3, 128.3, 128.0, 127.6, 127.5, 127.4, 127.0, 126.8, 77.4, 77.2, 77.0, 76.7, 72.7, 69.1, 31.0, 25.4. HRMS (EI, magnetic sector) calcd for $C_{23}H_{21}NO_2S$: 375.1293, found: 375.1286.

3.6.33 – Synthesis of *N*-(4-hydroxybutanoyl)phenothiazine (36)

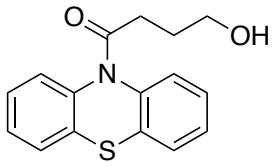

Compound **35** (187.7 mg, 0.5 mmol) was dissolved in 5 mL of 7:3 EtOAc:EtOH in a round bottom sealed with a rubber septum. The solution was sparged with an argon balloon for 20 minutes and then 30 wt% Pd/C (56.3 mg, 0.05 mmol) was added and the suspension sparged again for 5 minutes with an argon balloon. The solution was then sparged for 20 minutes with two balloons (double layered) of H_2 and was then maintained under an atmosphere of H_2 while stirring overnight. The mixture was then filtered through celite (frit already wet with DCM) and the filter cake was rinsed with DCM. The solvent was then evaporated in vacuo and the residue purified by column chromatography on silica gel (hexanes:EtOAc 7:3) to afford 68 mg (0.24 mmol) of the product as an off-white solid in 48% yield. ^{1}H NMR (400 MHz, DMSO-d6): δ 7.57-7.60 (2H, dd, J = 2.0, 10.5), 7.51-7.54 (2H, dd, J = 1.4, 10.0), 7.34-7.39 (2H, td, J = 2.0, 10.3), 7.24-7.30 (2H, td, J = 1.9, 10.1), 4.35-4.3.9 (1H, t), 3.24-3.30 (2H, q), 2.41-2.45 (2H, t), 1.52-1.62 (2H, m). ^{13}C NMR (100 MHz, $CDCl_3$) δ 172.7, 138.7, 128.1, 127.1, 77.4, 77.0, 76.7, 68.5, 62.3, 31.7, 27.9, 27.8, 22.2. HRMS (EI, magnetic sector) calcd for $C_{16}H_{15}NO_2S$: 285.0823, found: 285.0804.

3.6.34 – Synthesis of *N*-(5-benzyloxypentanoyl)phenoxazine (37)

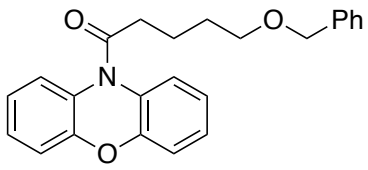

The crude acid chloride **28** (500 mg) and DMAP (50 mg, 0.4 mmol) was dissolved in 7.5 mL of dry and argon-purged toluene in a Schlenk flask under an inert atmosphere. The mixture was heated to 55 °C, PNX (556 mg, 3.03 mmol) was added and the mixture was stirred for 2h. Once cooled, the mixture was poured into water and extracted thrice with EtOAc and washed once with brine. The organic phases were combined and dried with magnesium sulphate, filtered and solvent removed in vacuo. The residue was purified by column chromatography on silica gel (hexanes:EtOAc 4:1) to afford 460 mg (1.18 mmol) of the product as an off-white/grey solid in 39% yield. ^{1}H NMR (400 MHz, $CDCl_3$): δ 7.44-7.47 (2H, dd, J = 7.8, 1.3), 7.23-7.33 (5H, m), 7.15-7.19 (2H, m), 7.07-7.12 (4H, m), 4.43 (2H, s), 3.40-3.43 (2H, t), 2.61-2.65 (2H, t), 1.73-1.80 (2H, m), 1.57-1.64 (2H, m). ^{13}C NMR (100 MHz, $CDCl_3$): δ 172.1, 151.3, 138.6, 129.5, 128.4, 127.6, 127.5, 126.9, 125.3, 123.3, 117.0, 77.4, 77.1, 76.7, 72.9, 70.0, 33.9, 29.1, 22.2. HRMS (EI, magnetic sector) calcd for $C_{24}H_{23}NO_3$: 373.1677, found: 373.1684.

3.6.35 – Synthesis of *N*-(4-hydroxypentanoyl)phenoxazine (38)

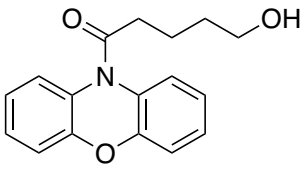

Compound **37** (600 mg, 1.54 mmol) was dissolved in 15 mL of 7:3 EtOH:EtOAc and purged with argon for 20 minutes. Pd/C 30 wt% (60.0 mg, 0.06 mmol) was added to the flask and the suspension was purged with argon for another 10 minutes. The flask was then purged with two balloons of hydrogen gas. Once purged twice, the two balloons were refilled and replaced, and the system closed. The reaction was left to stir overnight. The mixture was then filtered through celite (frit already wet with DCM) and the filter cake rinsed with additional DCM. The solvent

was then evaporated in vacuo and the residue purified via column chromatography on silica gel (hexanes:EtOAc 7:3) to afford 373 mg (1.32 mmol) of the product as an off-white solid in 82% yield. ^{1}H NMR (400 MHz, DMSO-d6): δ 7.55-7.57 (2H, dd, J = 1.6, 7.9), 7.13-7.25 (6H, m), 4.31-4.33 (1H, t), 3.26-3.36 (2H, q), 2.57-2.61 (2H, t), 1.47-1.54 (2H, m), 1.27-1.34 (2H, m). ^{13}C NMR (100 MHz, DMSO-d6): δ 172.0, 151.1, 129.7, 127.5, 126.0, 124.1, 171.1, 60.8, 33.9, 33.6, 21.7. HRMS (EI, magnetic sector) calcd for $C_{17}H_{17}NO_3$: 283.1208, found: 283.1180.

3.6.36 – Synthesis of *N*-(6-benzyloxyhexanoyl)phenoxazine (39)

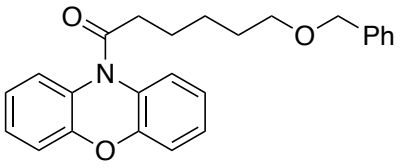

The crude acyl chloride **29** (722 mg) and DMAP (72 mg, X mmol) was dissolved in 10 mL of dry and argon-purged toluene in a Schlenk flask under an inert atmosphere. The mixture was heated to 60 °C, PNX (556 mg, 3.03 mmol) was added and the mixture stirred for 2h. Once cooled, the mixture was poured into water and extracted thrice with EtOAc and washed once with brine. The organic phases were combined and dried with magnesium sulphate, filtered and solvent removed in vacuo. The residue was purified by column chromatography on silica gel (hexanes and EtOAc 4:1) to afford 939 mg (2.4 mmol) of the product as a white waxy solid in 80% yield. ^{1}H NMR (400 MHz, $CDCl_3$): 7.44-7.47 (2H, m), 7.23-7.34 (5H, m), 7.16-7.20 (2H, m), 7.08-7.13 (4H, m). ^{13}C NMR (100 MHz, $CDCl_3$): δ 172.2, 151.3, 138.6, 129.5, 128.4, 127.7, 127.6, 127.5, 126.9, 125.3, 123.4, 117.0, 77.4, 77.3, 77.1, 76.7, 72.9, 70.2, 34.1, 29.5, 25.8, 25.2. HRMS (EI, magnetic sector) calcd for $C_{25}H_{25}NO_3$: 387.1834, found: 387.1807.

3.6.37 – Synthesis of *N*-(6-hydroxyhexanoyl)phenoxazine (40)

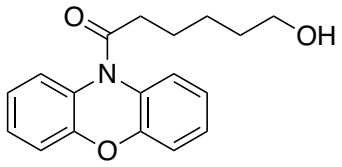

Compound **39** (763 mg, 1.97 mmol) was dissolved in 8.5 mL of EtOH:EtOAc 7:3 in a round bottom flask closed via septum. The solution was purged with an argon balloon for 20 minutes and then 30 wt% Pd/C (76.3 mg, 0.07 mmol) was added and the system was purged again for 5 minutes with an argon balloon. The solution was then purged for 20 minutes with two hydrogen gas balloons (double layered) before being sealed and hydrogen balloons refilled to maintain a hydrogen gas atmosphere and the suspension left to stir overnight. The mixture was then filtered through celite (frit already wet with DCM) and the filter cake rinsed with additional DCM. The solvent was then evaporated in vacuo and the residue purified via column chromatography on silica gel (hexanes:EtOAc 7:3) to afford 456 mg (1.5 mmol) of the product as a fine chalk-like white powder in 76% yield. ^{1}H NMR (400 MHz, DMSO-d6): δ 7.55-7.58 (2H, dd, J= 7.5, 1.5), 7.14-7.26 (6H, m), 4.28 (1H, t), 3.28 (2H, q), 2.57 (2H, t), 1.47 (2H, m), 1.29 (2H, m), 1.17 (2H, m). ^{13}C NMR (100 MHz, DMSO-d6): δ 172.0, 151.1, 129.7, 127.5, 126.0, 124.1, 117.1, 61.0, 40.6, 40.4, 40.2, 40.0, 39.8, 39.6, 39.4, 33.8, 32.7, 25.5, 24.9. HRMS (EI, magnetic sector) calcd for $C_{18}H_{19}NO_3$: 297.1364, found: 297.1430.

3.6.38 – Synthesis of N-acetylphenothiazine (41)

PTZ (2.0 g, 10.03 mmol) was stirred in 0.6 mL of glacial acetic acid at room temperature for 1 h After 1 h, the solution was cooled in an ice bath and acetyl chloride (10 mL, 140 mmol) was added. The mixture was then heated to reflux overnight. Upon cooling to room temperature, the crude product precipitated, was filtered and recrystallized from EtOH to afford 1.84 g (7.6 mmol) of the product as a white powder in 76% yield. ^{1}H NMR (400 MHz, $CDCl_3$): δ 7.53-7.55 (2H, d, J= 7.5), 7.46-7.49 (2H, dd, J= 7.6, 1.4), 7.34-7.39 (2H, td, J= 9.4, 7.9, 1.5), 7.24-7.29 (2H, td, J= 8.7, 7.5, 1.4), 2.24 (3H, s). The spectroscopic characterization was consistent with that reported in the literature [67]

3.6.39 – Synthesis of N-acetylphenoxazine (42)

PNX (2.75 g, 15 mmol) was dissolved in 10 mL of acetic anhydride and heated to reflux for 3 h. Once the mixture cooled, the product precipitated out of the acetic anhydride, was filtered and dried under vacuum to afford 2.01 g (9 mmol) of the product as a white powder in 60% yield. ^{1}H NMR (400 MHz, $CDCl_3$): δ 7.60-7.64 (2H, m), 7.14-7.26 (6H, m), 2.37 (3H, s). The spectroscopic characterization was consistent with that reported in the literature [68]

3.6.40 – General High Temperature Autoxidation Procedure

Using 20 mL test tubes, each test tube was filled with either 10 mL of purified *n*-hexadecane (Alfa Aesar 95%, treated by percolation through 2:1 alumina:silica, with the silica packed on top of the alumina) or a mixture of 9.5 mL of purified *n*-hexadecane and 0.5 mL of dodecanol. Teflon capillaries connected to the gas manifold were placed into each test tube, and the tubes were purged with N_2 at a flow rate of ~3 mL/min. After 20 minutes of purging the substrate, the heating block was set to 165 °C. For those experiments carried out in the presence of palmitic

acid, when the block reached ~155 °C, 12.7 mg of palmitic acid dissolved in a minimum of DCM were added in addition to the RTAs, which were added as solutions in HPLC-grade benzene. Once at 165 °C, the temperature was left to stabilize for 15 minutes and then an initial aliquot was removed. The gas flow was then switched to O_2 at a flow rate of 3 mL/min.

3.6.41 – Quantification of Hydroperoxides in Autoxidations via Microplate Assay

To quantify [ROOH], 5 μL aliquots were loaded into the wells of a 96-well microplate. Immediately before analysis 215 μL of a mixture of 1:4 iPrOH:MeOH and 30 μL of a solution containing fluorogenic coumarin phosphine dye (100 μM) were added using the automated reagent dispenser of the microplate reader at 37 °C. After stirring for 30 seconds followed by a 5 second delay, the fluorescence of the sample was measured every second for 60 seconds at an excitation wavelength of 340 nm and an emission wavelength of 425 nm. The concentration of the hydroperoxide in each well was determined from the rate of phosphine oxidation using the rate constant for the reaction of the dye with secondary peroxyl radicals (k = 5.1 M^{-1} s^{-1})[15] , assuming pseudo-first order kinetics. The response factor used to convert RFU to [ROOH] was 2.2 x 10^{10} a.u./[M].

3.6.42 – Monitoring Release of RTAs by HPLC

Following the same general setup as **3.6.40** except, the RTAs were added once the temperature stabilized at 165 °C, minimizing release before the first aliquots could be taken. The system was also left under N_2 for the duration of the experiment, with aliquots taken at the desired time intervals. Aliquots (100 μL) were diluted with 100 μL of purified *n*-hexadecane and then extracted with 200 μL of HPLC grade MeOH. The *n*-hexadecane/MeOH mixtures are vortexed to ensure mixing/extraction of the desired products into MeOH. 150 μL of the MeOH layer was

then extracted with a micropipette and loaded into an HPLC vial with a glass insert. Samples (10 μL) were injected via an autosampler onto a reverse-phase Kromasil Gold C18 column and eluted with 4:1 MeOH:H_2O at 0.35 mL/min. The chromatograms were monitored via PDA at 252.5 nm for the PTZ-based compounds and 238 nm for the PNX-based compounds.

3.7 – Appendix

3.7.1 – NMR Spectra

^{1}H-NMR ($CDCl_3$, 400 MHz)

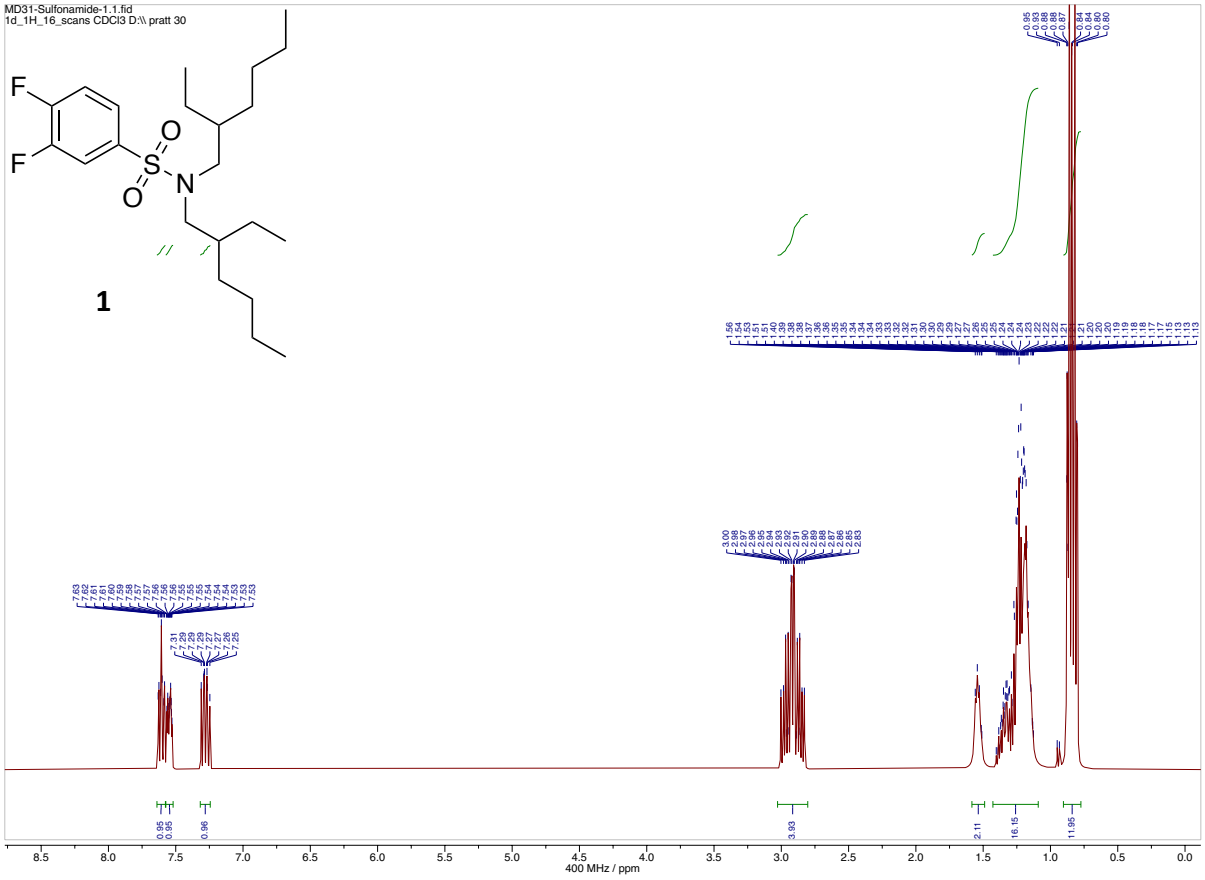

^{13}C-NMR ($CDCl_3$, 100 MHz)

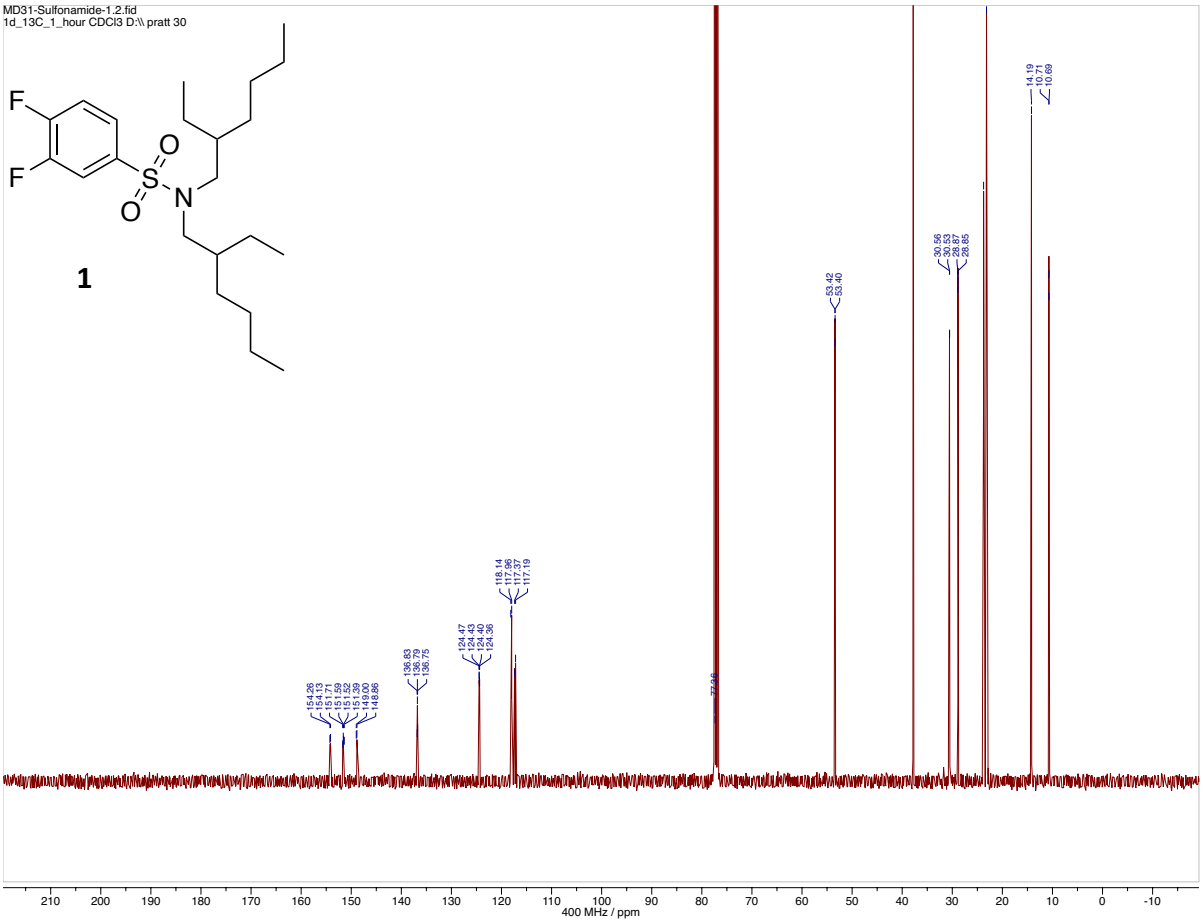

^{1}H-NMR (DMSO-d, 400 MHz)

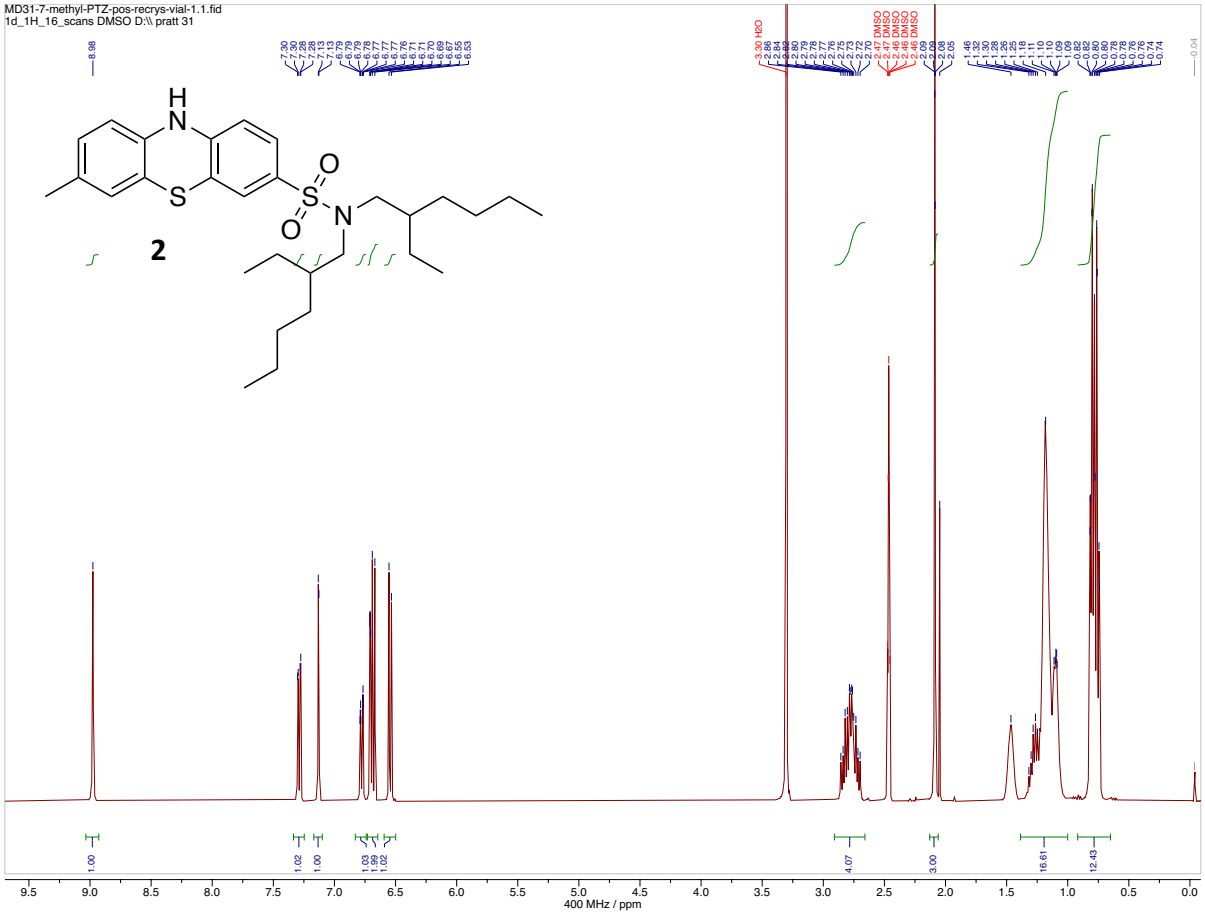

^{13}C-NMR (DMSO-d, 100 MHz)

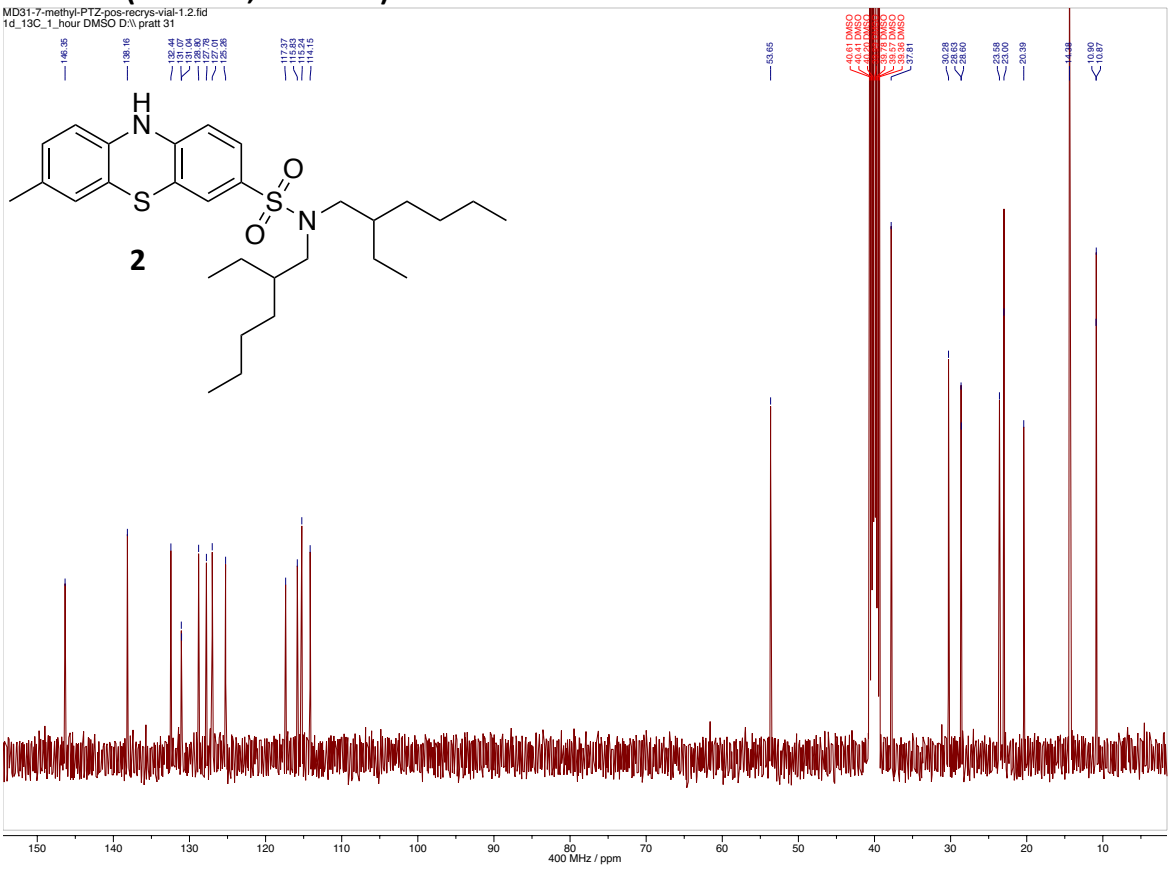

^{1}H-NMR ($CDCl_3$, 400 MHz)

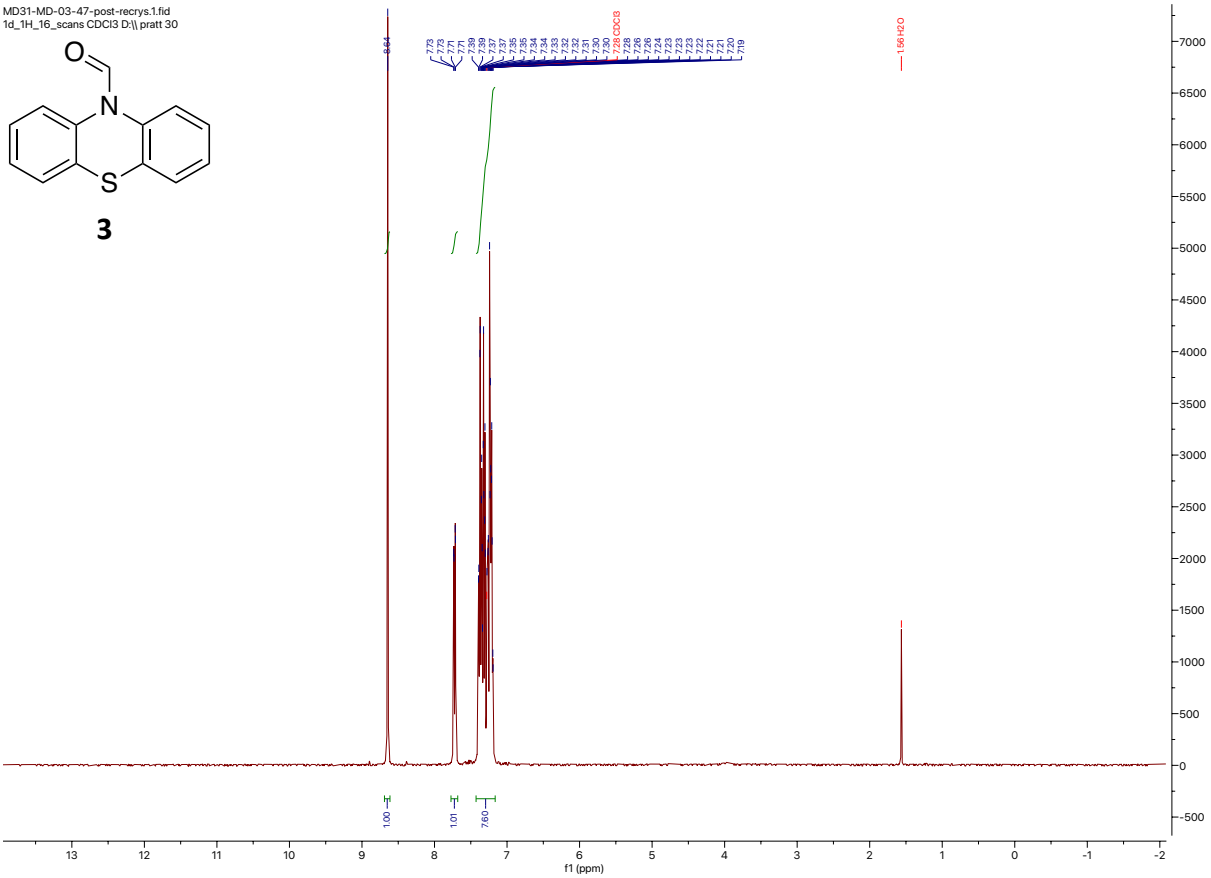

^{1}H-NMR ($CDCl_3$, 400 MHz)

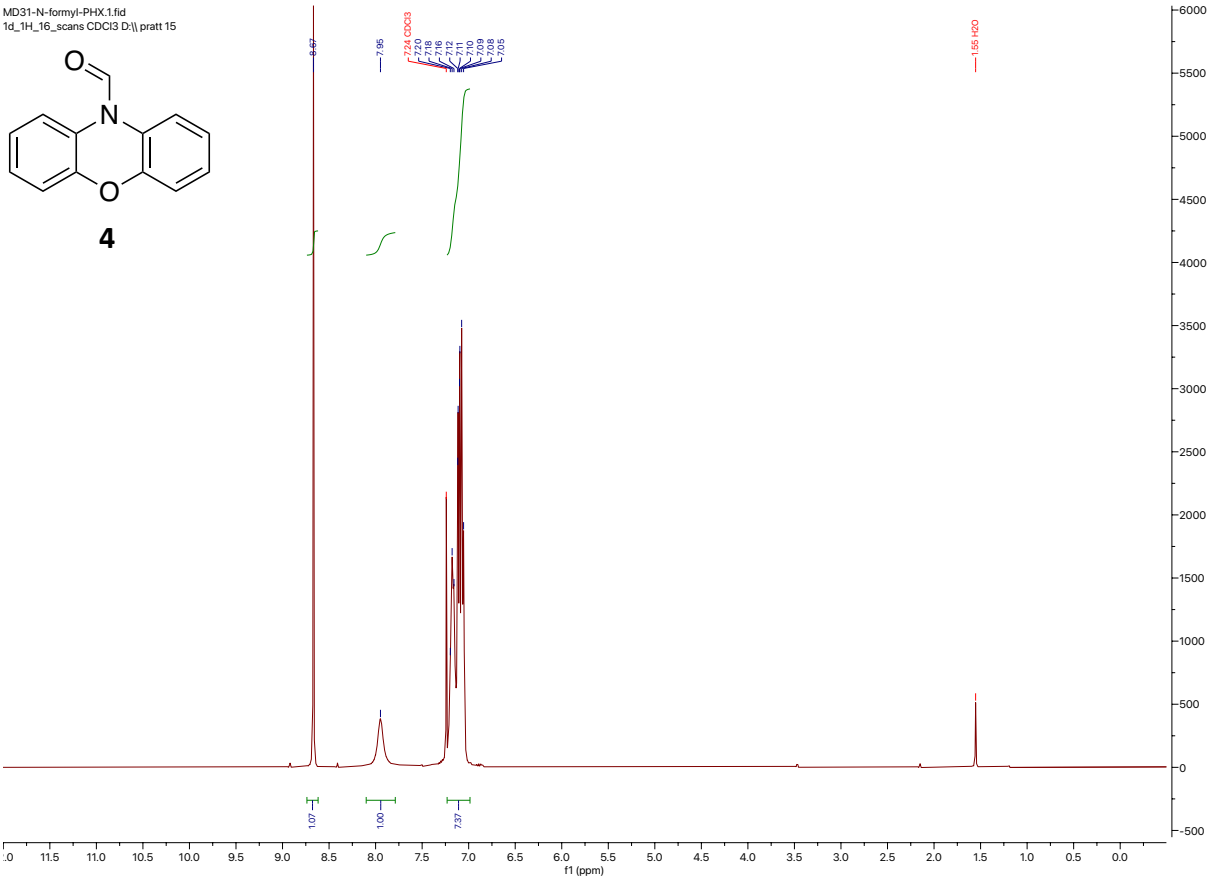

4

^{1}H-NMR (DMSO-d, 400 MHz)

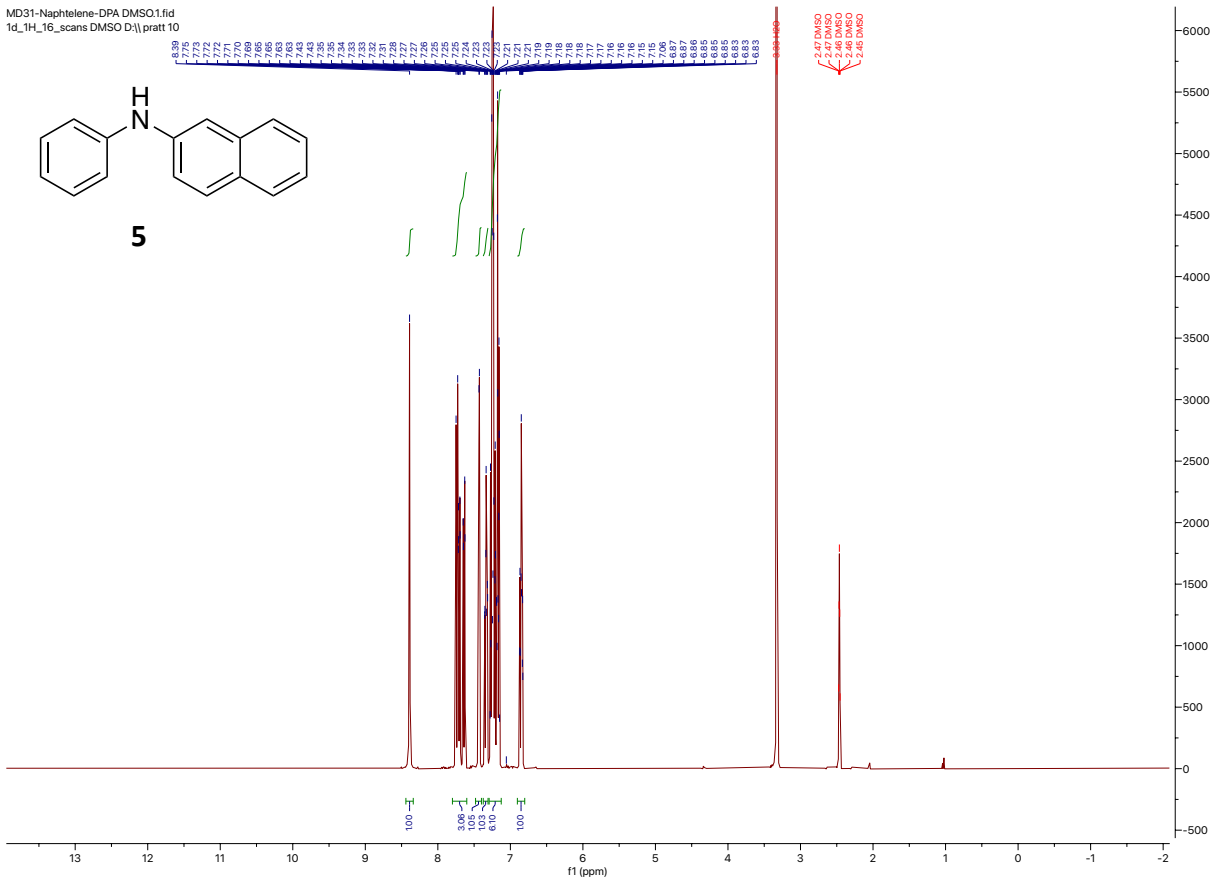

^{1}H-NMR (DMSO-d, 400 MHz)

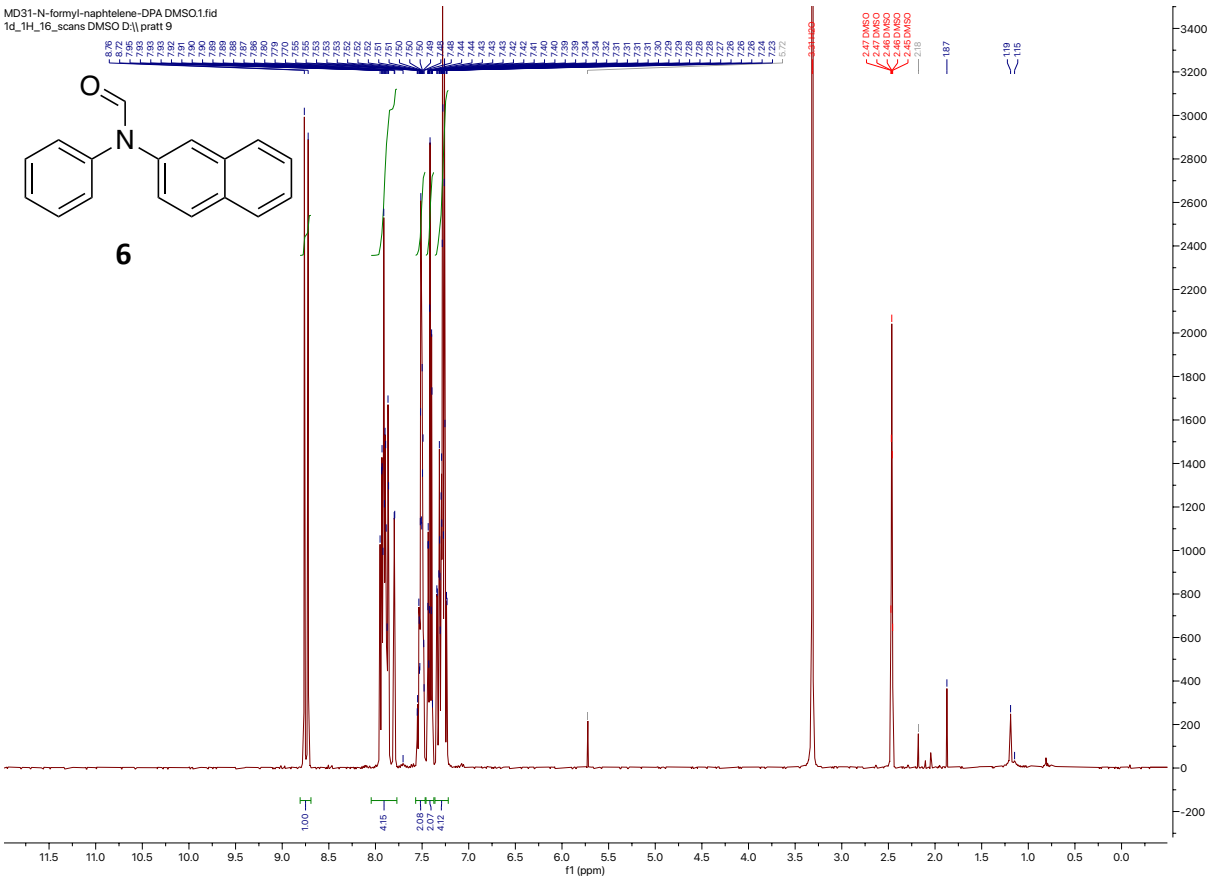

^{1}H-NMR ($CDCl_3$, 400 MHz)

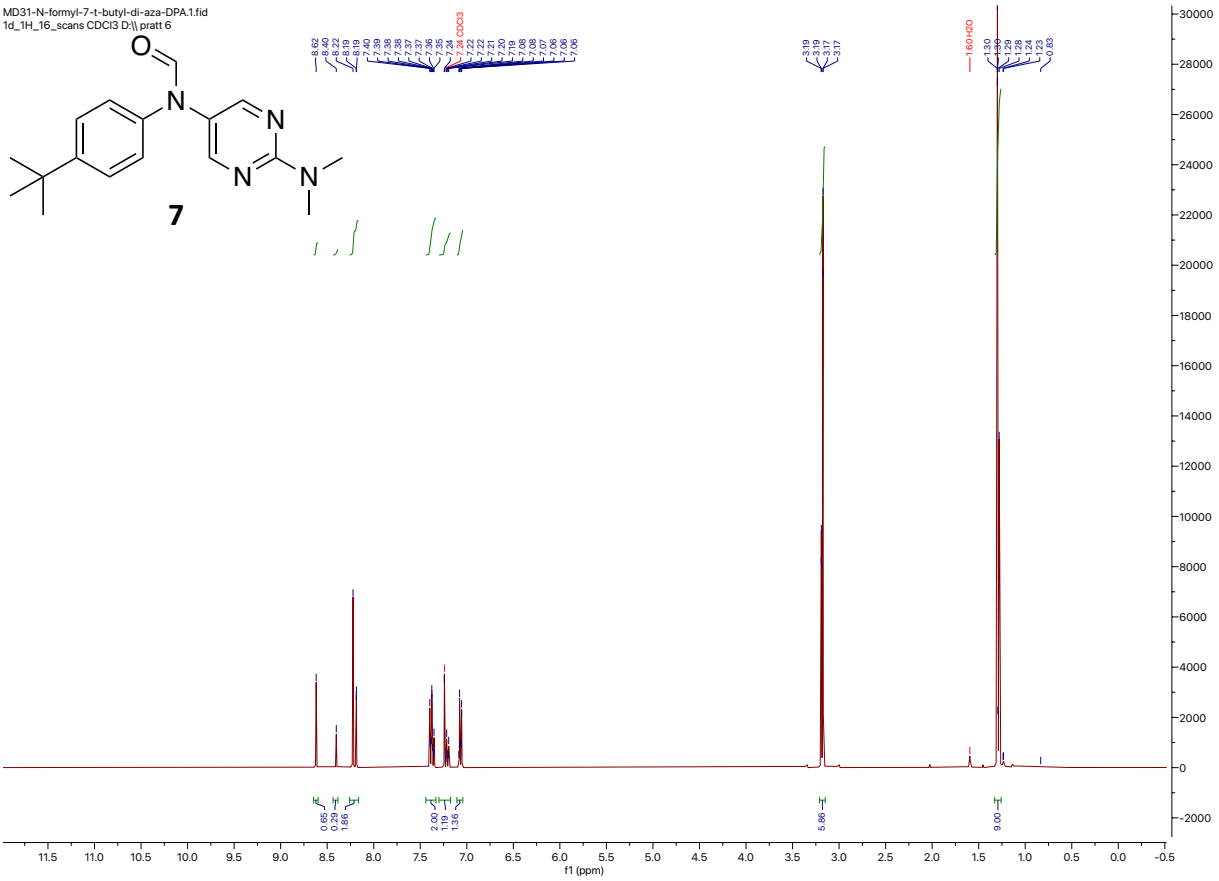

^{13}C-NMR ($CDCl_3$, 100 MHz)

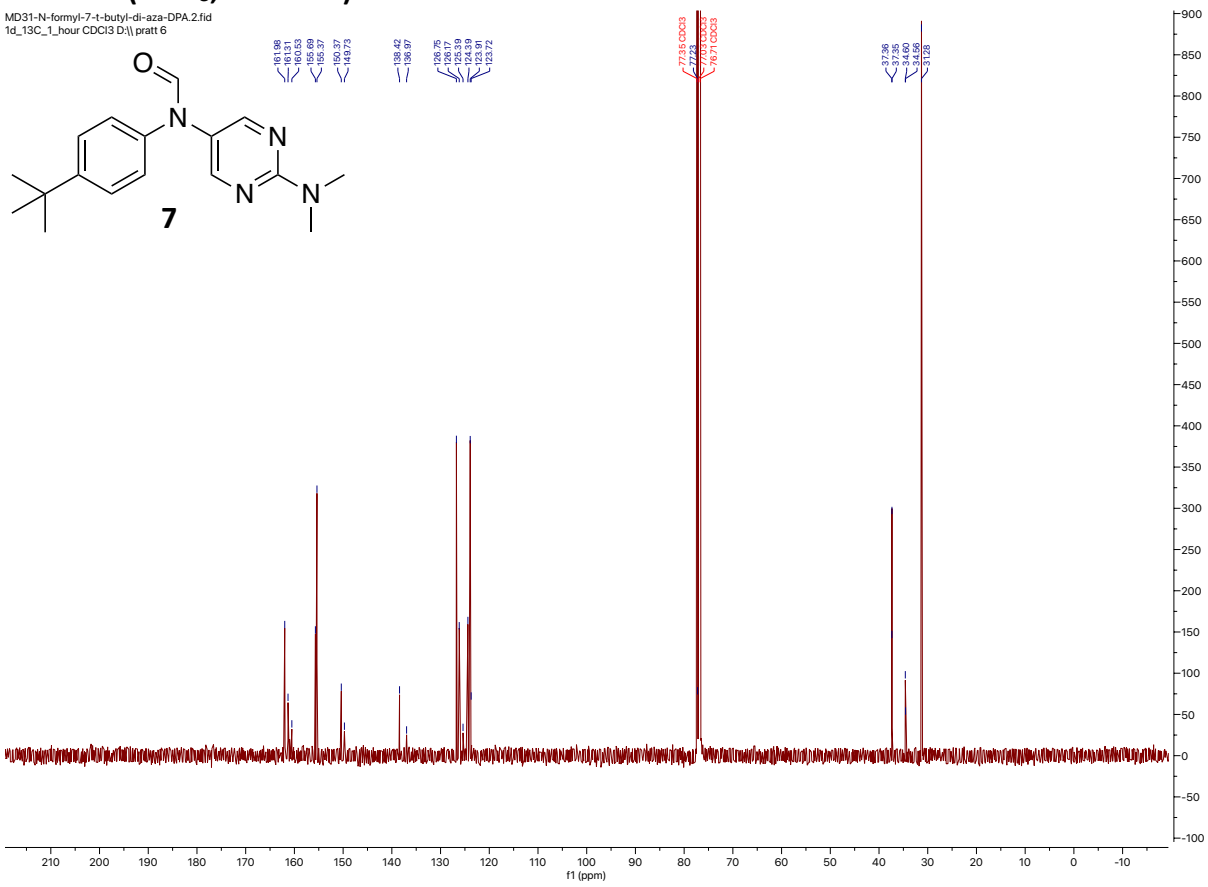

^{1}H-NMR ($CDCl_3$, 400 MHz)

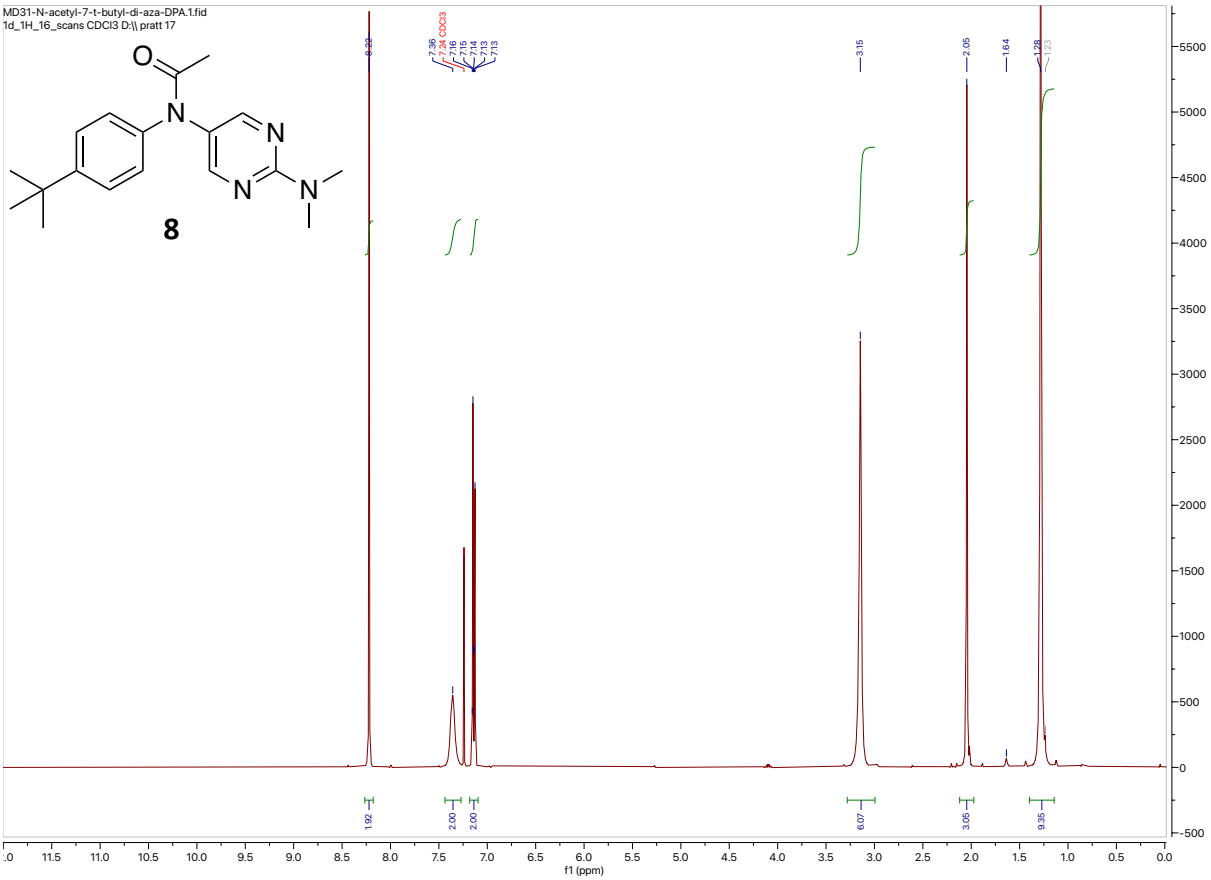

^{13}C-NMR ($CDCl_3$, 100 MHz)

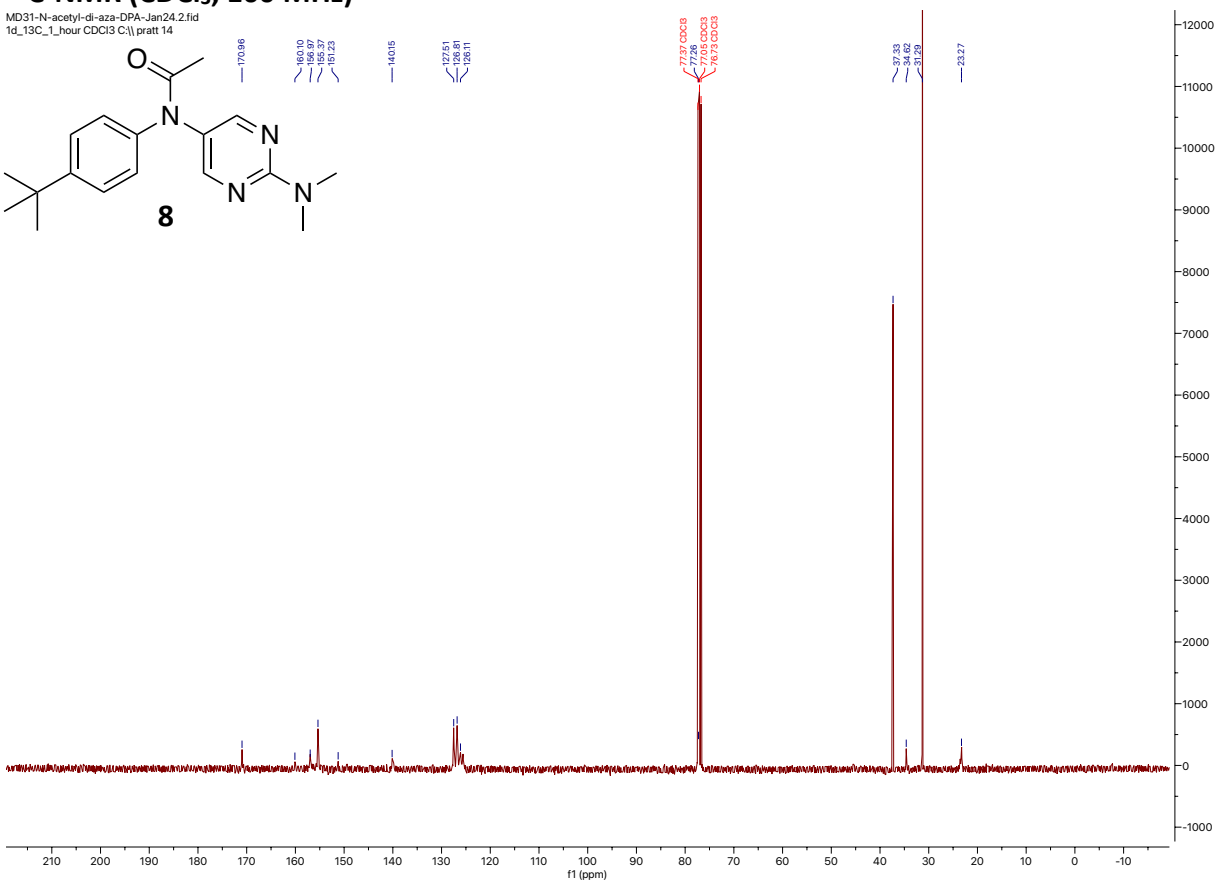

^{1}H-NMR ($CDCl_3$, 400 MHz)

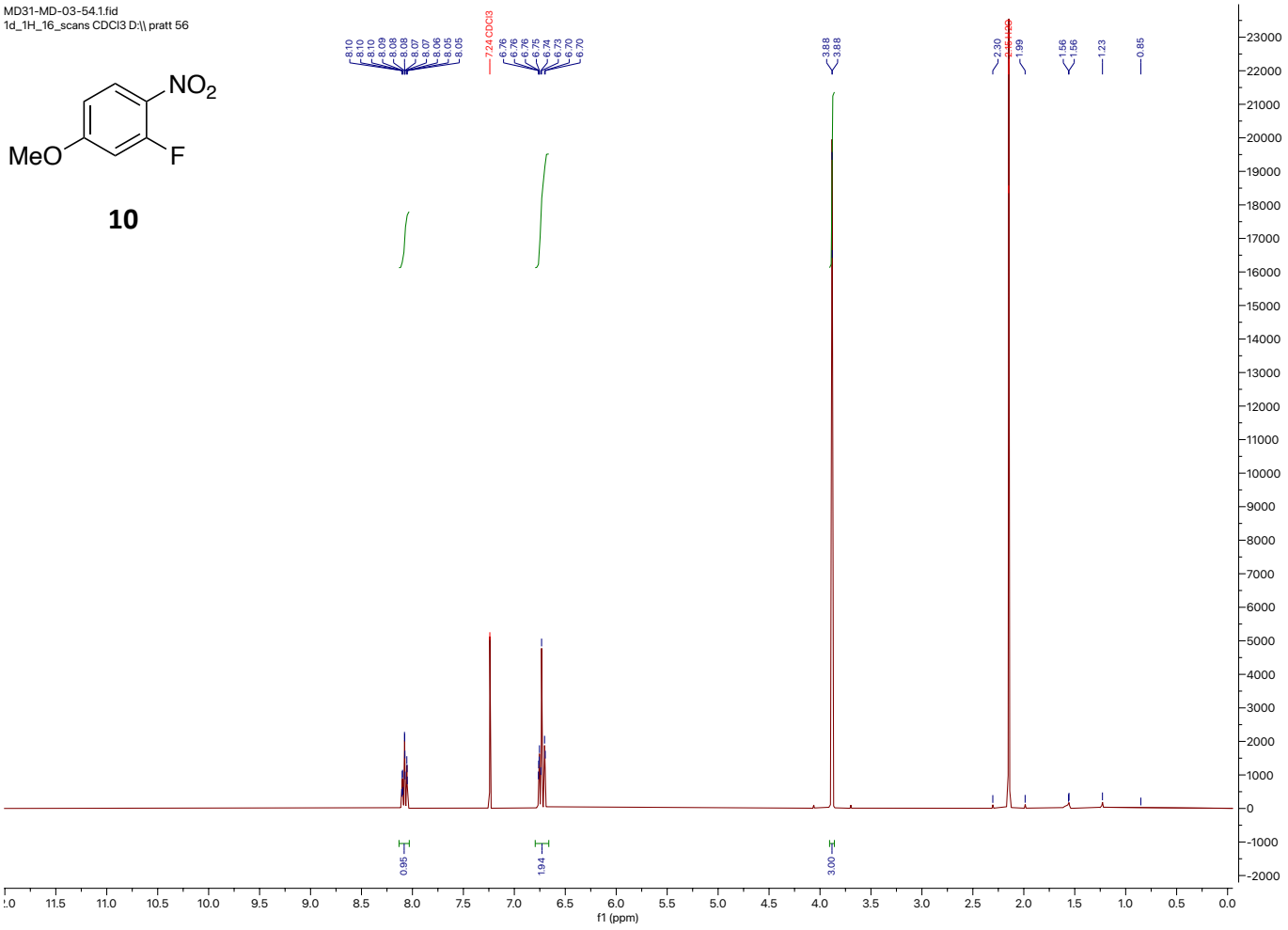

10

^{1}H-NMR ($CDCl_3$, 400 MHz)

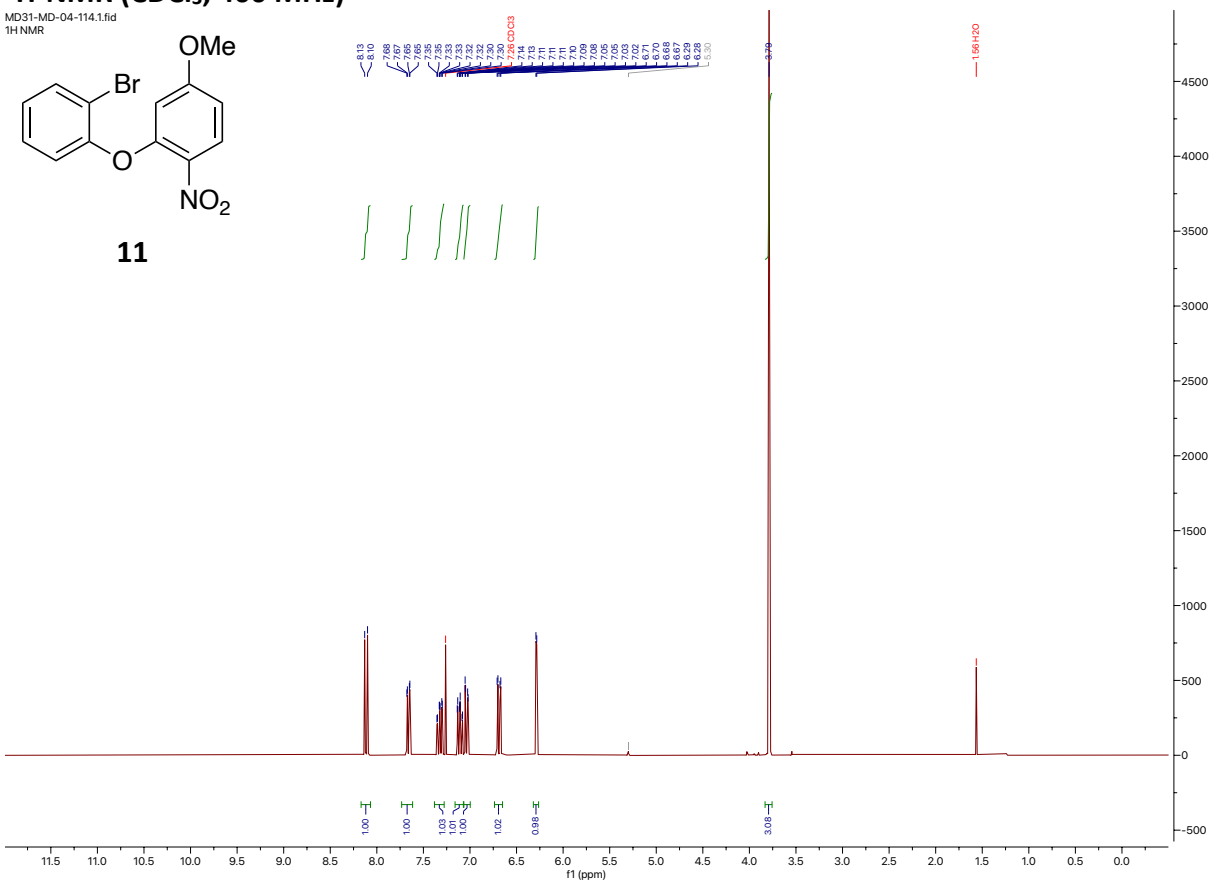

^{13}C-NMR ($CDCl_3$, 100 MHz)

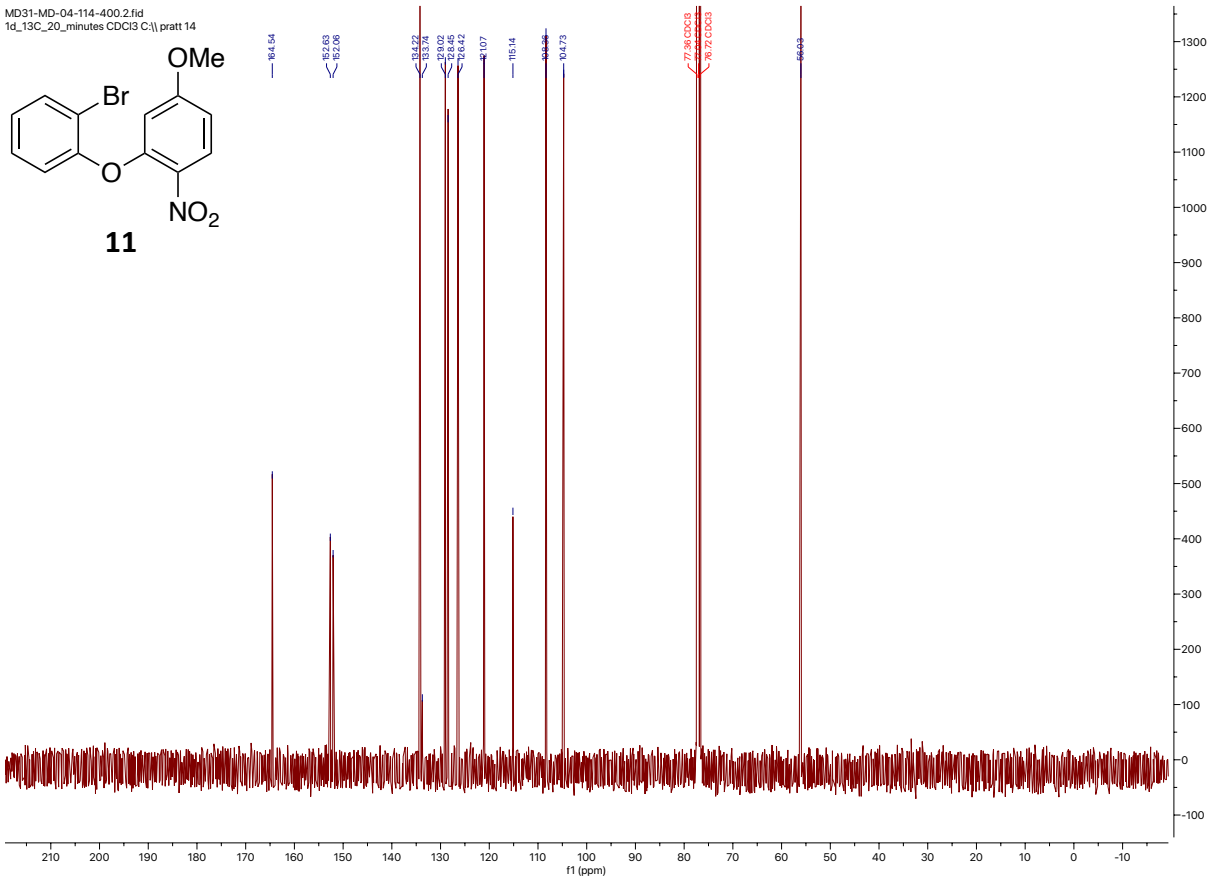

^{1}H-NMR ($CDCl_3$, 400 MHz)

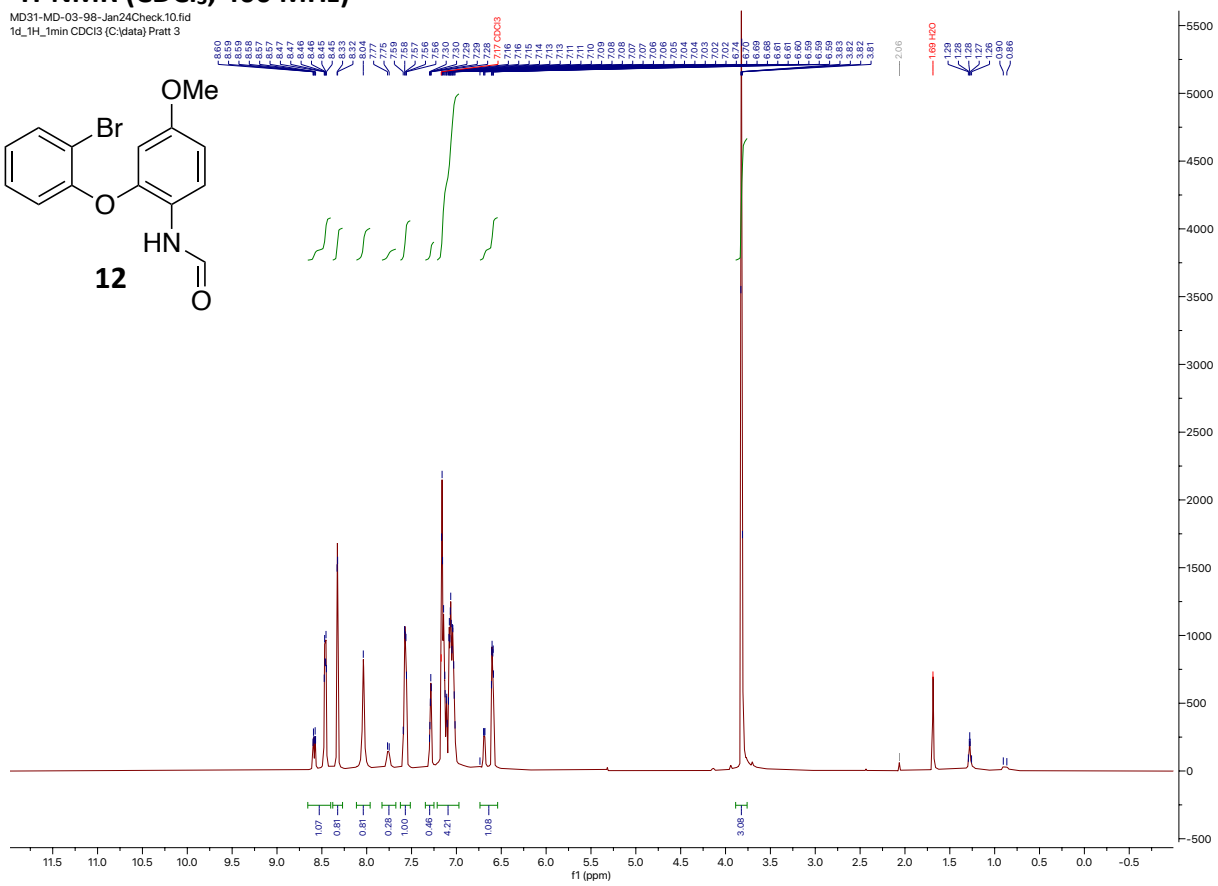

^{13}C-NMR ($CDCl_3$, 150 MHz)

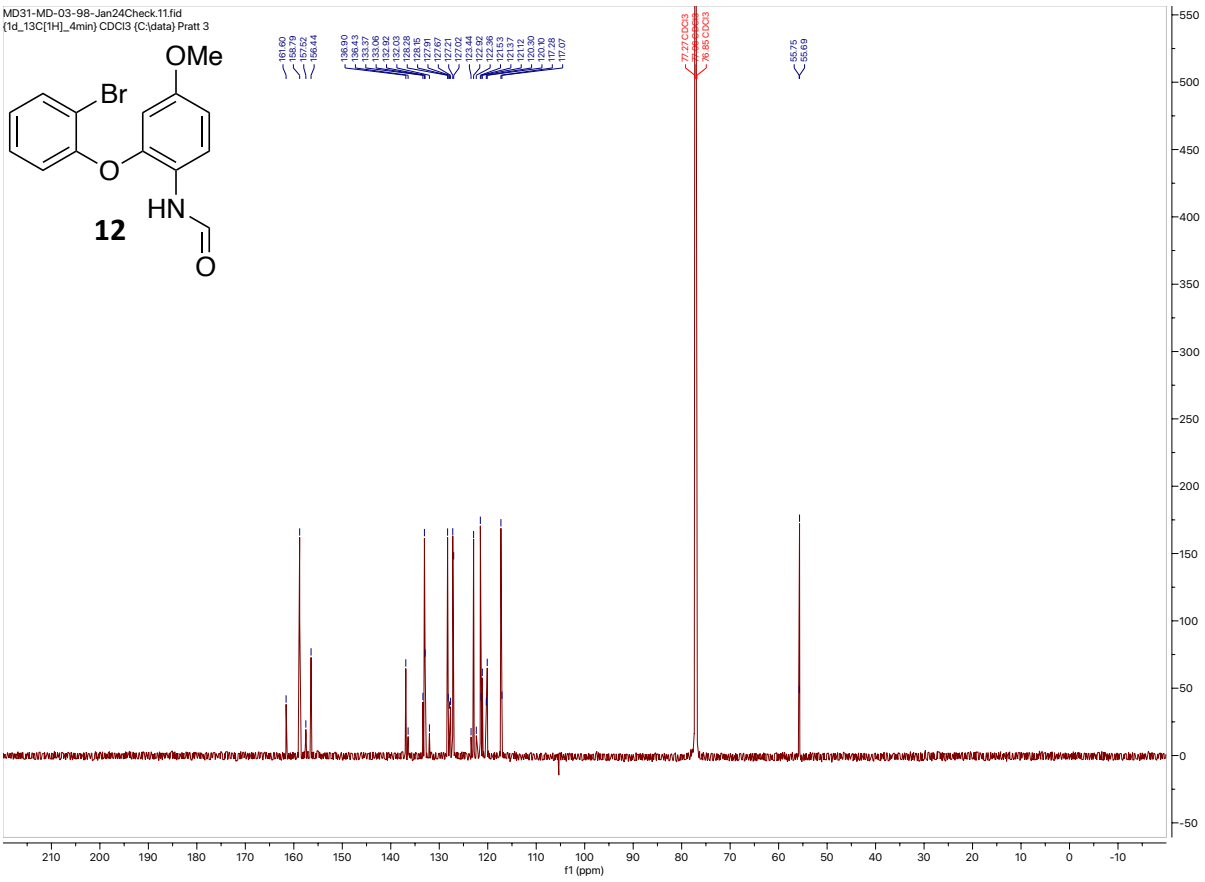

^{1}H-NMR ($CDCl_3$, 400 MHz)

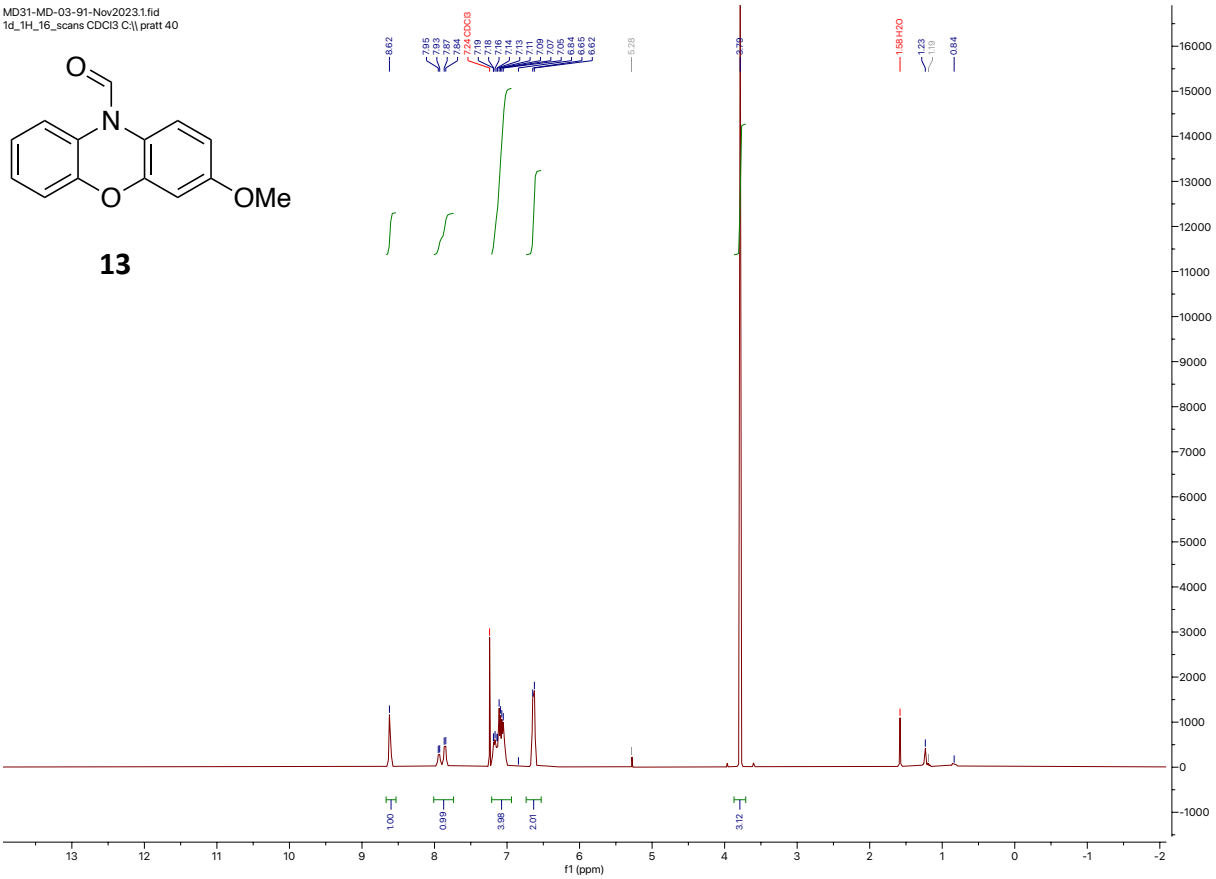

13

^{13}C-NMR ($CDCl_3$, 100 MHz)

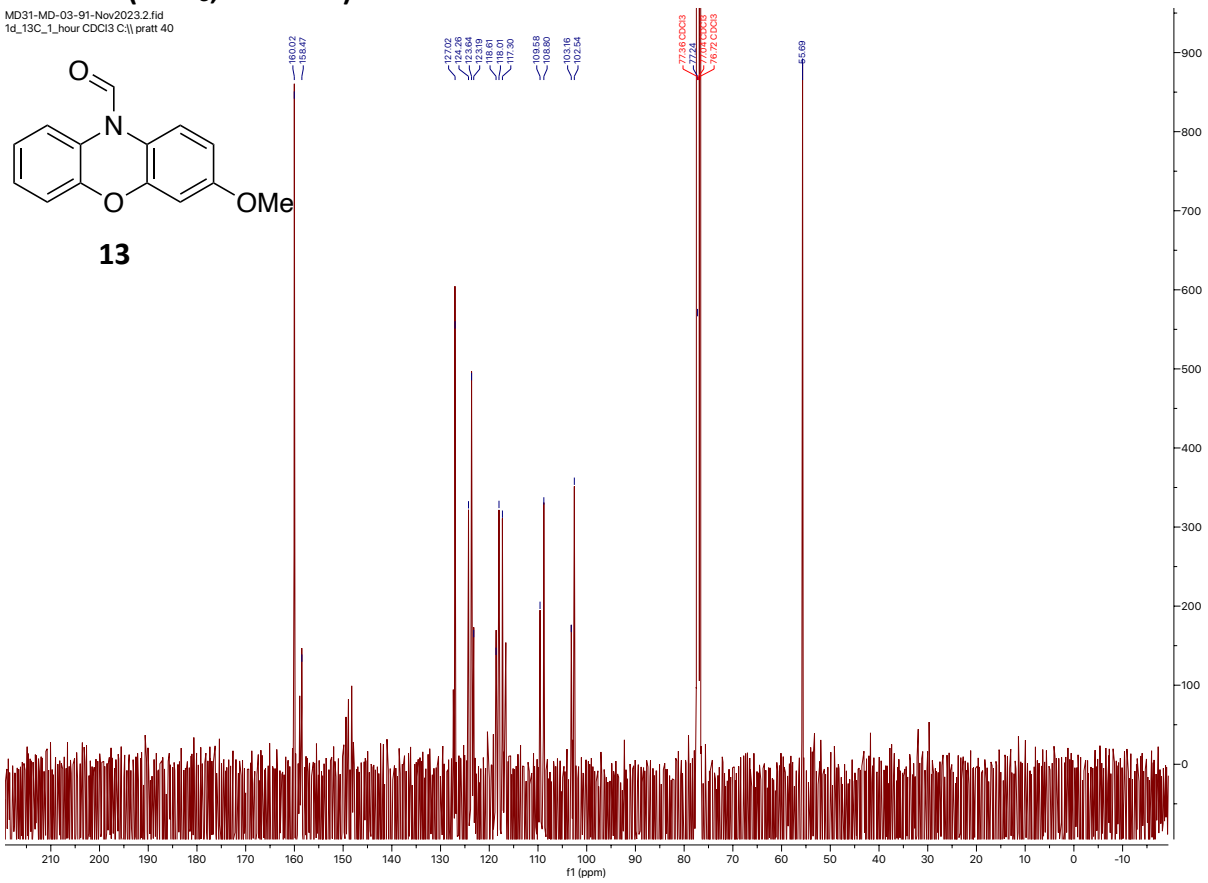

13

^{1}H-NMR ($CDCl_3$, 400 MHz)

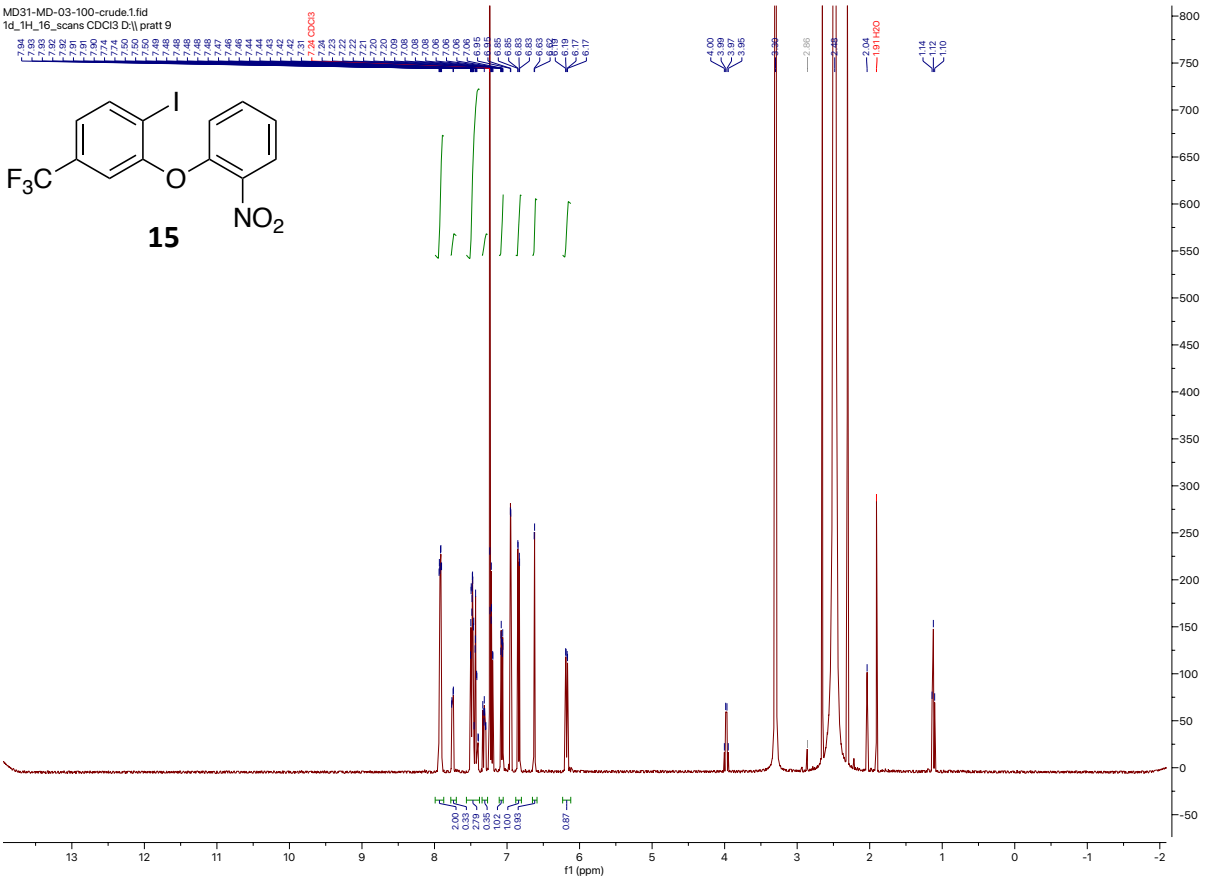

^{1}H-NMR ($CDCl_3$, 400 MHz)

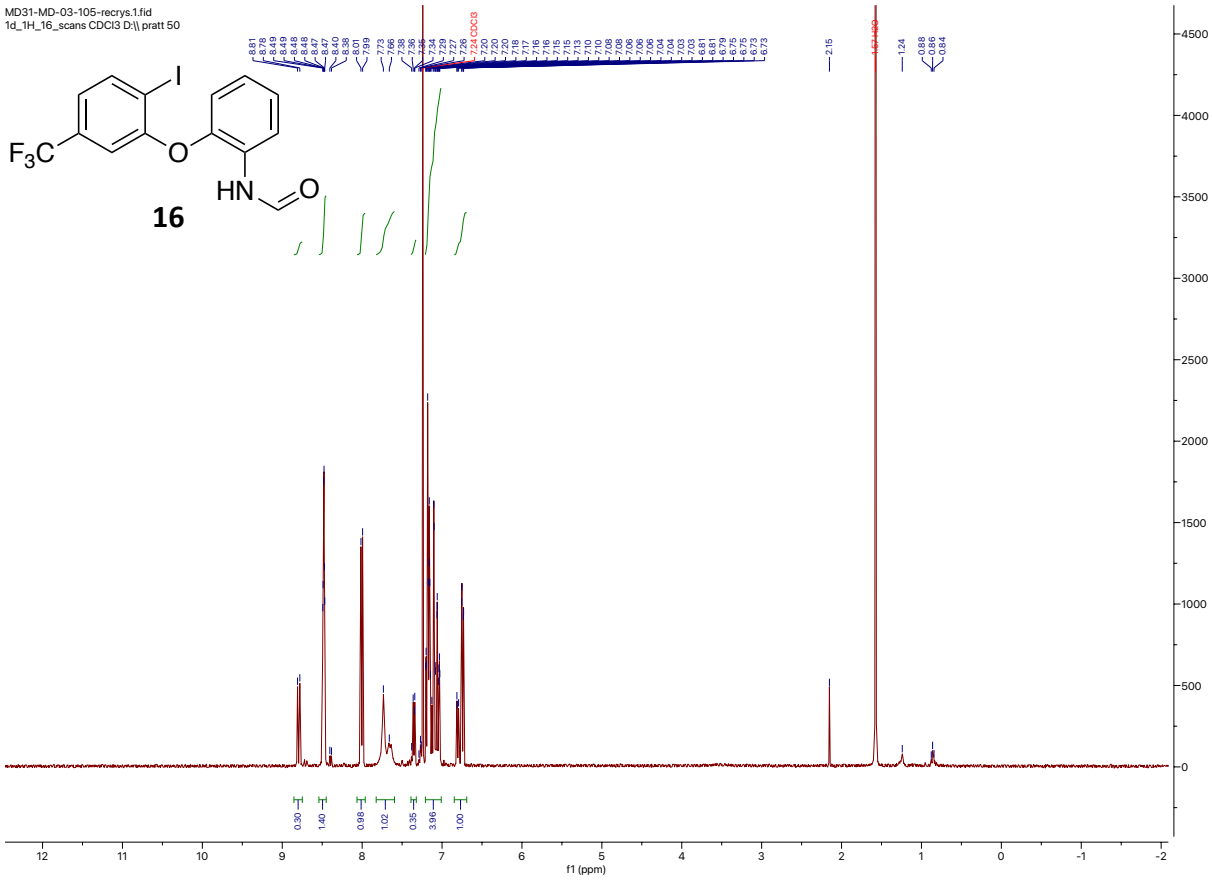

^{13}C-NMR ($CDCl_3$, 150 MHz)

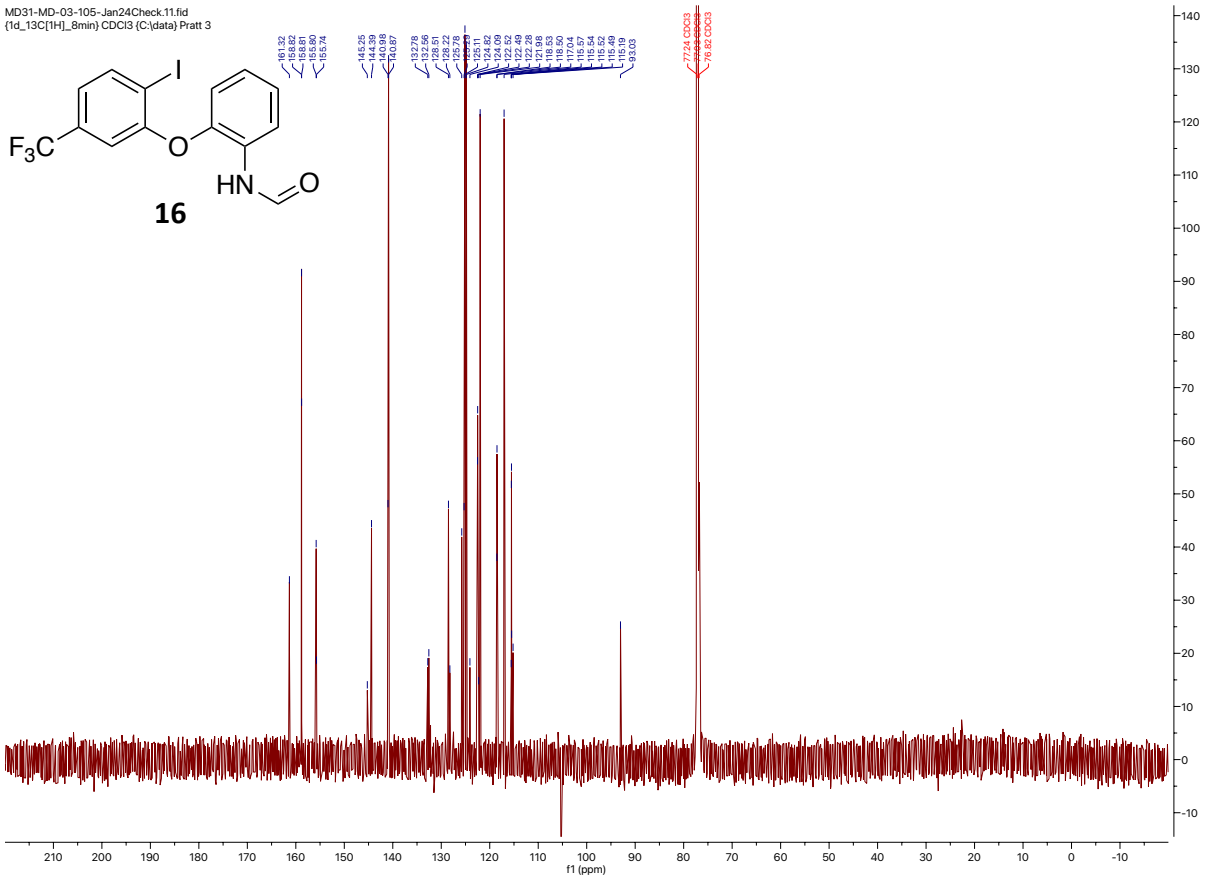

^{1}H-NMR ($CDCl_3$, 400 MHz)

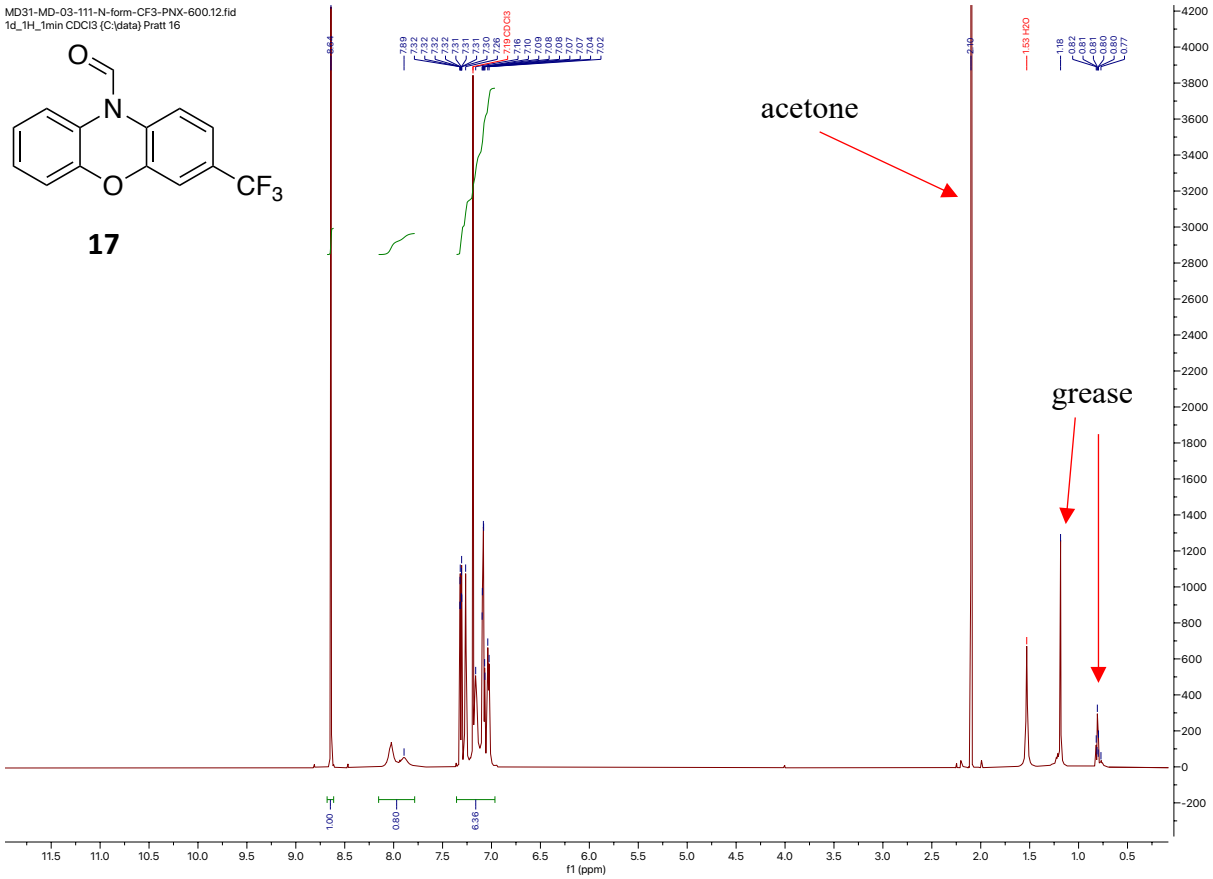

17

^{13}C-NMR ($CDCl_3$, 150 MHz)

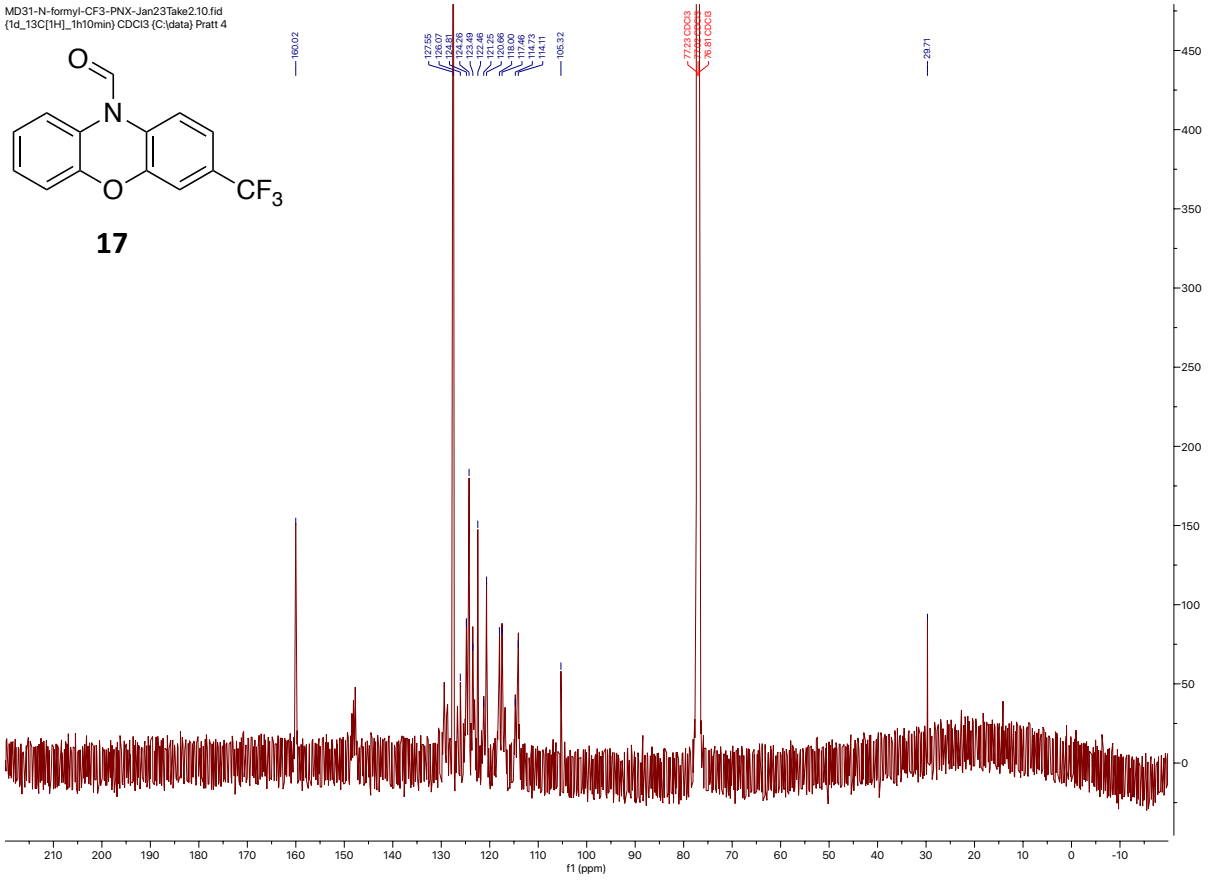

17

^{19}F-NMR ($CDCl_3$, 300 MHz)

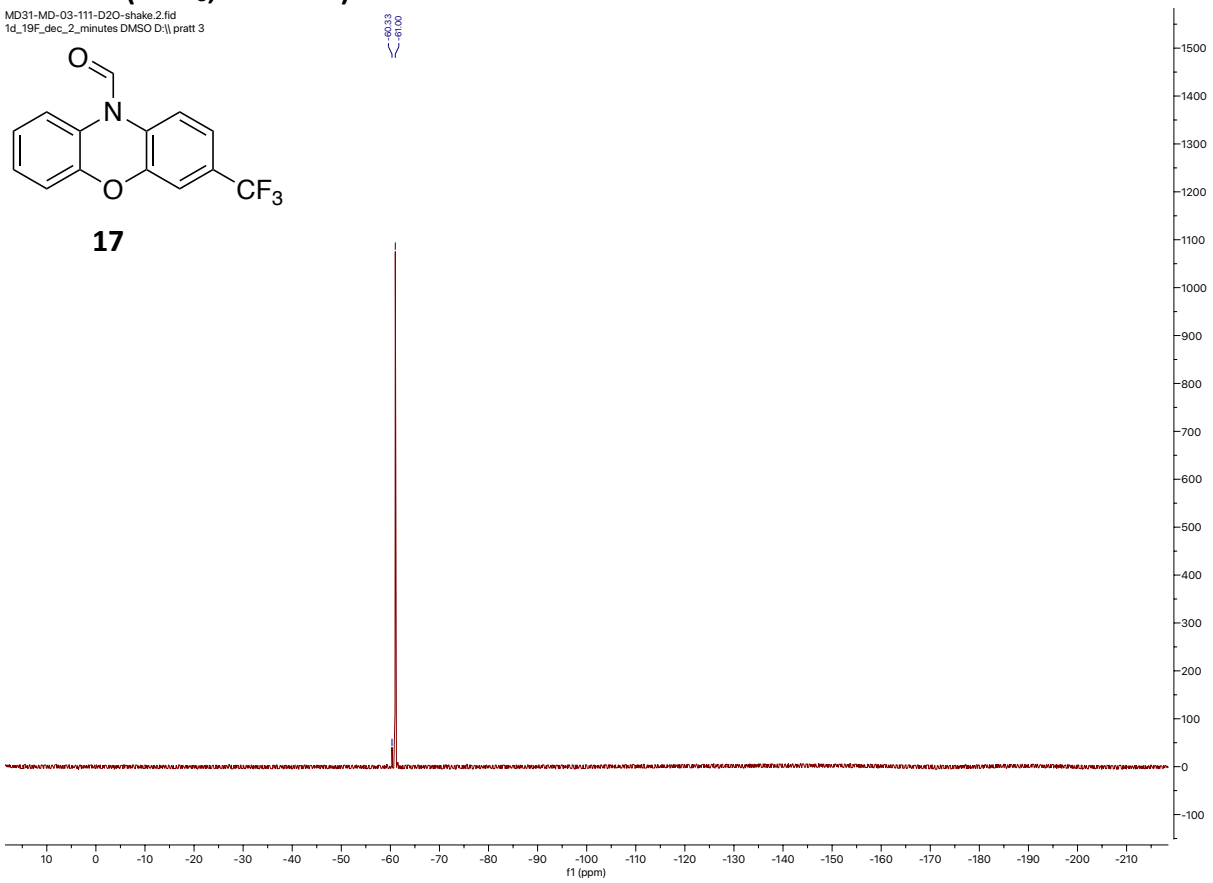

^{1}H-NMR (C_6D_6, 400 MHz)

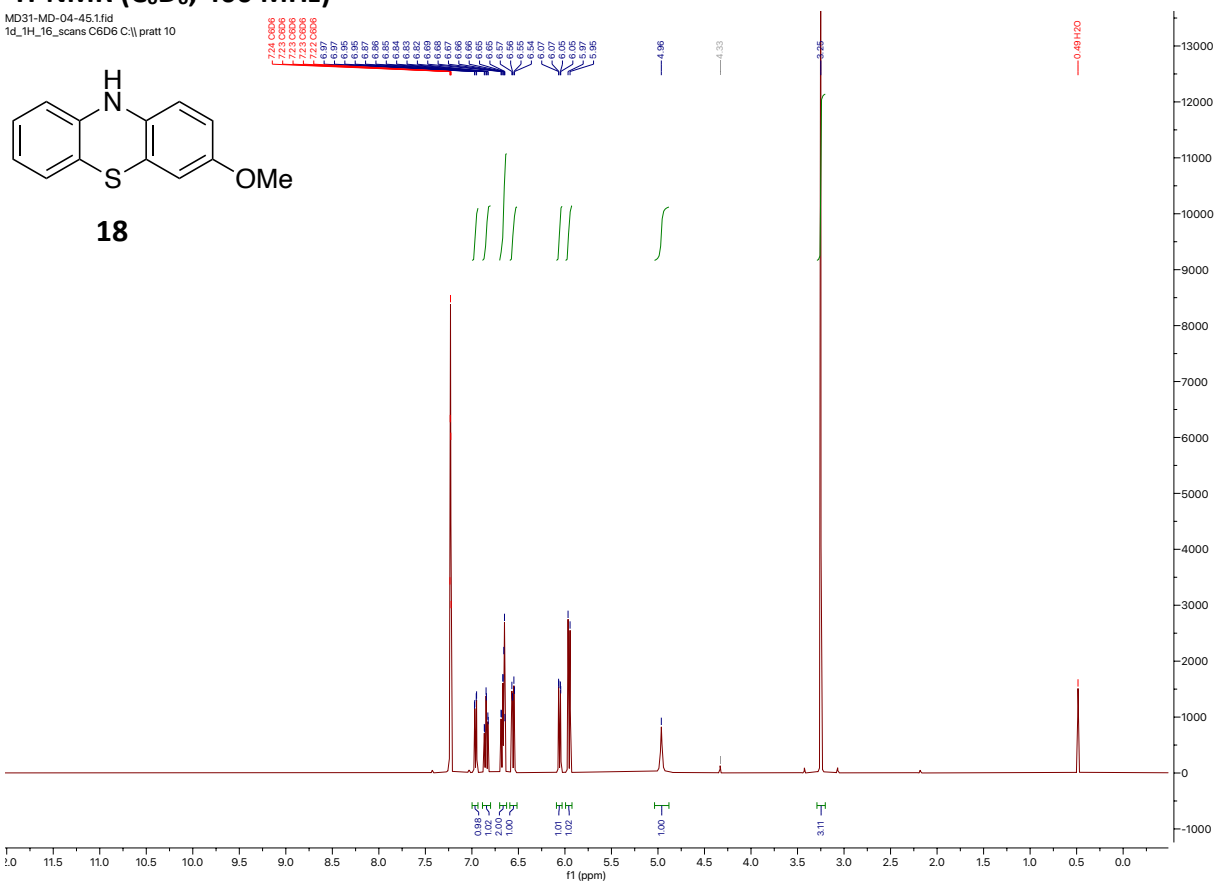

^{1}H-NMR (C_6D_6, 400 MHz)

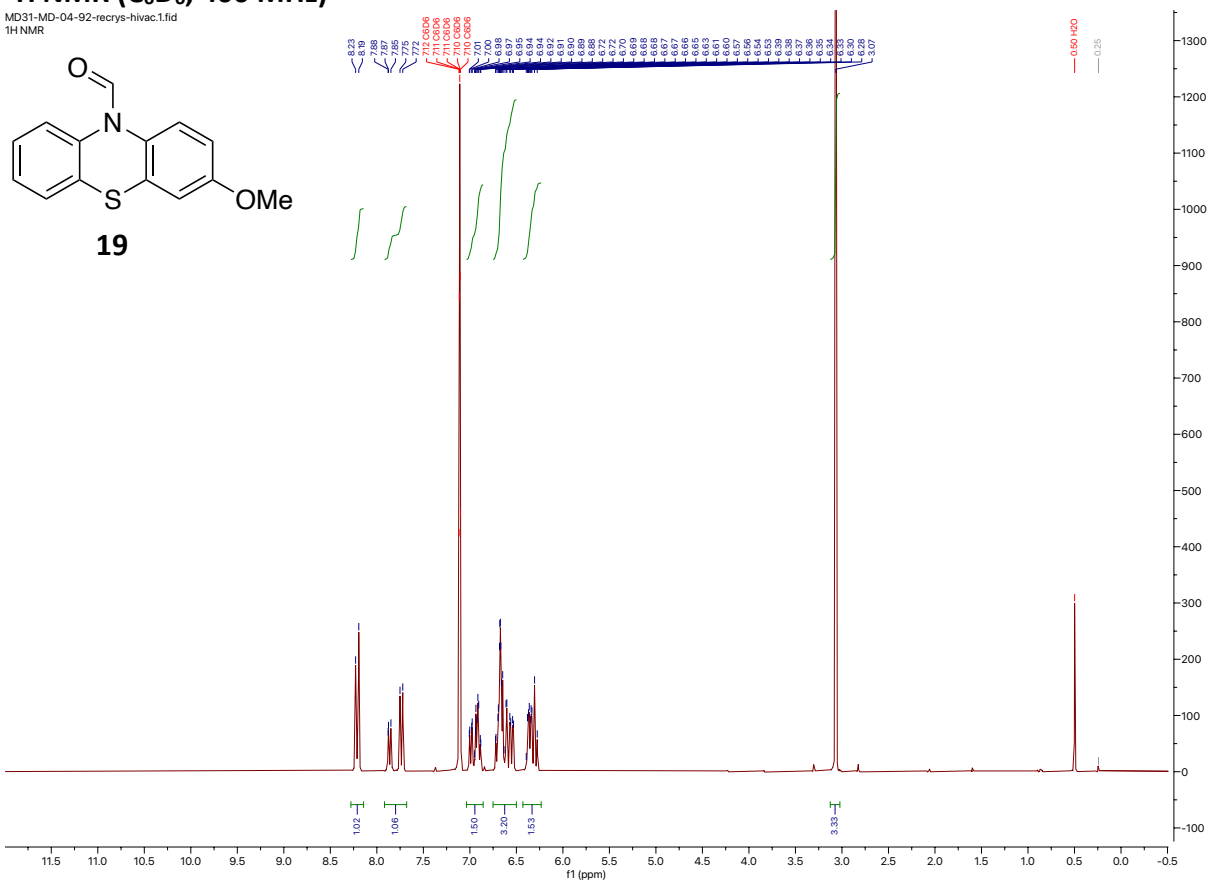

^{13}C-NMR ($CDCl_3$, 150 MHz)

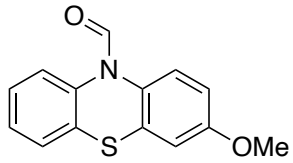

19

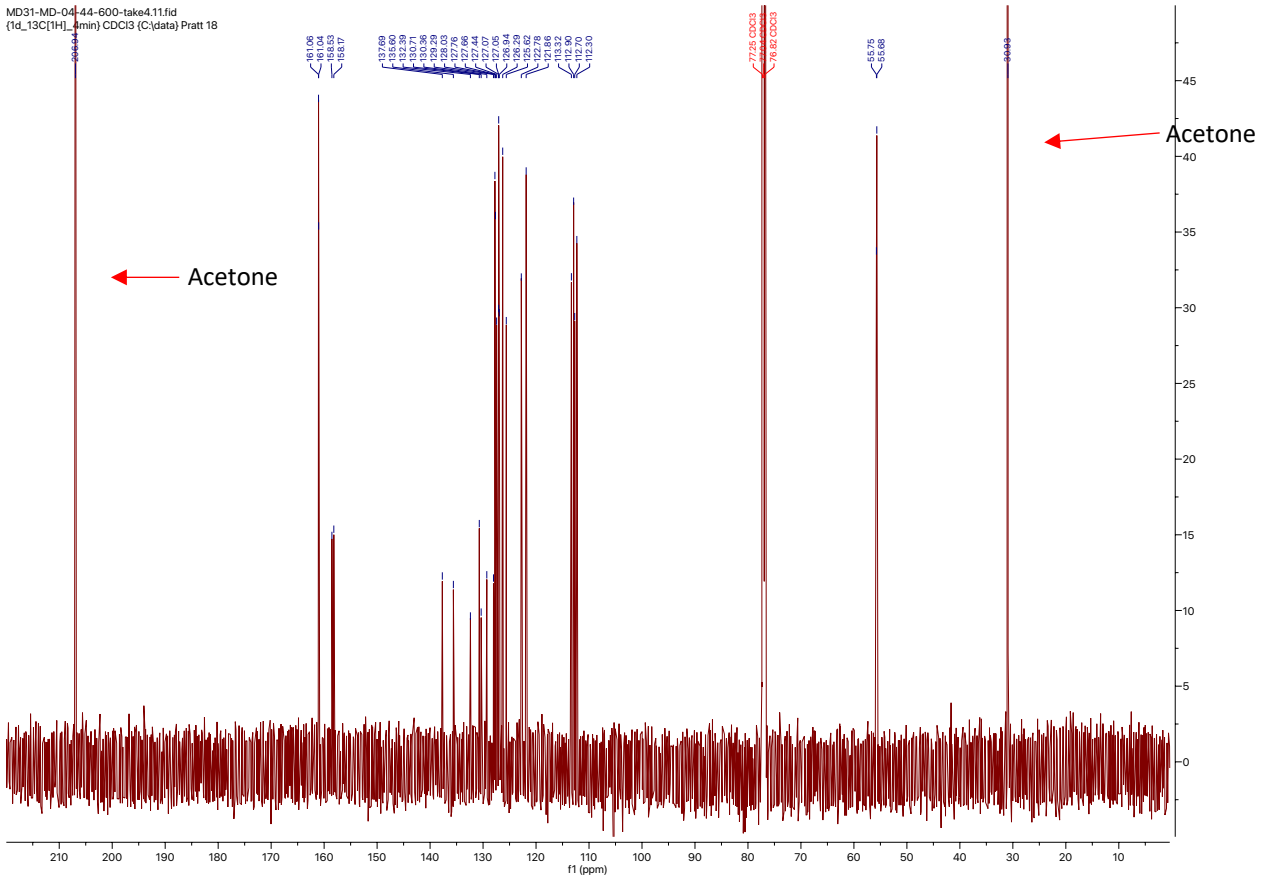

^{1}H-NMR (DMSO-d, 400 MHz)

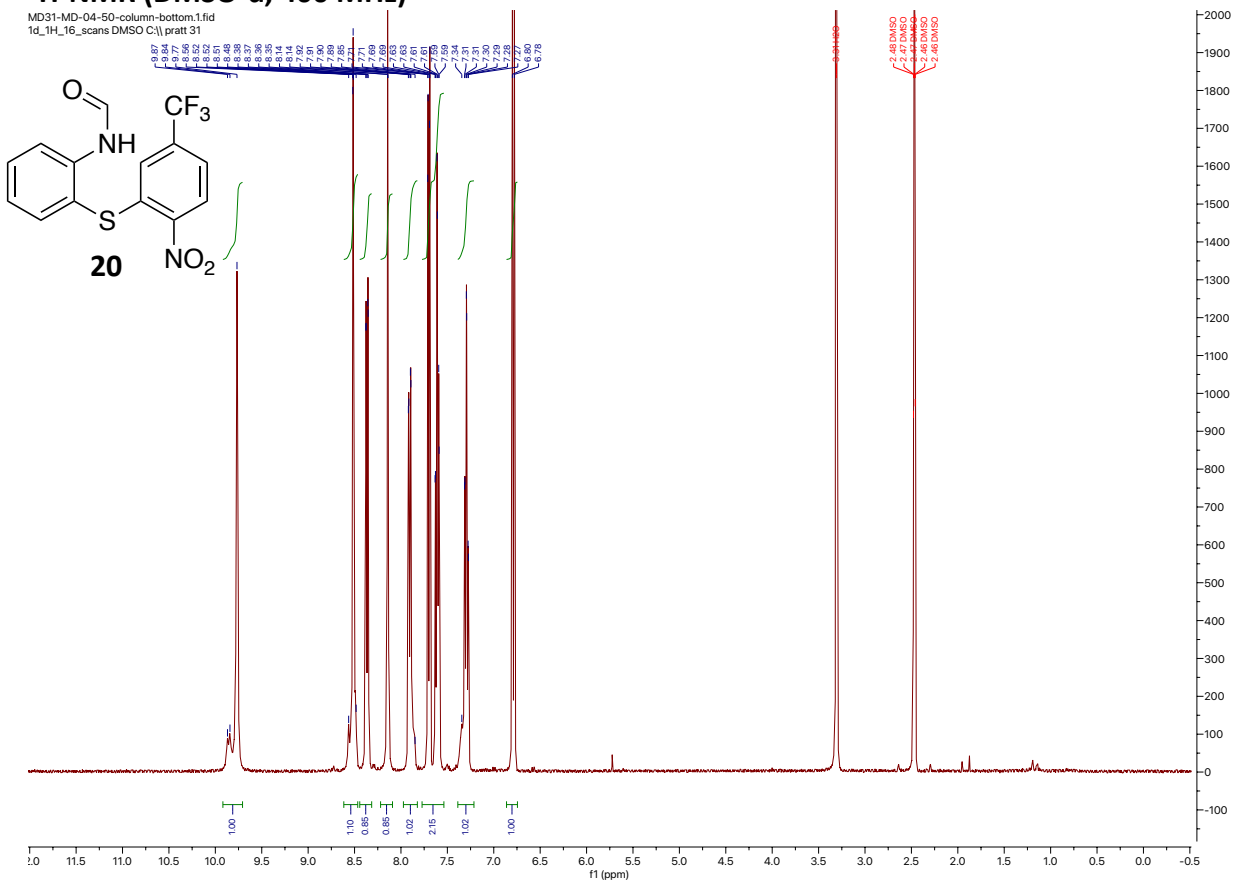

^{1}H-NMR (DMSO-d, 100 MHz)

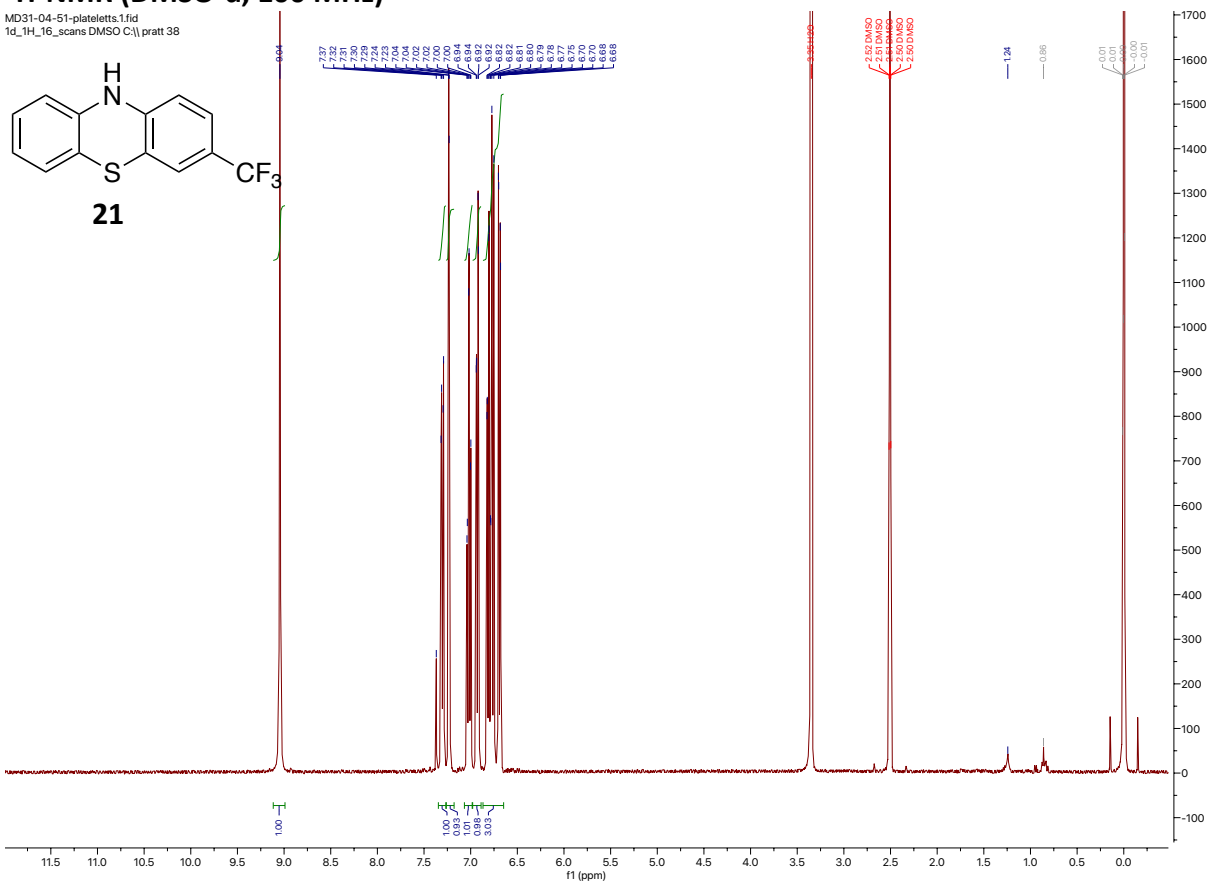

^{1}H-NMR (DMSO-d, 400 MHz)

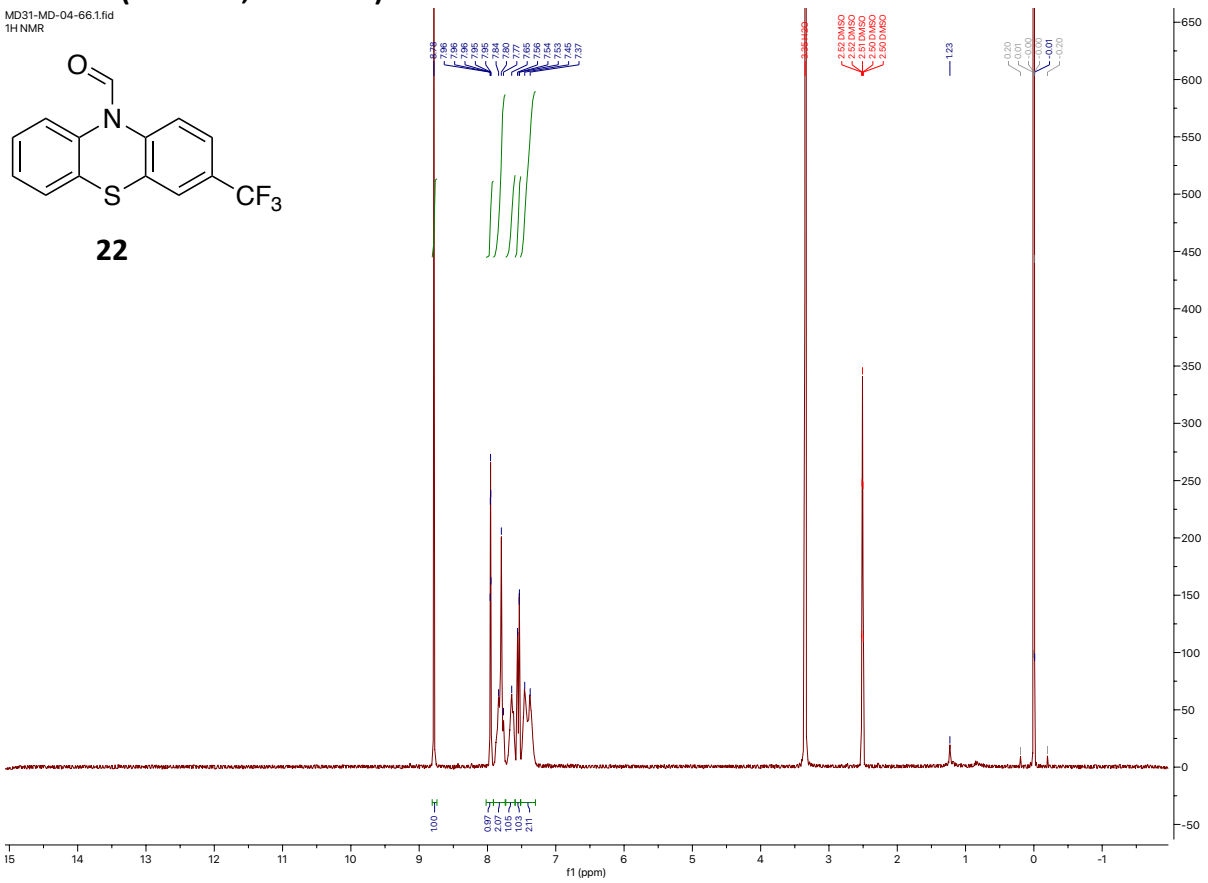

22

^{13}C-NMR ($CDCl_3$, 150 MHz)

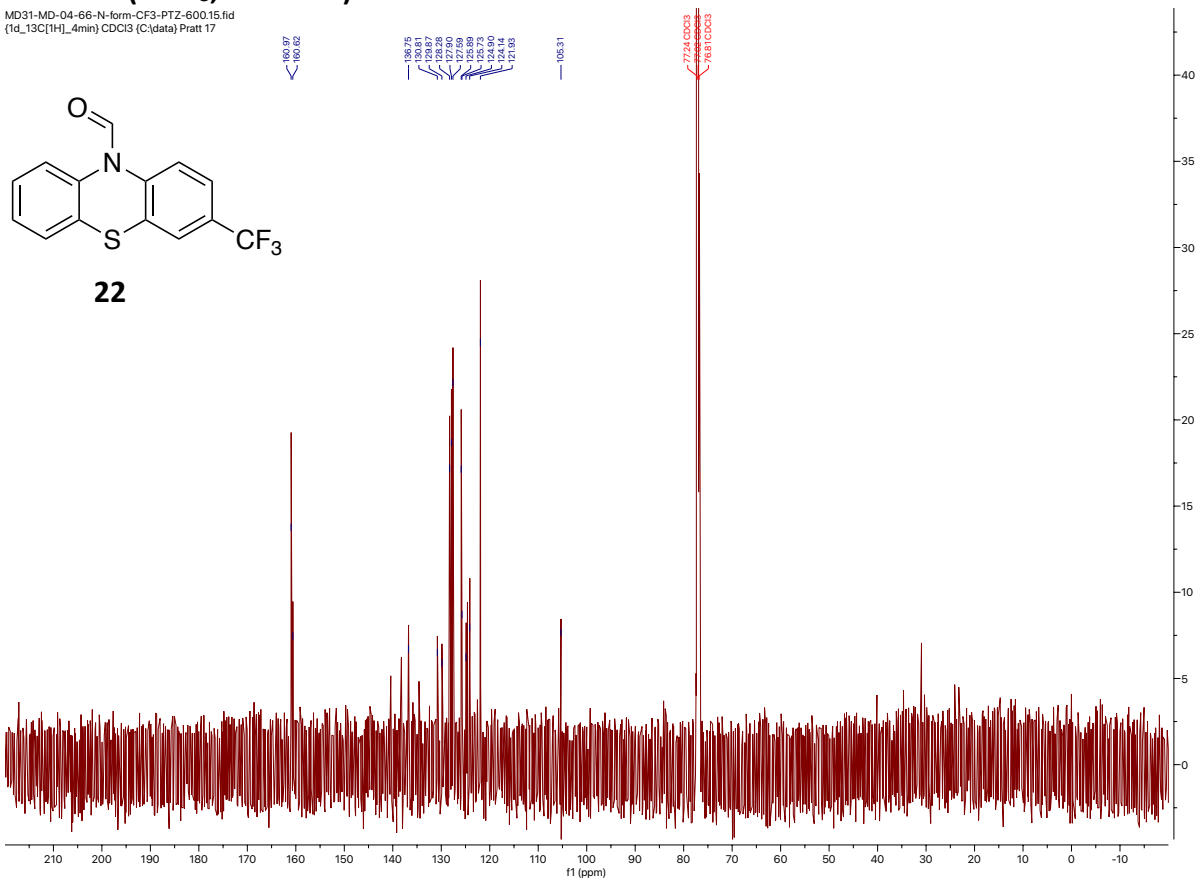

22

^{19}F-NMR ($CDCl_3$, 300 MHz)

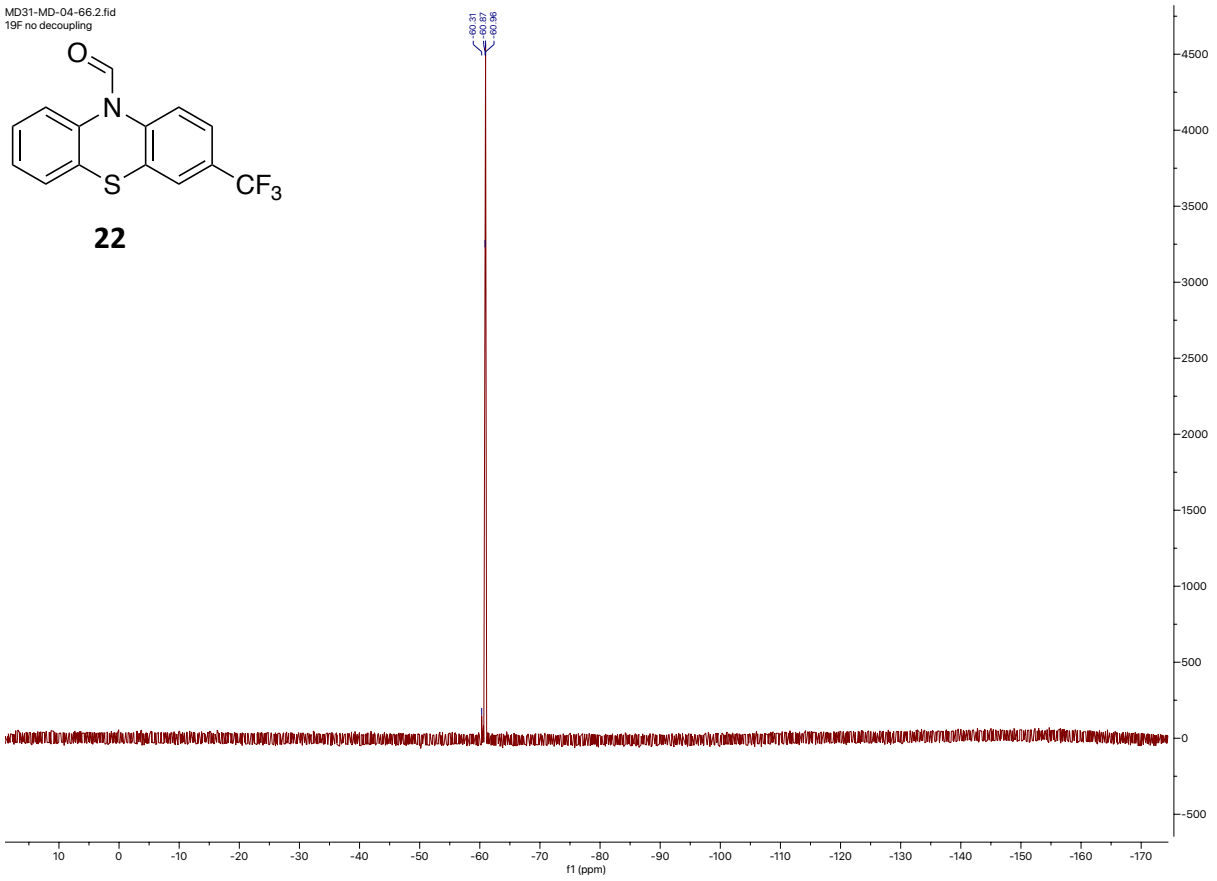

22

^{1}H-NMR ($CDCl_3$, 400 MHz)

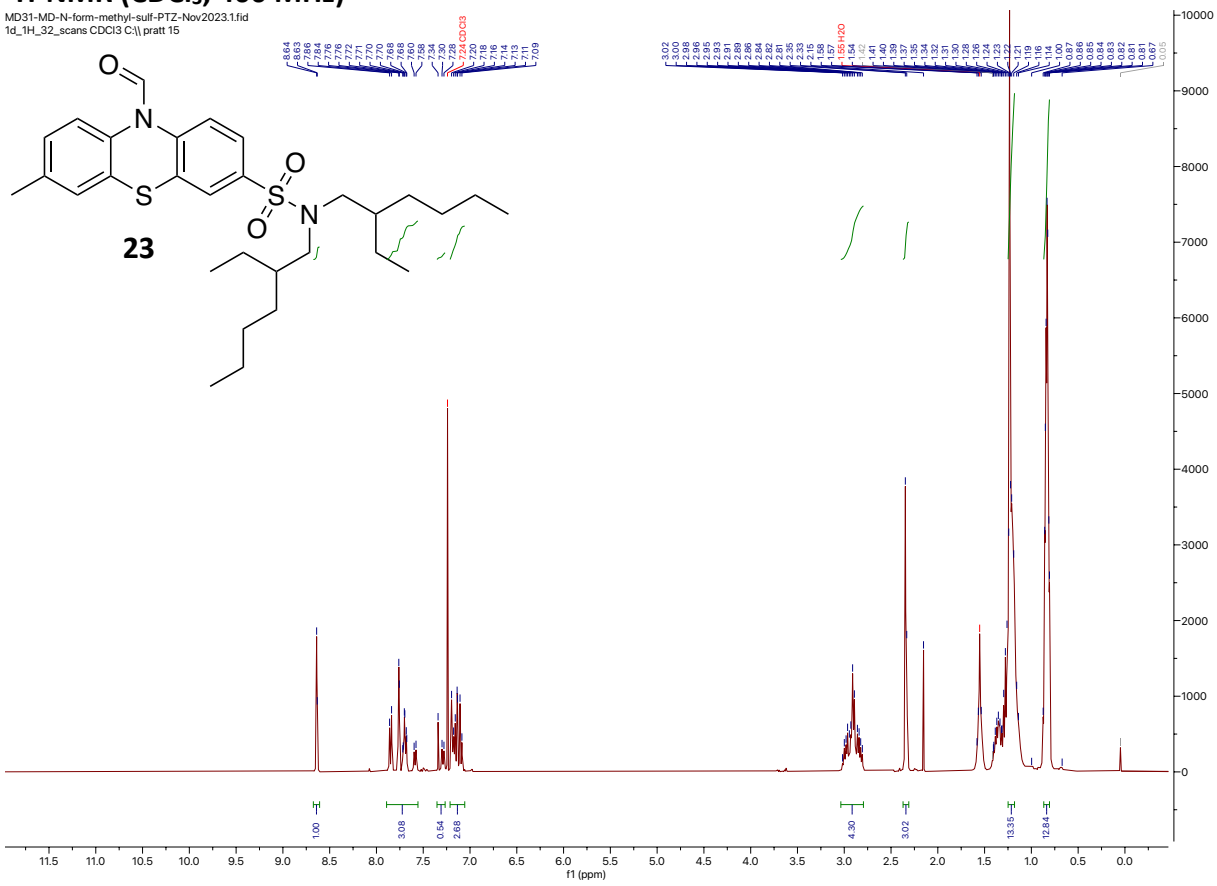

^{13}C-NMR ($CDCl_3$, 100 MHz)

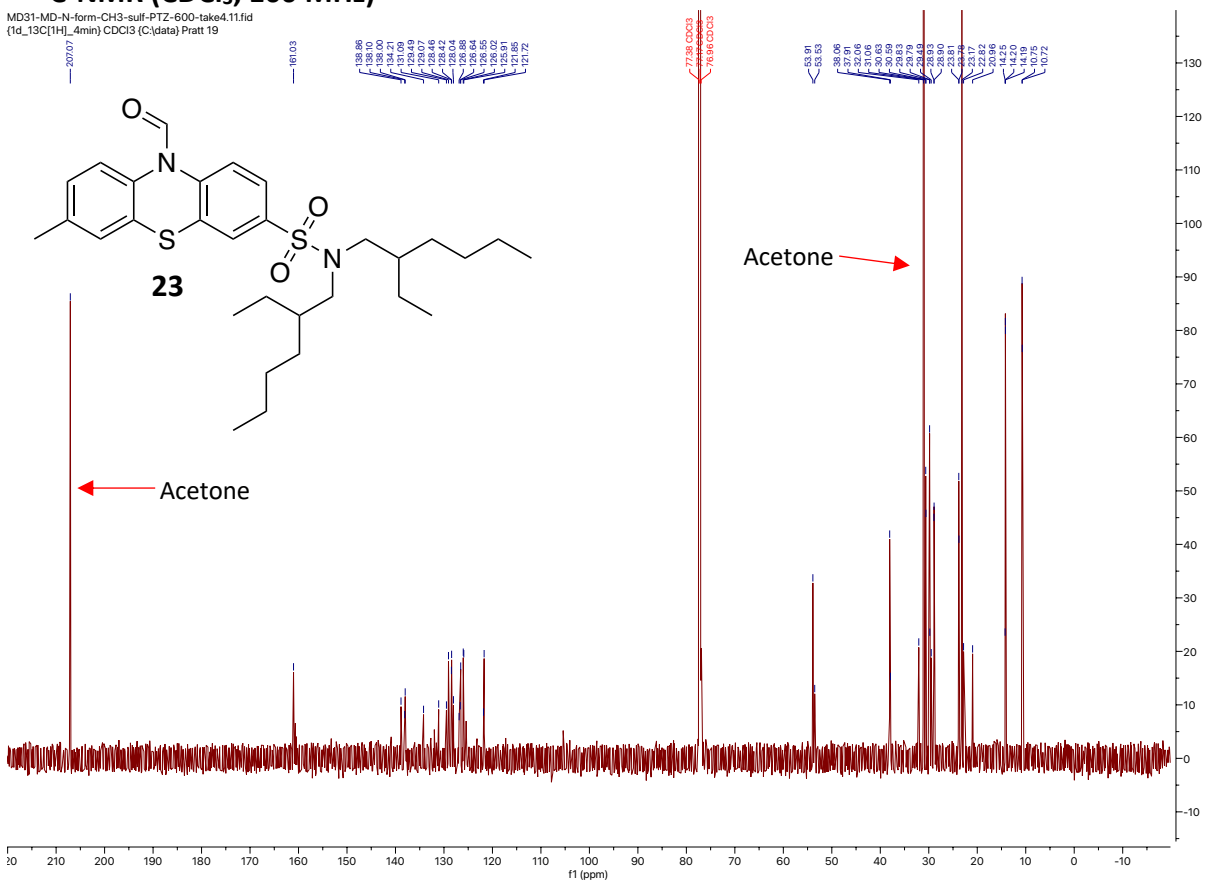

^{1}H-NMR ($CDCl_3$, 400 MHz)

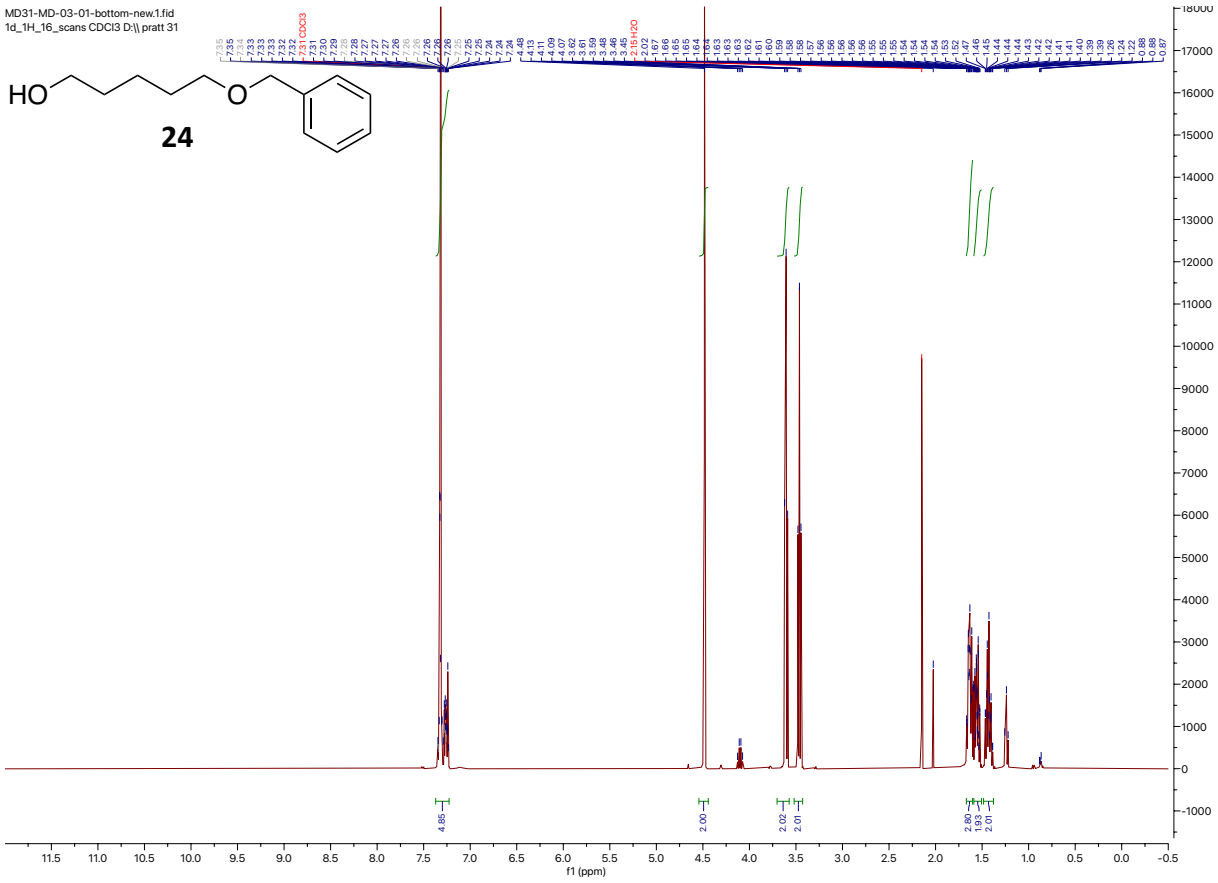

^{1}H-NMR ($CDCl_3$, 400 MHz)

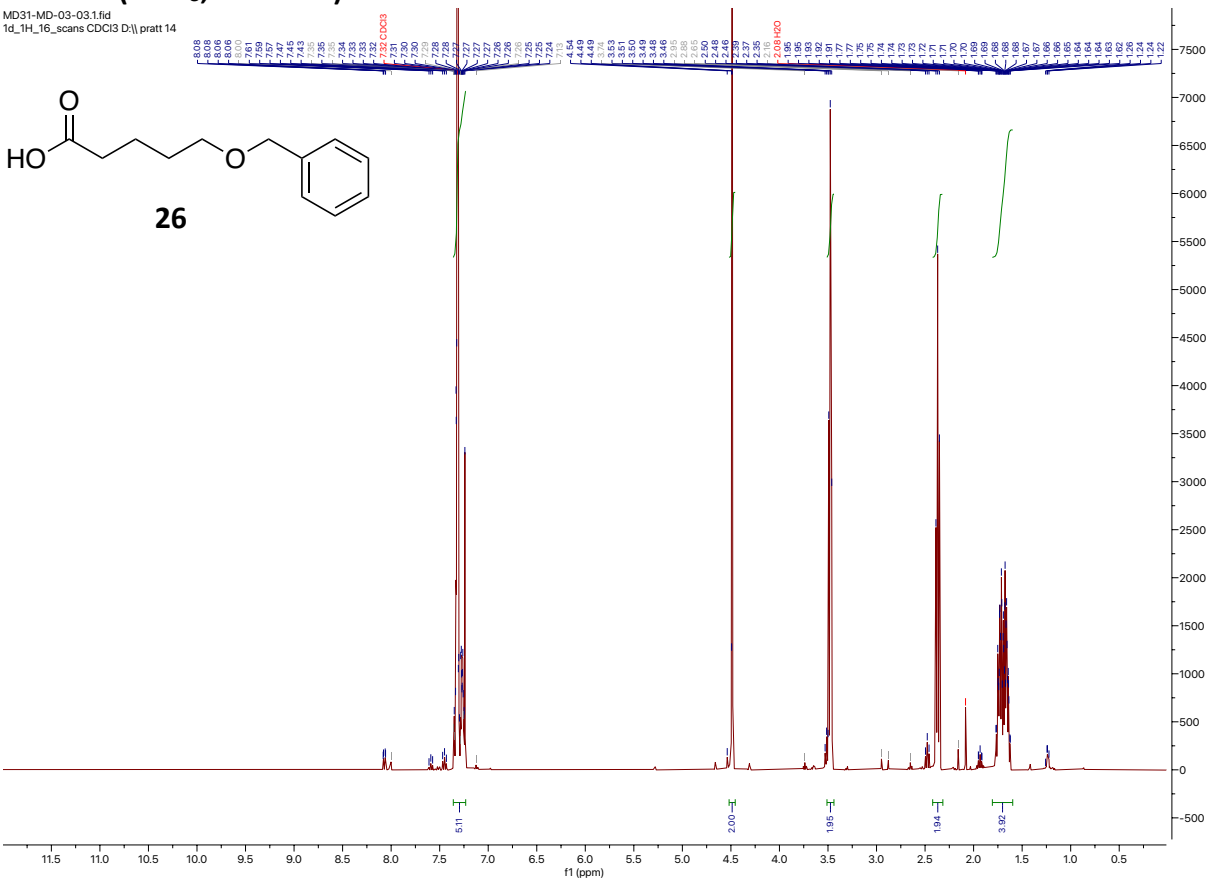

^{1}H-NMR ($CDCl_3$, 400 MHz)

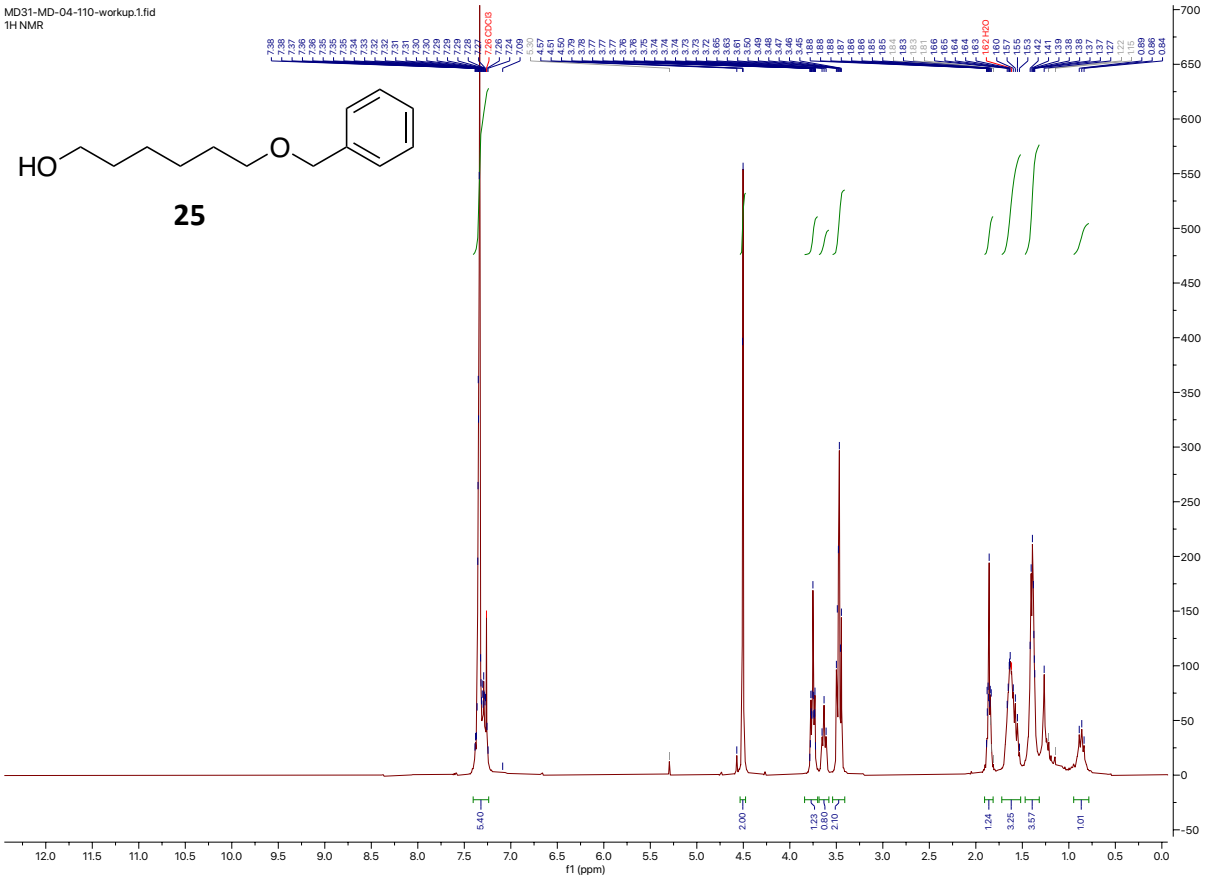

^{1}H-NMR ($CDCl_3$, 400 MHz)

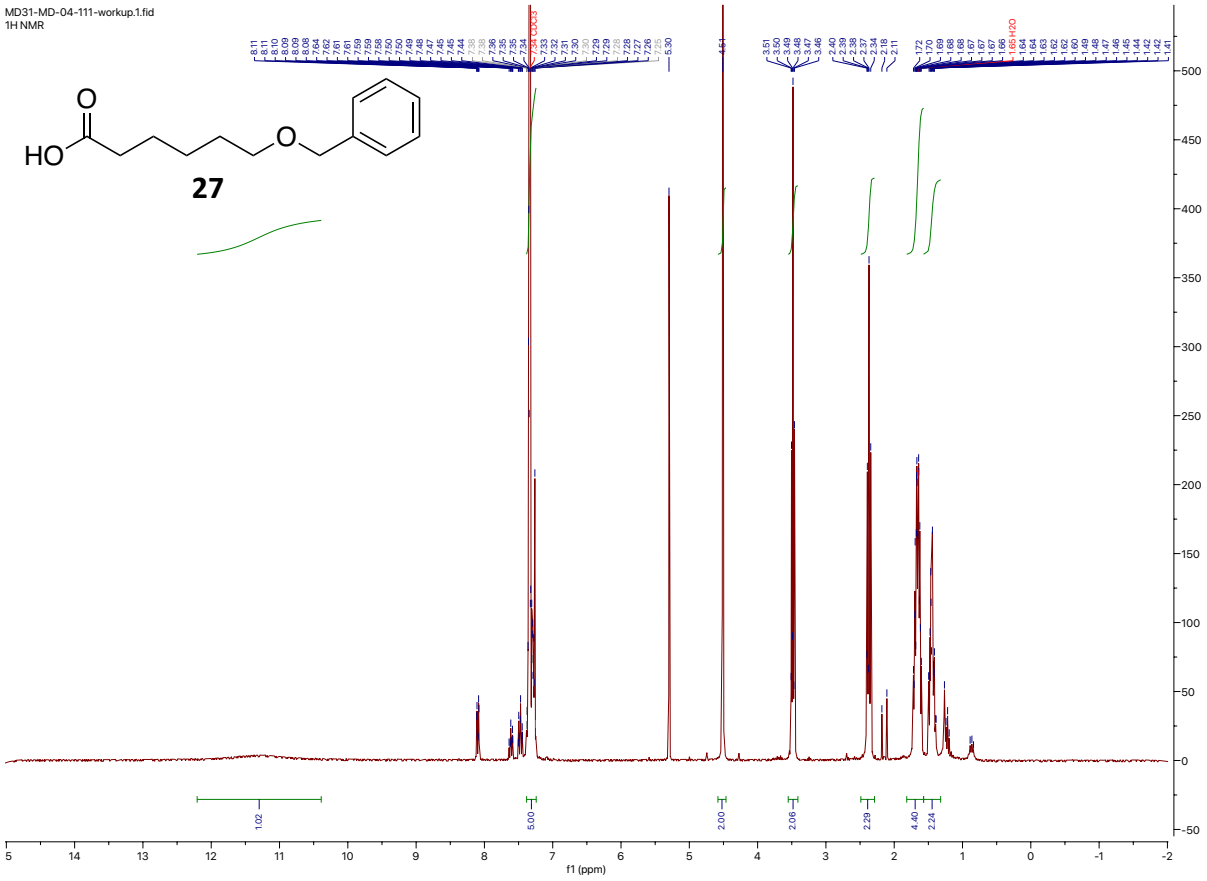

^{1}H-NMR ($CDCl_3$, 400 MHz)

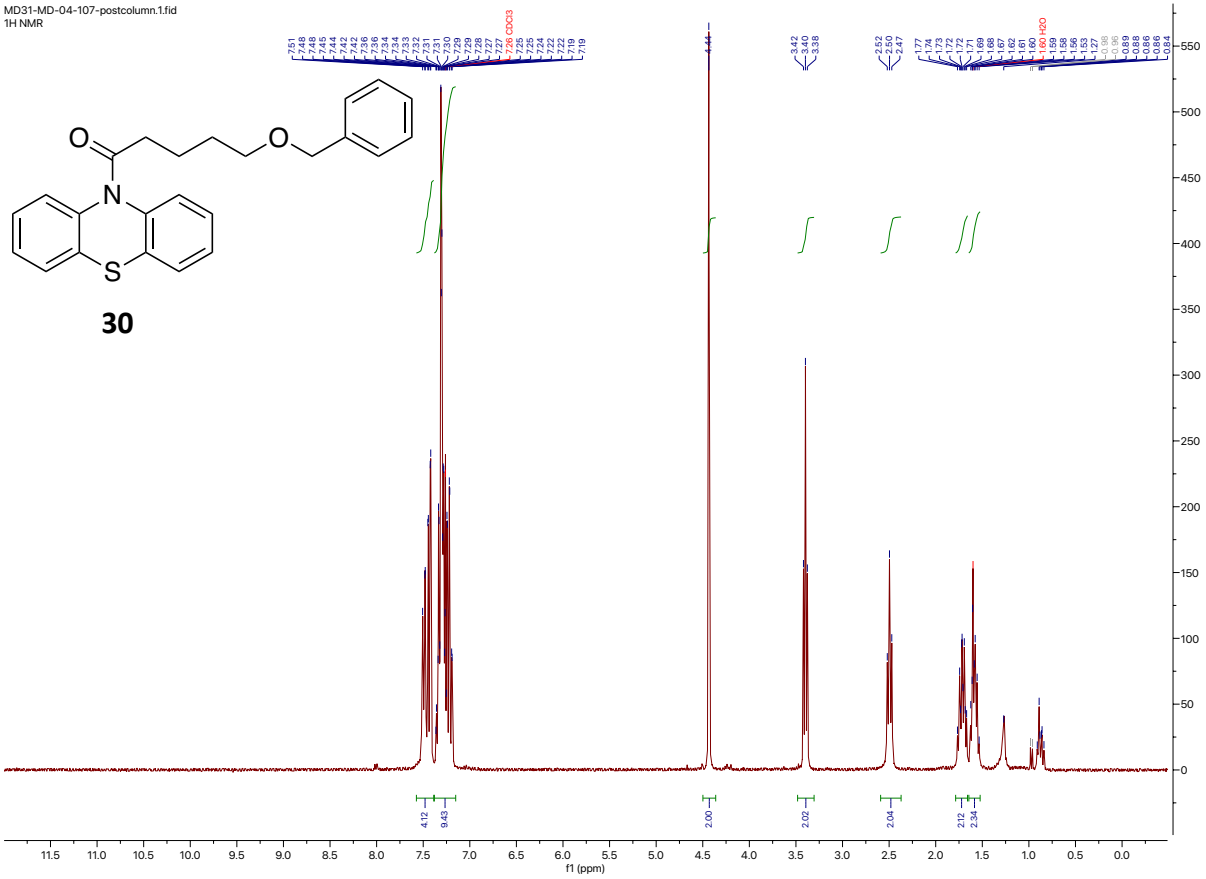

^{13}C-NMR ($CDCl_3$, 100 MHz)

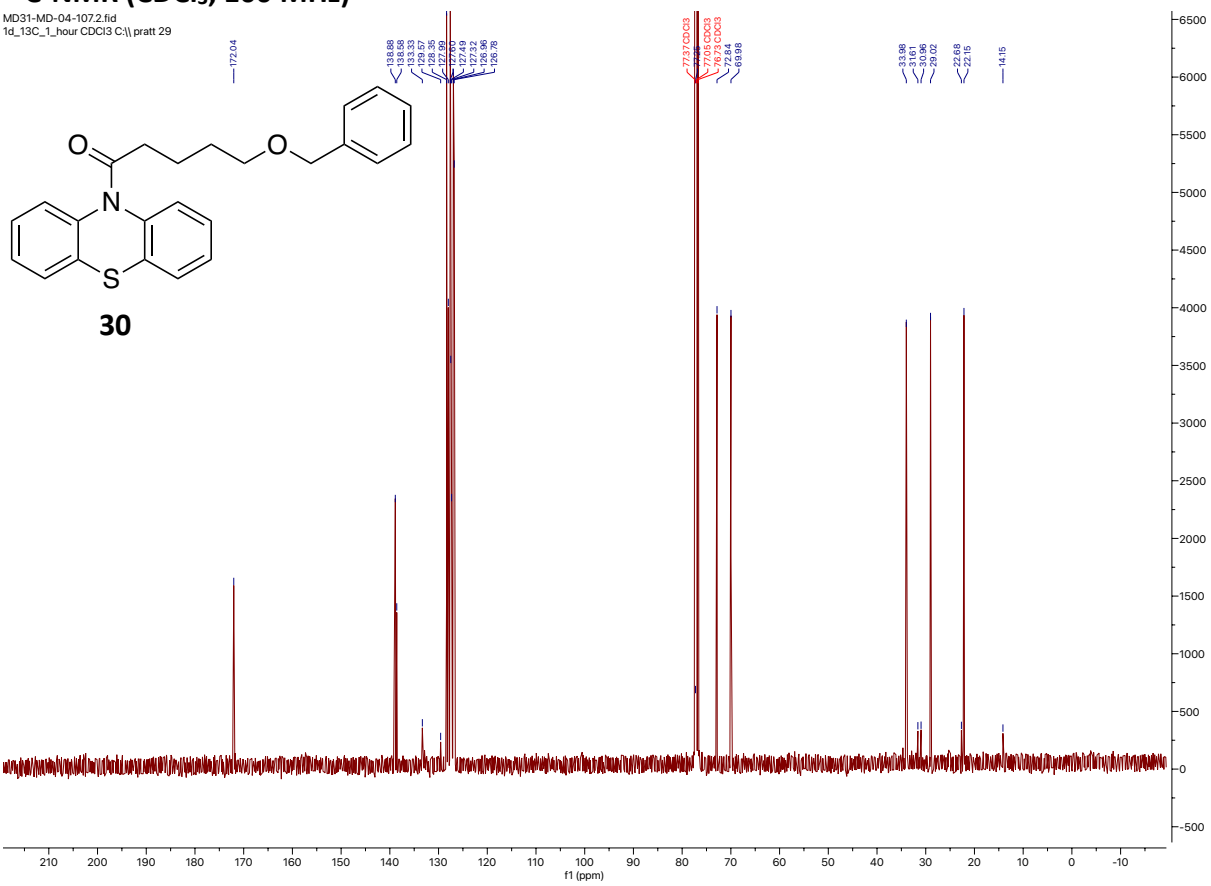

^{1}H-NMR (DMSO-d, 400 MHz)

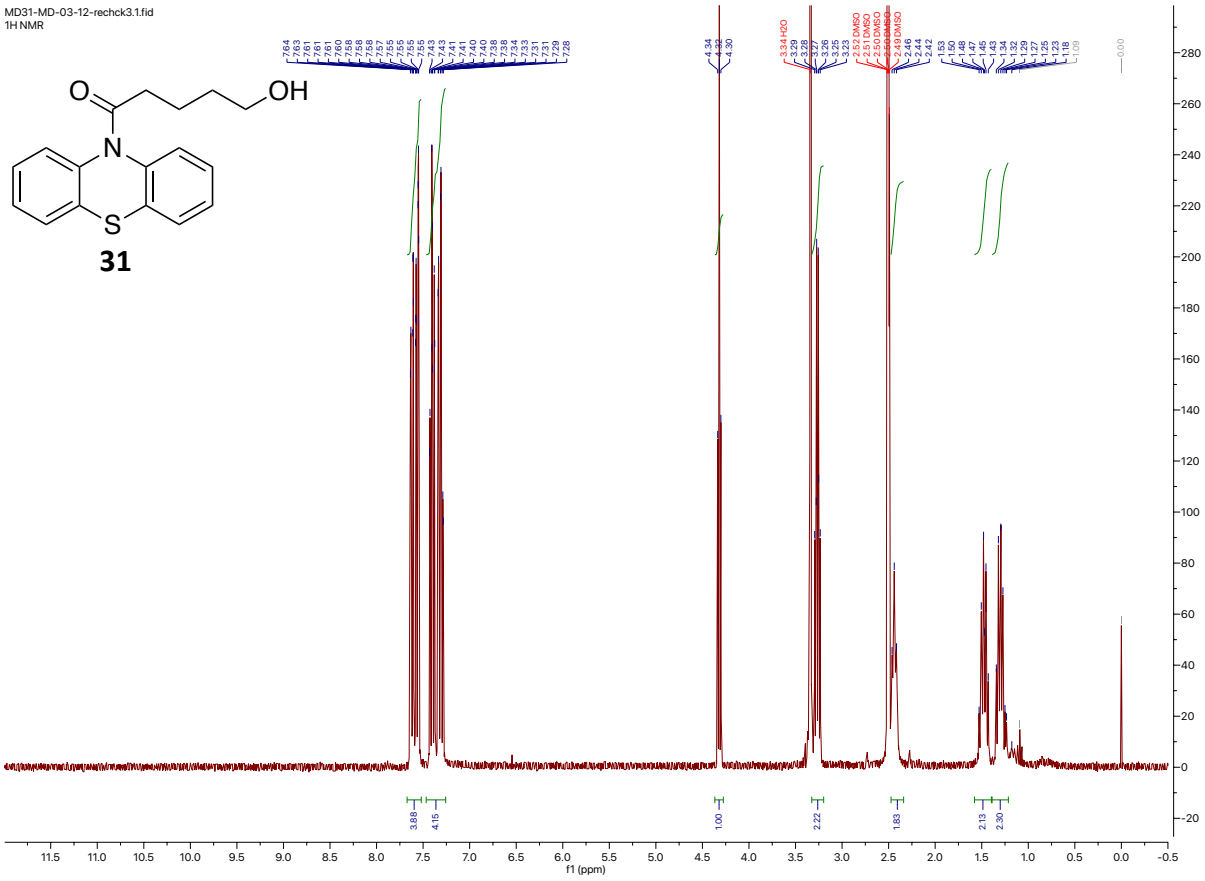

^{13}C-NMR ($CDCl_3$, 150 MHz)

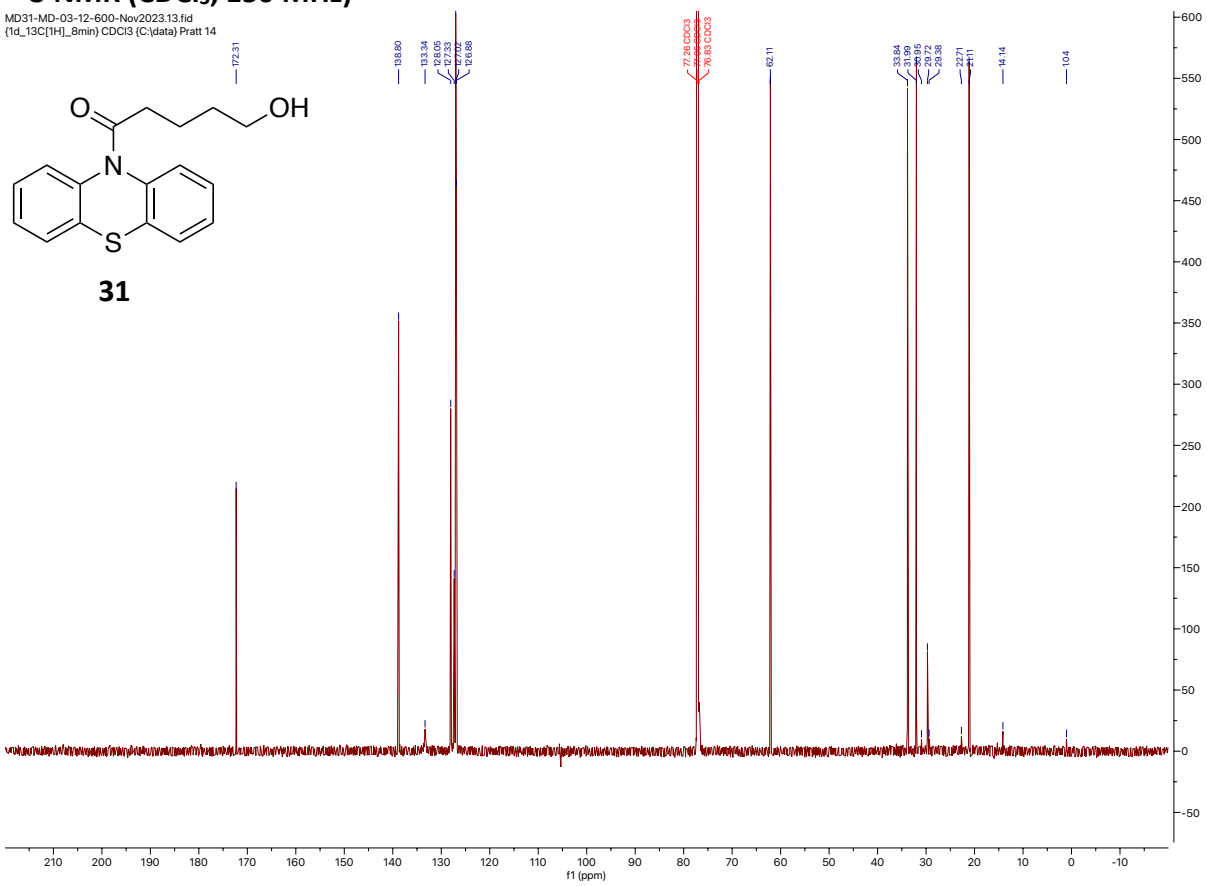

^{1}H-NMR ($CDCl_3$, 400 MHz)

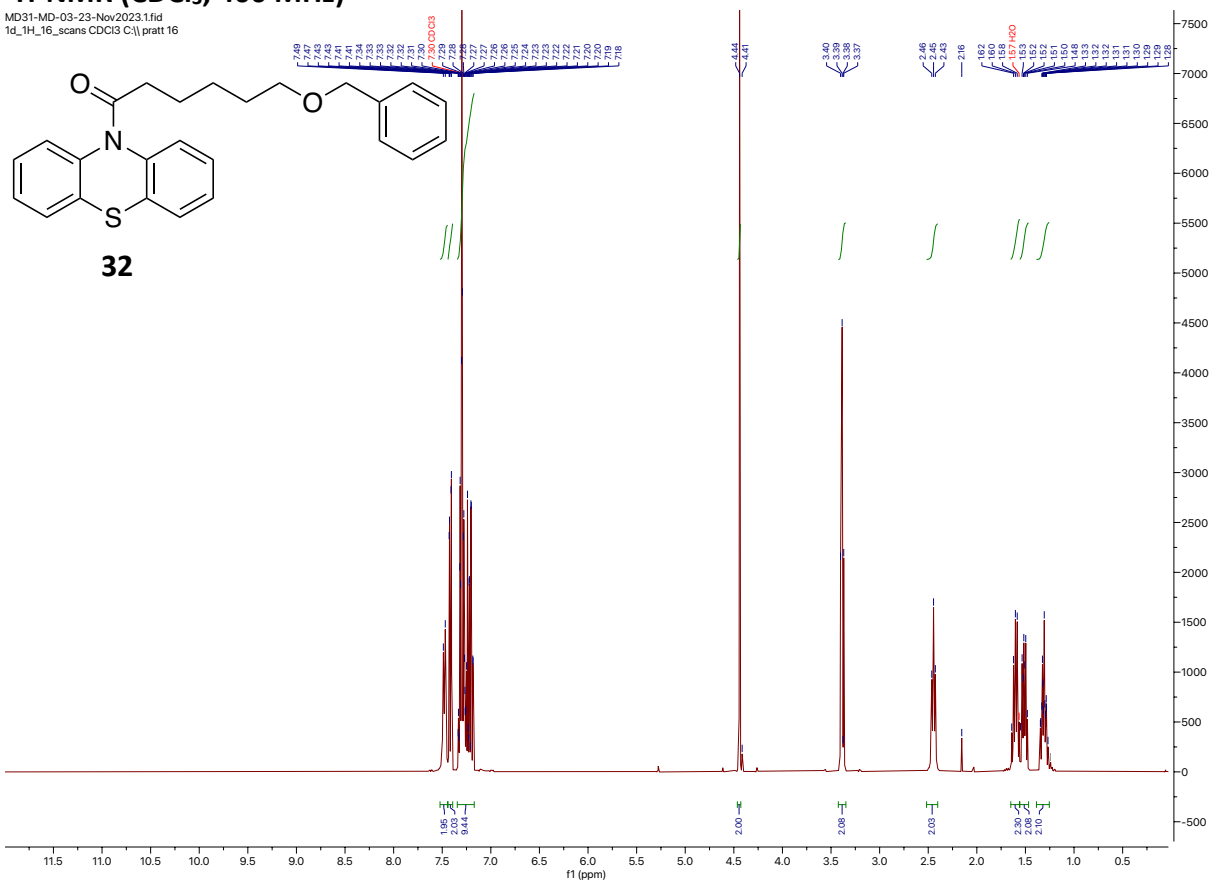

^{13}C-NMR ($CDCl_3$, 100 MHz)

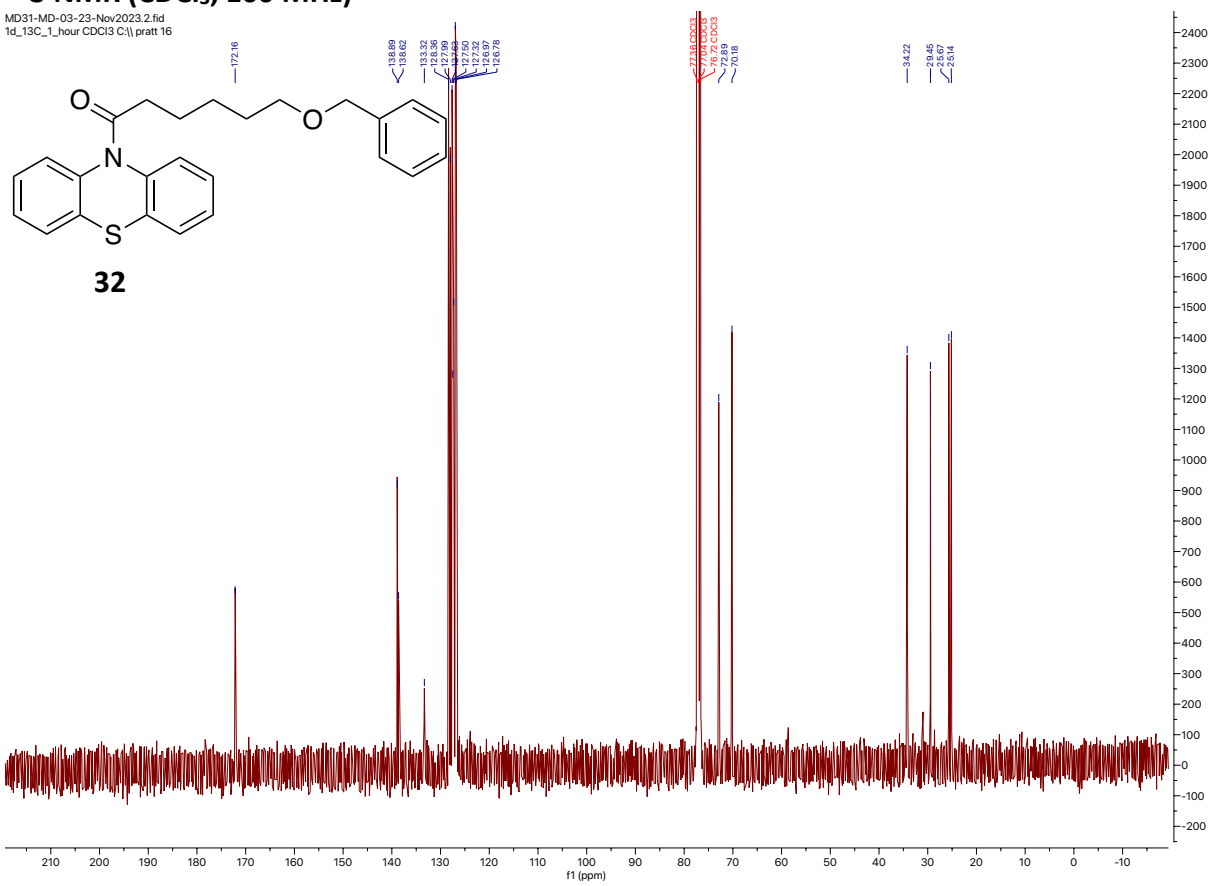

32

^{1}H-NMR ($CDCl_3$, 400 MHz)

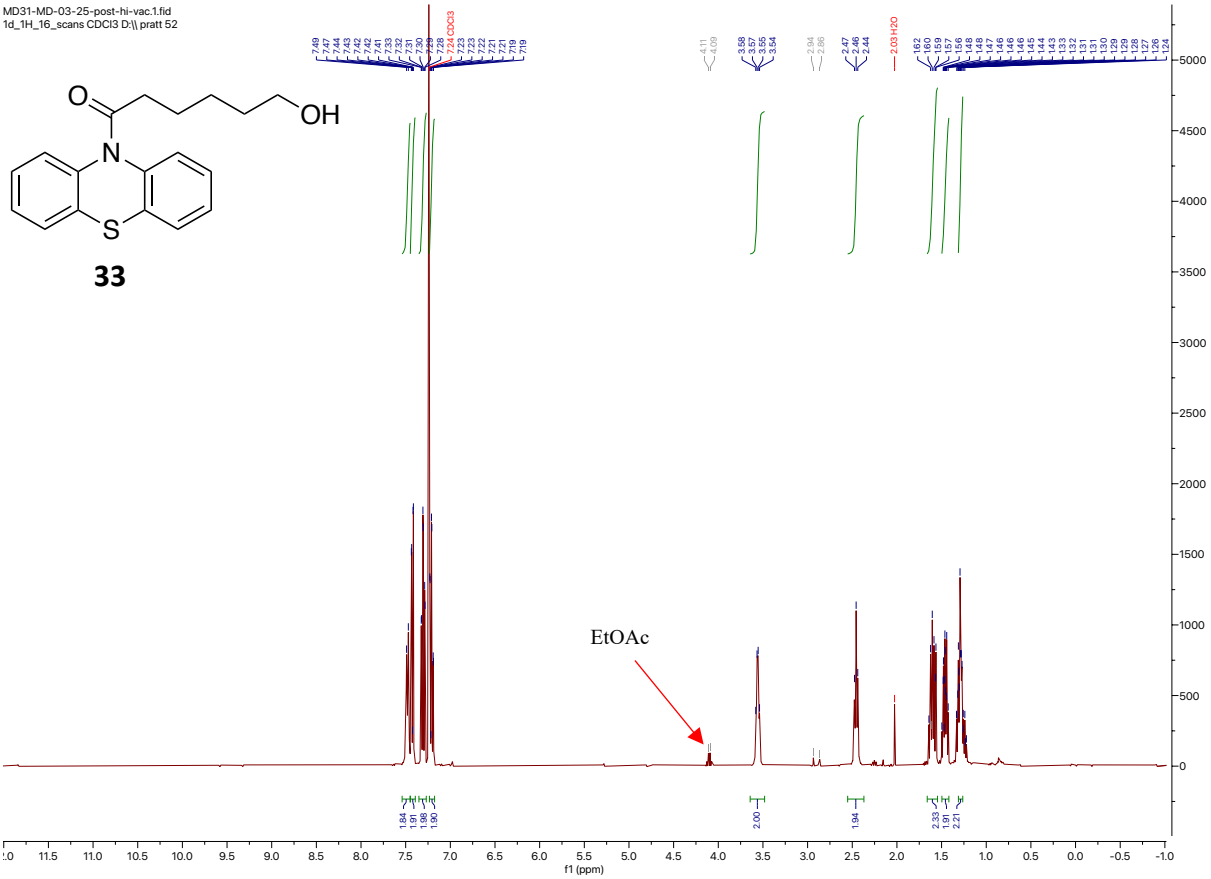

^{13}C-NMR ($CDCl_3$, 100 MHz)

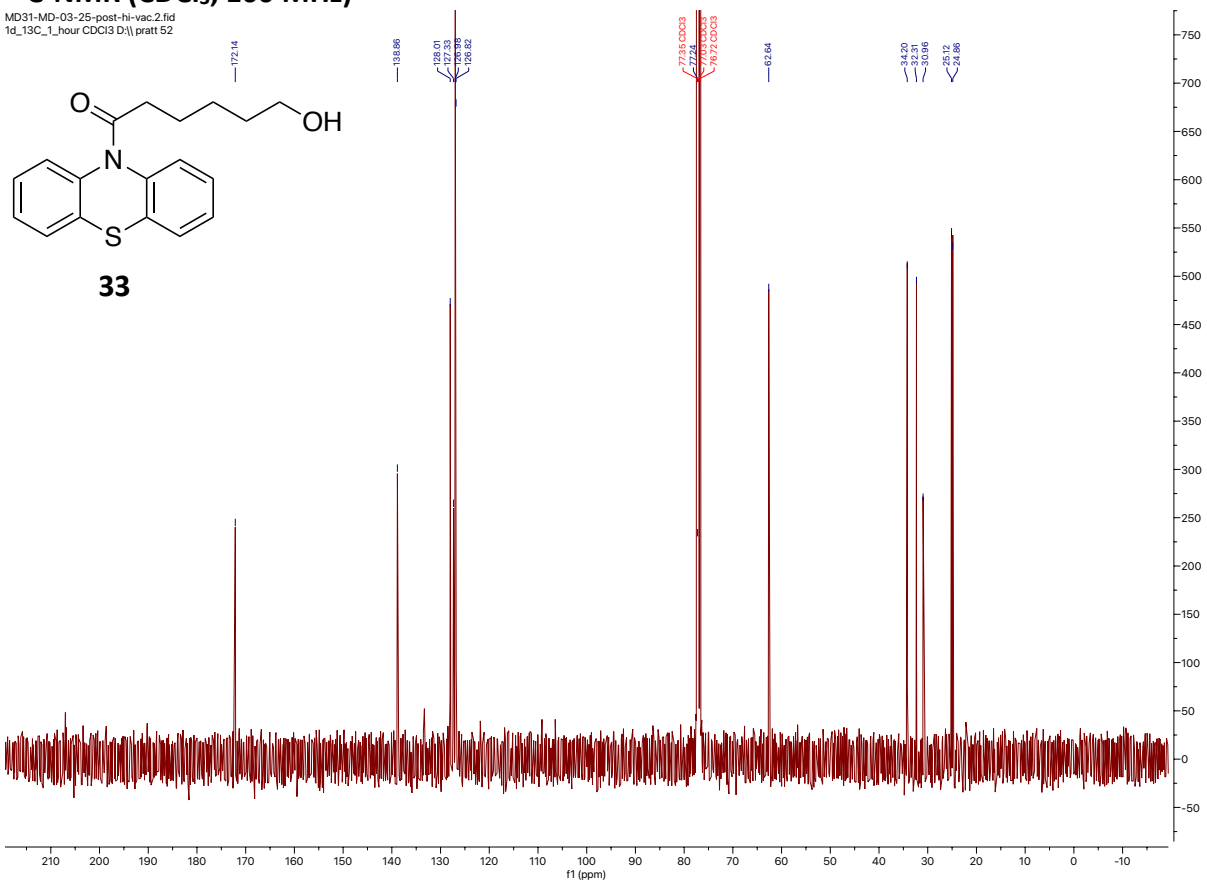

33

^{1}H-NMR ($CDCl_3$, 400 MHz)

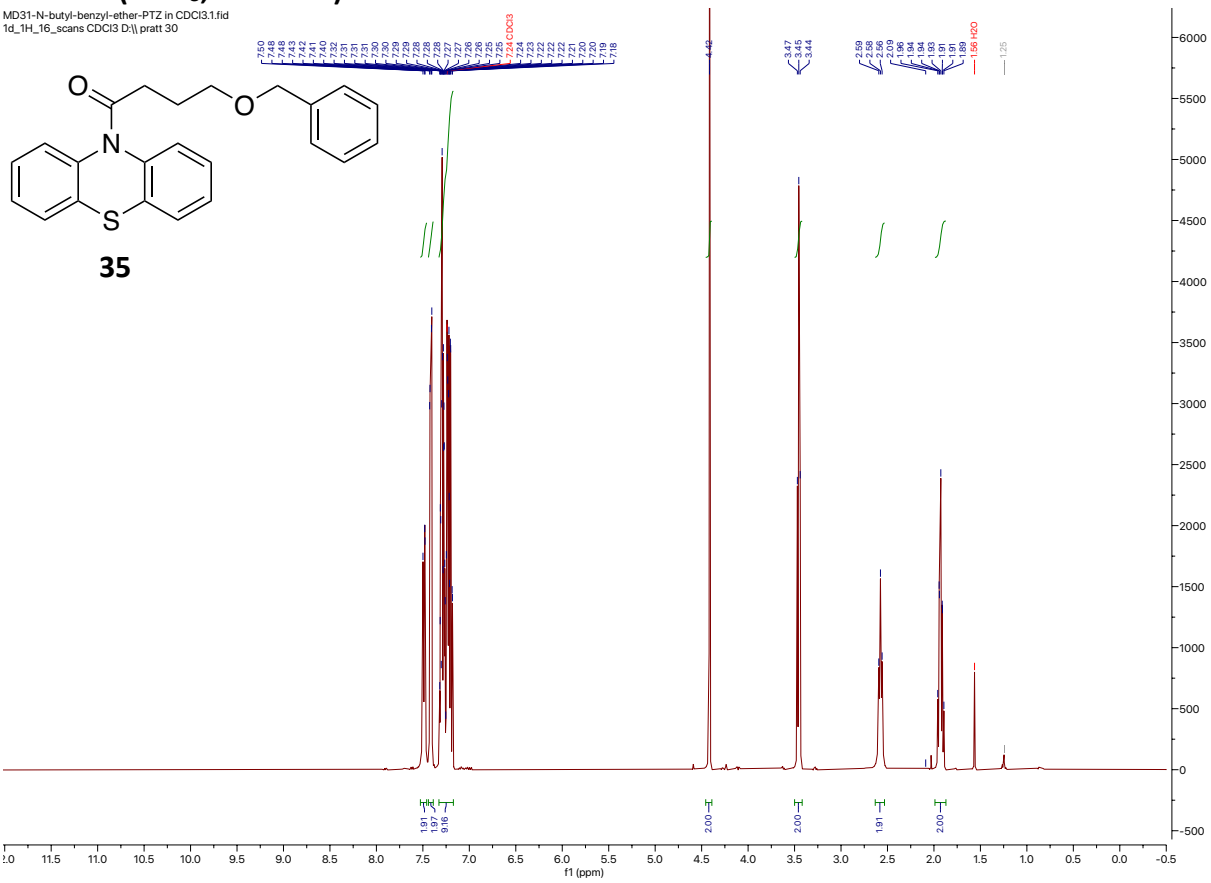

35

^{13}C-NMR ($CDCl_3$, 100 MHz)

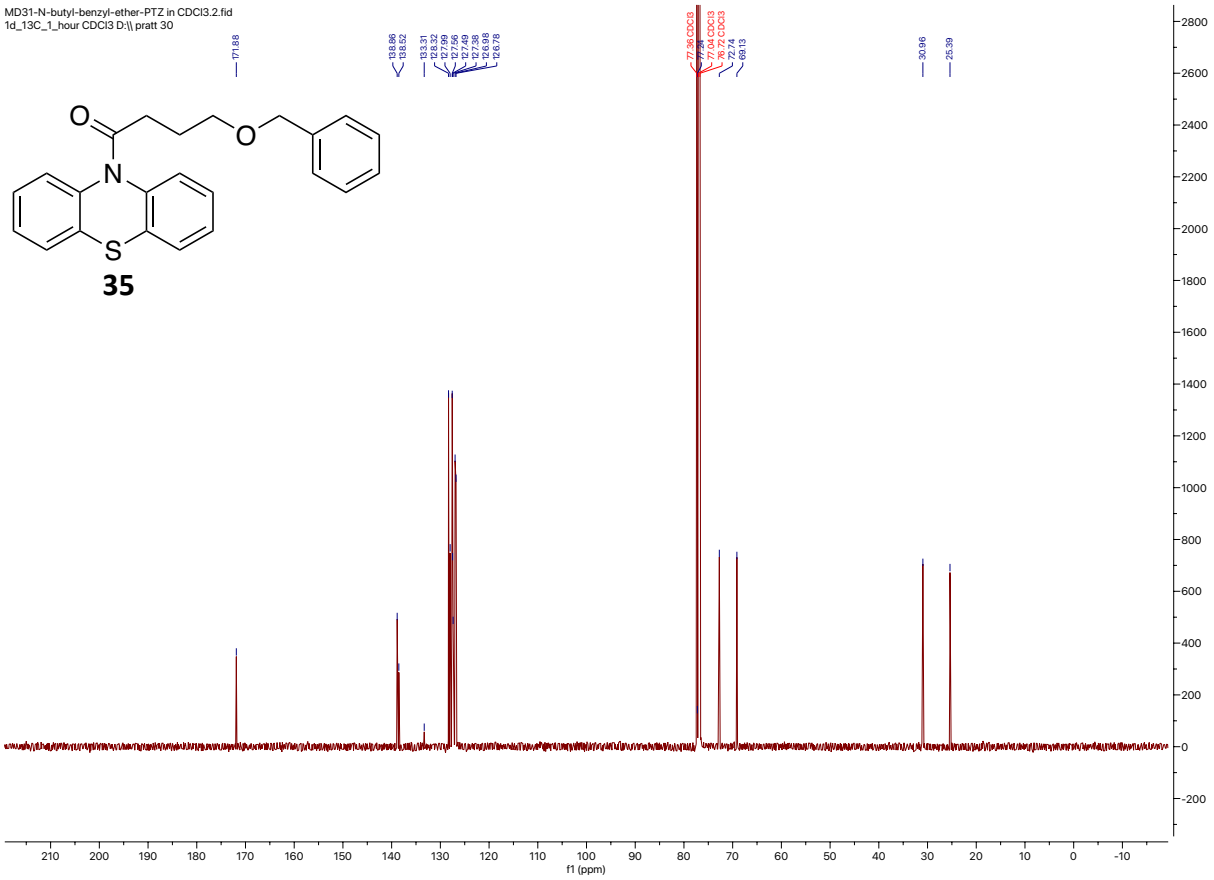

^{1}H-NMR ($CDCl_3$, 400 MHz)

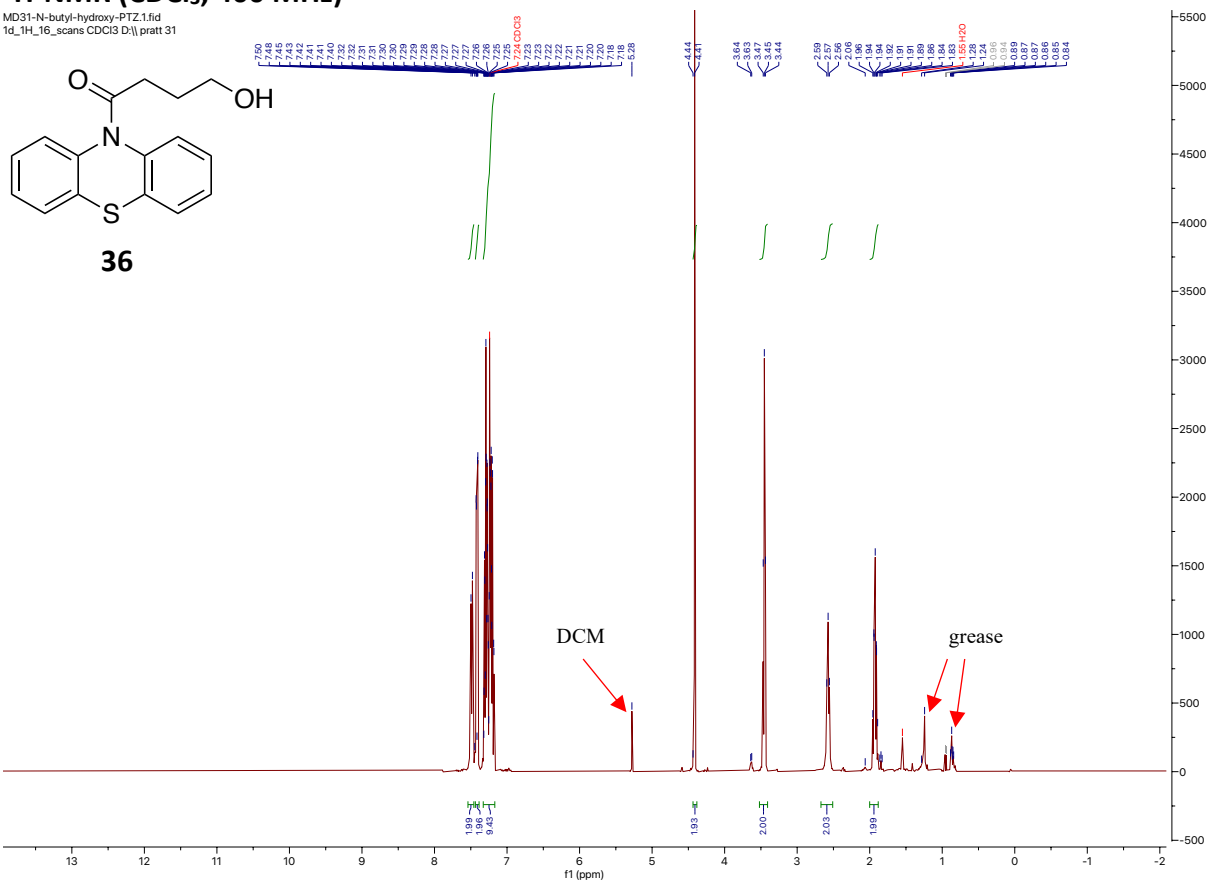

^{13}C-NMR ($CDCl_3$, 100 MHz)

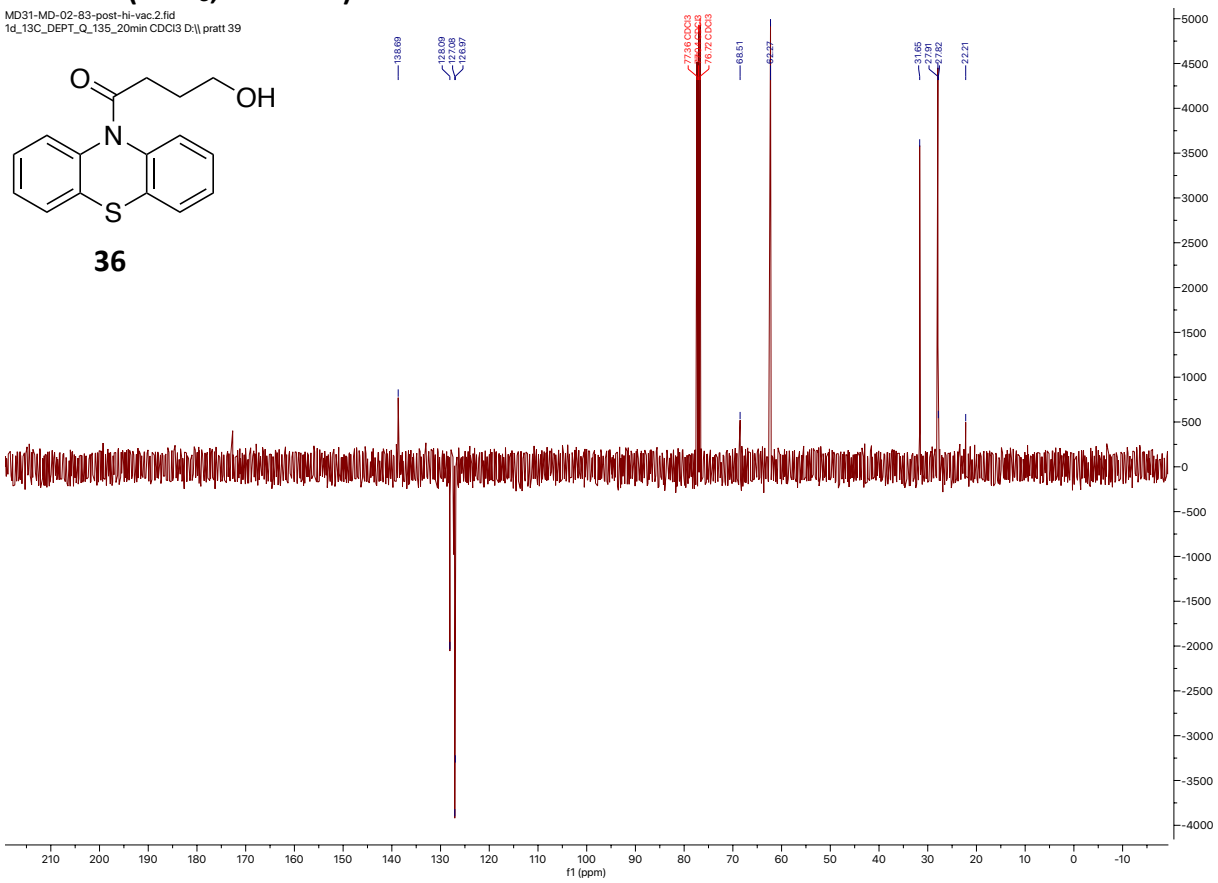

36

^{1}H-NMR ($CDCl_3$, 400 MHz)

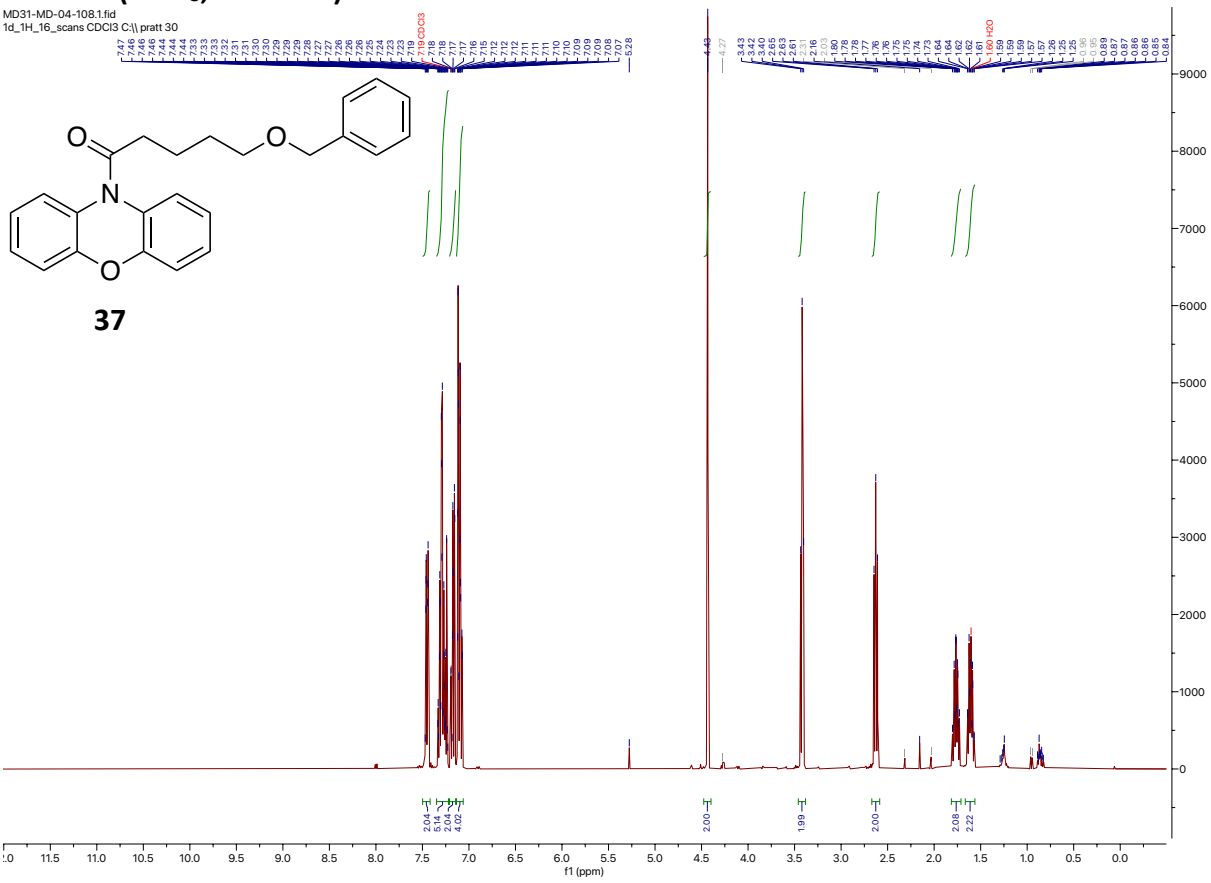

37

^{13}C-NMR ($CDCl_3$, 400 MHz)

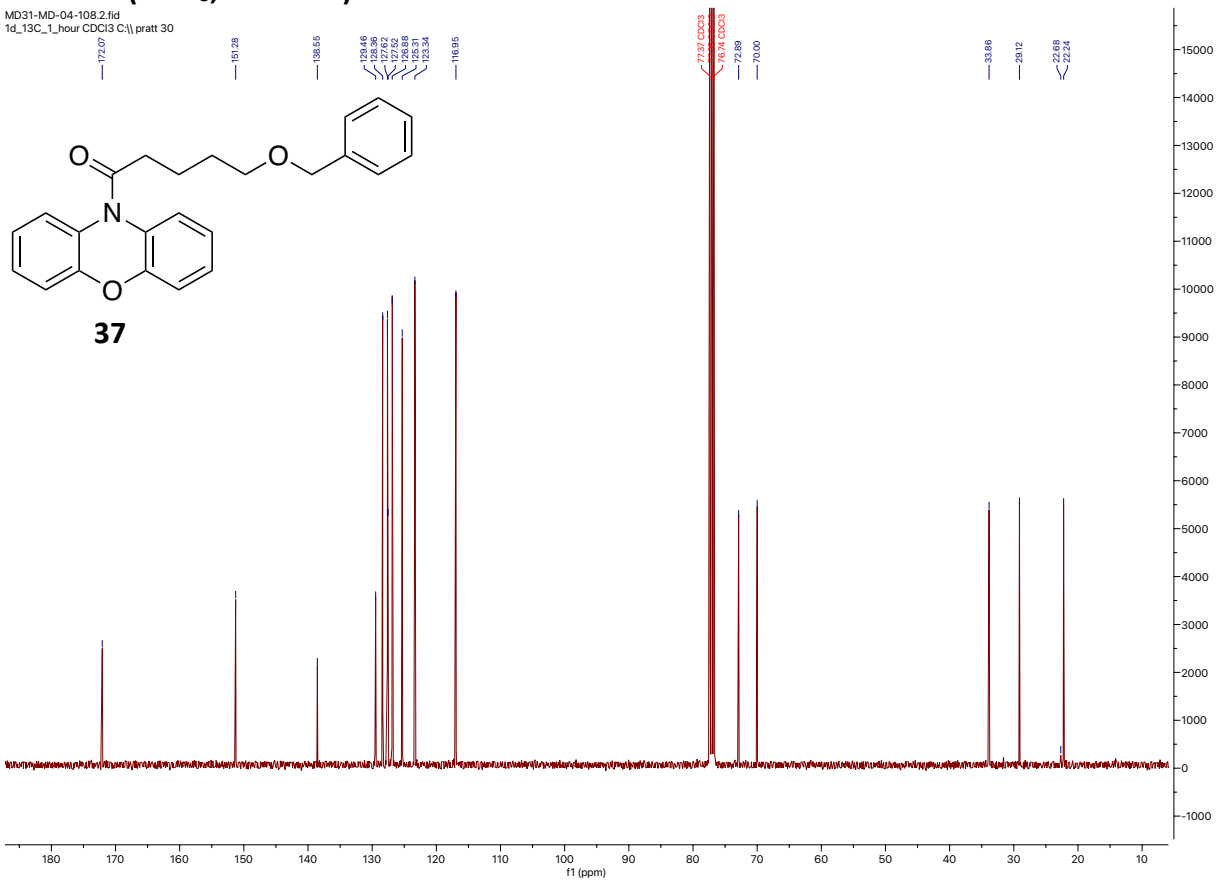

^{1}H-NMR (DMSO-d, 400 MHz)

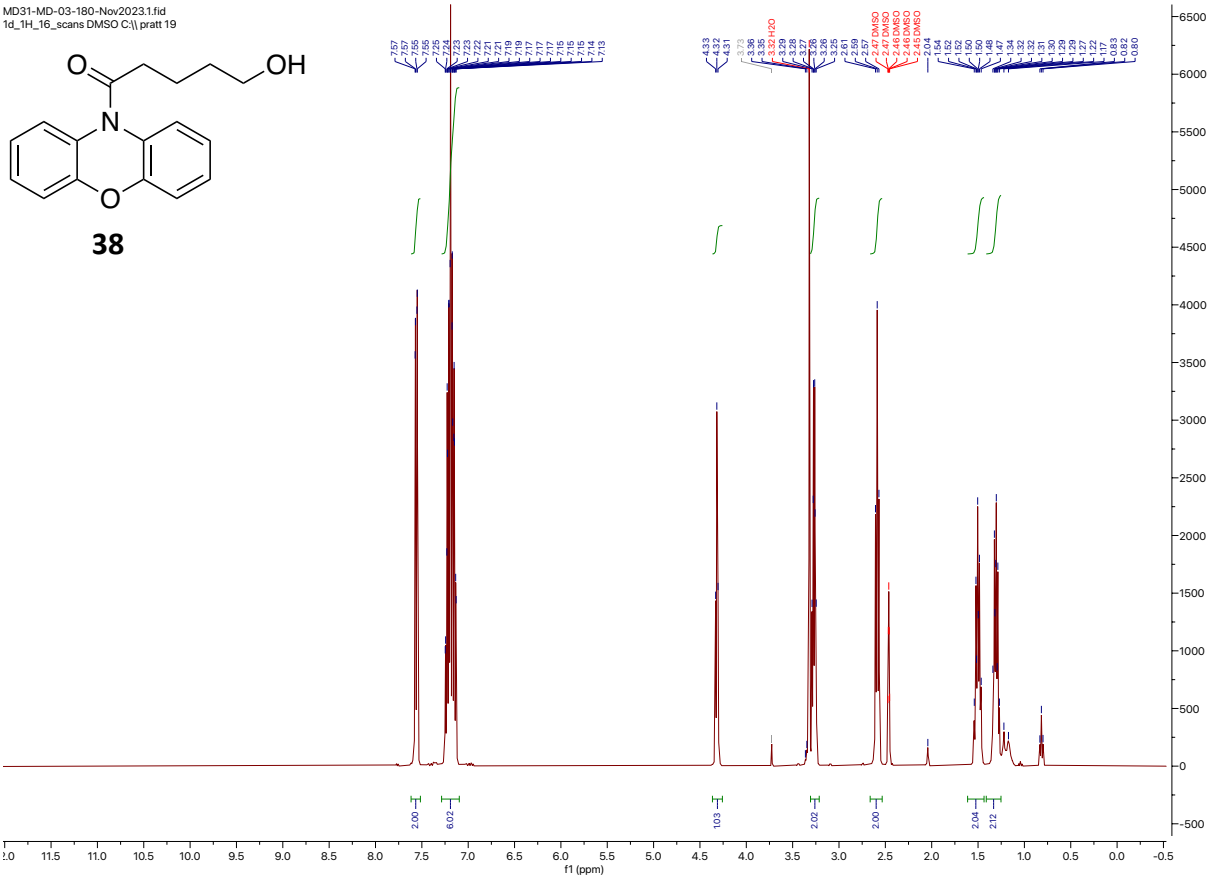

^{13}C-NMR (DMSO-d, 100 MHz)

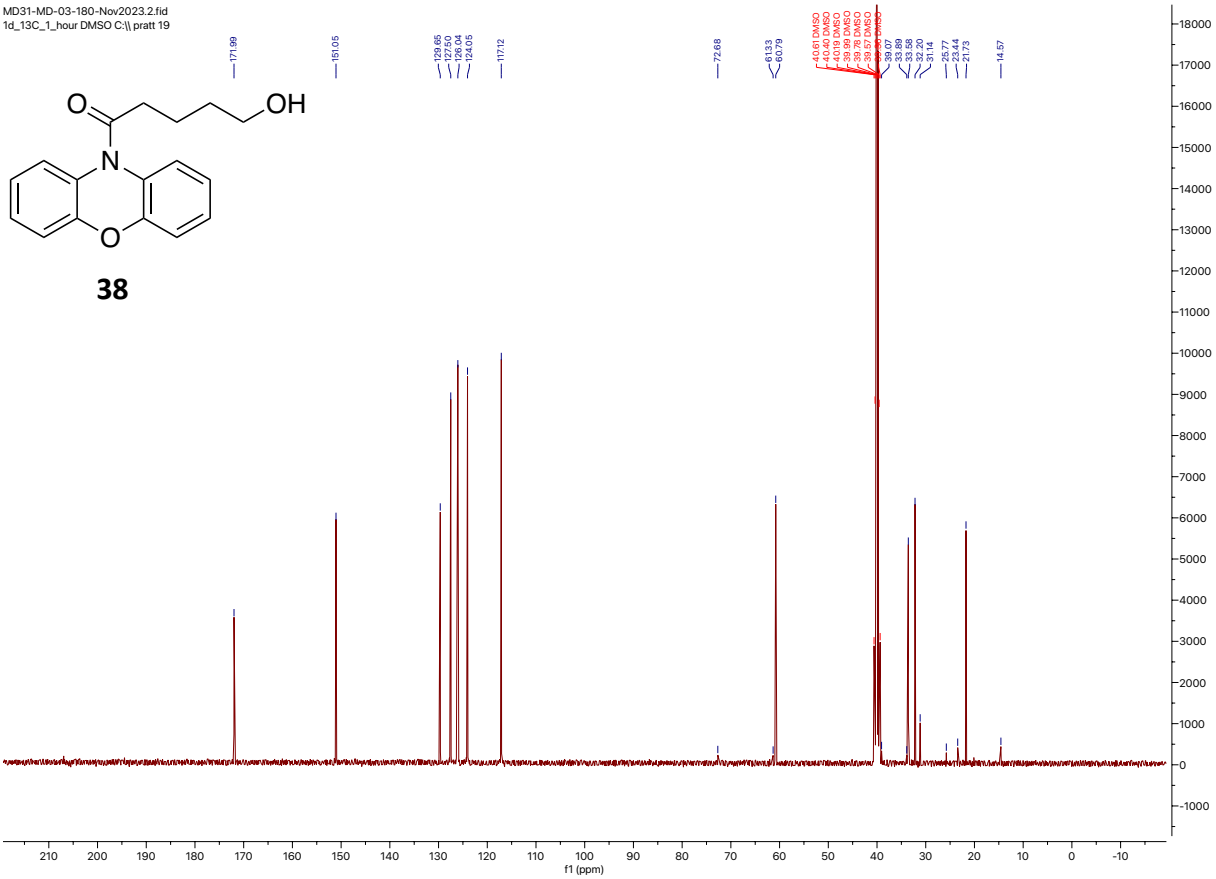

^{1}H-NMR ($CDCl_3$, 400 MHz)

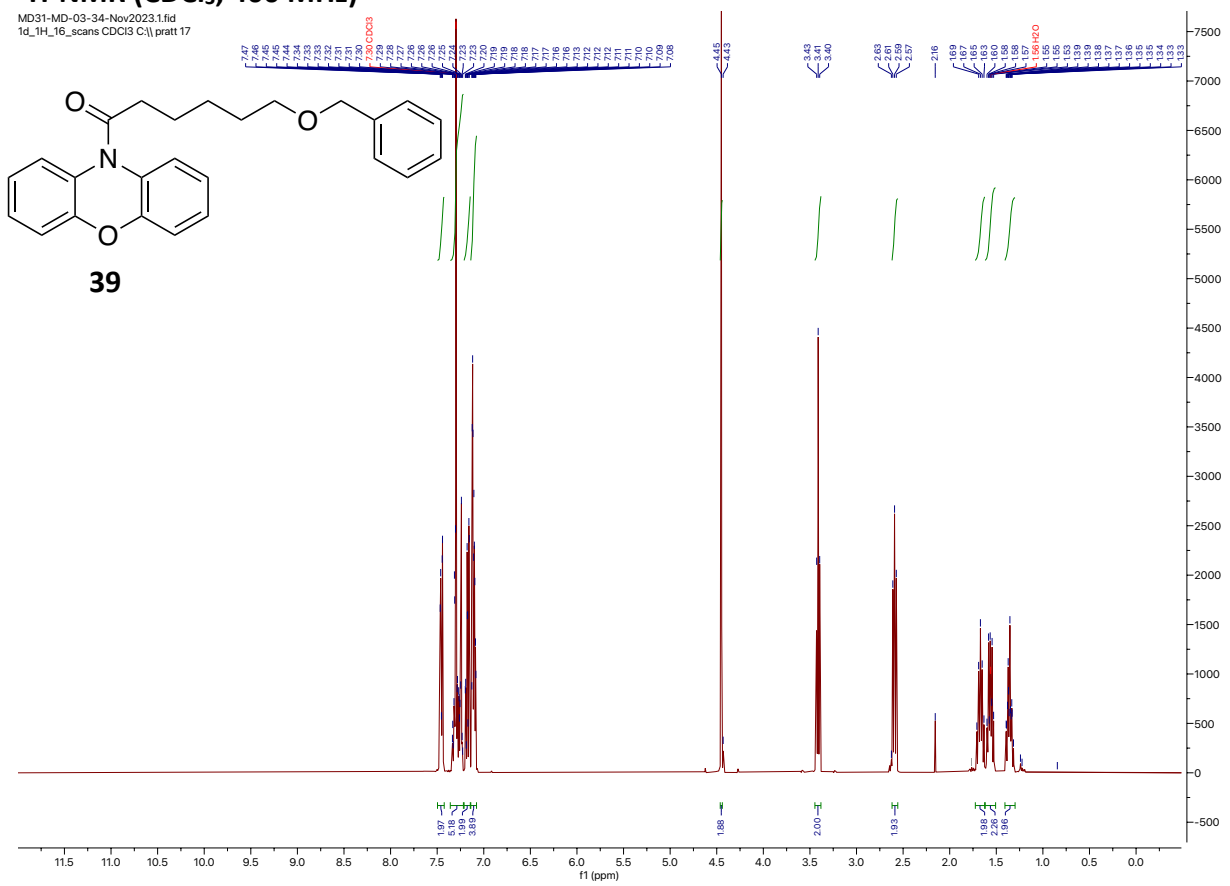

^{13}C-NMR ($CDCl_3$, 400 MHz)

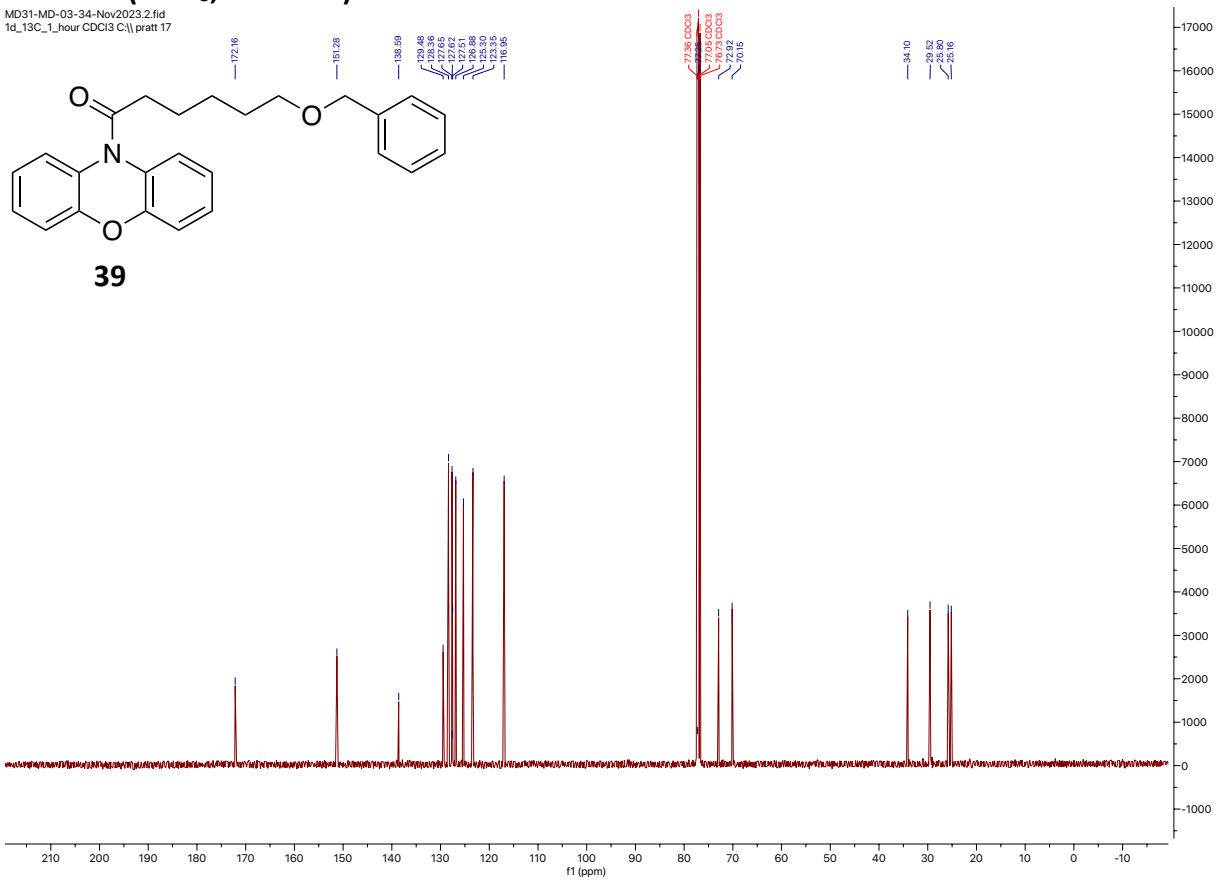

^{1}H-NMR (DMSO-d, 400 MHz)

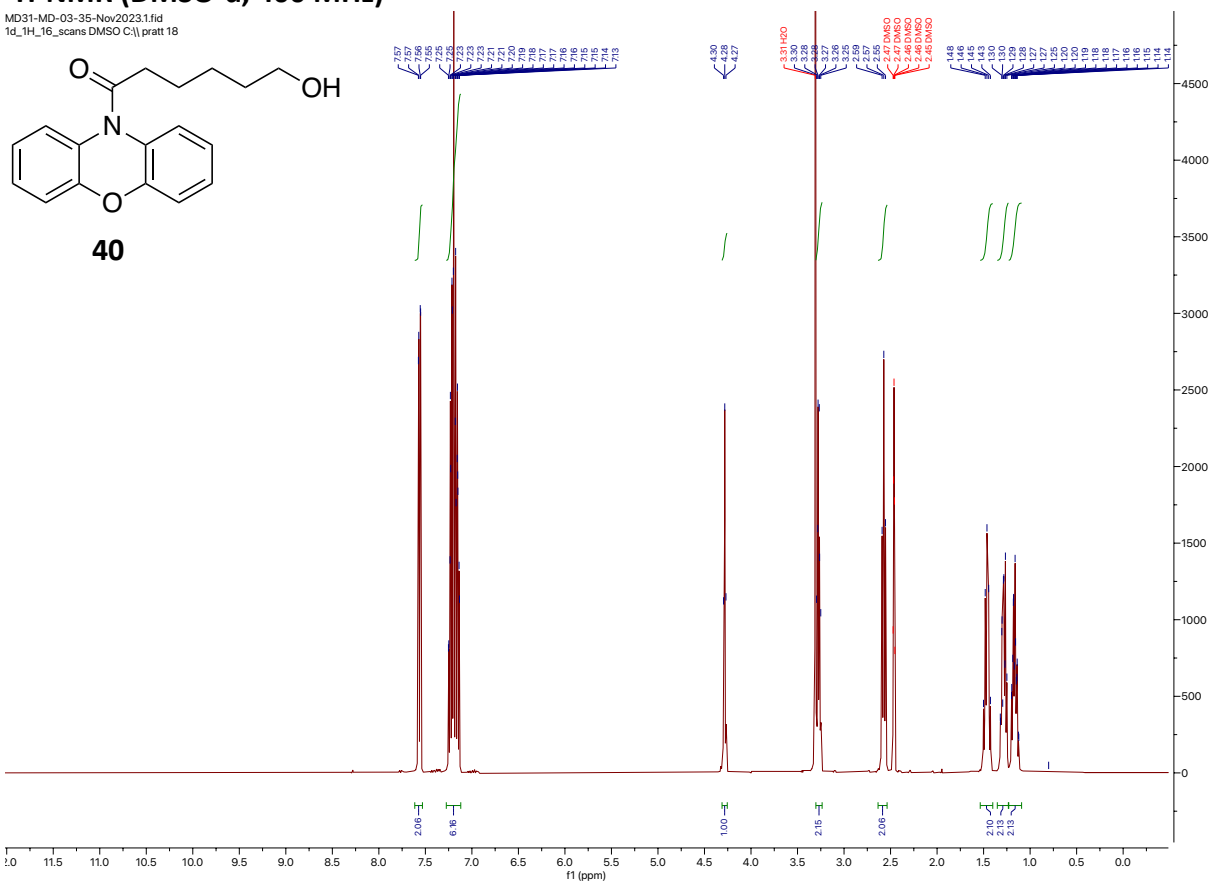

^{13}C-NMR (DMSO-d, 100 MHz)

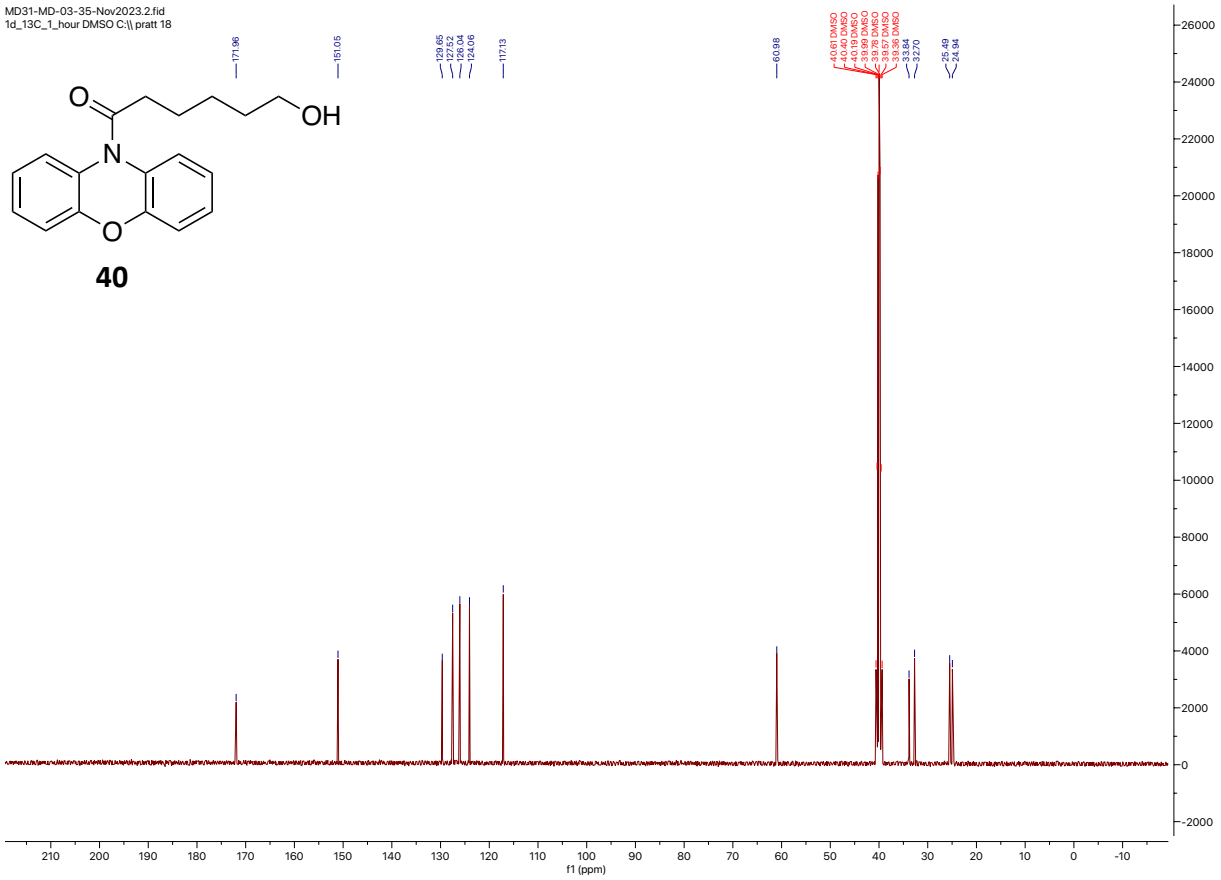

40

^{1}H-NMR ($CDCl_3$, 400 MHz)

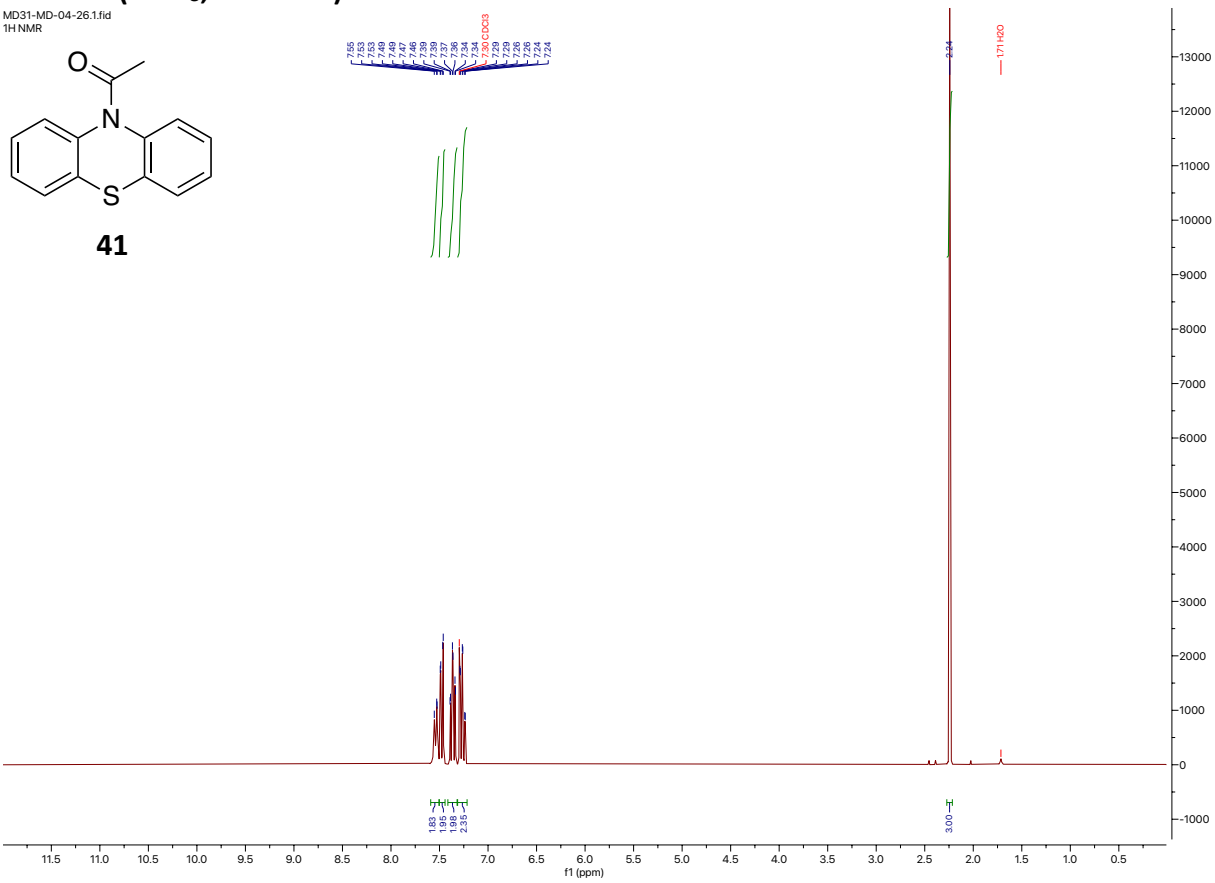

^{1}H-NMR ($CDCl_3$, 400 MHz)